

Spring 1-1-2018

Modular Software Architecture for Complex Multi-Body Fully-Coupled Spacecraft Dynamics

Cody J. Allard

University of Colorado at Boulder, cody.allard28@gmail.com

Follow this and additional works at: https://scholar.colorado.edu/asen_gradetds

 Part of the [Aerospace Engineering Commons](#), and the [Computer Sciences Commons](#)

Recommended Citation

Allard, Cody J., "Modular Software Architecture for Complex Multi-Body Fully-Coupled Spacecraft Dynamics" (2018). *Aerospace Engineering Sciences Graduate Theses & Dissertations*. 197.

https://scholar.colorado.edu/asen_gradetds/197

This Dissertation is brought to you for free and open access by Aerospace Engineering Sciences at CU Scholar. It has been accepted for inclusion in Aerospace Engineering Sciences Graduate Theses & Dissertations by an authorized administrator of CU Scholar. For more information, please contact cuscholaradmin@colorado.edu.

**Modular Software Architecture for Complex Multi-Body
Fully-Coupled Spacecraft Dynamics**

by

Cody J. Allard

B.S., Mechanical Engineering, University of Missouri

Columbia, Missouri, 2013

B.S., Physics, University of Missouri

Columbia, Missouri, 2013

M.S., Mechanical & Aerospace Engineering, University of Missouri

Columbia, Missouri, 2015

A thesis submitted to the

Faculty of the Graduate School of the

University of Colorado in partial fulfillment

of the requirements for the degree of

Doctor of Philosophy

Department of Aerospace Engineering Sciences

2018

This thesis entitled:
Modular Software Architecture for Complex Multi-Body Fully-Coupled Spacecraft Dynamics
written by Cody J. Allard
has been approved for the Department of Aerospace Engineering Sciences

Prof. Hanspeter Schaub

Prof. John Evans

Dr. Daniel Kubitschek

Prof. Steven Nerem

Prof. Christoffer Heckman

Date _____

The final copy of this thesis has been examined by the signatories, and we find that both the content and the form meet acceptable presentation standards of scholarly work in the above mentioned discipline.

Allard, Cody J. (Ph.D., Aerospace Engineering Sciences)

Modular Software Architecture for Complex Multi-Body Fully-Coupled Spacecraft Dynamics

Thesis directed by Prof. Hanspeter Schaub

Computer simulations of spacecraft dynamics are widely used in industry and academia to predict how spacecraft will behave during proposed mission concepts. Current technology and performance requirements have placed pressure on simulations to be increasingly more representative of the environment and the physics that spacecraft will encounter. This results in increasingly complex computer simulations. Designing the software architecture in a modular way is a crucial step to allow for ease of testing, maintaining, and scaling of the software code base. However, for complex spacecraft modeling including flexible or multi-body dynamics, modularizing the software is not a trivial task because the resulting equations of motion are fully-coupled nonlinear equations. In this dissertation, a software architecture is presented for creating complex fully-coupled spacecraft simulations with a modular framework.

One obstacle when attempting to modularize spacecraft dynamics formulations is that depending on the method used to derive the equations of motion, the state variables chosen, the choice of coordinate frames, and the assumptions made dictate the final form. Therefore, there can be an infinite number of ways to describe the equations of motion for a particular dynamics problem. This poses a problem when implementing in software because determining a pattern to modularize the equations can be difficult or sometimes impossible. This dissertation provides a solution to this problem by defining a systematic approach and a general form for developing equations of motion of spacecraft that will enable agreement between different dynamics problems and the final form of the equations of motion. The development makes minimal assumptions to make the solution applicable to a wide variety of problems commonly seen by spacecraft. Additionally, the approach is shown to be applicable to Newtonian/Eulerian mechanics and Kane's Method.

In addition to the general form for the equations of motion, this dissertation introduces a

back-substitution method that analytically modularizes the equations of motion. A major issue with dynamics problems from an software architecture standpoint, is that the second order state derivatives are coupled resulting a non-diagonal system mass matrix. Breaking a part this coupling while retaining the fully-couple nature of the problem is solved by analytically manipulating the equations to solve the system mass matrix in a two-step process called the back-substitution method which allows the math to be computed in a modular fashion. Additionally, energy and momentum conservation is a key tool to verify the equations of motion and software implementation are correct, and this dissertation provides a modular form for the energy and momentum calculations.

Since the development of the equations of motion can result in an infinite number of solutions, the literature is lacking on common dynamics problems solutions seen by spacecraft that agree with a common form. This results in the necessity to re-derive the equations of motion for complex problems which can be a time consuming task and is susceptible to analytical development errors. This dissertation provides ready-to-implement solutions to prevalent spacecraft dynamics problems that all conform to the general equation of motion form presented. Some examples are flexing appended bodies, fuel slosh, and imbalanced VSCMGs.

The final contribution of this dissertation is introducing a modular software architecture using the general equation of motion form, the back-substitution method, and the modularized energy/momentum calculations. This architecture is introduced by UML class diagrams and pseudo code to help explain the software implementation. The architecture allows for ease of testing, maintaining and scaling that is usually cumbersome with regards to dynamics problems. This architecture is implemented in the Basilisk astrodynamics software package and is a fully tested example of the proposed software architecture.

Dedication

To my wife, Jordon Allard.

You are my all, and your support throughout this process is immeasurable.

Acknowledgements

I would like to first and foremost thank my advisor, Dr. Hanspeter Schaub, for his mentorship, guidance and support throughout my degree. His enthusiasm for fundamental spacecraft dynamics not only made my research efficient and driven, but also made the research very enjoyable. The countless whiteboard discussions will be missed. Also, I would like to thank him for always pushing me and encouraging me towards all of my goals. Thank you to my committee members Dr. John Evans, Dr. Daniel Kubitschek, Dr. Steven Nerem and Dr. Christoffer Heckman for their support of my work and all of the time they took out of their busy schedules to be a part of my committee.

Thank you to Patrick Kenneally for all of the time he spent helping me with my programming skills, version control, Jira, and all other things that he helped me with throughout my time at CU. Additionally I would like to thank Manuel Diaz Ramos for his support with this research, his input and time taken to help develop the modular software architecture, and his willingness to provide support when I needed it.

I am especially grateful to my collaborators Manuel Diaz Ramos, John Alcorn, Paolo Panicucci, Paolo Cappuccio, and Iosto Fodde for the research projects that I was able to collaborate with them on. These projects were immensely helpful in my pursuit of the PhD and I thoroughly enjoyed working with each of them.

Special thanks to the EMM/Basilisk team in the AVS Lab that I was lucky enough to be apart of. It showed me how enjoyable working on a software development team can be. Thanks to the entire AVS Lab for the great conversations and the distractions from my research!

All of this work would also not have been possible without the support of the ADCS team

at LASP. The support from Scott Piggott and Dan Kubitschek has been astonishing. Scott is a genius, was extraordinarily helpful, and helped me even when he did not have the time for it. Dan is an incredible leader and motivates people around him to deliver their best work. I will miss getting to work with both of them!

Finally, I would like to thank my parents, my brother and my wife. Their support throughout the PhD but also throughout my life has been incredible. I would not be accomplishing this goal without all of them.

Contents

Chapter	
1	Introduction 1
1.1	Motivation 1
1.2	Background 2
1.2.1	General Form for Spacecraft Specific Equations of Motion 2
1.2.2	Development of Common Spacecraft Dynamics Problems Solutions 6
1.2.3	Software Architecture for Spacecraft Dynamics Simulations 6
1.3	Research Goals 9
2	Modularization of Spacecraft Equations 12
2.1	Spacecraft Specific Compact Equations of Motion Form 12
2.2	Multi-Rigidly Connected Spacecraft Equations of Motion Form 16
2.3	Back-Substitution Method 18
2.4	Back-Substitution Method Computational Performance 22
2.5	Modularization of Energy and Momentum Calculations 24
3	Spacecraft Equations of Motion Solutions 28
3.1	Development of Spacecraft Equations of Motion 29
3.1.1	Hinged Rigid-Bodies 29
3.1.2	Fuel Slosh - Lumped Mass Spring Mass Damper Model 45
3.1.3	Imbalanced Reaction Wheels 55

3.1.4	Thruster Based Mass Depletion	63
3.1.5	Dual-Hinged Rigid-Bodies	67
3.1.6	Imbalanced Variable Speed Control Moment Gyroscopes	87
3.1.7	Fuel Slosh - Pendulum Based Model	96
3.1.8	N-Connected Hinged Rigid-Bodies	105
3.2	Kane's Method Derivation Comparisons	111
3.2.1	Hinged Rigid-Bodies	112
3.2.2	Fuel Slosh - Lumped Mass Spring Mass Damper Model	116
3.2.3	Dual-Hinged Rigid-Bodies	119
4	Modular Software Architecture for Spacecraft Dynamics Simulations	126
4.1	Single Spacecraft Architecture	126
4.2	Multiple Spacecraft Architecture	131
5	Basilisk Astrodynamics Software Package Validation and Verification	137
5.1	Validation Examples	138
5.1.1	SpacecraftPlus	138
5.1.2	HingedRigidBodyStateEffector	149
5.1.3	ReactionWheelStateEffector	159
5.2	Energy and Momentum Conservation Verification	163
5.2.1	Hinged Rigid-Bodies Verification	163
5.2.2	Multiple Attached Spacecraft Verification	163
6	Applications, Simulations and Results	166
6.1	Linearization and Stability Analysis	166
6.1.1	Introduction	166
6.1.2	Derivation of Equations	167
6.1.3	Results	174

6.1.4	Conclusion	178
6.2	Force and Torque Calculation Example	179
6.2.1	Force on Spacecraft from Hinged Rigid Bodies and Fuel Slosh	180
6.2.2	Torque on Spacecraft from Hinged Rigid Bodies and Fuel Slosh	181
6.3	Hinged Rigid-Bodies Numerical Simulations	182
6.4	Fuel Slosh and Hinged Rigid-Bodies Numerical Simulations	185
7	Conclusion and Future Work	188
7.1	Summary and Conclusion	188
7.2	Recommendations for Future Work	190
	Bibliography	191
	Appendix	
A	Energy and Momentum Verification	198
A.1	Rigid-Body Hub Verification	198
A.2	Fuel Slosh - Lumped Mass Spring Mass Damper Model Verification	200
A.3	Reaction Wheels Verification	201
A.3.1	Balanced Reaction Wheels	201
A.3.2	Imbalanced Reaction Wheels	202
A.4	Dual-Hinged Rigid-Bodies Verification	203
A.5	Variable Speed Control Moment Gyroscopes Verification	204
A.5.1	Balanced Variable Speed Control Moment Gyroscopes	204
A.5.2	Imbalanced Variable Speed Control Moment Gyroscopes	205
A.6	N-Connected Hinged Rigid-Bodies Verification	206
A.7	Fuel Slosh - Pendulum Model	207
A.8	Multi-Spacecraft Verification - Attached Spacecraft and Unattached Spacecraft	208

Tables

Table

3.1	Partial velocity table for hinged rigid-bodies	113
3.2	Partial velocity table for fuel slosh	117
3.3	Partial velocity table for dual-hinged rigid-bodies	120
5.1	Frequency and amplitude test results for hinged rigid-bodies	156
6.1	Spacecraft parameters for stability analysis	174
6.2	Gain descriptions for the three scenarios for stability analysis	175
6.3	Gain and phase margins for each scenario	176
6.4	Simulation parameters for the flexing model	182
6.5	Simulation parameters for the rigid-body model	183
6.6	Flexing simulation initial conditions	183
6.7	Hub simulation parameters	185
6.8	Solar panel simulation parameters	185
6.9	Slosh simulation parameters	186

Figures

Figure

1.1	Artist rendition of ATV docking with Russian Zvezda module, http://www.dlr.de . . .	2
1.2	Two degrees of freedom dynamics problem	3
2.1	Complex spacecraft with multiple degrees of freedom	13
2.2	Multiple spacecraft diagram for multi-spacecraft dynamics	17
2.3	Dual-hinged rigid-bodies frame and variable definitions	19
2.4	Computational efficiency of back-substitution method	23
3.1	Components, variables and coordinate frames used for this derivation.	31
3.2	Frame and variable definitions used for formulation	47
3.3	Detailed description of single slosh particle	47
3.4	Reaction wheel static and dynamic imbalance.	57
3.5	Reference frame and variable definitions.	58
3.6	Thruster based mass depletion schematic	65
3.7	Frame and variable definitions used for dual-hinged rigid-bodies formulation	67
3.8	Reference frame setup and variable definitions for the spacecraft + VSCMG problem.	88
3.9	Frame and variable definitions used for formulation	97
3.10	Further detail of propellant slosh and reference frames	98
3.11	Frame and variable definitions for the system discussed here, where $N_p = 2$	106
4.1	UML Diagram for Modular Architecture.	127

4.2	Pseudo code for the <code>equationsOfMotion()</code> method within <code>spacecraftPlus</code>	129
4.3	Pseudo code for <code>hubEffector computeDerivatives()</code> method	130
4.4	Pseudo code for <code>hingedRigidBody computeDerivatives()</code> method	131
4.5	UML diagram for multi-spacecraft modular architecture	133
4.6	Pseudo code for the <code>equationsOfMotionSys()</code> method within <code>spacecraftDynamics</code>	134
4.7	Pseudo code for the <code>equationsOfMotion()</code> method within <code>spacecraftDynamics</code>	135
4.8	Pseudo code for the <code>integrateState()</code> method within <code>spacecraftDynamics</code>	136
5.1	Attitude of Spacecraft in MRPs	141
5.2	MRP Switching	142
5.3	Basilisk vs Validation Test Calculation For Rotation	143
5.4	Schematic of translational validation example	144
5.5	Velocity vs time curve for translational validation example	145
5.6	Translation Velocity Validation Test	146
5.7	Translation Position Validation Test	147
5.8	PointB vs PointC Translation	148
5.9	PointB vs PointC Attitude	148
5.10	Steady state deflection validation problem description	151
5.11	Validation Test Calculation for Steady State Theta 1 Deflection vs Simulation	152
5.12	Validation Test Calculation for Steady State Theta 2 Deflection vs Simulation	152
5.13	Max Theta While Forcing	156
5.14	X Position Lagrangian Vs Basilisk	157
5.15	Y Position Lagrangian Vs Basilisk	157
5.16	Theta Lagrangian Vs Basilisk	157
5.17	Theta 1 Position Lagrangian Vs Basilisk	158
5.18	Theta 2 Lagrangian Vs Basilisk	158
5.19	Schematic for validation example of reaction wheels	160

5.20	Reaction Wheel BOE Theta	162
5.21	Reaction Wheel BOE Body Rate	162
5.22	Reaction Wheel BOE RW Rate	162
5.23	Simulation verification results for a rigid hub with two hinged panels	164
5.24	Simulation verification results for two spacecraft attached to the primary spacecraft with two solar panels attached	165
6.1	Hinged rigid bodies frame and variable definitions	168
6.2	Open loop bode plot for Scenario 1 gains (blue is rigid response, green is flexible body response)	175
6.3	Open loop bode plot for Scenario 2 gains	175
6.4	Open loop bode plot for Scenario 3 gains	176
6.5	Closed loop bode plot for Scenario 1 gains	177
6.6	Closed loop bode plot for Scenario 2 gains	178
6.7	Closed loop bode plot for Scenario 3 gains	179
6.8	Inertial Velocity of Point B and Inertial Angular Velocity of the Body Frame	184
6.9	Angular Deflection of the Hinged Rigid-Bodies	184
6.10	Solar panel, slosh, and rotational motion.	186
6.11	Translational motion of spacecraft.	187
A.1	Simulation verification results for a rigid hub	199
A.2	Simulation verification results for a rigid hub with three spring mass damper fuel slosh particles	200
A.3	Simulation verification results for a rigid hub with three balanced reaction wheels . .	201
A.4	Simulation verification results for a rigid hub with three imbalanced reaction wheels	202
A.5	Simulation verification results for a rigid hub with two sets of dual-hinged rigid-bodies	203
A.6	Simulation verification results for a rigid hub with two balanced variable speed con- trol moment gyroscopes	204

A.7 Simulation verification results for a rigid hub with two imbalanced variable speed control moment gyroscopes	205
A.8 Simulation verification results for a rigid hub with one panel with four sections and another panel with three sections	206
A.9 Simulation verification results for a rigid hub with three pendulum based fuel slosh particles	207
A.10 Simulation verification results for two spacecraft attached to the primary spacecraft with two solar panels attached	208
A.11 Simulation verification results for first unattached spacecraft	209
A.12 Simulation verification results for second unattached spacecraft	209

Chapter 1

Introduction

1.1 Motivation

Spacecraft are becoming more and more complex which results in spacecraft exhibiting complicated dynamics. For example, spacecraft can have many appended bodies that have flexible behavior, spacecraft structures are becoming large enough that a large portion of the structure can no longer be assumed to be rigid, and robotic structures attached to spacecraft can have complex interrelations between appendages. Figure 1.1 shows an illustrative example of a complex spacecraft exhibiting such features. Furthermore, spacecraft mission performance requirements are becoming more strict resulting in the need to have a more complete knowledge of the dynamics. For example, some missions have extremely tight requirements on the fine pointing of the spacecraft, which requires high fidelity simulations of the dynamics to show adherence to these tight requirements. If the simulation is not high enough fidelity, the results might not be able to be trusted.

This increase in complexity results in a huge increase in the complexity of the governing equations and the resulting software implementation of the equations. To implement simulation code attempting to describe the motion of a spacecraft like the one shown in Figure 1.1, usually results in massive interconnected code that is extremely difficult to test, maintain, and scale. For example, for a project of that size, sometimes something as simple as adding or removing a flexible solar panel to/from the equations of motion can take a lengthy amount of time to change in the software and result in non-functioning code or bugs that result in disagreement between the code and the underlying physics.



Figure 1.1: Artist rendition of ATV docking with Russian Zvezda module, <http://www.dlr.de>

Additionally, the complexity of the underlying physics for the problems can result in lengthy derivations, are prone to errors, and are sometimes spacecraft specific which results in re-derivation for different spacecraft. There is a need to have general solutions to common physical phenomenon that spacecraft encounter that can be applied to a wide range of spacecraft. Finally, computational efficiency needs to be considered due to the length of simulation time required for spacecraft analysis, and the complexity of the mathematics required to solve the dynamics. This dissertation is aimed at developing general spacecraft Equations of Motion (EOMs) and developing a modular software architecture to avoid these common problems.

1.2 Background

1.2.1 General Form for Spacecraft Specific Equations of Motion

An issue with multi-body dynamics is the EOMs can come in many different forms [1, 2]. This is a drawback from a software implementation perspective because having such variability can lead to disorganized and inconsistent implementation of different dynamical systems. The form of the EOMs depends on the chosen state variables, the method used to develop the EOMs, the coordinate frames chosen, and the assumptions used. This results in an infinite number of solutions available to describe the motion of an individual dynamics problem. To give further context, a simple example

shown in Figure 1.2 is used to show how different state variables and methods used to develop the EOMs can lead to different results.

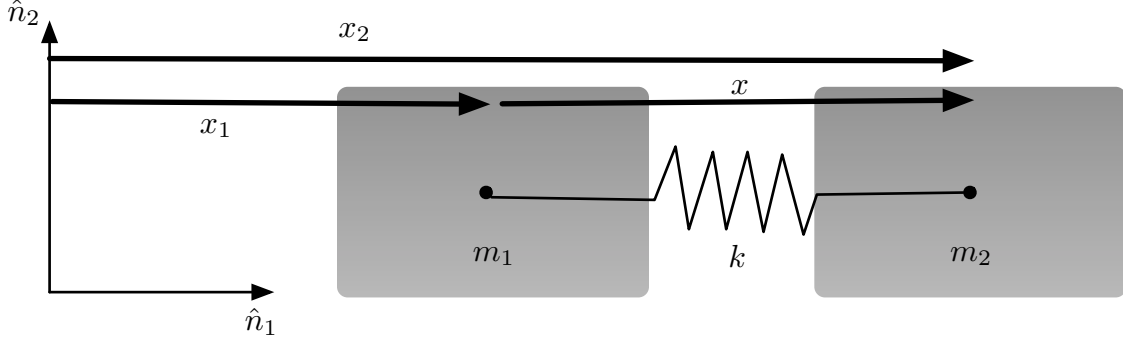


Figure 1.2: Two degrees of freedom dynamics problem

In Figure 1.2, the problem represented is two masses, m_1 and m_2 , connected by a spring with linear spring constant k . The masses are constrained to move freely only along the \hat{n}_1 axis and there are no external forces acting on the system. Since this system has two degrees of freedom, two state variables are needed, at a minimum, to completely describe the motion. There are three variables defined that could be used as state variables: the inertial position of m_1 , x_1 ; the inertial position of m_2 , x_2 ; and the relative distance between m_1 and m_2 , x .

For this example, there are three cases chosen to compare the form of the solutions. Case 1 uses the state variables x_1 and x and the EOMs are derived using Newtonian mechanics. To solve Case 1, Newton's Second Law is evaluated on both m_1 and m_2 and the results can be seen in Eqs. (1.1) and (1.2).

$$m_1 \ddot{x}_1 = kx \quad (1.1)$$

$$m_2(\ddot{x}_1 + \ddot{x}) = -kx_2 \quad (1.2)$$

Putting these equations into State Space Representation [3] yields

$$\begin{bmatrix} m_1 & 0 \\ m_2 & m_2 \end{bmatrix} \begin{bmatrix} \ddot{x}_1 \\ \ddot{x} \end{bmatrix} = \begin{bmatrix} 0 & k \\ 0 & -k \end{bmatrix} \begin{bmatrix} x_1 \\ x \end{bmatrix} \quad (1.3)$$

Equation (1.3) is the matrix form of the differential equations that describe the motion of the two masses for Case 1.

Case 2 uses the state variables x_1 and x_2 , and Newtonian mechanics to derive the EOMs of the system. Similar to Case 1, Newton's Second Law is performed on both m_1 and m_2 and the results can be seen in Equations (1.4) and (1.5).

$$m_1\ddot{x}_1 = k(x_2 - x_1) \quad (1.4)$$

$$m_2\ddot{x}_2 = -k(x_2 - x_1) \quad (1.5)$$

The equations are placed into State Space Representation and the results can be seen in following equation:

$$\begin{bmatrix} m_1 & 0 \\ 0 & m_2 \end{bmatrix} \begin{bmatrix} \ddot{x}_1 \\ \ddot{x}_2 \end{bmatrix} = \begin{bmatrix} -k & k \\ k & -k \end{bmatrix} \begin{bmatrix} x_1 \\ x_2 \end{bmatrix} \quad (1.6)$$

Lastly, Case 3 uses the same state variables used in Case 1, x_1 and x , but uses Lagrangian mechanics to develop the EOMs. First, the Lagrangian is defined:

$$\mathcal{L} = \frac{1}{2}m_1\dot{x}_1^2 + \frac{1}{2}m_2(\dot{x}_1 + \dot{x})^2 - \frac{1}{2}kx^2 \quad (1.7)$$

Next, Lagrange's equation is performed on state variable x_1 :

$$\frac{\partial \mathcal{L}}{\partial x_1} - \frac{d}{dt} \left(\frac{\partial \mathcal{L}}{\partial \dot{x}_1} \right) = (m_1 + m_2)\ddot{x}_1 + m_2\ddot{x} = 0 \quad (1.8)$$

Similarly, Lagrange's equation is performed on state variable x :

$$\frac{\partial \mathcal{L}}{\partial x} - \frac{d}{dt} \left(\frac{\partial \mathcal{L}}{\partial \dot{x}} \right) = -kx - m_2\ddot{x}_1 - m_2\ddot{x} = 0 \quad (1.9)$$

Finally, Eqs (1.8) and (1.9) are placed into State Space Representation:

$$\begin{bmatrix} m_1 + m_2 & m_2 \\ m_2 & m_2 \end{bmatrix} \begin{bmatrix} \ddot{x}_1 \\ \ddot{x} \end{bmatrix} = \begin{bmatrix} 0 & 0 \\ 0 & -k \end{bmatrix} \begin{bmatrix} x_1 \\ x \end{bmatrix} \quad (1.10)$$

Comparing the forms of the solutions for Case 1, 2, and 3 in Eqs (1.3), (1.6), and (1.10), it shows that each form is different with respect to the system mass matrix on the left hand side of the

equations and the dynamics matrix on the right hand side of the equation. This is a simple example but highlights the difficulty at arriving at a common form because there are an infinite number of ways of representing the system dynamics. This non-conformity is an issue from a software architecture perspective because the design has to incorporate the variability of the form of the EOMs which can lead to disorganized and unmaintainable code, or a highly complex architecture.

In the literature on spacecraft dynamics, there is a strong history of development of solutions for complex spacecraft dynamics. For example, flexible solar arrays is a common phenomenon affecting spacecraft and there is a breadth of research presenting models of flexing solar arrays. However, similar to the simple example provided, the models presented often vary in form and there is not a standard way to arrive at the EOMs. For example References [4, 5, 6] present models of spacecraft dynamics with appended solar panels but each have a different form. From a software implementation stand point, this non-conformity provides difficulty because as new models are added, they do not fit a specific pattern. This results in scalability issues[7] because adding new models can result in losing functionality of the code and requiring major architectural changes.

One method to combat this is to auto-generate equations of motion using software packages. Motion Genesis is a software package that uses Kane's Method [8] to programatically find the EOMs for complex multi-body dynamics [9]. MathWorks Simscape Multibody [10] can also generate EOMs to be integrated and can output simulation code to Matlab or C code. However this approach has a similar problem where each system will result in different equations depending on the spacecraft and configuration, therefore implementing these equations into software can be time consuming and not scalable [7]. Developing a software architecture surrounding one of the auto-generation software packages that would allow for scalability would be a difficult task. Also, the product would rely heavily on another code base that if changed could present maintainability [7] issues. Finally, validation and verification of software models is an important aspect of the spacecraft design process therefore the ease of testing [7] the code base can be a concern.

There is need to solve the issue of non-conformity between different dynamics problems commonly affecting spacecraft. More specifically, there is a need to develop a standard structure

for the EOMs that can be consistent for a wide variety of spacecraft configurations, assumptions and derivations.

1.2.2 Development of Common Spacecraft Dynamics Problems Solutions

As discussed in the previous section, there is a rich history on complex dynamics problem solutions for spacecraft, but the solutions provided come in many different forms, and because of this when implementing a new simulation model in software, often times re-derivation is required to fit in the form needed for the architecture.

In contrast to already developed solutions, there are systematic methods to develop EOMs for complex multi-body systems. The field of multi-body dynamics has extensive research on modeling dynamics but some of the EOMs presented in the literature are generalized for complex and diverse problems [11, 12]. This results in re-derivation of equations because of generality [13, 14, 15, 16, 17, 18, 19]. These re-derivations can be very time consuming and error prone.

There is a need in the literature to have ready-to-implement solutions to common physical phenomenon affecting spacecraft that have energy and momentum verification tools available. This removes the need for re-derivation and testing which can be a time consuming task. Also using a standard EOM form introduced in the previous section would allow for conformity between the solutions and allow for ease of implementation into software.

1.2.3 Software Architecture for Spacecraft Dynamics Simulations

An important aspect when considering software design is the scalability, maintainability, and testability of the software[7]. If the software is not designed well, adding complexity (scalability), maintaining functionality amidst a changing code base (maintainability) and the ease of verifying functionality (testability) can become extremely laborious [20]. For complex simulations of spacecraft, this methodology needs to be considered to avoid these complications. However, multi-body dynamics poses a difficult problem because of the coupled nature of the system through the non-diagonal system mass matrix [1]. This mass matrix relates the dynamical effect of the second order

state variables between all of the interconnected bodies.

Although multi-body dynamics is a complex challenge not only from an equation of motion (EOM) development perspective but from a software implementation perspective, there is an abundant amount of open source software packages simulating multi-body dynamics. Bullet [21] is an open source multi-body dynamics software package that utilizes the Gauss-Seidel Method to solve the system mass inverse for diagonally dominant matrices [22]. Project CHRONO is an open source multi-physics software package that utilizes parallel computing to solve multi-body dynamics with a large number of degrees of freedom [23]. Rigid Body Dynamics Library is an open source multi-body dynamics software package that utilizes the Articulated Body Algorithm and Composite Rigid Body Algorithm for solving the dynamics [24]. Moby is a multi-body dynamics software package that uses interior point quadratic solver to solve for constraints [25]. Although these software packages are powerful for simulating a large number of bodies at a time, adding spacecraft specific environmental factors and incorporating flight software into these open source packages can be laborious and is not the intended use of these software packages. Additionally, validation and verification of the simulation is important for spacecraft missions and the capability to provide the necessary information for that process is not always a key feature of these open source packages.

In contrast to the open source packages, there are commercial software packages that are solving multi-body dynamics problems. COMSOL is a multi-physics software package that has a multi-body dynamics module for simulating multi-body dynamics [26]. As this is a commercial software, the details of the software architecture and the method for solving the complex multi-body dynamics is not readily available. MathWorks Simscape Multibody [10] can generate EOMs to be integrated and can output simulation code to Matlab or C code. Motion Genesis uses Kanes method [2, 18] to output simulation code to Matlab, C, or Fortran and includes energy and momentum verification [9]. One downfall of these equation of motion generators is that the equations are specific to that system which introduces scalability, maintainability, and testability issues for software architecture. Additionally, these software packages, although general, present

issues with computational efficiency.

Computer graphics also has a strong influence in physics engine software, even though being visually realistic typically takes precedence over the dynamics accuracy. For example, Interactive Computer Graphics has a library called Position Based Dynamics Library [27] that uses position based dynamics. This method, which integrates position and velocity using kinematics, avoids physical constraints but is focused on being visually realistic. This results in the dynamics being not as accurate, but the computations being extremely fast. Indeed, the software can simulate a very large number of degrees of freedom and is visually appealing[28, 29]. Additionally, Interactive Computer Graphics has another physics engine called IBDS Physics Library which uses both forward dynamics and position based dynamics [30, 31]. Not only is the loss of accuracy a downfall of these methods with regards to spacecraft applications, but additionally energy and momentum verification tools are not available which makes validating and verifying the code difficult.

In contrast to general multi-body dynamics software, there are software packages that focus only on spacecraft simulation because of the unique environment that spacecraft encounter, and the specific challenges that modeling spacecraft dynamics entails. STK SOLIS is a software package for modeling spacecraft with both translational and attitude dynamics but does not model disturbances that can change the center of mass of the spacecraft, for example flexing solar arrays [32]. The Jet Propulsion Laboratory has a software package, Dynamics Algorithms for Real-Time Simulation (DARTS) [33]. This simulation software package utilizes spacial operator algebra for the development of the multibody dynamics [34] to create the system mass matrix in a form that can be solved efficiently with a recursive algorithm [35]. NASA's open source software package named 42 [36], allows for spacecraft composed of multiple rigid or flexible bodies using tree-topology [16] to formulate the dynamics resulting in a system mass matrix inversion solution. Orekit is an open source software package for spacecraft simulations and flight software and models the spacecraft as a rigid body and the dynamics are primarily focused on defining perturbations as external forces and torques [37].

The spacecraft specific software packages described that involve multi-body dynamics have

to populate a system mass matrix and either have to find the inverse of the matrix or use other linear algebra techniques [34, 35]. Populating the system mass matrix while retaining a modular software architecture is difficult because the system needs to know the locations of the states in the system mass matrix and also know the relative locations of other coupled states. Additionally, inverting the system mass matrix can be computationally expensive because the calculation scales with N^3 , with N being the number of states.

Removing the need to invert the full system mass matrix to solve the fully-coupled dynamics problem would greatly simplify the software architecture while retaining the full system dynamics. Additionally, arriving at a modular software architecture would be easier because the second order states would no longer be coupled in the system mass matrix. Additionally, energy and momentum verification would still be available because the full solution is being calculated.

1.3 Research Goals

In summary, the overarching novel contribution from this dissertation is to standardize the EOMs of spacecraft while being applicable to a wide range of spacecraft configurations, introduce a back-substitution method to remove the need to invert the entire system mass matrix which results in a modular form of the EOMs, and develop a modular software architecture that leverages the modularized equations. While prior methods allow for general multi-body setups, this method is specifically developed for common spacecraft configurations where there is a single rigid spacecraft hub onto which additional bodies (both rigid and flexible) are attached. This assumption is a key enabler that leads to an elegant modular framework that can be implemented in numerical simulations without dropping any dynamical coupling between the components. This allows for the underlying physics to be retained which enables energy and momentum conservation checks to be completed.

Additionally, this dissertation aims to develop EOMs to common physical phenomenon seen by spacecraft. This removes the need to re-derive EOMs for the chosen set of dynamics problems which can be time consuming and error prone task. The dissertation provides ready to implement

solutions that fit the generalized form of the EOMs introduced in the dissertation and also provides examples on the systematic approach for developing EOMs for the introduced modular software architecture.

The resulting dynamics software architecture and the solutions to common dynamics problems provide a ready-to-implement solution that allows the user to rapidly configure a broad range of spacecraft configurations without having to derive equations of motion or integrate auto-coded equations. The modular form allows for new types of dynamic forces and torques to be added without having to re-derive all the other spacecraft equations of motion, enabling a layered approach to increase the simulation modeling capabilities.

In summary, below is a list of the research goals providing the scope of the research project:

(1) Modularization of Equations of Motion

- Introduce a generalized EOM form for spacecraft dynamics that applies to a wide variety spacecraft applications
- Manipulate these generalized EOMs into a modular form using a method called the back-substitution method
- Manipulate the energy and momentum calculations into a modular form
- Expand the modular EOMs to multiple spacecraft which can dock and detach

(2) Spacecraft Specific Equations of Motion Solutions

- Develop and provide ready-to-implement solutions for common phenomenon seen by spacecraft that avoids the need for re-derivation and provides examples to arrive at the general equation of motion form
- Provide examples that confirm Kane's method can be used to also arrive at the generalized EOM form

(3) Modular Software Architecture for Spacecraft Dynamics Simulations

- Introduce a modular software architecture that will leverage the equations of motion form and result in code that is easy to test, scale, maintain and is computationally efficient
- Expand this architecture to allow for multiple spacecraft to dock and detach from one another

Chapter 2

Modularization of Spacecraft Equations

There are an infinite number of ways to describe the motion of a system with EOMs. The final form of the EOMs depend on the chosen assumptions, state variables, coordinate frames and methods used to arrive at the solutions. In Section 1.2.1 the simple example seen in 1.2, three different forms of the EOMs are shown depending on the state variables and the derivation method used. This shows that when deriving EOMs for spacecraft, which can be much more complicated, quickly there is a disagreement on the form of the EOMs for a single system. Additionally, when considering a new system with different dynamics, the form of the EOMs can look even further different.

This section's goal is to develop a standard form for spacecraft EOMs that is applicable to a wide range of spacecraft. Using this standard form, a back-substitution method is used to modularize the EOMs that removes the need to invert the full system mass matrix while retaining the full solution. Finally, the modularized energy and momentum calculations are introduced that provides an efficient way to verify the implementation of equations in software.

2.1 Spacecraft Specific Compact Equations of Motion Form

An important consideration when first developing the EOMs are the associated assumptions because they will ultimately dictate how applicable the mathematical structure is to different dynamical systems. Figure 2.1 shows an example spacecraft with flexing solar arrays and lumped mass fuel slosh and will be the reference when discussing the assumptions[38]. Since both of these

Now that the rigid-body hub is defined, the state variables that define the state of the hub at any given time are: the position of point B with respect to the origin of the inertial frame N , $\mathbf{r}_{B/N}$, the inertial velocity of point B with respect to point N , $\dot{\mathbf{r}}_{B/N}$, the Modified Rodrigues Parameters (MRPs) representation of the body frame \mathcal{B} with respect to the inertial frame \mathcal{N} , $\boldsymbol{\sigma}_{\mathcal{B}/\mathcal{N}}$ and the inertial angular velocity vector of the body frame \mathcal{B} with respect to the inertial frame \mathcal{N} , $\boldsymbol{\omega}_{\mathcal{B}/\mathcal{N}}$. The MRPs are the chosen attitude parameterization set because its a minimal set of 3 parameters with elegant non-singular implementations [39]. However, the dynamics are independent of the chosen attitude parameterization, therefore any attitude description can be used. These 4 variables represent the 6 degrees of freedom that the rigid-body hub exhibits and represents the 12 state variables that are needed to implement a second order differential equation in software. These, at a minimum, are the states required for the system. All of the additional degrees of freedom on the system will be referenced to the body frame, \mathcal{B} .

Now that the important parameters have been defined for the rigid-body hub, other degrees of freedom need to be introduced and generalized. Figure 2.1 shows an example with flexing solar panels and lumped mass fuel slosh as additional degrees of freedom as an example system. Each of these models are labeled as “effectors”. Each effector is assumed to have a mass, m_{eff} , a center mass location, E_c , and a position vector from point B to E_c , $\mathbf{r}_{E_c/B}$. If the effector has inertia properties, it also has a frame, $\mathcal{E} : \{\hat{e}_1, \hat{e}_2, \hat{e}_3\}$, and an inertia tensor, $[I_{\text{eff}, E_c}]$, that is defined about its center of mass, E_c .

With the hub parameters and the effector parameters defined, the general form proposed in this research for the hub’s EOMs is shown in Eqs. (2.1) and (2.2). This general form is formalized by using a systematic approach for multiple dynamics problem formulations including flexible solar arrays[41], lumped mass fuel slosh[38], imbalanced reaction wheels[42], fully-coupled mass depletion[43], and imbalanced variable speed control moment gyroscopes[44, 45]. The first

equation proposed for this general form is the translational motion equation:

$$m_{sc}\ddot{\mathbf{r}}_{B/N} - m_{sc}\mathbf{c} \times \dot{\boldsymbol{\omega}}_{B/N} + \sum_{i=1}^{N_{\text{eff}}} \sum_{j=1}^{N_{\text{DOF},i}} \mathbf{v}_{\text{Trans,LHS}_{ij}} \ddot{\alpha}_{ij} = \mathbf{F}_{\text{ext}} - 2m_{sc}\boldsymbol{\omega}_{B/N} \times \mathbf{c}' - m_{sc}\boldsymbol{\omega}_{B/N} \times (\boldsymbol{\omega}_{B/N} \times \mathbf{c}) + \sum_{i=1}^{N_{\text{eff}}} \mathbf{v}_{\text{Trans,RHS}_i} \quad (2.1)$$

The system parameters in Eq. (2.1) include the total mass of the spacecraft, m_{sc} , the vector from point B to the instantaneous center of mass of the entire spacecraft, \mathbf{c} , and the body frame relative time derivative with respect to the body frame of \mathbf{c} , \mathbf{c}' . N_{eff} is the number of effectors, $N_{\text{DOF},i}$ is the i^{th} effector's degrees of freedom, $\mathbf{v}_{\text{Trans,LHS}_{ij}}$ is a vector for the translational equation that corresponds with the j^{th} degree of freedom of the i^{th} effector's second order derivative of its state, α_{ij} , and $\mathbf{v}_{\text{Trans,RHS}_i}$ is the i^{th} effector's vector contribution to the forces on the right hand side of Eq. (2.1). This proposed equation of motion form is general and common for any effector attached to a spacecraft. Later in this dissertation specific formulations are illustrated for a select set of effectors.

The rotational EOMs form are proposed to be of the following form

$$m_{sc}\mathbf{c} \times \ddot{\mathbf{r}}_{B/N} + [I_{sc,B}]\dot{\boldsymbol{\omega}}_{B/N} + \sum_{i=1}^{N_{\text{eff}}} \sum_{j=1}^{N_{\text{DOF},i}} \mathbf{v}_{\text{Rot,LHS}_{ij}} \ddot{\alpha}_{ij} = \mathbf{L}_B - \boldsymbol{\omega}_{B/N} \times ([I_{sc,B}]\boldsymbol{\omega}_{B/N}) - [I'_{sc,B}]\boldsymbol{\omega}_{B/N} + \sum_{i=1}^{N_{\text{eff}}} \mathbf{v}_{\text{Rot,RHS}_i} \quad (2.2)$$

where $[I_{sc,B}]$ is the inertia tensor of the total spacecraft (hub and effectors) about point B , $[I'_{sc,B}]$ is the time derivative with respect to the body frame of $[I_{sc,B}]$, $\mathbf{v}_{\text{Rot,LHS}_{ij}}$ is a vector for the rotational equation that corresponds with the j^{th} degree of freedom of i^{th} effector's second order derivative of its state, α_{ij} , and $\mathbf{v}_{\text{Rot,RHS}_i}$ is the i^{th} effector's vector contribution to the torques on the right hand side of Eq. (2.2).

Finally, the individual effector degree of freedom EOMs are proposed to fit the following form:

$$a_{jj_i} \ddot{\alpha}_{ij} + \sum_{k=1; k \neq j}^{N_{\text{DOF},i}} a_{jk_i} \ddot{\alpha}_{ik} = \mathbf{a}_{\alpha_{ij}} \cdot \ddot{\mathbf{r}}_{B/N} + \mathbf{b}_{\alpha_{ij}} \cdot \dot{\boldsymbol{\omega}}_{B/N} + c_{\alpha_{ij}} \quad (2.3)$$

where each effector has $N_{\text{DOF},i}$ EOMs needed to fully describe the motion of that effector. If $N_{\text{DOF},i} = 1$ for an effector, Eq. (2.3) simplifies to:

$$\ddot{\alpha}_i = \mathbf{a}_{\alpha_i} \cdot \ddot{\mathbf{r}}_{B/N} + \mathbf{b}_{\alpha_i} \cdot \dot{\boldsymbol{\omega}}_{B/N} + c_{\alpha_i} \quad (2.4)$$

Eqs. (2.1)-(2.4) are the generalized EOMs that can apply to a wide-variety of spacecraft. Utilizing this common form yields consistent EOMs that enable the modular software architecture. While looking at Eqs. (2.3) and (2.4), it should be pointed out that the i^{th} effector EOM does not include the second order state variables from other effectors, only the individual effectors and their corresponding degrees of freedom. This is a key assumption that will allow for modularity between all of the effectors attached to the rigid-body hub.

2.2 Multi-Rigidly Connected Spacecraft Equations of Motion Form

A goal of this dissertation is to allow for multiple spacecraft to simulated at a time and allow for docking and detachment of spacecraft. A diagram depicting this multi-spacecraft architecture can be seen in Figure 2.2. In the diagram the primary spacecraft has the primary hub frame \mathcal{P} in which all of the dynamics will be computed with respect to. However, this only corresponds to the connected spacecraft. In Figure 2.2 the unconnected spacecraft will act just like the independent spacecraft introduced in the previous section. An assumption with this research is that when the spacecraft are attached, they are connected rigidly through their rigid-body hubs. This assumption allows for the dynamics to retain a standard form. In other words, the resulting spacecraft system has a larger rigid hub section but has the same form of the EOMs as presented in the previous section. However, from a software architecture perspective, the EOMs of the system need to be generalized. The translational equation is defined in Equation (2.5).

$$m_{\text{sys}} \ddot{\mathbf{r}}_{P/N} - m_{\text{sys}} [\tilde{\mathbf{c}}_P] \dot{\boldsymbol{\omega}}_{P/N} + \sum_{i=1}^{N_{\text{eff}}} \sum_{j=1}^{N_{\text{DOF},i}} \mathbf{v}_{\text{Trans,LHS}_{ij}} \ddot{\alpha}_{ij} = \mathbf{F}_{\text{ext}} - 2m_{\text{sc}} [\tilde{\boldsymbol{\omega}}_{P/N}] \mathbf{c}'_P - m_{\text{sc}} [\tilde{\boldsymbol{\omega}}_{P/N}] [\tilde{\boldsymbol{\omega}}_{P/N}] \mathbf{c}_P + \sum_{i=1}^{N_{\text{eff}}} \mathbf{v}_{\text{Trans,RHS}_i} \quad (2.5)$$

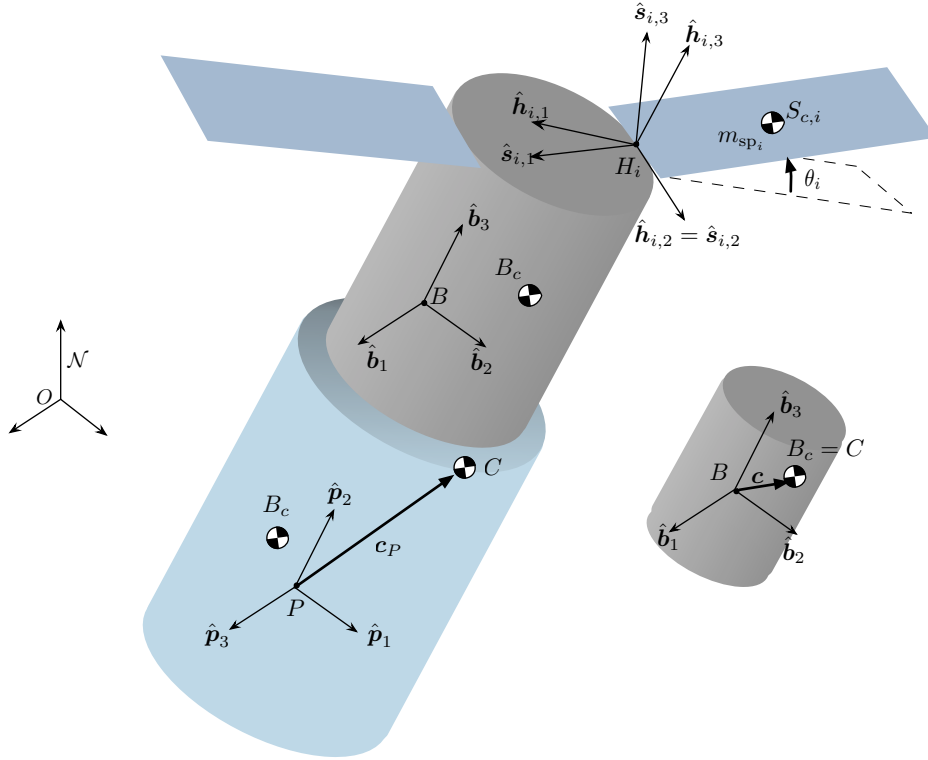


Figure 2.2: Multiple spacecraft diagram for multi-spacecraft dynamics

The total mass of the spacecraft system is labeled m_{sys} , the vector from point P to the center of mass of the spacecraft system is defined as \mathbf{c}_P , and the time derivative with respect to the body fixed frame \mathcal{P} of \mathbf{c}_P , is $\dot{\mathbf{c}}_P$.

Similarly, the proposed rotational EOMs form can be seen in Eq. (2.6). $[I_{\text{sys},P}]$ is the inertia of the spacecraft system about point P , and $[I'_{\text{sys},P}]$ is the time derivative with respect to the body frame of $[I_{\text{sys},P}]$.

$$m_{\text{sys}}[\tilde{\mathbf{c}}_P]\ddot{\mathbf{r}}_{P/N} + [I_{\text{sys},P}]\dot{\boldsymbol{\omega}}_{\mathcal{P}/N} + \sum_{i=1}^{N_{\text{eff}}} \sum_{j=1}^{N_{\text{DOF},i}} \mathbf{v}_{\text{Rot,LHS},ij} \ddot{\alpha}_{ij} = \mathbf{L}_P - [\tilde{\boldsymbol{\omega}}_{\mathcal{P}/N}][I_{\text{sys},P}]\boldsymbol{\omega}_{\mathcal{P}/N} - [I'_{\text{sys},P}]\boldsymbol{\omega}_{\mathcal{P}/N} + \sum_{i=1}^{N_{\text{eff}}} \mathbf{v}_{\text{Rot,RHS},i} \quad (2.6)$$

Finally, the individual effector degree of freedom EOMs are similar to the EOMs in the

previous section, but are now about the body frame origin of the system point P :

$$a_{jj_i} \ddot{\alpha}_{ij} + \sum_{k=1; k \neq j}^{N_{\text{DOF},i}} a_{jk_i} \ddot{\alpha}_{ik} = \mathbf{a}_{\alpha_{ij}} \cdot \ddot{\mathbf{r}}_{P/N} + \mathbf{b}_{\alpha_{ij}} \cdot \dot{\boldsymbol{\omega}}_{P/N} + c_{\alpha_{ij}} \quad (2.7)$$

$$\ddot{\alpha}_i = \mathbf{a}_{\alpha_i} \cdot \ddot{\mathbf{r}}_{P/N} + \mathbf{b}_{\alpha_i} \cdot \dot{\boldsymbol{\omega}}_{P/N} + c_{\alpha_i} \quad (2.8)$$

These equations will be used in software when the spacecraft are attached to each other. $\ddot{\mathbf{r}}_{P/N}$ and $\dot{\boldsymbol{\omega}}_{P/N}$ would only need to be found for one of the spacecraft, the primary spacecraft, with their states being integrated using those accelerations. Once the states $\mathbf{r}_{P/N}$, $\dot{\mathbf{r}}_{P/N}$, $\boldsymbol{\sigma}_{P/N}$, $\boldsymbol{\omega}_{P/N}$ of the primary spacecraft are found the states of the other attached spacecraft can be found by kinematic relationships. This results in the minimum amount of math required to solve the problem while retaining the full system dynamics.

2.3 Back-Substitution Method

A product of multi-body dynamics is the dynamic coupling between the second order state variables that results in a non-diagonal system mass matrix [8]. This can be troublesome in attempting to integrate the EOMs in software. When integrating EOMs the form that is beneficial is $\dot{\mathbf{X}} = \mathbf{f}(\mathbf{X}, t)$ where \mathbf{X} is the state vector, $\dot{\mathbf{X}}$ is the time derivative of \mathbf{X} , and $\mathbf{f}(\mathbf{X}, t)$ is a function of the current state and time, t . When there is a system mass matrix, $[M]$, present, the form changes to $[M]\dot{\mathbf{X}} = \mathbf{f}(\mathbf{X}, t)$. Therefore, a system mass matrix needs to be inverted to solve this complex problem. This results in two problems with inverting a system mass matrix. Firstly, inverting a matrix can be computational inefficient because the calculation scales with cube of the number of states. Secondly, the modularization of the dynamics from software implementation perspective is a difficult task because the system needs to know the location of each effector within the system mass matrix and locations relative to the other effectors. A back-substitution method is developed to solve this problem.

To visualize the impact of the EOMs generalized form, the spacecraft seen in Figure 2.3 is used as an example. The spacecraft has panels modeled as two interconnected rigid-bodies with a

single rotational degree of freedom each. Figure 2.3 only shows 2 sets of dual-connected solar panels, but the example is generalized to N_s number of sets. If the EOMs were put into the generalized form from the previous section, the dynamical coupling of this complex system would be visualized in the following schematic of the resulting coupled differential equations:

$$\begin{bmatrix}
 3 \times 3 & 3 \times 3 & 3 \times 1 & 3 \times 1 & 3 \times 1 & 3 \times 1 & \cdot & 3 \times 1 & 3 \times 1 \\
 3 \times 3 & 3 \times 3 & 3 \times 1 & 3 \times 1 & 3 \times 1 & 3 \times 1 & \cdot & 3 \times 1 & 3 \times 1 \\
 1 \times 3 & 1 \times 3 & 1 \times 1 & 1 \times 1 & 0 & 0 & \cdot & 0 & 0 \\
 1 \times 3 & 1 \times 3 & 1 \times 1 & 1 \times 1 & 0 & 0 & \cdot & 0 & 0 \\
 1 \times 3 & 1 \times 3 & 0 & 0 & 1 \times 1 & 1 \times 1 & \cdot & 0 & 0 \\
 1 \times 3 & 1 \times 3 & 0 & 0 & 1 \times 1 & 1 \times 1 & \cdot & 0 & 0 \\
 \cdot & \cdot & \cdot & \cdot & \cdot & \cdot & \cdot & \cdot & \cdot \\
 1 \times 3 & 1 \times 3 & 0 & 0 & 0 & 0 & \cdot & 1 \times 1 & 1 \times 1 \\
 1 \times 3 & 1 \times 3 & 0 & 0 & 0 & 0 & \cdot & 1 \times 1 & 1 \times 1
 \end{bmatrix}
 \begin{bmatrix}
 \ddot{\mathbf{r}}_{B/N} \\
 \dot{\boldsymbol{\omega}}_{B/N} \\
 \ddot{\theta}_{11} \\
 \ddot{\theta}_{12} \\
 \ddot{\theta}_{21} \\
 \ddot{\theta}_{22} \\
 \cdot \\
 \ddot{\theta}_{N_s1} \\
 \ddot{\theta}_{N_s2}
 \end{bmatrix}
 =
 \begin{bmatrix}
 3 \times 1 \\
 3 \times 1 \\
 1 \times 1 \\
 1 \times 1 \\
 1 \times 1 \\
 1 \times 1 \\
 \cdot \\
 1 \times 1 \\
 1 \times 1
 \end{bmatrix}
 \quad (2.9)$$

Eq. (2.9) shows the form of the second order state variable coupling that results from this configuration. It confirms that the individual degrees of freedom for the sets of solar panels are coupled with each other, but are not directly coupled through second order state derivatives with the other sets of panels. This is a key insight and is exploited in the following back-substitution method.

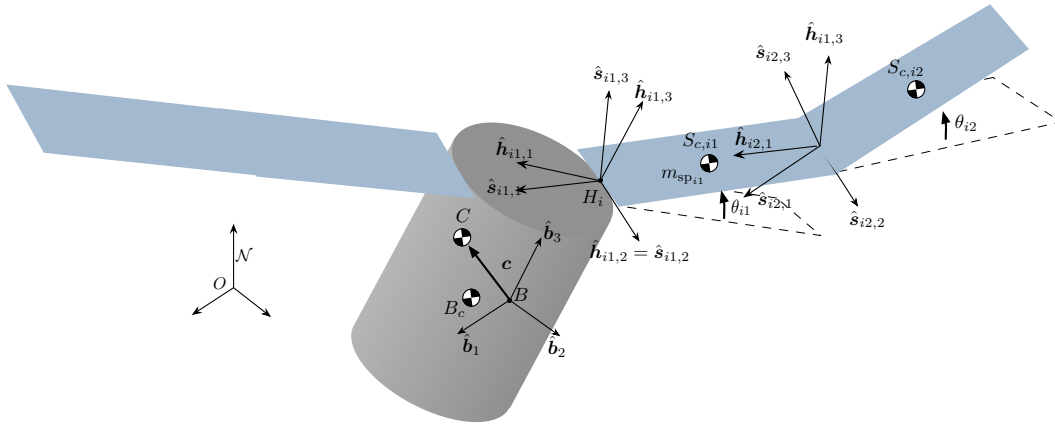


Figure 2.3: Dual-hinged rigid-bodies frame and variable definitions

Looking further into Eq. (2.9), all of the solar panel second order state derivatives are present in the hub translational and rotational equations. On the other hand, the hub translational and rotational second order state variables are present in the individual solar panel EOMs. This dynamic coupling through the hub is another key insight that the back-substitution method will use to modularize the EOMs.

This section of the dissertation expresses the vector equations shown in the past section as matrix equations. These equations do not specify a frame in which the matrix components are expressed with respect to but one must use a single frame when implementing these equations in software. A common frame to express the equations in would be the body frame, \mathcal{B} . Since these equations are matrix equations the following notation will be used: the cross product is expressed as $[\tilde{\mathbf{a}}]\mathbf{b}$, is expressed as $\mathbf{a}^T \mathbf{b}$ and the outer product is expressed as $\mathbf{a}\mathbf{b}^T$.

The back-substitution method is presented for effectors that have $N_{\text{DOF},i} = 1$ for this section but is extended to effectors with multiple degrees of freedom in Section 3.1.6. The first step in the back substitution method is to substitute Eq. (2.4) into both the translational and rotational EOMs for the rigid-body hub. First, the substitution into the translational motion for $N_{\text{DOF},i} = 1$ is shown in the following equation:

$$m_{\text{sc}}\ddot{\mathbf{r}}_{B/N} - m_{\text{sc}}[\tilde{\mathbf{c}}]\dot{\boldsymbol{\omega}}_{B/N} + \sum_{i=1}^{N_{\text{eff}}} \mathbf{v}_{\text{Trans,LHS}_i} \left[\mathbf{a}_{\alpha_i}^T \ddot{\mathbf{r}}_{B/N} + \mathbf{b}_{\alpha_i}^T \dot{\boldsymbol{\omega}}_{B/N} + c_{\alpha_i} \right] = \mathbf{F}_{\text{ext}} \\ - 2m_{\text{sc}}[\tilde{\boldsymbol{\omega}}_{B/N}]\mathbf{c}' - m_{\text{sc}}[\tilde{\boldsymbol{\omega}}_{B/N}][\tilde{\boldsymbol{\omega}}_{B/N}]\mathbf{c} + \sum_{i=1}^{N_{\text{eff}}} \mathbf{v}_{\text{Trans,RHS}_i} \quad (2.10)$$

Simplifying and combining like terms yields the translational EOM that has been decoupled from the other effector accelerations:

$$\left[m_{\text{sc}}[I_{3 \times 3}] + \sum_{i=1}^{N_{\text{eff}}} \mathbf{v}_{\text{Trans,LHS}_i} \mathbf{a}_{\alpha_i}^T \right] \ddot{\mathbf{r}}_{B/N} + \left[-m_{\text{sc}}[\tilde{\mathbf{c}}] + \sum_{i=1}^{N_{\text{eff}}} \mathbf{v}_{\text{Trans,LHS}_i} \mathbf{b}_{\alpha_i}^T \right] \dot{\boldsymbol{\omega}}_{B/N} = \mathbf{F}_{\text{ext}} \\ - 2m_{\text{sc}}[\tilde{\boldsymbol{\omega}}_{B/N}]\mathbf{c}' - m_{\text{sc}}[\tilde{\boldsymbol{\omega}}_{B/N}][\tilde{\boldsymbol{\omega}}_{B/N}]\mathbf{c} + \sum_{i=1}^{N_{\text{eff}}} \left[\mathbf{v}_{\text{Trans,RHS}_i} - \mathbf{v}_{\text{Trans,LHS}_i} c_{\alpha_i} \right] \quad (2.11)$$

Following the same pattern for the rotational hub EOM, Eq. (2.2), yields:

$$\begin{aligned} \left[m_{sc}[\tilde{\mathbf{c}}] + \sum_{i=1}^{N_{\text{eff}}} \mathbf{v}_{\text{Rot,LHS}_i} \mathbf{a}_{\alpha_i}^T \right] \ddot{\mathbf{r}}_{B/N} + \left[[I_{sc,B}] + \sum_{i=1}^{N_{\text{eff}}} \mathbf{v}_{\text{Rot,LHS}_i} \mathbf{b}_{\alpha_i}^T \right] \dot{\boldsymbol{\omega}}_{B/N} = \mathbf{L}_B \\ - [\tilde{\boldsymbol{\omega}}_{B/N}] [I_{sc,B}] \boldsymbol{\omega}_{B/N} - [I'_{sc,B}] \boldsymbol{\omega}_{B/N} + \sum_{i=1}^{N_{\text{eff}}} \left[\mathbf{v}_{\text{Rot,RHS}_i} - \mathbf{v}_{\text{Rot,LHS}_i} c_{\alpha_i} \right] \end{aligned} \quad (2.12)$$

The following matrices are defined to yield a more compact notation:

$$[A] = m_{sc} [I_{3 \times 3}] + \sum_{i=1}^{N_{\text{eff}}} \mathbf{v}_{\text{Trans,LHS}_i} \mathbf{a}_{\alpha_i}^T \quad (2.13)$$

$$[B] = -m_{sc} [\tilde{\mathbf{c}}] + \sum_{i=1}^{N_{\text{eff}}} \mathbf{v}_{\text{Trans,LHS}_i} \mathbf{b}_{\alpha_i}^T \quad (2.14)$$

$$[C] = m_{sc} [\tilde{\mathbf{c}}] + \sum_{i=1}^{N_{\text{eff}}} \mathbf{v}_{\text{Rot,LHS}_i} \mathbf{a}_{\alpha_i}^T \quad (2.15)$$

$$[D] = [I_{sc,B}] + \sum_{i=1}^{N_{\text{eff}}} \mathbf{v}_{\text{Rot,LHS}_i} \mathbf{b}_{\alpha_i}^T \quad (2.16)$$

$$\mathbf{v}_{\text{Trans}} = \mathbf{F}_{\text{ext}} - 2m_{sc} [\tilde{\boldsymbol{\omega}}_{B/N}] \mathbf{c}' - m_{sc} [\tilde{\boldsymbol{\omega}}_{B/N}] [\tilde{\boldsymbol{\omega}}_{B/N}] \mathbf{c} + \sum_{i=1}^{N_{\text{eff}}} \left[\mathbf{v}_{\text{Trans,RHS}_i} - \mathbf{v}_{\text{Trans,LHS}_i} c_{\alpha_i} \right] \quad (2.17)$$

$$\mathbf{v}_{\text{Rot}} = \mathbf{L}_B - [\tilde{\boldsymbol{\omega}}_{B/N}] [I_{sc,B}] \boldsymbol{\omega}_{B/N} - [I'_{sc,B}] \boldsymbol{\omega}_{B/N} + \sum_{i=1}^{N_{\text{eff}}} \left[\mathbf{v}_{\text{Rot,RHS}_i} - \mathbf{v}_{\text{Rot,LHS}_i} c_{\alpha_i} \right] \quad (2.18)$$

Using these definitions, the coupled translation and rotation hub EOMs are written compactly as

$$\begin{bmatrix} [A] & [B] \\ [C] & [D] \end{bmatrix} \begin{bmatrix} \ddot{\mathbf{r}}_{B/N} \\ \dot{\boldsymbol{\omega}}_{B/N} \end{bmatrix} = \begin{bmatrix} \mathbf{v}_{\text{Trans}} \\ \mathbf{v}_{\text{Rot}} \end{bmatrix} \quad (2.19)$$

Equation (2.19) represents a system of 6 equations, that can be solved using the Schur complement matrix formulation[46] for the partitioned form of the hub system mass matrix:

$$\dot{\boldsymbol{\omega}}_{B/N} = \left([D] - [C][A]^{-1}[B] \right)^{-1} (\mathbf{v}_{\text{Rot}} - [C][A]^{-1} \mathbf{v}_{\text{Trans}}) \quad (2.20)$$

$$\ddot{\mathbf{r}}_{B/N} = [A]^{-1}(\mathbf{v}_{\text{Trans}} - [B]\dot{\boldsymbol{\omega}}_{B/N}) \quad (2.21)$$

This shows that the back-substitution method only requires two 3×3 matrix inverses. The additional degree of freedom second order state derivatives are found by back-substituting these solutions into Eqs. (2.3) and (2.4).

This back-substitution method, by leveraging the pattern of the system mass matrix, has provided a way to avoid inverting the full system mass matrix, and perform the minimum amount of math required to solve the fully-coupled problem. Energy and momentum tools are still available because no compromising assumptions were made. The second order state variables are no longer coupled in the system mass matrix which will allow for a modular software architecture. This allows the software to not need to manage the interrelations between different effectors in the system mass matrix. This will be further explained in Section 4.

2.4 Back-Substitution Method Computational Performance

The resulting formulation for the back-substitution method removes the necessity of inverting the system mass matrix and only requires two 3×3 matrix inversions using the Schur matrix formulation seen in Eqs. (2.20) and (2.21). This form of the solution is the same no matter what system is being considered as long as the system adheres generalized EOM form introduced in this dissertation. This results in a fixed size matrix implementation in software. In contrast, in solutions having to populate a full system mass matrix the mass matrix can change in size which will result in dynamically sized matrices and can impact computational performance.

To analyze these effects with respect to computational performance, a simulation was created to attach a varying number of fuel slosh particles and flexing appended bodies [38] to see how the performance scales with respect to the number of degrees of freedom. Both the back-substitution method introduced in this paper for this system and the full system matrix solution is considered in this analysis. The specific spacecraft parameters for the hub, fuel slosh and flexing appended bodies

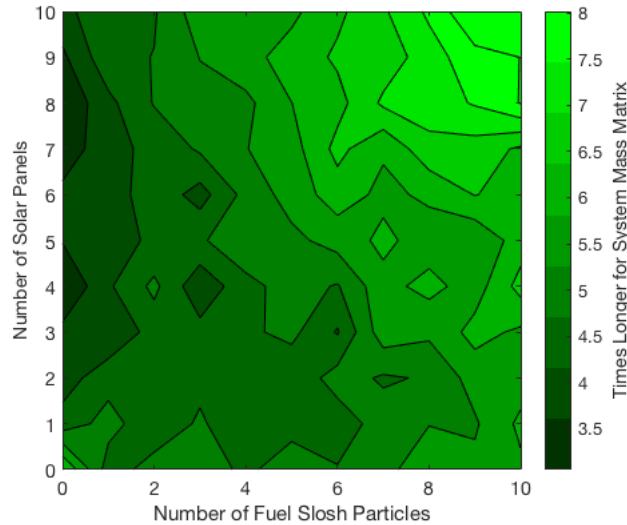


Figure 2.4: Computational efficiency of back-substitution method

are not included here because the computational performance is independent to those parameters. The associated mathematical operations are the critical component, not the numerical values being computed.

A computationally efficient C++ library named Eigen [47] is used for all of the matrix algebra. Eigen has different methods included on how to solve a system of equations and one of these methods is called QR decomposition. This method does not require the solution of the system mass matrix inverse, but rather solves directly for the solution to the system which will increase the speed of calculations. The method also leverages the pattern of the matrix being solved [47] and therefore is more applicable to diagonally dominant matrices which is common in dynamics formulations [34]. Because the back-substitution method is solving the full solution, the QR decomposition method was chosen because other methods can affect the accuracy of the solution.

The computational performance results are illustrated in Figure 2.4. The quantity used to define the performance is the times longer for the system mass matrix solution. Therefore, the higher the number the more efficient the back-substitution method is. Also, it should be noted that the figure uses an interpolation function to try and smooth the curves between the different data points. The data points are discrete integer values with respect the number of fuel slosh particles

and solar panels and so the discontinuities are expected. The results shows that at a minimum the back-substitution method is 3 times as fast and the speed improvements positively scale with the number of attached fuel slosh particles and flexing appended bodies. When there are 10 fuel slosh particles and 10 appended flexing bodies, the system mass matrix solution takes 8 times longer to compute the solution. The back-substitution method is always more efficient because a dynamically allocated size matrix is not required for this solution. The reason that the number of solar panels does not scale as quickly as fuel slosh particles is because of the complexity of the EOMs. There are more calculations required when implementing the flexing equations than the fuel slosh equations, therefore the speed up is not as high as the fuel slosh. These results quantify the expected computational performance of the the back-substitution method and furthers the applicability of the back-substitution method for complex spacecraft simulations.

2.5 Modularization of Energy and Momentum Calculations

A key part of EOM development is expressing the total energy and momentum of the spacecraft for verification purposes. This section describes the proposed method for how the energy and momentum is calculated and modularized for each effector to add their contributions to the overall total energy. It is advantageous to define energy and momentum of the center of mass of the spacecraft (orbital) and about its center of mass (rotational). This is because the orbital and rotational energies typically have different orders of magnitude and so separating these terms will avoid numerical issues in the verification process, and both quantities should be conserved in applicable scenarios.

First, the orbital energy is analytically expressed to be in terms of the state variables. The total orbital kinetic energy (i.e. kinetic energy of the center of mass) of the spacecraft is

$$T_{\text{orb}} = \frac{1}{2} m_{sc} \dot{\mathbf{r}}_{C/N} \cdot \dot{\mathbf{r}}_{C/N} \quad (2.22)$$

Expanding $\dot{\mathbf{r}}_{C/N}$ to be in terms of $\dot{\mathbf{r}}_{B/N}$ and $\dot{\mathbf{c}}$ results in

$$T_{\text{orb}} = \frac{1}{2} m_{sc} (\dot{\mathbf{r}}_{B/N} + \dot{\mathbf{c}}) \cdot (\dot{\mathbf{r}}_{B/N} + \dot{\mathbf{c}}) \quad (2.23)$$

This simplifies to the final desired equation

$$T_{\text{orb}} = \frac{1}{2}m_{sc}(\dot{\mathbf{r}}_{B/N} \cdot \dot{\mathbf{r}}_{B/N} + 2\dot{\mathbf{r}}_{B/N} \cdot \dot{\mathbf{c}} + \dot{\mathbf{c}} \cdot \dot{\mathbf{c}}) \quad (2.24)$$

Each effector contributes to \mathbf{c} and $\dot{\mathbf{c}}$, but does not have direct individual contributions. Additionally, in this form each effector does not need to know about the center of mass location of the spacecraft which is advantageous from a modularity perspective.

The total orbital potential energy depends on what type of gravity model is being used or if other conservative external forces are acting on the spacecraft. For simplicity, the orbital potential energy due to point gravity is included here but spherical harmonics and other higher order effects could be included.

$$V_{\text{orb}} = -\frac{\mu}{|\mathbf{r}_{C/N}|} \quad (2.25)$$

It is convenient to combine the kinetic and potential energies into one term, E_{orb} , because the total orbital energy of the spacecraft must be conserved when there are no non-conservative external forces and torques acting on the spacecraft. This is shown in the following equation.

$$E_{\text{orb}} = T_{\text{orb}} + V_{\text{orb}} \quad (2.26)$$

Next, there is the expression of the rotational energy. The total rotational and deformational kinetic energy (i.e. kinetic energy about the center of mass) of the spacecraft is

$$T_{\text{rot}} = \frac{1}{2}\boldsymbol{\omega}_{B/N} \cdot [I_{\text{hub},B_c}]\boldsymbol{\omega}_{B/N} + \frac{1}{2}m_{\text{hub}}\dot{\mathbf{r}}_{B_c/C} \cdot \dot{\mathbf{r}}_{B_c/C} + \sum_{i=1}^{N_{\text{eff}}} \left(\frac{1}{2}\boldsymbol{\omega}_{\mathcal{E}_i/N} \cdot [I_{\text{eff},E_{c,i}}]\boldsymbol{\omega}_{\mathcal{E}_i/N} + \frac{1}{2}m_{\text{eff}}\dot{\mathbf{r}}_{E_{c,i}/C} \cdot \dot{\mathbf{r}}_{E_{c,i}/C} \right) \quad (2.27)$$

Expanding and combining like terms results in

$$T_{\text{rot}} = \frac{1}{2}\boldsymbol{\omega}_{B/N} \cdot [I_{\text{hub},B_c}]\boldsymbol{\omega}_{B/N} + \frac{1}{2}m_{\text{hub}}\dot{\mathbf{r}}_{B_c/B} \cdot \dot{\mathbf{r}}_{B_c/B} + \sum_{i=1}^{N_{\text{eff}}} \left[\frac{1}{2}\boldsymbol{\omega}_{\mathcal{E}_i/N} \cdot [I_{\text{eff},E_{c,i}}]\boldsymbol{\omega}_{\mathcal{E}_i/N} + \frac{1}{2}m_{\text{eff}}\dot{\mathbf{r}}_{E_{c,i}/B} \cdot \dot{\mathbf{r}}_{E_{c,i}/B} \right] - \left[m_{\text{hub}}\dot{\mathbf{r}}_{B_c/B} + \sum_{i=1}^{N_{\text{eff}}} m_{\text{eff}}\dot{\mathbf{r}}_{E_{c,i}/B} \right] \cdot \dot{\mathbf{c}} + \frac{1}{2} \left[m_{\text{hub}} + \sum_{i=1}^{N_{\text{eff}}} m_{\text{eff}} \right] \dot{\mathbf{c}} \cdot \dot{\mathbf{c}} \quad (2.28)$$

Performing a final simplification yields the desired result where each effector adds its contributions to the rotational energy

$$T_{\text{rot}} = \frac{1}{2} \boldsymbol{\omega}_{B/N} \cdot [I_{\text{hub}, B_c}] \boldsymbol{\omega}_{B/N} + \frac{1}{2} m_{\text{hub}} \dot{\mathbf{r}}_{B_c/B} \cdot \dot{\mathbf{r}}_{B_c/B} + \sum_{i=1}^{N_{\text{eff}}} \left[\frac{1}{2} \boldsymbol{\omega}_{\mathcal{E}_i/N} \cdot [I_{\text{eff}, E_{c,i}}] \boldsymbol{\omega}_{\mathcal{E}_i/N} + \frac{1}{2} m_{\text{eff}} \dot{\mathbf{r}}_{E_{c,i}/B} \cdot \dot{\mathbf{r}}_{E_{c,i}/B} \right] - \frac{1}{2} m_{sc} \dot{\mathbf{c}} \cdot \dot{\mathbf{c}} \quad (2.29)$$

This form is advantageous because each effector does not need to know the location of the center of mass of the spacecraft but rather they define their contributions with respect to point B . From software architecture stand point, this form will prove to be desirable.

The total rotational potential energy is specific to each effector. For example, the spring joint potential energy for a hinged rigid-body is shown in the following equation.

$$V_{\text{rot}} = \frac{1}{2} k_{\theta} \theta^2 \quad (2.30)$$

Each effector might not have a potential energy contribution, however each effector will have the ability to add their contribution to the total potential energy. Since the total rotational energy of the system is conserved when there are no non-conservative internal or external forces or torques acting on the system, it is convenient to combine the kinetic and potential energies into one term, E_{rot} . This is shown in the following equation.

$$E_{\text{rot}} = T_{\text{rot}} + V_{\text{rot}} \quad (2.31)$$

The total orbital angular momentum of the spacecraft about point N is

$$\mathbf{H}_{\text{orb}, N} = m_{sc} \mathbf{r}_{C/N} \times \dot{\mathbf{r}}_{C/N} \quad (2.32)$$

Expanding in terms of the state variables yields

$$\mathbf{H}_{\text{orb}, N} = m_{sc} (\mathbf{r}_{B/N} + \mathbf{c}) \times (\dot{\mathbf{r}}_{B/N} + \dot{\mathbf{c}}) \quad (2.33)$$

The final form of this equation which does not have direct contribution from effectors outside of their contributions to \mathbf{c} and $\dot{\mathbf{c}}$ is

$$\mathbf{H}_{\text{orb}, N} = m_{sc} \left[\mathbf{r}_{B/N} \times \dot{\mathbf{r}}_{B/N} + \mathbf{r}_{B/N} \times \dot{\mathbf{c}} + \mathbf{c} \times \dot{\mathbf{r}}_{B/N} + \mathbf{c} \times \dot{\mathbf{c}} \right] \quad (2.34)$$

The total rotational angular momentum of the spacecraft about point C is

$$\mathbf{H}_{\text{rot},C} = [I_{\text{hub},B_c}] \boldsymbol{\omega}_{B/\mathcal{N}} + m_{\text{hub}} \mathbf{r}_{B_c/C} \times \dot{\mathbf{r}}_{B_c/C} + \sum_{i=1}^{N_{\text{eff}}} \left[[I_{\text{eff},E_{c,i}}] \boldsymbol{\omega}_{\mathcal{E}_i/\mathcal{N}} + m_{\text{eff}} \mathbf{r}_{E_{c,i}/C} \times \dot{\mathbf{r}}_{E_{c,i}/C} \right] \quad (2.35)$$

Expanding these terms yields

$$\begin{aligned} \mathbf{H}_{\text{rot},C} = & [I_{\text{hub},B_c}] \boldsymbol{\omega}_{B/\mathcal{N}} + m_{\text{hub}} (\mathbf{r}_{B_c/B} - \mathbf{c}) \times (\dot{\mathbf{r}}_{B_c/B} - \dot{\mathbf{c}}) \\ & + \sum_{i=1}^{N_{\text{eff}}} \left[[I_{\text{eff},E_{c,i}}] \boldsymbol{\omega}_{\mathcal{E}_i/\mathcal{N}} + m_{\text{eff}} (\mathbf{r}_{E_{c,i}/B} - \mathbf{c}) \times (\dot{\mathbf{r}}_{E_{c,i}/B} - \dot{\mathbf{c}}) \right] \end{aligned} \quad (2.36)$$

Distributing this result and simplifying yields the final equation

$$\begin{aligned} \mathbf{H}_{\text{rot},C} = & [I_{\text{hub},B_c}] \boldsymbol{\omega}_{B/\mathcal{N}} + m_{\text{hub}} \mathbf{r}_{B_c/B} \times \dot{\mathbf{r}}_{B_c/B} \\ & + \sum_{i=1}^{N_{\text{eff}}} \left[[I_{\text{eff},E_{c,i}}] \boldsymbol{\omega}_{\mathcal{E}_i/\mathcal{N}} + m_{\text{eff}} \mathbf{r}_{E_{c,i}/B} \times \dot{\mathbf{r}}_{E_{c,i}/B} \right] - m_{sc} \mathbf{c} \times \dot{\mathbf{c}} \end{aligned} \quad (2.37)$$

Again, this form is desirable because the effectors define their contributions with respect to the body fixed point B as opposed to the commonly used center of mass location point C which is varying and depends on the other effectors. This will be leveraged in the modular form of the software architecture.

The results seen in Eqs. (2.26), (2.31), (2.34), and (2.37) are the modularized equations for energy and momentum where effectors provide contributions to orbital terms through \mathbf{c} and $\dot{\mathbf{c}}$ and to rotational terms through direct contributions. This form is vital to retain the modularity of the system, and also validate the software implementation of the dynamics.

Chapter 3

Spacecraft Equations of Motion Solutions

Since EOMs come in many different forms, the literature involving dynamics solutions for spacecraft varies widely on the form of the solutions. This section aims to develop EOMs for common phenomenon affecting spacecraft. This will remove the need to re-derive EOMs for the provided problems and are tested, ready to implement solutions. The solutions all conform the generalized EOM form introduced in Section 2, and provide examples on using the systematic approach to arrive at the generalized EOM form and can be readily implemented in the modular software architecture presented in Section 4.

This dissertation develops EOMs for spacecraft with a variety of effectors attached to it, and extend this to multi-rigidly connected spacecraft where each spacecraft can have general number of effectors attached to them and spacecraft can detach and dock to one another. These solutions are developed in a frame independent and compact vector notation, which is beneficial for both analytical development and when implementing in software. Additionally, the EOMs are derived in a fully-coupled manner meaning that the dynamics retains the ability to check for energy and momentum conservation when applicable. Having energy and momentum checks is a crucial tool when developing the equations for simulations.

When developing EOMs of multi-body systems, an important consideration is determining what analytical method to use to arrive at the EOMs. Lagrangian mechanics [1, 2, 48, 49, 50], Newtonian and Eulerian Mechanics [39, 40], and Kane's Method [8, 51] are the three most common methods for spacecraft. Each have their advantages and disadvantages [2], and in some situations

a certain method can be more beneficial than the others. For example, the Lagrangian mechanics approach is a desirable method based on the simple form of the method, however special identities and algebraic manipulation are required to convert from generalized coordinates and generalized coordinate rates to the desired angular velocity vector form [49, 50]. The EOMs developed in this section can be found by using both Newtonian/Eulerian mechanics and Kane's Method and both methods are included to show agreement.

3.1 Development of Spacecraft Equations of Motion

For single spacecraft it is proposed to develop general models for flexing solar arrays or appended bodies, spring mass damper based fuel slosh, pendulum based fuel slosh, thruster based mass depletion, imbalanced reaction wheels, and imbalanced variable speed control moment gyroscopes. These are common physical phenomenon affecting many spacecraft and the derivations to arrive at these solutions can be time consuming and error prone.

3.1.1 Hinged Rigid-Bodies

3.1.1.1 Introduction

Spacecraft designs include a range of shapes and sizes, as well as deployable structural components such as large solar panels or antennas. Typically these components are connected to the spacecraft as cantilevered elements, therefore they are susceptible to flexing behavior. In many situations, this behavior needs to be included in the dynamics. Consider the scenario of performing an orbit insertion about a planet where the attitude is controlled with the primary thrusters off-pulsing and the attitude thrusters control the rotation about the primary thrust axis. In this common scenario the on-off behavior of the thrusters provides sharp impulses to the spacecraft system which can excite flexing. The spacecraft is typically assumed to be a rigid-body in initial modeling, but this assumption degrades the fidelity of the simulation if there are components that flex. Flexing impacts both the translational and rotational motion (and associated stability

margins) of the spacecraft, as well as sensor modeling such as accelerometers and rate gyros. For simulation and analysis purposes flexing is very important because it can impact performance, requirements and success of the mission.

There are many different ways to model flexible dynamics [12]. One method is to assume that the primary impact will be on the attitude dynamics of the spacecraft so the translational motion coupling is ignored [40]. Also, in some scenarios the effects of flexing can be assumed to only impact one plane of motion [40, 48, 1]. These methods are helpful in the early stages of a mission, but lack fidelity and are limited in application in that they do not allow general three-dimensional closed loop dynamics to be considered. In the orbit insertion problem it is critical to model scenarios where vehicle is tumbling after a fault and needs to recover aggressively to apply the needed burn during in the insertion time window. Here the spacecraft would be performing a general three-dimensional rotation, and the general cross-coupling terms between the flexing and rigid hub must be considered.

The field of multi-body dynamics has extensive research on modeling flexible dynamics and the equations of motion presented are generalized for complex and diverse problems [11, 12]. This results in re-derivation of equations because of generality [13, 14, 15, 16, 17, 18, 19]. These methods are required for unique and complex systems because the equations of motion depend on how many joints are interconnected. For example, in robotic systems, the number of interconnected joints varies widely, and the equations of motion are specific to that system [52, 53]. Since there are many spacecraft that have similar designs with appended rigid-bodies, there is a need to develop equations of motion that could be readily applied to these spacecraft. However, as is illustrated in this dissertation, deriving complete equations of motion for a general spacecraft configuration is a challenging and time consuming task.

Related to the work in this dissertation, multiple publications present models of spacecraft dynamics with appended solar panels [4, 5, 6]. However, this previous research is mainly focused on the deployment of solar panels and how the deployment affects the dynamics of the spacecraft [4, 5, 6]. Also, the previous research on deployable solar panels are specific to solar panels that are

composed of interconnected bodies. This dissertation considers systems where the solar panels are single rigid-bodies.

There is a need for a general solution to model flexing behavior of spacecraft that can be readily implemented into software and be computationally efficient. This dissertation introduces a solution for modeling the flexible dynamics of the solar panels by assuming that the hub of the spacecraft and the solar panels are rigid-bodies, but the solar panels are connected to the hub by single degree-of-freedom torsional springs. This is a first-order approximation to the actual structural deflection phenomenon, but from a simulation and analysis purposes this approximation is beneficial to computational speed and control system performance analysis. The torsional spring constants can be attenuated to match the natural first-order frequencies of the solar panels found from Finite Element Analysis or testing.

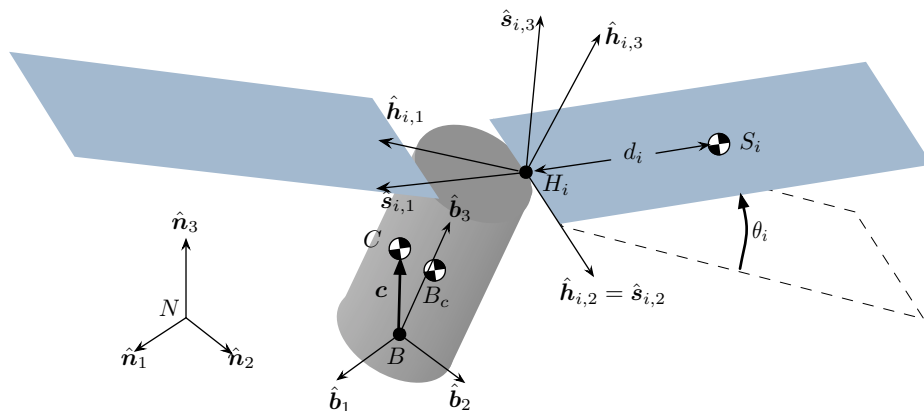


Figure 3.1: Components, variables and coordinate frames used for this derivation.

3.1.1.2 Problem Statement

A goal of this dissertation is to develop differential equations of motion describing a general spacecraft configuration with flexible appendage dynamics that can be readily integrated into a computer simulation. This avoids the need of deriving equations of motion for future spacecraft mission concepts. This formulation is developed in a general manner that applies to a wide range of spacecraft configurations and panel locations. The description of the spacecraft, components,

coordinate frames and variables are introduced in Figure 3.1.

The particular spacecraft in Figure 3.1 is composed of a rigid-body hub connected to two solar panels by one degree-of-freedom joints. These joints are modeled as torsional hinges with a linear spring constant of k_i , and an angular rate damping term, c_i . Two panels are shown for simplicity, however, the following formulation assumes there are N_s number of solar panels, each with a general location and hinge axis.

There are four coordinate frames defined for this formulation. The inertial reference frame is indicated by $\mathcal{N} : \{\hat{\mathbf{n}}_1, \hat{\mathbf{n}}_2, \hat{\mathbf{n}}_3\}$ and is the reference frame that the dynamics are developed with respect to. The body fixed coordinate frame, $\mathcal{B} : \{\hat{\mathbf{b}}_1, \hat{\mathbf{b}}_2, \hat{\mathbf{b}}_3\}$, is defined with its origin, B , which can be located anywhere fixed to the hub and the \mathcal{B} frame can be oriented in any configuration. The i^{th} solar panel frame, $\mathcal{S}_i : \{\hat{\mathbf{s}}_{i,1}, \hat{\mathbf{s}}_{i,2}, \hat{\mathbf{s}}_{i,3}\}$, has its basis vectors oriented in the same direction as the principle axes of the solar panel and its origin is coincident with the i^{th} hinge joint, H_i . The \mathcal{S}_i frame is oriented such that $\hat{\mathbf{s}}_{i,1}$ points anti-parallel to the center of mass of the solar panel, S_i , and the variable d_i defines the distance between points H_i and S_i . The $\hat{\mathbf{s}}_{i,2}$ axis is defined as the rotation axis that would yield a positive θ_i using the right-hand rule. The i^{th} hinge frame, $\mathcal{H}_i : \{\hat{\mathbf{h}}_{i,1}, \hat{\mathbf{h}}_{i,2}, \hat{\mathbf{h}}_{i,3}\}$, is a frame fixed with respect to the body frame, and is equivalent to the respective \mathcal{S}_i frame when the solar panel is undeflected. As it can be seen in Figure 3.1, $\hat{\mathbf{s}}_{i,2} = \hat{\mathbf{h}}_{i,2}$, therefore θ_i defines a single axis rotation of the \mathcal{S}_i with respect to the \mathcal{H}_i frame.

The location C is the center of mass location of the entire spacecraft, and B_c is the body-fixed center of mass location of the the rigid-body hub. The vector \mathbf{c} points from the origin of the body frame to the center of mass of the spacecraft. It is important to acknowledge that points B , B_c and C are not necessarily coincident and this assumption can be very useful when defining the spacecraft parameters. Simulation teams typically work very closely with structural engineering teams to define the spacecraft mass properties and the general point B assumption gives much more flexibility in this technical interchange.

3.1.1.3 Derivation of Equations of Motion

Next the equations of motion (EOMs) are derived using Newtonian and Eulerian mechanics. This approach allows for a general set of rigid hub attitude coordinates to be used while still describing the hub rotation rate through the convenient body angular velocity vector. EOMs are required for the translational, rotational, and solar panel motion.

3.1.1.4 Spacecraft Translational Equations of Motion

The derivation of the hub translational equations of motion begins with Newton's second law for the center of mass of the spacecraft

$$\ddot{\mathbf{r}}_{C/N} = \frac{\mathbf{F}_{\text{ext}}}{m_{\text{sc}}} \quad (3.1)$$

where $\mathbf{r}_{C/N}$ defines the vector pointing from point N to point C , \mathbf{F}_{ext} is the sum of the external forces acting on the spacecraft and m_{sc} is the total mass of the spacecraft. Finding the hub EOM requires describing the acceleration of the origin of the body frame, point B

$$\ddot{\mathbf{r}}_{B/N} = \ddot{\mathbf{r}}_{C/N} - \ddot{\mathbf{c}} \quad (3.2)$$

where the center of mass vector, \mathbf{c} is

$$\mathbf{c} = \frac{m_{\text{hub}}\mathbf{r}_{B_c/B} + \sum_{i=1}^{N_s} m_{\text{sp}_i}\mathbf{r}_{S_i/B}}{m_{\text{sc}}} \quad (3.3)$$

with the total mass of the spacecraft defined as

$$m_{\text{sc}} = m_{\text{hub}} + \sum_{i=1}^{N_s} m_{\text{sp}_i} \quad (3.4)$$

To find the inertial time derivative of \mathbf{c} , it is first convenient to find the time derivative of \mathbf{c} with respect to the body frame. A time derivative of a vector \mathbf{v} with respect to the body frame \mathcal{B} is denoted by \mathbf{v}' ; the inertial time derivative is labeled as $\dot{\mathbf{v}}$. The first and second body-relative time derivatives of \mathbf{c} are shown in Eqs. (3.5) and (3.6).

$$\mathbf{c}' = \frac{\sum_{i=1}^{N_s} m_{\text{sp}_i}\mathbf{r}'_{S_i/H_i}}{m_{\text{sc}}} \quad (3.5)$$

$$\mathbf{c}'' = \frac{\sum_{i=1}^{N_s} m_{\text{sp}_i} \mathbf{r}''_{S_i/H_i}}{m_{\text{sc}}} \quad (3.6)$$

The variable \mathbf{r}_{S_i/H_i} is easily defined using the $\hat{\mathbf{s}}_{i,1}$ axis

$$\mathbf{r}_{S_i/H_i} = -d_i \hat{\mathbf{s}}_{i,1} \quad (3.7)$$

To populate Eqs. (3.5) and (3.6), the first and second time derivatives with respect to the body frame of \mathbf{r}_{S_i/H_i} are taken

$$\mathbf{r}'_{S_i/H_i} = d_i \dot{\theta}_i \hat{\mathbf{s}}_{i,3} \quad (3.8)$$

$$\mathbf{r}''_{S_i/H_i} = d_i \left(\ddot{\theta}_i \hat{\mathbf{s}}_{i,3} + \dot{\theta}_i^2 \hat{\mathbf{s}}_{i,1} \right) \quad (3.9)$$

Substituting these results into Eqs. (3.5) and (3.6) yields

$$\mathbf{c}' = \frac{\sum_{i=1}^{N_s} m_{\text{sp}_i} d_i \dot{\theta}_i \hat{\mathbf{s}}_{i,3}}{m_{\text{sc}}} \quad (3.10)$$

$$\mathbf{c}'' = \frac{\sum_{i=1}^{N_s} m_{\text{sp}_i} d_i \left(\ddot{\theta}_i \hat{\mathbf{s}}_{i,3} + \dot{\theta}_i^2 \hat{\mathbf{s}}_{i,1} \right)}{m_{\text{sc}}} \quad (3.11)$$

The transport theorem [39] maps the time derivative of a vector \mathbf{v} as seen by one frame \mathcal{B} into the time derivative as seen by another frame \mathcal{N} through

$$\frac{\mathcal{N}d\mathbf{v}}{dt} = \dot{\mathbf{v}} = \frac{\mathcal{B}d\mathbf{v}}{dt} + \boldsymbol{\omega}_{\mathcal{B}/\mathcal{N}} \times \mathbf{v} = \mathbf{v}' + \boldsymbol{\omega}_{\mathcal{B}/\mathcal{N}} \times \mathbf{v} \quad (3.12)$$

Using the transport theorem the inertial second derivative $\ddot{\mathbf{c}}$ is expressed in terms of body relative derivatives of \mathbf{c} as

$$\ddot{\mathbf{c}} = \mathbf{c}'' + 2\boldsymbol{\omega}_{\mathcal{B}/\mathcal{N}} \times \mathbf{c}' + \dot{\boldsymbol{\omega}}_{\mathcal{B}/\mathcal{N}} \times \mathbf{c} + \boldsymbol{\omega}_{\mathcal{B}/\mathcal{N}} \times (\boldsymbol{\omega}_{\mathcal{B}/\mathcal{N}} \times \mathbf{c}) \quad (3.13)$$

where $\boldsymbol{\omega}_{\mathcal{B}/\mathcal{N}}$ is the angular velocity vector of frame \mathcal{B} with respect to frame \mathcal{N} . Substituting Eq. (3.13) into the translational equations of motion in Eq. (3.2) results in

$$\ddot{\mathbf{r}}_{B/N} = \ddot{\mathbf{r}}_{C/N} - \mathbf{c}'' - 2\boldsymbol{\omega}_{\mathcal{B}/\mathcal{N}} \times \mathbf{c}' - \dot{\boldsymbol{\omega}}_{\mathcal{B}/\mathcal{N}} \times \mathbf{c} - \boldsymbol{\omega}_{\mathcal{B}/\mathcal{N}} \times (\boldsymbol{\omega}_{\mathcal{B}/\mathcal{N}} \times \mathbf{c}) \quad (3.14)$$

It is evident by looking at Eqs. (3.11) and (3.14) that the angular acceleration of the body, $\dot{\boldsymbol{\omega}}_{B/N}$, and the angular acceleration of each solar panel angle, $\ddot{\theta}_i$, are coupled with the translational acceleration, $\ddot{\mathbf{r}}_{B/N}$. Because these are accelerations of state variables and will ultimately populate a system mass matrix, Eq. (3.14) is rearranged with the second order state variable terms isolated on the left-hand side of the equation. The mass of the spacecraft m_{sc} is multiplied on both sides of the equation which results in the substitution of the sum of the external forces applied on the spacecraft seen in Eq. (3.1).

It is also convenient to replace the cross products with the matrix equivalent skew symmetric matrix. Here the vector equation $\mathbf{a} \times \mathbf{b}$ is equivalent to the matrix expression $[\tilde{\mathbf{a}}]\mathbf{b}$ of these vectors [39].

$$m_{sc}\ddot{\mathbf{r}}_{B/N} - m_{sc}[\tilde{\mathbf{c}}]\dot{\boldsymbol{\omega}}_{B/N} + \sum_{i=1}^{N_s} m_{sp_i} d_i \hat{\mathbf{s}}_{i,3} \ddot{\theta}_i = \mathbf{F}_{ext} - 2m_{sc}[\tilde{\boldsymbol{\omega}}_{B/N}]\mathbf{c}' - m_{sc}[\tilde{\boldsymbol{\omega}}_{B/N}][\tilde{\boldsymbol{\omega}}_{B/N}]\mathbf{c} - \sum_{i=1}^{N_s} m_{sp_i} d_i \dot{\theta}_i^2 \hat{\mathbf{s}}_{i,1} \quad (3.15)$$

This equation describes the translational motion of the body frame point B with respect to the inertial frame and is in terms of the rotational motion and solar panel motion. This equation conforms with the general translational EOM form introduced in Eq. (2.1).

3.1.1.5 Spacecraft Rotational Equations of Motion

Next the EOM for the hub rotational motion is developed. The rigid-body rotational motion is most conveniently expressed by separating the kinematic and kinetic differential equations. This allows for any choice of attitude coordinates to be used to describe the orientation, while the convenient use of the quasi-velocity vector $\boldsymbol{\omega}_{B/N}$ is retained. In this dissertation the three-dimensional hub attitude is expressed using the Modified Rodrigues Parameters (MRPs) $\boldsymbol{\sigma}_{B/N}$ [54, 55, 56]. Combined with their shadow sets the MRPs form a convenient non-singular 3-parameter description with a discontinuity at 180 degrees principal rotations [57, 58]. The associated MRP differential

kinematic equations of motion are given by [39]

$$\dot{\boldsymbol{\sigma}}_{B/N} = \frac{1}{4}[B(\boldsymbol{\sigma}_{B/N})]^{\mathcal{B}}\boldsymbol{\omega}_{B/N} \quad (3.16)$$

where

$$[B(\boldsymbol{\sigma})] = (1 - \boldsymbol{\sigma}^T \boldsymbol{\sigma})[I_{3 \times 3}] + 2[\tilde{\boldsymbol{\sigma}}] + 2\boldsymbol{\sigma}\boldsymbol{\sigma}^T \quad (3.17)$$

and ${}^{\mathcal{B}}\boldsymbol{\omega}_{B/N}$ is the \mathcal{B} -frame matrix representation of the $\boldsymbol{\omega}_{B/N}$ vector. The following derivations are not tied to the use of MRPs, and other rigid-body attitude coordinates could readily be substituted.

The kinetic rotational EOM derivation starts with Euler's equation when the body fixed coordinate frame origin is not coincident with the center of mass of the body [39]

$$\dot{\mathbf{H}}_{sc,B} = \mathbf{L}_B + m_{sc}\ddot{\mathbf{r}}_{B/N} \times \mathbf{c} \quad (3.18)$$

Here the vector \mathbf{L}_B is the total external torque about point B . The definition of the angular momentum vector of the spacecraft about point B is:

$$\begin{aligned} \mathbf{H}_{sc,B} = & [I_{hub,B_c}]\boldsymbol{\omega}_{\mathcal{B}/N} + m_{hub}\mathbf{r}_{B_c/B} \times \dot{\mathbf{r}}_{B_c/B} \\ & + \sum_{i=1}^{N_s} \left([I_{sp_i,S_i}]\boldsymbol{\omega}_{\mathcal{B}/N} + \dot{\theta}_i I_{s_i,2} \hat{\mathbf{h}}_{i,2} + m_{sp_i} \mathbf{r}_{S_i/B} \times \dot{\mathbf{r}}_{S_i/B} \right) \end{aligned} \quad (3.19)$$

The solar panel frame \mathcal{S}_i is assumed to be a principle frame such that the solar panel inertia tensor about its center of mass is

$$[I_{sp_i,S_i}] = {}^{S_i} \begin{bmatrix} I_{s_i,1} & 0 & 0 \\ 0 & I_{s_i,2} & 0 \\ 0 & 0 & I_{s_i,3} \end{bmatrix} \quad (3.20)$$

The inertial time derivative of Eq. (3.19) is evaluated again using the Transport Theorem [39] to related vector derivatives as seen by different rotating frames and yields

$$\begin{aligned} \dot{\mathbf{H}}_{sc,B} = & [I_{hub,B_c}]\dot{\boldsymbol{\omega}}_{\mathcal{B}/N} + \boldsymbol{\omega}_{\mathcal{B}/N} \times [I_{hub,B_c}]\boldsymbol{\omega}_{\mathcal{B}/N} + m_{hub}\mathbf{r}_{B_c/B} \times \ddot{\mathbf{r}}_{B_c/B} \\ & + \sum_{i=1}^{N_s} \left([I'_{sp_i,S_i}]\boldsymbol{\omega}_{\mathcal{B}/N} + [I_{sp_i,S_i}]\dot{\boldsymbol{\omega}}_{\mathcal{B}/N} + \boldsymbol{\omega}_{\mathcal{B}/N} \times [I_{sp_i,S_i}]\boldsymbol{\omega}_{\mathcal{B}/N} \right. \\ & \left. + \ddot{\theta}_i I_{s_i,2} \hat{\mathbf{h}}_{i,2} + \boldsymbol{\omega}_{\mathcal{B}/N} \times \dot{\theta}_i I_{s_i,2} \hat{\mathbf{h}}_{i,2} + m_{sp_i} \mathbf{r}_{S_i/B} \times \ddot{\mathbf{r}}_{S_i/B} \right) \end{aligned} \quad (3.21)$$

The terms $\ddot{\mathbf{r}}_{B_c/B}$ and $\ddot{\mathbf{r}}_{S_i/B}$ are also found using the Transport Theorem and taking advantage of $\mathbf{r}_{B_c/B}$ being fixed with respect to the body frame.

$$\ddot{\mathbf{r}}_{B_c/B} = \dot{\boldsymbol{\omega}}_{\mathcal{B}/\mathcal{N}} \times \mathbf{r}_{B_c/B} + \boldsymbol{\omega}_{\mathcal{B}/\mathcal{N}} \times (\boldsymbol{\omega}_{\mathcal{B}/\mathcal{N}} \times \mathbf{r}_{B_c/B}) \quad (3.22)$$

$$\ddot{\mathbf{r}}_{S_i/B} = \mathbf{r}''_{S_i/B} + 2\boldsymbol{\omega}_{\mathcal{B}/\mathcal{N}} \times \mathbf{r}'_{S_i/B} + \dot{\boldsymbol{\omega}}_{\mathcal{B}/\mathcal{N}} \times \mathbf{r}_{S_i/B} + \boldsymbol{\omega}_{\mathcal{B}/\mathcal{N}} \times (\boldsymbol{\omega}_{\mathcal{B}/\mathcal{N}} \times \mathbf{r}_{S_i/B}) \quad (3.23)$$

Incorporating Eqs. (3.22) and (3.23) into Eq. (3.21) and simplifying the extensive algebra results in the intermediate result:

$$\begin{aligned} \dot{\mathbf{H}}_{sc,B} = & [I_{hub,B_c}] \dot{\boldsymbol{\omega}}_{\mathcal{B}/\mathcal{N}} + \boldsymbol{\omega}_{\mathcal{B}/\mathcal{N}} \times [I_{hub,B_c}] \boldsymbol{\omega}_{\mathcal{B}/\mathcal{N}} + m_{hub} \mathbf{r}_{B_c/B} \times (\dot{\boldsymbol{\omega}}_{\mathcal{B}/\mathcal{N}} \times \mathbf{r}_{B_c/B}) \\ & + m_{hub} \mathbf{r}_{B_c/B} \times \left[\boldsymbol{\omega}_{\mathcal{B}/\mathcal{N}} \times (\boldsymbol{\omega}_{\mathcal{B}/\mathcal{N}} \times \mathbf{r}_{B_c/B}) \right] + \sum_{i=1}^{N_s} \left([I'_{sp_i,S_i}] \boldsymbol{\omega}_{\mathcal{B}/\mathcal{N}} + [I_{sp_i,S_i}] \dot{\boldsymbol{\omega}}_{\mathcal{B}/\mathcal{N}} + \boldsymbol{\omega}_{\mathcal{B}/\mathcal{N}} \times [I_{sp_i,S_i}] \boldsymbol{\omega}_{\mathcal{B}/\mathcal{N}} \right. \\ & + \dot{\theta}_i I_{s_i,2} \hat{\mathbf{h}}_{i,2} + \boldsymbol{\omega}_{\mathcal{B}/\mathcal{N}} \times \dot{\theta}_i I_{s_i,2} \hat{\mathbf{h}}_{i,2} + m_{sp_i} \mathbf{r}_{S_i/B} \times \mathbf{r}''_{S_i/B} + 2m_{sp_i} \mathbf{r}_{S_i/B} \times (\boldsymbol{\omega}_{\mathcal{B}/\mathcal{N}} \times \mathbf{r}'_{S_i/B}) \\ & \left. + m_{sp_i} \mathbf{r}_{S_i/B} \times (\dot{\boldsymbol{\omega}}_{\mathcal{B}/\mathcal{N}} \times \mathbf{r}_{S_i/B}) + m_{sp_i} \mathbf{r}_{S_i/B} \times [\boldsymbol{\omega}_{\mathcal{B}/\mathcal{N}} \times (\boldsymbol{\omega}_{\mathcal{B}/\mathcal{N}} \times \mathbf{r}_{S_i/B})] \right) \quad (3.24) \end{aligned}$$

Applying the matrix tilde operator to replace the vector cross product, and using the inertia tensor parallel axis theorem [39] the following are defined:

$$[I_{hub,B}] = [I_{hub,B_c}] + m_{hub} [\tilde{\mathbf{r}}_{B_c/B}] [\tilde{\mathbf{r}}_{B_c/B}]^T \quad (3.25)$$

$$[I_{sp_i,B}] = [I_{sp_i,S_i}] + m_{sp_i} [\tilde{\mathbf{r}}_{S_i/B}] [\tilde{\mathbf{r}}_{S_i/B}]^T \quad (3.26)$$

$$[I_{sc,B}] = [I_{hub,B}] + \sum_i^P [I_{sp_i,B}] \quad (3.27)$$

$$[I'_{sc,B}] = \sum_{i=1}^{N_s} \left[[I'_{sp_i,S_i}] - m_{sp_i} \left([\tilde{\mathbf{r}}'_{S_i/B}] [\tilde{\mathbf{r}}_{S_i/B}] + [\tilde{\mathbf{r}}_{S_i/B}] [\tilde{\mathbf{r}}'_{S_i/B}] \right) \right] \quad (3.28)$$

$[I'_{sp_i,S_i}]$ needs to be defined and is conveniently expressed by leveraging the assumption that the inertia matrix is diagonal and can be written in terms of its base vectors:

$$[I_{sp_i,S_i}] = I_{s_i,1} \hat{\mathbf{s}}_{i,1} \hat{\mathbf{s}}_{i,1}^T + I_{s_i,2} \hat{\mathbf{s}}_{i,2} \hat{\mathbf{s}}_{i,2}^T + I_{s_i,3} \hat{\mathbf{s}}_{i,3} \hat{\mathbf{s}}_{i,3}^T \quad (3.29)$$

Taking the body time derivative of Eq. (3.29) results in

$$[I'_{sp_i,S_i}] = I_{s_i,1} \hat{\mathbf{s}}'_{i,1} \hat{\mathbf{s}}_{i,1}^T + I_{s_i,1} \hat{\mathbf{s}}_{i,1} \hat{\mathbf{s}}'^T_{i,1} + I_{s_i,2} \hat{\mathbf{s}}'_{i,2} \hat{\mathbf{s}}_{i,2}^T + I_{s_i,2} \hat{\mathbf{s}}_{i,2} \hat{\mathbf{s}}'^T_{i,2} + I_{s_i,3} \hat{\mathbf{s}}'_{i,3} \hat{\mathbf{s}}_{i,3}^T + I_{s_i,3} \hat{\mathbf{s}}_{i,3} \hat{\mathbf{s}}'^T_{i,3} \quad (3.30)$$

The \mathcal{B} -frame relative time derivatives of $\hat{\mathbf{s}}_{i,j}$ are

$$\hat{\mathbf{s}}'_{i,j} = \boldsymbol{\omega}_{S_i/B} \times \hat{\mathbf{s}}_{i,j} = \dot{\theta}_i \hat{\mathbf{s}}_{i,2} \times \hat{\mathbf{s}}_{i,j}; \quad j = 1, 2, 3 \quad (3.31)$$

Substituting Eq. (3.31) into Eq. (3.30) and simplifying results in the following body-relative time derivative expression of the solar panel inertia tensor.

$$[I'_{\text{sp}_i, S_i}] = \dot{\theta}_i (I_{S_i,3} - I_{S_i,1}) (\hat{\mathbf{s}}_{i,1} \hat{\mathbf{s}}_{i,3}^T + \hat{\mathbf{s}}_{i,3} \hat{\mathbf{s}}_{i,1}^T) \quad (3.32)$$

Using these definitions greatly simplifies the expression in Eq. (3.24) yielding the compact expression

$$\begin{aligned} \dot{\mathbf{H}}_{\text{sc}, B} = & [I_{\text{sc}, B}] \dot{\boldsymbol{\omega}}_{B/N} + \boldsymbol{\omega}_{B/N} \times [I_{\text{sc}, B}] \boldsymbol{\omega}_{B/N} + [I'_{\text{sc}, B}] \boldsymbol{\omega}_{B/N} + \sum_{i=1}^{N_s} \left\{ \ddot{\theta}_i I_{S_i,2} \hat{\mathbf{h}}_{i,2} \right. \\ & \left. + \boldsymbol{\omega}_{B/N} \times \dot{\theta}_i I_{S_i,2} \hat{\mathbf{h}}_{i,2} + m_{\text{sp}_i} \mathbf{r}_{S_i/B} \times \mathbf{r}''_{S_i/B} + m_{\text{sp}_i} \boldsymbol{\omega}_{B/N} \times \left(\mathbf{r}_{S_i/B} \times \mathbf{r}'_{S_i/B} \right) \right\} \quad (3.33) \end{aligned}$$

Next Eqs. (3.18) and (3.33) are equated to yield

$$\begin{aligned} \mathbf{L}_B + m_{\text{sc}} \ddot{\mathbf{r}}_{B/N} \times \mathbf{c} = & [I_{\text{sc}, B}] \dot{\boldsymbol{\omega}}_{B/N} + \boldsymbol{\omega}_{B/N} \times [I_{\text{sc}, B}] \boldsymbol{\omega}_{B/N} + [I'_{\text{sc}, B}] \boldsymbol{\omega}_{B/N} + \sum_{i=1}^{N_s} \left\{ \ddot{\theta}_i I_{S_i,2} \hat{\mathbf{h}}_{i,2} \right. \\ & \left. + \boldsymbol{\omega}_{B/N} \times \dot{\theta}_i I_{S_i,2} \hat{\mathbf{h}}_{i,2} + m_{\text{sp}_i} \mathbf{r}_{S_i/B} \times \mathbf{r}''_{S_i/B} + m_{\text{sp}_i} \boldsymbol{\omega}_{B/N} \times \left(\mathbf{r}_{S_i/B} \times \mathbf{r}'_{S_i/B} \right) \right\} \quad (3.34) \end{aligned}$$

Finally, Eq. (3.34) is written into compact matrix form and rearranged to have all acceleration terms on the left hand side again.

$$\begin{aligned} m_{\text{sc}} [\tilde{\mathbf{c}}] \ddot{\mathbf{r}}_{B/N} + [I_{\text{sc}, B}] \dot{\boldsymbol{\omega}}_{B/N} + \sum_{i=1}^{N_s} \left\{ I_{S_i,2} \hat{\mathbf{h}}_{i,2} + m_{\text{sp}_i} d_i [\tilde{\mathbf{r}}_{S_i/B}] \hat{\mathbf{s}}_{i,3} \right\} \ddot{\theta}_i = \\ - [\tilde{\boldsymbol{\omega}}_{B/N}] [I_{\text{sc}, B}] \boldsymbol{\omega}_{B/N} - [I'_{\text{sc}, B}] \boldsymbol{\omega}_{B/N} - \sum_{i=1}^{N_s} \left\{ \dot{\theta}_i [\tilde{\boldsymbol{\omega}}_{B/N}] \left(I_{S_i,2} \hat{\mathbf{h}}_{i,2} + m_{\text{sp}_i} d_i [\tilde{\mathbf{r}}_{S_i/B}] \hat{\mathbf{s}}_{i,3} \right) \right. \\ \left. + m_{\text{sp}_i} d_i \dot{\theta}_i^2 [\tilde{\mathbf{r}}_{S_i/B}] \hat{\mathbf{s}}_{i,1} \right\} + \mathbf{L}_B \quad (3.35) \end{aligned}$$

This expanded rotational equations of motion a rigid hub with N_s hinged panels illustrates the additional terms required to account for the panel flexing and thus the system center of mass location shift relative to the body. This equation conforms with the general rotational EOM form introduced in Eq. (2.2).

3.1.1.6 Hinged Panel Equations of Motion

The set of EOMs required to solve this system of differential equations are related to the hinged rigid panels which can represent solar panel flexing. In this development the i^{th} solar panel frame \mathcal{S}_i is assumed to be a principal coordinate frame of the panel, yielding the diagonal inertia tensor representation shown in Eq. (3.20).

Let $\mathbf{L}_{H_i} = L_{i,1}\hat{\mathbf{s}}_{i,1} + L_{i,2}\hat{\mathbf{s}}_{i,2} + L_{i,3}\hat{\mathbf{s}}_{i,3}$ be the total torque acting on the solar panel about the hinge point H_i . The corresponding hinge torque component about the body-fixed hinge axis $\hat{\mathbf{s}}_{i,2}$ is given through

$$L_{i,2} = -k_i\theta_i - c_i\dot{\theta}_i + \hat{\mathbf{s}}_{i,2} \cdot \boldsymbol{\tau}_{\text{ext},H_i} \quad (3.36)$$

The hinge structure produces the other two torques $L_{i,1}$ and $L_{i,3}$. The vector $\boldsymbol{\tau}_{\text{ext},H_i}$ is the net external torque on the solar panel and is projected onto the $\hat{\mathbf{s}}_{i,2}$ direction to find its contribution to $L_{i,2}$. Gravity, for example would apply the following torque on the solar panel about point H_i

$$\boldsymbol{\tau}_{g,H_i} = \mathbf{r}_{\mathcal{S}_i/H_i} \times \mathbf{F}_g \quad (3.37)$$

The inertial angular velocity vector for the solar panel frame is

$$\boldsymbol{\omega}_{\mathcal{S}_i/\mathcal{N}} = \boldsymbol{\omega}_{\mathcal{S}_i/\mathcal{H}_i} + \boldsymbol{\omega}_{\mathcal{H}_i/\mathcal{B}} + \boldsymbol{\omega}_{\mathcal{B}/\mathcal{N}} \quad (3.38)$$

where $\boldsymbol{\omega}_{\mathcal{S}_i/\mathcal{H}_i} = \dot{\theta}_i\hat{\mathbf{s}}_{i,2}$. Because the hinge frame \mathcal{H}_i is fixed relative to the body frame \mathcal{B} the relative angular velocity vector is $\boldsymbol{\omega}_{\mathcal{H}_i/\mathcal{B}} = \mathbf{0}$. The body angular velocity vector is written in \mathcal{S}_i -frame components as

$$\boldsymbol{\omega}_{\mathcal{B}/\mathcal{N}} = (\hat{\mathbf{s}}_{i,1} \cdot \boldsymbol{\omega}_{\mathcal{B}/\mathcal{N}})\hat{\mathbf{s}}_{i,1} + (\hat{\mathbf{s}}_{i,2} \cdot \boldsymbol{\omega}_{\mathcal{B}/\mathcal{N}})\hat{\mathbf{s}}_{i,2} + (\hat{\mathbf{s}}_{i,3} \cdot \boldsymbol{\omega}_{\mathcal{B}/\mathcal{N}})\hat{\mathbf{s}}_{i,3} \quad (3.39)$$

$$= \omega_{s_{i,1}}\hat{\mathbf{s}}_{i,1} + \omega_{s_{i,2}}\hat{\mathbf{s}}_{i,2} + \omega_{s_{i,3}}\hat{\mathbf{s}}_{i,3} \quad (3.40)$$

Fortunately using this definition greatly simplifies the following algebraic development. Finally, the inertial solar panel angular velocity vector is written as

$$\boldsymbol{\omega}_{\mathcal{S}_i/\mathcal{N}} = \omega_{s_{i,1}}\hat{\mathbf{s}}_{i,1} + (\omega_{s_{i,2}} + \dot{\theta}_i)\hat{\mathbf{s}}_{i,2} + \omega_{s_{i,3}}\hat{\mathbf{s}}_{i,3} \quad (3.41)$$

As $\hat{\mathbf{s}}_{i,2}$ is a body-fixed vector, note that

$$\dot{\omega}_{s_{i,2}} = \frac{\mathcal{B}d}{dt} (\boldsymbol{\omega}_{\mathcal{B}/\mathcal{N}} \cdot \hat{\mathbf{s}}_{i,2}) = \frac{\mathcal{B}d}{dt} (\boldsymbol{\omega}_{\mathcal{B}/\mathcal{N}}) \cdot \hat{\mathbf{s}}_{i,2} = \dot{\boldsymbol{\omega}}_{\mathcal{B}/\mathcal{N}} \cdot \hat{\mathbf{s}}_{i,2} \quad (3.42)$$

The notation $\mathcal{B}d/dt(\mathbf{x})$ denotes a body-frame \mathcal{B} relative time derivative operation of the vector \mathbf{x} .

Substituting these angular velocity components into the rotational equations of motion of a rigid-body with torques taken about its center of mass [39], the general solar panel equations of motion are written as

$$I_{s_{i,1}} \dot{\omega}_{s_{i,1}} = -(I_{s_{i,3}} - I_{s_{i,2}})(\omega_{s_{i,2}} + \dot{\theta}_i) \omega_{s_{i,3}} + L_{s_{i,1}} \quad (3.43)$$

$$I_{s_{i,2}} (\dot{\omega}_{s_{i,2}} + \ddot{\theta}_i) = -(I_{s_{i,1}} - I_{s_{i,3}}) \omega_{s_{i,3}} \omega_{s_{i,1}} + L_{s_{i,2}} \quad (3.44)$$

$$I_{s_{i,3}} \dot{\omega}_{s_{i,3}} = -(I_{s_{i,2}} - I_{s_{i,1}}) \omega_{s_{i,1}} (\omega_{s_{i,2}} + \dot{\theta}_i) + L_{s_{i,3}} \quad (3.45)$$

where $\mathbf{L}_{S_i} = L_{s_{i,1}} \hat{\mathbf{s}}_{i,1} + L_{s_{i,2}} \hat{\mathbf{s}}_{i,2} + L_{s_{i,3}} \hat{\mathbf{s}}_{i,3}$ is the net torque acting on the solar panel about its center of mass. Note that the second differential equation in Eq. (3.44) is used to get the desired equations of motion of θ_i . The first and third equation could be used to back-solve for the structural hinge torques embedded in $L_{s_{i,1}}$ and $L_{s_{i,3}}$ if needed.

Let \mathbf{F}_{S_i} be the net force acting on the solar panel. Using the superparticle theorem [39] yields

$$\mathbf{F}_{S_i} = m_{\text{sp}_i} \ddot{\mathbf{r}}_{S_i/N} \quad (3.46)$$

The torque about the solar panel center of mass can be related to the torque about the hinge point H_i using

$$\mathbf{L}_{H_i} = \mathbf{L}_{S_i} + \mathbf{r}_{S_i/H_i} \times \mathbf{F}_{S_i} \quad (3.47)$$

Solving for the torque about S_i yields

$$\mathbf{L}_{S_i} = \mathbf{L}_{H_i} - \mathbf{r}_{S_i/H_i} \times m_{\text{sp}_i} \ddot{\mathbf{r}}_{S_i/N} \quad (3.48)$$

Taking the vector dot product of Eq. (3.48) with $\hat{\mathbf{s}}_{i,2}$ and using $\mathbf{r}_{S_i/H_i} = -d_i \hat{\mathbf{s}}_{i,1}$ allows for a scalar

equation to be developed that relates the hinge axis torque $L_{s_{i,2}}$.

$$L_{s_{i,2}} = \hat{\mathbf{s}}_{i,2} \cdot \mathbf{L}_{S_i} = \underbrace{\hat{\mathbf{s}}_{i,2} \cdot \mathbf{L}_{H_i}}_{L_{i,2}} - \hat{\mathbf{s}}_{i,2} \cdot (\mathbf{r}_{S_i/H_i} \times m_{\text{sp}_i} \ddot{\mathbf{r}}_{S_i/N}) \quad (3.49)$$

$$= -k_i \theta - c_i \dot{\theta}_i + \hat{\mathbf{s}}_{i,2} \cdot \boldsymbol{\tau}_{\text{ext},H_i} + m_{\text{sp}_i} d_i \hat{\mathbf{s}}_{i,2} \cdot (\hat{\mathbf{s}}_{i,1} \times \ddot{\mathbf{r}}_{S_i/N}) \quad (3.50)$$

Solving for the second order inertial time derivative of $\mathbf{r}_{S_i/N} = \mathbf{r}_{H_i/N} - d\hat{\mathbf{s}}_{i,1}$ yields

$$\ddot{\mathbf{r}}_{S_i/N} = \ddot{\mathbf{r}}_{H_i/N} - \dot{\boldsymbol{\omega}}_{S_i/N} \times (d\hat{\mathbf{s}}_{i,1}) - \boldsymbol{\omega}_{S_i/N} \times (\boldsymbol{\omega}_{S_i/N} \times (d\hat{\mathbf{s}}_{i,1})) \quad (3.51)$$

Substituting this inertial acceleration into the above $L_{s_{i,2}}$ expression provides

$$\begin{aligned} L_{s_{i,2}} = & -k_i \theta - c_i \dot{\theta}_i + m_{\text{sp}_i} d_i \hat{\mathbf{s}}_{i,2} \cdot (\hat{\mathbf{s}}_{i,1} \times \ddot{\mathbf{r}}_{H_i/N}) + m_{\text{sp}_i} d_i^2 \hat{\mathbf{s}}_{i,2} \cdot (\hat{\mathbf{s}}_{i,1} \times (\hat{\mathbf{s}}_{i,1} \times \dot{\boldsymbol{\omega}}_{S_i/N})) \\ & - m_{\text{sp}_i} d_i^2 \hat{\mathbf{s}}_{i,2} \cdot (\hat{\mathbf{s}}_{i,1} \times (\boldsymbol{\omega}_{S_i/N} \times (\boldsymbol{\omega}_{S_i/N} \times \hat{\mathbf{s}}_{i,1}))) \end{aligned} \quad (3.52)$$

Using the double vector cross product identity, as well as $\mathbf{a} \cdot (\mathbf{b} \times \mathbf{c}) = (\mathbf{a} \times \mathbf{b}) \cdot \mathbf{c}$, the $L_{s_{i,2}}$ torque component is simplified to

$$\begin{aligned} L_{s_{i,2}} = & -k_i \theta - c_i \dot{\theta}_i + \hat{\mathbf{s}}_{i,2} \cdot \boldsymbol{\tau}_{\text{ext},H_i} - m_{\text{sp}_i} d_i \hat{\mathbf{s}}_{i,3} \cdot \ddot{\mathbf{r}}_{H_i/N} \\ & - m_{\text{sp}_i} d_i^2 \hat{\mathbf{s}}_{i,2} \cdot \dot{\boldsymbol{\omega}}_{B/N} - m_{\text{sp}_i} d_i^2 \ddot{\theta}_i + m_{\text{sp}_i} d_i^2 \omega_{s_{i,3}} \omega_{s_{i,1}} \end{aligned} \quad (3.53)$$

Substituting this torque into the differential equation seen in Eq. (3.45), yields the desired scalar hinged solar panel equation of motion

$$\begin{aligned} (I_{s_{i,2}} + m_{\text{sp}_i} d_i^2) \hat{\mathbf{s}}_{i,2}^T \dot{\boldsymbol{\omega}}_{B/N} + (I_{s_{i,2}} + m_{\text{sp}_i} d_i^2) \ddot{\theta}_i + m_{\text{sp}_i} d_i \hat{\mathbf{s}}_{i,3}^T \ddot{\mathbf{r}}_{H_i/N} + k_i \theta + c_i \dot{\theta}_i \\ - \hat{\mathbf{s}}_{i,2}^T \boldsymbol{\tau}_{\text{ext},H_i} + (I_{s_{i,1}} - I_{s_{i,3}} - m_{\text{sp}_i} d_i^2) \omega_{s_{i,3}} \omega_{s_{i,1}} = 0 \end{aligned} \quad (3.54)$$

The final task is to expand $\ddot{\mathbf{r}}_{H_i/N}$ in terms of the translational motion $\ddot{\mathbf{r}}_{B/N}$. Recalling that the hinge location is a fixed point on the body, Eq. (3.54) is changed to the following form:

$$\begin{aligned} (I_{s_{i,2}} + m_{\text{sp}_i} d_i^2) \hat{\mathbf{s}}_{i,2}^T \dot{\boldsymbol{\omega}}_{B/N} + m_{\text{sp}_i} d_i \hat{\mathbf{s}}_{i,3}^T (\ddot{\mathbf{r}}_{B/N} + \dot{\boldsymbol{\omega}}_{B/N} \times \mathbf{r}_{H_i/B} + \boldsymbol{\omega}_{B/N} \times (\boldsymbol{\omega}_{B/N} \times \mathbf{r}_{H_i/B})) \\ + (I_{s_{i,2}} + m_{\text{sp}_i} d_i^2) \ddot{\theta}_i + k_i \theta + c_i \dot{\theta}_i - \hat{\mathbf{s}}_{i,2}^T \boldsymbol{\tau}_{\text{ext},H_i} + (I_{s_{i,1}} - I_{s_{i,3}} - m_{\text{sp}_i} d_i^2) \omega_{s_{i,3}} \omega_{s_{i,1}} = 0 \end{aligned} \quad (3.55)$$

The final expression again groups the second order state variables conveniently to the left-hand side of the equation and the cross products are replaced with the skew symmetric matrix operators:

$$\begin{aligned}
m_{\text{sp}_i} d_i \hat{\mathbf{s}}_{i,3}^T \ddot{\mathbf{r}}_{B/N} + \left[(I_{s_{i,2}} + m_{\text{sp}_i} d_i^2) \hat{\mathbf{s}}_{i,2}^T - m_{\text{sp}_i} d_i \hat{\mathbf{s}}_{i,3}^T [\tilde{\mathbf{r}}_{H_i/B}] \right] \dot{\boldsymbol{\omega}}_{B/N} \\
+ (I_{s_{i,2}} + m_{\text{sp}_i} d_i^2) \ddot{\theta}_i = -k_i \theta_i - c_i \dot{\theta}_i + \hat{\mathbf{s}}_{i,2}^T \boldsymbol{\tau}_{\text{ext}, H_i} + (I_{s_{i,3}} - I_{s_{i,1}} + m_{\text{sp}_i} d_i^2) \omega_{s_{i,3}} \omega_{s_{i,1}} \\
- m_{\text{sp}_i} d_i \hat{\mathbf{s}}_{i,3}^T [\tilde{\boldsymbol{\omega}}_{B/N}] [\tilde{\boldsymbol{\omega}}_{B/N}] \mathbf{r}_{H_i/B} \quad (3.56)
\end{aligned}$$

Eq. (3.56) provides N_s scalar hinged panel EOM required to describe the motion of the spacecraft. This equation conforms with the general effector EOM form introduced in Eq. 2.4.

3.1.1.7 Back-Substitution Formulation

The equations presented in the previous sections result in $N_s + 6$ coupled kinetic differential equations. Note that the various kinematic differential equation for hub motion and rotation, as well as the flexing angles, are already decoupled in this formulation. Therefore, if the remaining $N + 6$ kinetic EOMs were placed into state space form, a system mass matrix of size $N_s + 6$ would need to be inverted to numerically integrate the dynamical system. This can result in a computationally expensive simulation for a large number of panels. In the following developments the EOMs are manipulated using the back-substitution method introduced in Section 2.3.

3.1.1.8 Solar Panel Motion Manipulation

In Eq. (3.56), the solar panel motion is coupled with both the translational motion and the rotational motion. In addition, both the translational and rotational EOMs include the solar panel accelerations. To decouple the hub acceleration vectors from the panel accelerations, Eq. (3.56) is

solved for the angular accelerations $\ddot{\theta}_i$.

$$\ddot{\theta}_i = \frac{1}{(I_{s_{i,2}} + m_{\text{sp}_i} d_i^2)} \left(-m_{\text{sp}_i} d_i \hat{\mathbf{s}}_{i,3}^T \ddot{\mathbf{r}}_{B/N} - \left[(I_{s_{i,2}} + m_{\text{sp}_i} d_i^2) \hat{\mathbf{s}}_{i,2}^T - m_{\text{sp}_i} d_i \hat{\mathbf{s}}_{i,3}^T [\tilde{\mathbf{r}}_{H_i/B}] \right] \dot{\boldsymbol{\omega}}_{B/N} \right. \\ \left. - k_i \theta_i - c_i \dot{\theta}_i + \hat{\mathbf{s}}_{i,2}^T \boldsymbol{\tau}_{\text{ext}, H_i} + (I_{s_{i,3}} - I_{s_{i,1}} + m_{\text{sp}_i} d_i^2) \omega_{s_{i,3}} \omega_{s_{i,1}} \right. \\ \left. - m_{\text{sp}_i} d_i \hat{\mathbf{s}}_{i,3}^T [\tilde{\boldsymbol{\omega}}_{B/N}] [\tilde{\boldsymbol{\omega}}_{B/N}] \mathbf{r}_{H_i/B} \right) \quad (3.57)$$

Eq. (3.57) is rewritten into the following compact form and will be utilized multiple times throughout this formulation

$$\ddot{\theta}_i = \mathbf{a}_{\theta_i}^T \ddot{\mathbf{r}}_{B/N} + \mathbf{b}_{\theta_i}^T \dot{\boldsymbol{\omega}}_{B/N} + c_{\theta_i} \quad (3.58)$$

where \mathbf{a}_{θ_i} , \mathbf{b}_{θ_i} , and c_{θ_i} are defined as

$$\mathbf{a}_{\theta_i} = -\frac{m_{\text{sp}_i} d_i}{(I_{s_{i,2}} + m_{\text{sp}_i} d_i^2)} \hat{\mathbf{s}}_{i,3} \quad (3.59a)$$

$$\mathbf{b}_{\theta_i} = -\frac{1}{(I_{s_{i,2}} + m_{\text{sp}_i} d_i^2)} \left[(I_{s_{i,2}} + m_{\text{sp}_i} d_i^2) \hat{\mathbf{s}}_{i,2} + m_{\text{sp}_i} d_i [\tilde{\mathbf{r}}_{H_i/B}] \hat{\mathbf{s}}_{i,3} \right] \quad (3.59b)$$

$$c_{\theta_i} = \frac{1}{(I_{s_{i,2}} + m_{\text{sp}_i} d_i^2)} \left(-k_i \theta_i - c_i \dot{\theta}_i + \hat{\mathbf{s}}_{i,2} \cdot \boldsymbol{\tau}_{\text{ext}, H_i} + (I_{s_{i,3}} - I_{s_{i,1}} + m_{\text{sp}_i} d_i^2) \omega_{s_{i,3}} \omega_{s_{i,1}} \right. \\ \left. - m_{\text{sp}_i} d_i \hat{\mathbf{s}}_{i,3}^T [\tilde{\boldsymbol{\omega}}_{B/N}] [\tilde{\boldsymbol{\omega}}_{B/N}] \mathbf{r}_{H_i/B} \right) \quad (3.59c)$$

3.1.1.9 Decoupled Translational and Rotational Accelerations

To solve for the translational and rotational accelerations, Eq. (3.58) is substituted into the translational and rotational EOMs. The result of this substitution for the translation EOM, Eq. (3.15), is seen in the following equation:

$$m_{\text{sc}} \ddot{\mathbf{r}}_{B/N} - m_{\text{sc}} [\tilde{\mathbf{c}}] \dot{\boldsymbol{\omega}}_{B/N} + \sum_{i=1}^{N_s} m_{\text{sp}_i} d_i \hat{\mathbf{s}}_{i,3} \left(\mathbf{a}_{\theta_i}^T \ddot{\mathbf{r}}_{B/N} + \mathbf{b}_{\theta_i}^T \dot{\boldsymbol{\omega}}_{B/N} + c_{\theta_i} \right) \\ = F_{\text{ext}} - 2m_{\text{sc}} [\tilde{\boldsymbol{\omega}}_{B/N}] \mathbf{c}' - m_{\text{sc}} [\tilde{\boldsymbol{\omega}}_{B/N}] [\tilde{\boldsymbol{\omega}}_{B/N}] \mathbf{c} - \sum_{i=1}^{N_s} m_{\text{sp}_i} d_i \dot{\theta}_i^2 \hat{\mathbf{s}}_{i,1} \quad (3.60)$$

Simplifying and combining like terms yields the translational EOM that has been decoupled from the solar panel acceleration:

$$\begin{aligned} & \left(m_{sc}[I_{3 \times 3}] + \sum_{i=1}^N m_{sp_i} d_i \hat{\mathbf{s}}_{i,3} \mathbf{a}_{\theta_i}^T \right) \ddot{\mathbf{r}}_{B/N} + \left(-m_{sc}[\tilde{\mathbf{c}}] + \sum_{i=1}^N m_{sp_i} d_i \hat{\mathbf{s}}_{i,3} \mathbf{b}_{\theta_i}^T \right) \dot{\boldsymbol{\omega}}_{B/N} \\ & = m_{sc} \ddot{\mathbf{r}}_{C/N} - 2m_{sc}[\tilde{\boldsymbol{\omega}}_{B/N}] \mathbf{c}' - m_{sc}[\tilde{\boldsymbol{\omega}}_{B/N}][\tilde{\boldsymbol{\omega}}_{B/N}] \mathbf{c} - \sum_{i=1}^N \left(m_{sp_i} d_i \dot{\theta}_i^2 \hat{\mathbf{s}}_{i,1} + m_{sp_i} d_i c_{\theta_i} \hat{\mathbf{s}}_{i,3} \right) \end{aligned} \quad (3.61)$$

Following the same pattern for the rotational hub EOM, Eq. (3.35), yields:

$$\begin{aligned} & \left[m_{sc}[\tilde{\mathbf{c}}] + \sum_{i=1}^N (I_{s_{i,2}} \hat{\mathbf{s}}_{i,2} + m_{sp_i} d_i [\tilde{\mathbf{r}}_{S_{c,i}/B}] \hat{\mathbf{s}}_{i,3}) \mathbf{a}_{\theta_i}^T \right] \ddot{\mathbf{r}}_{B/N} \\ & + \left[[I_{sc,B}] + \sum_{i=1}^N (I_{s_{i,2}} \hat{\mathbf{s}}_{i,2} + m_{sp_i} d_i [\tilde{\mathbf{r}}_{S_{c,i}/B}] \hat{\mathbf{s}}_{i,3}) \mathbf{b}_{\theta_i}^T \right] \dot{\boldsymbol{\omega}}_{B/N} = -[\tilde{\boldsymbol{\omega}}_{B/N}][I_{sc,B}] \boldsymbol{\omega}_{B/N} - [I'_{sc,B}] \boldsymbol{\omega}_{B/N} \\ & - \sum_{i=1}^N \left\{ (\dot{\theta}_i [\tilde{\boldsymbol{\omega}}_{B/N}] + c_{\theta_i} [I_{3 \times 3}]) (I_{s_{i,2}} \hat{\mathbf{s}}_{i,2} + m_{sp_i} d_i [\tilde{\mathbf{r}}_{S_{c,i}/B}] \hat{\mathbf{s}}_{i,3}) + m_{sp_i} d_i \dot{\theta}_i^2 [\tilde{\mathbf{r}}_{S_{c,i}/B}] \hat{\mathbf{s}}_{i,1} \right\} + \mathbf{L}_B \end{aligned} \quad (3.62)$$

The following matrices are defined to adhere to the back-substitution method as seen in Section 2.3:

$$[A] = m_{sc}[I_{3 \times 3}] + \sum_{i=1}^N m_{sp_i} d_i \hat{\mathbf{s}}_{i,3} \mathbf{a}_{\theta_i}^T \quad (3.63)$$

$$[B] = -m_{sc}[\tilde{\mathbf{c}}] + \sum_{i=1}^N m_{sp_i} d_i \hat{\mathbf{s}}_{i,3} \mathbf{b}_{\theta_i}^T \quad (3.64)$$

$$[C] = m_{sc}[\tilde{\mathbf{c}}] + \sum_{i=1}^N (I_{s_{i,2}} \hat{\mathbf{s}}_{i,2} + m_{sp_i} d_i [\tilde{\mathbf{r}}_{S_{c,i}/B}] \hat{\mathbf{s}}_{i,3}) \mathbf{a}_{\theta_i}^T \quad (3.65)$$

$$[D] = [I_{sc,B}] + \sum_{i=1}^N (I_{s_{i,2}} \hat{\mathbf{s}}_{i,2} + m_{sp_i} d_i [\tilde{\mathbf{r}}_{S_{c,i}/B}] \hat{\mathbf{s}}_{i,3}) \mathbf{b}_{\theta_i}^T \quad (3.66)$$

$$\begin{aligned} \mathbf{v}_{trans} & = m_{sc} \ddot{\mathbf{r}}_{C/N} - 2m_{sc}[\tilde{\boldsymbol{\omega}}_{B/N}] \mathbf{c}' - m_{sc}[\tilde{\boldsymbol{\omega}}_{B/N}][\tilde{\boldsymbol{\omega}}_{B/N}] \mathbf{c} \\ & - \sum_{i=1}^N \left(m_{sp_i} d_i \dot{\theta}_i^2 \hat{\mathbf{s}}_{i,1} + m_{sp_i} d_i c_{\theta_i} \hat{\mathbf{s}}_{i,3} \right) \end{aligned} \quad (3.67)$$

$$\begin{aligned} \mathbf{v}_{rot} & = - \sum_{i=1}^N \left\{ (\dot{\theta}_i [\tilde{\boldsymbol{\omega}}_{B/N}] + c_{\theta_i} [I_{3 \times 3}]) (I_{s_{i,2}} \hat{\mathbf{s}}_{i,2} + m_{sp_i} d_i [\tilde{\mathbf{r}}_{S_{c,i}/B}] \hat{\mathbf{s}}_{i,3}) \right. \\ & \left. + m_{sp_i} d_i \dot{\theta}_i^2 [\tilde{\mathbf{r}}_{S_{c,i}/B}] \hat{\mathbf{s}}_{i,1} \right\} - [\tilde{\boldsymbol{\omega}}_{B/N}][I_{sc,B}] \boldsymbol{\omega}_{B/N} - [I'_{sc,B}] \boldsymbol{\omega}_{B/N} + \mathbf{L}_B \end{aligned} \quad (3.68)$$

Defining these matrices was the final step required to adhere to the general EOM form introduced in Section 2. Now the EOMs can readily be implemented in software to approximate the flexing phenomenon.

3.1.1.10 Conclusion

Spacecraft with large appended solar panels have flexing effects that are generally non-negligible and should be included in simulations of the spacecraft. This dissertation presents a very convenient and compact closed-form formulation for a first-order approximation of flexible dynamics that can be applied to spacecraft with appended solar panels or hinged structural sub-components that can be modeled as single rigid-bodies. It is not applicable to appended solar panels that consist of multiple interconnected panels. Numerical simulation results for a spacecraft with flexing solar arrays using this model can be seen in Section 6.3.

The equations produced in this dissertation are compact, frame independent, and modular equations of motion which will result in organized and flexible software implementations. Additionally the back-substitution method equations are more computationally efficient because it removes the need for a fully-coupled system mass matrix inverse. Modeling the flexing effect using this first-order approximation is an excellent way to analyze the impact of flexing on the spacecraft by running simulations through the life of missions and narrow down scenarios susceptible to unwanted flexing behavior. Formulating the equations of motion for flexible multi-body dynamics can be a time consuming task and this dissertation provides a solution that can readily implemented in software.

3.1.2 Fuel Slosh - Lumped Mass Spring Mass Damper Model

3.1.2.1 Introduction

Another important physical phenomenon that affects many spacecraft is fuel slosh. Mathematically, the EOMs of the structure and the liquid are tightly coupled[59, 60]. In space, the liquid is subjected not only to inertial forces, but also to microgravity, viscous, and surface tension forces[61, 62]. Furthermore, a moving liquid inside a tank produces a change in the position of the center of mass of the whole system in addition to internal torques and forces when a liquid wave hits the walls of the tank.

The most rigorous mathematical approach to sloshing phenomena is given by the Navier-Stokes equations with nonlinear boundary conditions[63]. Several Computational Fluid Dynamics (CFD) methods have been applied to solve this problem using different formulations[59, 64, 60, 65, 66]. Quasi-simultaneous methods can be used to solve the coupled EOMs[59]. The combined CFD-rigid-body model, although more exact, has some drawbacks from a simulation point of view. First, the inherent complexity of the combined model might not be feasible in early stages of the design. Second, integrating continuum and lumped models can be computationally time consuming[67, 68].

To avoid these complications, often simplified slosh models are used for control loop modeling [61, 62, 69, 70]. Slosh is comprised of several different kinds of movement, many of which are highly nonlinear. Small-amplitude waves and stable nonlinear rotary slosh can be approximated using lumped mechanical multi-mode models[61, 62, 71], including either masses, springs, and dampers or pendulums. Using a lumped model may be a useful simplification in a dynamic model for control design purposes. It can be viewed as a complement of the more accurate CFD approach. In this work, a systematic approach to slosh modeling is proposed using approximated multi-mode mechanical models.

3.1.2.2 Problem Statement

The formulation assumes that there is a rigid hub, with N_P lumped masses in the tank for the fuel. Subscript j is used to indicate the j_{th} fuel slosh mass, m_j . Figure 3.2 displays the frame and variable definitions used for this formulation.

There are two coordinate frames defined for this formulation. The inertial reference frame is indicated by $\mathcal{N} : \{\hat{n}_1, \hat{n}_2, \hat{n}_3\}$. The body fixed coordinate frame, $\mathcal{B} : \{\hat{b}_1, \hat{b}_2, \hat{b}_3\}$, which is anchored to the hub and can be oriented in any direction.

There are a few more key locations that need to be defined. Point B is the origin of the body frame, and can have any location with respect to the hub. Point B_c is the location of the center of mass of the rigid hub. P_j is the undeflected or equilibrium position of each corresponding slosh mass, while point $P_{c,j}$ is the current position of that slosh mass.

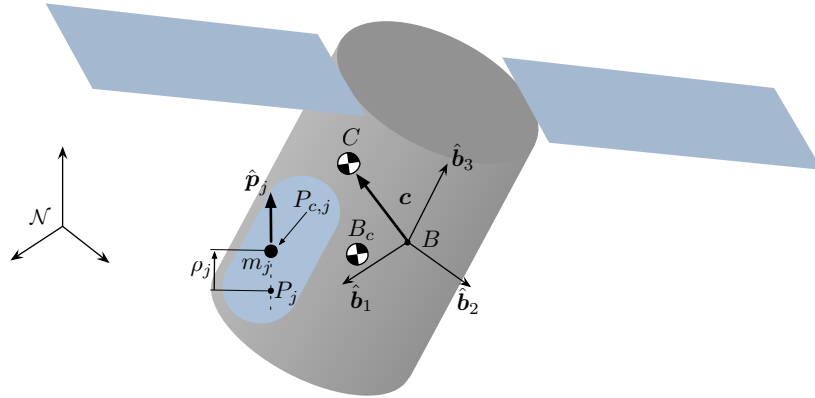


Figure 3.2: Frame and variable definitions used for formulation

Figure 3.3 provides further detail of the fuel slosh parameters. As seen in Figure 3.3, an individual slosh particle is constrained to move along its corresponding \hat{p}_j direction while connected by a spring with a linear spring constant value k_j and by a linear damper with a damping coefficient, c_j . The variable, ρ_j is a state variable and quantifies the displacement from equilibrium for the corresponding slosh mass.

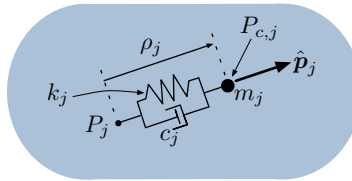


Figure 3.3: Detailed description of single slosh particle

Using the variables and frames defined, the following section outlines the derivation of equations of motion for the spacecraft.

3.1.2.3 Rigid Spacecraft Hub Translational Motion

The derivation begins with Newton's first law for the center of mass of the spacecraft.

$$\ddot{\mathbf{r}}_{C/N} = \frac{\mathbf{F}}{m_{sc}} \quad (3.69)$$

Ultimately the acceleration of the body frame or point B is desired

$$\ddot{\mathbf{r}}_{B/N} = \ddot{\mathbf{r}}_{C/N} - \ddot{\mathbf{c}} \quad (3.70)$$

The definition of \mathbf{c} can be seen in Eq. (3.71).

$$\mathbf{c} = \frac{1}{m_{sc}} \left(m_{hub} \mathbf{r}_{B_c/B} + \sum_{j=1}^{N_P} m_j \mathbf{r}_{P_{c,j}/B} \right) \quad (3.71)$$

To find the inertial time derivative of \mathbf{c} , it is first necessary to find the time derivative of \mathbf{c} with respect to the body frame. A time derivative of any vector, \mathbf{v} , with respect to the body frame is denoted by \mathbf{v}' ; the inertial time derivative is labeled as $\dot{\mathbf{v}}$. The first and second body-relative time derivatives of \mathbf{c} can be seen in Eqs. (3.72) and (3.73).

$$\mathbf{c}' = \frac{1}{m_{sc}} \left(\sum_{j=1}^{N_P} m_j \mathbf{r}'_{P_{c,j}/B} \right) \quad (3.72)$$

$$\mathbf{c}'' = \frac{1}{m_{sc}} \left(\sum_{j=1}^{N_P} m_j \mathbf{r}''_{P_{c,j}/B} \right) \quad (3.73)$$

$\mathbf{r}_{P_{c,j}/B}$ is defined in the following

$$\mathbf{r}_{P_{c,j}/B} = \mathbf{r}_{P_j/B} + \rho_j \hat{\mathbf{p}}_j \quad (3.74)$$

And, the first and second body time derivatives of $\mathbf{r}_{P_{c,j}/B}$ are

$$\mathbf{r}'_{P_{c,j}/B} = \dot{\rho}_j \hat{\mathbf{p}}_j \quad (3.75)$$

$$\mathbf{r}''_{P_{c,j}/B} = \ddot{\rho}_j \hat{\mathbf{p}}_j \quad (3.76)$$

Eqs. (3.72) and (3.73) are next reformulated to include these new definitions:

$$\mathbf{c}' = \frac{1}{m_{sc}} \left(\sum_{j=1}^{N_P} m_j \dot{\rho}_j \hat{\mathbf{p}}_j \right) \quad (3.77)$$

$$\mathbf{c}'' = \frac{1}{m_{sc}} \left(\sum_{j=1}^{N_P} m_j \ddot{\rho}_j \hat{\mathbf{p}}_j \right) \quad (3.78)$$

Using the transport theorem[39] yields the following definition for $\ddot{\mathbf{c}}$

$$\ddot{\mathbf{c}} = \mathbf{c}'' + 2\boldsymbol{\omega}_{B/N} \times \mathbf{c}' + \dot{\boldsymbol{\omega}}_{B/N} \times \mathbf{c} + \boldsymbol{\omega}_{B/N} \times (\boldsymbol{\omega}_{B/N} \times \mathbf{c}) \quad (3.79)$$

Eq. (3.70) is updated to include Eq. (3.79)

$$\ddot{\mathbf{r}}_{B/N} = \ddot{\mathbf{r}}_{C/N} - \mathbf{c}'' - 2\boldsymbol{\omega}_{B/N} \times \mathbf{c}' - \dot{\boldsymbol{\omega}}_{B/N} \times \mathbf{c} - \boldsymbol{\omega}_{B/N} \times (\boldsymbol{\omega}_{B/N} \times \mathbf{c}) \quad (3.80)$$

Substituting Eq.(3.78) into Eq.(3.80) results in

$$\ddot{\mathbf{r}}_{B/N} = \ddot{\mathbf{r}}_{C/N} - \frac{1}{m_{sc}} \left[\sum_{j=1}^{N_P} m_j \ddot{\rho}_j \hat{\mathbf{p}}_j \right] - 2\boldsymbol{\omega}_{B/N} \times \mathbf{c}' - \dot{\boldsymbol{\omega}}_{B/N} \times \mathbf{c} - \boldsymbol{\omega}_{B/N} \times (\boldsymbol{\omega}_{B/N} \times \mathbf{c}) \quad (3.81)$$

Moving second order terms to the left hand side and introducing the tilde matrix[39] to replace the cross product operators simplifies the equation to

$$\ddot{\mathbf{r}}_{B/N} - [\tilde{\mathbf{c}}]\dot{\boldsymbol{\omega}}_{B/N} + \frac{1}{m_{sc}} \sum_{j=1}^{N_P} m_j \hat{\mathbf{p}}_j \ddot{\rho}_j = \ddot{\mathbf{r}}_{C/N} - 2[\tilde{\boldsymbol{\omega}}_{B/N}]\mathbf{c}' - [\tilde{\boldsymbol{\omega}}_{B/N}][\tilde{\boldsymbol{\omega}}_{B/N}]\mathbf{c} \quad (3.82)$$

Equation (3.82) is the translational motion equation and is the first EOM needed to describe the motion of the spacecraft. The following section develops the rotational EOM.

3.1.2.4 Rigid Spacecraft Hub Rotational Motion

Starting with Euler's equation when the body fixed coordinate frame origin is not coincident with the center of mass of the body[39]

$$\dot{\mathbf{H}}_{sc,B} = \mathbf{L}_B + m_{sc}\ddot{\mathbf{r}}_{B/N} \times \mathbf{c} \quad (3.83)$$

where \mathbf{L}_B is the total external torque about point B . The definition of the angular momentum vector of the spacecraft about point B is

$$\mathbf{H}_{sc,B} = [I_{hub,B_c}]\boldsymbol{\omega}_{B/N} + m_{hub}\mathbf{r}_{B_c/B} \times \dot{\mathbf{r}}_{B_c/B} + \sum_{j=1}^{N_P} m_j \mathbf{r}_{P_{c,j}/B} \times \dot{\mathbf{r}}_{P_{c,j}/B} \quad (3.84)$$

Now the inertial time derivative of Eq. (3.84) is taken and yields

$$\begin{aligned} \dot{\mathbf{H}}_{sc,B} = & [I_{hub,B_c}]\dot{\boldsymbol{\omega}}_{B/N} + \boldsymbol{\omega}_{B/N} \times [I_{hub,B_c}]\boldsymbol{\omega}_{B/N} + m_{hub}\mathbf{r}_{B_c/B} \times \ddot{\mathbf{r}}_{B_c/B} \\ & + \sum_{j=1}^{N_P} m_j \mathbf{r}_{P_{c,j}/B} \times \ddot{\mathbf{r}}_{P_{c,j}/B} \end{aligned} \quad (3.85)$$

The terms $\ddot{\mathbf{r}}_{B_c/B}$ and $\ddot{\mathbf{r}}_{P_{c,j}/B}$ are found using the transport theorem and knowing that $\mathbf{r}_{B_c/B}$ is fixed with respect to the body frame.

$$\ddot{\mathbf{r}}_{B_c/B} = \dot{\boldsymbol{\omega}}_{\mathcal{B}/\mathcal{N}} \times \mathbf{r}_{B_c/B} + \boldsymbol{\omega}_{\mathcal{B}/\mathcal{N}} \times (\boldsymbol{\omega}_{\mathcal{B}/\mathcal{N}} \times \mathbf{r}_{B_c/B}) \quad (3.86)$$

$$\ddot{\mathbf{r}}_{P_{c,j}/B} = \mathbf{r}''_{P_{c,j}/B} + 2\boldsymbol{\omega}_{\mathcal{B}/\mathcal{N}} \times \mathbf{r}'_{P_{c,j}/B} + \dot{\boldsymbol{\omega}}_{\mathcal{B}/\mathcal{N}} \times \mathbf{r}_{P_{c,j}/B} + \boldsymbol{\omega}_{\mathcal{B}/\mathcal{N}} \times (\boldsymbol{\omega}_{\mathcal{B}/\mathcal{N}} \times \mathbf{r}_{P_{c,j}/B}) \quad (3.87)$$

Incorporating Eqs. (3.86) - (3.87) into Eq. (3.85) results in

$$\begin{aligned} \dot{\mathbf{H}}_{sc,B} = & [I_{hub,B_c}] \dot{\boldsymbol{\omega}}_{\mathcal{B}/\mathcal{N}} + \boldsymbol{\omega}_{\mathcal{B}/\mathcal{N}} \times [I_{hub,B_c}] \boldsymbol{\omega}_{\mathcal{B}/\mathcal{N}} + m_{hub} \mathbf{r}_{B_c/B} \times (\dot{\boldsymbol{\omega}}_{\mathcal{B}/\mathcal{N}} \times \mathbf{r}_{B_c/B}) \\ & + m_{hub} \mathbf{r}_{B_c/B} \times \left[\boldsymbol{\omega}_{\mathcal{B}/\mathcal{N}} \times (\boldsymbol{\omega}_{\mathcal{B}/\mathcal{N}} \times \mathbf{r}_{B_c/B}) \right] + \sum_{j=1}^{N_P} m_j \mathbf{r}_{P_{c,j}/B} \times \left[\mathbf{r}''_{P_{c,j}/B} + 2\boldsymbol{\omega}_{\mathcal{B}/\mathcal{N}} \times \mathbf{r}'_{P_{c,j}/B} + \dot{\boldsymbol{\omega}}_{\mathcal{B}/\mathcal{N}} \times \mathbf{r}_{P_{c,j}/B} \right. \\ & \left. + \boldsymbol{\omega}_{\mathcal{B}/\mathcal{N}} \times (\boldsymbol{\omega}_{\mathcal{B}/\mathcal{N}} \times \mathbf{r}_{P_{c,j}/B}) \right] \quad (3.88) \end{aligned}$$

Applying the parallel axis theorem the following inertia tensor terms are defined as

$$[I_{hub,B}] = [I_{hub,B_c}] + m_{hub} [\tilde{\mathbf{r}}_{B_c/B}] [\tilde{\mathbf{r}}_{B_c/B}]^T \quad (3.89)$$

$$[I_{sc,B}] = [I_{hub,B}] + \sum_{j=1}^{N_P} m_j [\tilde{\mathbf{r}}_{P_{c,j}/B}] [\tilde{\mathbf{r}}_{P_{c,j}/B}]^T \quad (3.90)$$

Taking the body-relative time derivative of Equation (3.90) yields

$$[I'_{sc,B}] = - \sum_{j=1}^{N_P} m_j \left([\tilde{\mathbf{r}}'_{P_{c,j}/B}] [\tilde{\mathbf{r}}_{P_{c,j}/B}] + [\tilde{\mathbf{r}}_{P_{c,j}/B}] [\tilde{\mathbf{r}}'_{P_{c,j}/B}] \right) \quad (3.91)$$

Using Eq. (3.90) to simplify results in Eq. (3.92). The Jacobi Identity, $(\mathbf{a} \times \mathbf{b}) \times \mathbf{c} = \mathbf{a} \times (\mathbf{b} \times \mathbf{c}) - \mathbf{b} \times (\mathbf{a} \times \mathbf{c})$, is used to combine terms and produce the following simplified equation

$$\begin{aligned} \dot{\mathbf{H}}_{sc,B} = & [I_{sc,B}] \dot{\boldsymbol{\omega}}_{\mathcal{B}/\mathcal{N}} + \boldsymbol{\omega}_{\mathcal{B}/\mathcal{N}} \times [I_{sc,B}] \boldsymbol{\omega}_{\mathcal{B}/\mathcal{N}} + [I'_{sc,B}] \boldsymbol{\omega}_{\mathcal{B}/\mathcal{N}} + \sum_{j=1}^{N_P} \left[m_j \mathbf{r}_{P_{c,j}/B} \times \mathbf{r}''_{P_{c,j}/B} \right. \\ & \left. + m_j \boldsymbol{\omega}_{\mathcal{B}/\mathcal{N}} \times \left(\mathbf{r}_{P_{c,j}/B} \times \mathbf{r}'_{P_{c,j}/B} \right) \right] \quad (3.92) \end{aligned}$$

Eqs. (3.83) and (3.92) are equated and yield

$$\begin{aligned} \mathbf{L}_B + m_{sc} \dot{\mathbf{r}}_{B/N} \times \mathbf{c} = & [I_{sc,B}] \dot{\boldsymbol{\omega}}_{\mathcal{B}/\mathcal{N}} + \boldsymbol{\omega}_{\mathcal{B}/\mathcal{N}} \times [I_{sc,B}] \boldsymbol{\omega}_{\mathcal{B}/\mathcal{N}} + [I'_{sc,B}] \boldsymbol{\omega}_{\mathcal{B}/\mathcal{N}} + \sum_{j=1}^{N_P} \left[m_j \mathbf{r}_{P_{c,j}/B} \times \mathbf{r}''_{P_{c,j}/B} \right. \\ & \left. + m_j \boldsymbol{\omega}_{\mathcal{B}/\mathcal{N}} \times \left(\mathbf{r}_{P_{c,j}/B} \times \mathbf{r}'_{P_{c,j}/B} \right) \right] \quad (3.93) \end{aligned}$$

Finally, using tilde matrix and simplifying yields the modified Euler equation, which is the second EOM necessary to describe the motion of the spacecraft.

$$[I_{sc,B}]\dot{\boldsymbol{\omega}}_{B/N} = -[\tilde{\boldsymbol{\omega}}_{B/N}][I_{sc,B}]\boldsymbol{\omega}_{B/N} - [I'_{sc,B}]\boldsymbol{\omega}_{B/N} - \sum_{j=1}^{N_P} \left(m_j [\tilde{\mathbf{r}}_{P_{c,j}/B}] \mathbf{r}''_{P_{c,j}/B} + m_j [\tilde{\boldsymbol{\omega}}_{B/N}] [\tilde{\mathbf{r}}_{P_{c,j}/B}] \mathbf{r}'_{P_{c,j}/B} \right) + \mathbf{L}_B - m_{sc} [\tilde{\mathbf{c}}] \ddot{\mathbf{r}}_{B/N} \quad (3.94)$$

Rearranging Eq. (3.94) to be in the same form as the previous sections results in:

$$m_{sc} [\tilde{\mathbf{c}}] \ddot{\mathbf{r}}_{B/N} + [I_{sc,B}]\dot{\boldsymbol{\omega}}_{B/N} + \sum_{j=1}^{N_P} m_j [\tilde{\mathbf{r}}_{P_{c,j}/B}] \hat{\mathbf{p}}_j \ddot{\rho}_j = -[\tilde{\boldsymbol{\omega}}_{B/N}][I_{sc,B}]\boldsymbol{\omega}_{B/N} - [I'_{sc,B}]\boldsymbol{\omega}_{B/N} - \sum_{j=1}^{N_P} m_j [\tilde{\boldsymbol{\omega}}_{B/N}] [\tilde{\mathbf{r}}_{P_{c,j}/B}] \mathbf{r}'_{P_{c,j}/B} + \mathbf{L}_B \quad (3.95)$$

3.1.2.5 Fuel Slosh Motion

The fuel slosh motion is being approximated by a lumped mechanical multi-mode model[61, 62, 71]. Figure 3.9 shows that a single fuel slosh particle is free to move along its corresponding $\hat{\mathbf{p}}_j$ direction and this formulation is generalized to include N_P number of fuel slosh particles. The derivation begins with Newton's law for each fuel slosh particle:

$$m_j \ddot{\mathbf{r}}_{P_{c,j}/N} = \mathbf{F}_G + \mathbf{F}_C - k_j \rho_j \hat{\mathbf{p}}_j - c_j \dot{\rho}_j \hat{\mathbf{p}}_j \quad (3.96)$$

Where \mathbf{F}_G is the force of gravity and \mathbf{F}_C is the constraint force that maintains the fuel slosh mass to travel along the direction $\hat{\mathbf{p}}_j$. The forces due to the spring and damper are explicitly included in Eq. (3.96) and result in a restoring force and damping force. $\ddot{\mathbf{r}}_{P_{c,j}/N}$ is defined in the following equation.

$$\ddot{\mathbf{r}}_{P_{c,j}/N} = \ddot{\mathbf{r}}_{B/N} + \ddot{\mathbf{r}}_{P_{c,j}/B} \quad (3.97)$$

The inertial acceleration vector $\ddot{\mathbf{r}}_{P_{c,j}/B}$ is defined in Eq. (3.87). Plugging this definition into Eq. (3.96) results in

$$m_j \left[\ddot{\mathbf{r}}_{B/N} + \ddot{\rho}_j \hat{\mathbf{p}}_j + 2\boldsymbol{\omega}_{B/N} \times \mathbf{r}'_{P_{c,j}/B} + \dot{\boldsymbol{\omega}}_{B/N} \times \mathbf{r}_{P_{c,j}/B} + \boldsymbol{\omega}_{B/N} \times (\boldsymbol{\omega}_{B/N} \times \mathbf{r}_{P_{c,j}/B}) \right] = \mathbf{F}_G + \mathbf{F}_C - k_j \rho_j \hat{\mathbf{p}}_j - c_j \dot{\rho}_j \hat{\mathbf{p}}_j \quad (3.98)$$

Equation (3.98) is the dynamical equation for a fuel slosh particle, however, the constraint force, \mathbf{F}_C , is undefined. Since the fuel slosh particle is free to move in the $\hat{\mathbf{p}}_j$ direction, the component of \mathbf{F}_C along the $\hat{\mathbf{p}}_j$ direction is zero. Leveraging this insight, Eq. (3.98) is projected into the $\hat{\mathbf{p}}_j$ direction by multiplying both sides of the equation by $\hat{\mathbf{p}}_j^T$.

$$\begin{aligned} m_j \left(\hat{\mathbf{p}}_j^T \ddot{\mathbf{r}}_{B/N} + \ddot{\rho}_j + 2\hat{\mathbf{p}}_j^T \boldsymbol{\omega}_{B/N} \times \mathbf{r}'_{P_{c,j}/B} + \hat{\mathbf{p}}_j^T \dot{\boldsymbol{\omega}}_{B/N} \times \mathbf{r}_{P_{c,j}/B} + \hat{\mathbf{p}}_j^T \boldsymbol{\omega}_{B/N} \times (\boldsymbol{\omega}_{B/N} \times \mathbf{r}_{P_{c,j}/B}) \right) \\ = \hat{\mathbf{p}}_j^T \mathbf{F}_G - k_j \rho_j - c_j \dot{\rho}_j \end{aligned} \quad (3.99)$$

Moving the second order terms to the left hand side and introducing the tilde matrix notation yields the final equation needed to describe the motion of the spacecraft with fuel slosh. These EOMs match the generalized EOM form introduced in Section 2.

$$\begin{aligned} m_j \hat{\mathbf{p}}_j^T \ddot{\mathbf{r}}_{B/N} - m_j \hat{\mathbf{p}}_j^T [\tilde{\mathbf{r}}_{P_{c,j}/B}] \dot{\boldsymbol{\omega}}_{B/N} + m_j \ddot{\rho}_j \\ = \hat{\mathbf{p}}_j^T \mathbf{F}_G - k_j \rho_j - c_j \dot{\rho}_j - 2m_j \hat{\mathbf{p}}_j^T [\tilde{\boldsymbol{\omega}}_{B/N}] \mathbf{r}'_{P_{c,j}/B} - m_j \hat{\mathbf{p}}_j^T [\tilde{\boldsymbol{\omega}}_{B/N}] [\tilde{\boldsymbol{\omega}}_{B/N}] \mathbf{r}_{P_{c,j}/B} \end{aligned} \quad (3.100)$$

3.1.2.6 Back-substitution Method

The equations presented in the previous sections result in $N_P + 6$ coupled differential equations. Therefore, if the EOMs were placed into state space form, a system mass matrix of size $N_P + 6$ would need to be inverted to numerically integrate the EOMs. This can result in a computationally expensive simulation. In the following section, the EOMs are manipulated to fit the form of the back-substitution method seen in Section 2.3.

First, the slosh equation is manipulated to isolate the slosh acceleration to the left hand side of the equation:

$$\begin{aligned} \ddot{\rho}_j = \frac{1}{m_j} \left(-m_j \hat{\mathbf{p}}_j^T \ddot{\mathbf{r}}_{B/N} + m_j \hat{\mathbf{p}}_j^T [\tilde{\mathbf{r}}_{P_{c,j}/B}] \dot{\boldsymbol{\omega}}_{B/N} \right. \\ \left. + \hat{\mathbf{p}}_j^T \mathbf{F}_G - k_j \rho_j - c_j \dot{\rho}_j - 2m_j \hat{\mathbf{p}}_j^T [\tilde{\boldsymbol{\omega}}_{B/N}] \mathbf{r}'_{P_{c,j}/B} - m_j \hat{\mathbf{p}}_j^T [\tilde{\boldsymbol{\omega}}_{B/N}] [\tilde{\boldsymbol{\omega}}_{B/N}] \mathbf{r}_{P_{c,j}/B} \right) \end{aligned} \quad (3.101)$$

The equation is placed in a more compact form

$$\ddot{\rho}_j = \mathbf{a}_{\rho_j}^T \ddot{\mathbf{r}}_{B/N} + \mathbf{b}_{\rho_j}^T \dot{\boldsymbol{\omega}}_{B/N} + c_{\rho_j} \quad (3.102)$$

while utilizing the variables defined in the following equations:

$$\mathbf{a}_{\rho_j} = -\hat{\mathbf{p}}_j \quad (3.103)$$

$$\mathbf{b}_{\rho_j} = -[\tilde{\mathbf{r}}_{P_{c,j}/B}] \hat{\mathbf{p}}_j \quad (3.104)$$

$$c_{\rho_j} = \frac{1}{m_j} \left(\hat{\mathbf{p}}_j^T \mathbf{F}_G - k_j \rho_j - c_j \dot{\rho}_j - 2m_j \hat{\mathbf{p}}_j^T [\tilde{\boldsymbol{\omega}}_{B/N}] \mathbf{r}'_{P_{c,j}/B} - m_j \hat{\mathbf{p}}_j^T [\tilde{\boldsymbol{\omega}}_{B/N}] [\tilde{\boldsymbol{\omega}}_{B/N}] \mathbf{r}_{P_{c,j}/B} \right) \quad (3.105)$$

To decouple the translational EOM from the slosh equation, Eq. (3.102) is substituted into Eq (3.82) resulting in

$$\begin{aligned} \ddot{\mathbf{r}}_{B/N} - [\tilde{\mathbf{c}}] \dot{\boldsymbol{\omega}}_{B/N} + \frac{1}{m_{sc}} \sum_{j=1}^{N_P} m_j \hat{\mathbf{p}}_j \left(\mathbf{a}_{\rho_j}^T \ddot{\mathbf{r}}_{B/N} + \mathbf{b}_{\rho_j}^T \dot{\boldsymbol{\omega}}_{B/N} + c_{\rho_j} \right) &= \ddot{\mathbf{r}}_{C/N} - 2[\tilde{\boldsymbol{\omega}}_{B/N}] \mathbf{c}' \\ &- [\tilde{\boldsymbol{\omega}}_{B/N}] [\tilde{\boldsymbol{\omega}}_{B/N}] \mathbf{c} \end{aligned} \quad (3.106)$$

Simplifying this result and multiplying both sides by m_{sc} yields

$$\begin{aligned} \left(m_{sc} [I_{3 \times 3}] + \sum_{j=1}^{N_P} m_j \hat{\mathbf{p}}_j \mathbf{a}_{\rho_j}^T \right) \ddot{\mathbf{r}}_{B/N} + \left(-m_{sc} [\tilde{\mathbf{c}}] + \sum_{j=1}^{N_P} m_j \hat{\mathbf{p}}_j \mathbf{b}_{\rho_j}^T \right) \dot{\boldsymbol{\omega}}_{B/N} \\ = m_{sc} \ddot{\mathbf{r}}_{C/N} - 2m_{sc} [\tilde{\boldsymbol{\omega}}_{B/N}] \mathbf{c}' - m_{sc} [\tilde{\boldsymbol{\omega}}_{B/N}] [\tilde{\boldsymbol{\omega}}_{B/N}] \mathbf{c} - \sum_{j=1}^{N_P} m_j c_{\rho_j} \hat{\mathbf{p}}_j \end{aligned} \quad (3.107)$$

Following a similar pattern for the rotational dynamics, the slosh equation is plugged into the rotational EOM of the spacecraft and yields

$$\begin{aligned} m_{sc} [\tilde{\mathbf{c}}] \ddot{\mathbf{r}}_{B/N} + [I_{sc,B}] \dot{\boldsymbol{\omega}}_{B/N} + \sum_{j=1}^{N_P} m_j [\tilde{\mathbf{r}}_{P_{c,j}/B}] \hat{\mathbf{p}}_j \left(\mathbf{a}_{\rho_j}^T \ddot{\mathbf{r}}_{B/N} + \mathbf{b}_{\rho_j}^T \dot{\boldsymbol{\omega}}_{B/N} + c_{\rho_j} \right) = \\ - [\tilde{\boldsymbol{\omega}}_{B/N}] [I_{sc,B}] \boldsymbol{\omega}_{B/N} - [I'_{sc,B}] \boldsymbol{\omega}_{B/N} - \sum_{j=1}^{N_P} m_j [\tilde{\boldsymbol{\omega}}_{B/N}] [\tilde{\mathbf{r}}_{P_{c,j}/B}] \mathbf{r}'_{P_{c,j}/B} + \mathbf{L}_B \end{aligned} \quad (3.108)$$

Combining like terms and rearranging the equation to fit the back-substitution method form results

in the following equation:

$$\begin{aligned} \left[m_{sc}[\tilde{\mathbf{c}}] + \sum_{j=1}^{N_P} m_j [\tilde{\mathbf{r}}_{P_{c,j}/B}] \hat{\mathbf{p}}_j \mathbf{a}_{\rho_j}^T \right] \ddot{\mathbf{r}}_{B/N} + \left[[I_{sc,B}] + \sum_{j=1}^{N_P} m_j [\tilde{\mathbf{r}}_{P_{c,j}/B}] \hat{\mathbf{p}}_j \mathbf{b}_{\rho_j}^T \right] \dot{\boldsymbol{\omega}}_{B/N} = -[\tilde{\boldsymbol{\omega}}_{B/N}] [I_{sc,B}] \boldsymbol{\omega}_{B/N} \\ - [I'_{sc,B}] \boldsymbol{\omega}_{B/N} - \sum_{j=1}^{N_P} \left(m_j [\tilde{\boldsymbol{\omega}}_{B/N}] [\tilde{\mathbf{r}}_{P_{c,j}/B}] \mathbf{r}'_{P_{c,j}/B} + m_j c_{\rho_j} [\tilde{\mathbf{r}}_{P_{c,j}/B}] \hat{\mathbf{p}}_j \right) + \mathbf{L}_B \end{aligned} \quad (3.109)$$

Finally, the back-substitution matrices are defined in the following equations:

$$[A] = m_{sc} [I_{3 \times 3}] + \sum_{j=1}^{N_P} m_j \hat{\mathbf{p}}_j \mathbf{a}_{\rho_j}^T \quad (3.110)$$

$$[B] = -m_{sc} [\tilde{\mathbf{c}}] + \sum_{j=1}^{N_P} m_j \hat{\mathbf{p}}_j \mathbf{b}_{\rho_j}^T \quad (3.111)$$

$$[C] = m_{sc} [\tilde{\mathbf{c}}] + \sum_{j=1}^{N_P} m_j [\tilde{\mathbf{r}}_{P_{c,j}/B}] \hat{\mathbf{p}}_j \mathbf{a}_{\rho_j}^T \quad (3.112)$$

$$[D] = [I_{sc,B}] + \sum_{j=1}^{N_P} m_j [\tilde{\mathbf{r}}_{P_{c,j}/B}] \hat{\mathbf{p}}_j \mathbf{b}_{\rho_j}^T \quad (3.113)$$

$$\mathbf{v}_{\text{trans}} = m_{sc} \ddot{\mathbf{r}}_{C/N} - 2m_{sc} [\tilde{\boldsymbol{\omega}}_{B/N}] \mathbf{c}' - m_{sc} [\tilde{\boldsymbol{\omega}}_{B/N}] [\tilde{\boldsymbol{\omega}}_{B/N}] \mathbf{c} - \sum_{j=1}^{N_P} m_j c_{\rho_j} \hat{\mathbf{p}}_j \quad (3.114)$$

$$\begin{aligned} \mathbf{v}_{\text{rot}} = -[\tilde{\boldsymbol{\omega}}_{B/N}] [I_{sc,B}] \boldsymbol{\omega}_{B/N} - [I'_{sc,B}] \boldsymbol{\omega}_{B/N} \\ - \sum_{j=1}^{N_P} \left(m_j [\tilde{\boldsymbol{\omega}}_{B/N}] [\tilde{\mathbf{r}}_{P_{c,j}/B}] \mathbf{r}'_{P_{c,j}/B} + m_j c_{\rho_j} [\tilde{\mathbf{r}}_{P_{c,j}/B}] \hat{\mathbf{p}}_j \right) + \mathbf{L}_B \end{aligned} \quad (3.115)$$

This completes the necessary definitions to describe the motion of a spacecraft approximating the sloshing fuel with the lumped mass spring mass damper model. These equations fit the generalized EOM form introduced in Section 2 and can be readily implemented in software. Numerical simulations of this model can be seen in Section 6.4.

3.1.3 Imbalanced Reaction Wheels

3.1.3.1 Introduction

Momentum exchange devices are a fundamental component of most spacecraft for both coarse attitude control and precision pointing. Many modern spacecraft include three or more reaction wheels (RWs), which consist of a flywheel attached to a motor and bearing fixed to the spacecraft. A challenge to using RWs is that they may induce jitter due to mass imbalances in the RW. Characterization and mitigation of RW induced jitter on a spacecraft is important to many missions due to the increasingly rigorous attitude stability requirements and the necessity of avoiding excitation of the spacecraft's structural modes. Excessive vibration of a spacecraft may be detrimental to its instruments and operation. Additionally, many instruments require the spacecraft to be held extremely steady in order to effectively operate or collect data. Optical instruments in particular often require attitude stability of less than one arc-second per second in order to avoid optical smear or similar effects [72, 73]. Vibration isolation has long been a method of dulling the effects of wheel jitter [74]. Various methods of vibration isolation have been proposed, including magnetic suspension of RWs as a means of circumventing the jitter problem [75, 76].

RW induced vibration on a spacecraft is usually characterized through experimentation prior to flight in order to validate requirements. Empirical models of RWs allow static and dynamic imbalance parameters to be extracted [77]. In addition to experimental demonstration of RW performance on an integrated spacecraft, it is of interest to use an analytic model of a RW for simulation in the early stages of spacecraft development. A popular simplified model of RW jitter involves including forces and torques resulting from RW static and dynamic imbalances as external disturbances [78, 79, 74]. Static imbalance is when the center of mass of the reaction wheel is not coincident with the spin axis, and dynamic imbalance is due to off-diagonal inertia matrix terms with respect to the spin axis frame. This model is well established and attractive due to its low computational requirements – force and torque of jitter are simply proportional to wheel speed squared. Furthermore, the simplified formulation allows a model to be constructed directly from

the typical RW manufacturer imbalance specifications: static imbalance and dynamic imbalance. This allows RW mass imbalances to be implemented as lumped parameters instead of using specific terms such as RW center of mass location and inertia tensor [74]. Previous literature puts emphasis on empirical modeling of RW jitter and the effects of RW jitter within context of spacecraft flexible dynamics [80, 81, 82].

Regarding modeling the momentum exchange device jitter with a first-principles approach, Zhang and Zhang discuss a fully-coupled model of control moment gyro (CMG) imbalance[83]. While this contains gyro frame imbalance modeling not required for RWs, the results are presented without a full derivation and the paper does not provide the complete system equations of motion. This partial imbalanced momentum exchange device results also does not discuss how to tie typical manufacturers' imbalance specifications directly to the imbalance parameter modeling. Reference [76] develops the spacecraft equations of motion with magnetically suspended RWs where the RW center of mass moves relative to the body. However, this magnetic levitation introduces additional degrees of freedom and modeling challenges not present in a body-locked imbalanced RW as studied in this dissertation.

The simplified model for representing RW jitter due to static and dynamic imbalances is not physically realistic due to the nonconservative nature of adding a system-internal forcing effect as an external disturbance [39]. The resulting model only considers the impact of the wheel onto the spacecraft, but neglects how the spacecraft impacts the wheel motion. The resulting one-way coupled simplified model has the primary benefits of algebraic simplicity of the jitter equations and the associated fast computational evaluation. For spacecraft dynamics analysis purposes the non-physical nature of the simplified model does not necessarily present a problem if the RWs are well balanced with respect to the overall size of the spacecraft. However, depending on the quality of the reaction wheel balance in relation to the spacecraft size this approach may become problematic. Furthermore, the simplified model does not allow for energy and momentum code validation checks. When verifying the computer simulation code the spacecraft energy and momentum checks are critical tools of the dynamics validation process. Even for a spacecraft simulation that only includes

RW jitter, complete verification of the model is difficult because without energy and momentum checks a truth model is difficult to create. If the model of the spacecraft has other complex behaviors such as solar panel flexing or fuel slosh, the importance of energy and momentum checks increases rapidly. The coupled nature of these complex spacecraft systems results in severe challenges with debugging and verification. The energy and momentum checks become essential in this process.

An offset in the center of mass of the RW from the spin axis, denoted static imbalance, results in an internal force and torque on the spacecraft. An asymmetric distribution of mass about the RW spin axis is denoted as the dynamic imbalance and produces an internal disturbance torque onto the spacecraft. Figure 3.4 explains these imbalances geometrically. I_p is a line that is coincident with the center mass of the RW and illustrates a principal axis of the RW. The static imbalance results in a center of mass offset of the RW but does not change the direction of the principal axes. The dynamic imbalance is result of the principal axes not being aligned with the spin axis. Deflection of the RW wheel bearing due to static and dynamic imbalances further affects the vibrational modes of the system, however, this effect is beyond the scope of this work and is not being considered. This dissertation investigates modeling these classical static and dynamic imbalance behaviors in a first-principles based approach. With this jitter model the RW is still treated as a rigid component with a body-fixed rotation axis, but the rotation axis is not necessarily aligned with the RW principle axes, and the RW center of mass is off-set from this rotation axis by a distance d_i .

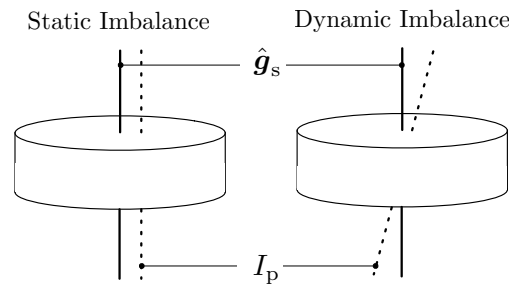


Figure 3.4: Reaction wheel static and dynamic imbalance.

When deriving the equations of motion (EOMs) for a spacecraft with N_{RW} reaction wheels,

an important assumption is made in that the reaction wheels are symmetric and results in the EOMs to be simplified to a convenient and compact form [39]. However, if the reaction wheels are imbalanced the EOMs have to be re-derived to account for the fully-coupled dynamics between the RWs and the spacecraft. This dissertation follows a development path using Newtonian and Eulerian mechanics using a formulation that uses a minimal coordinate description [39].

3.1.3.2 Problem Statement

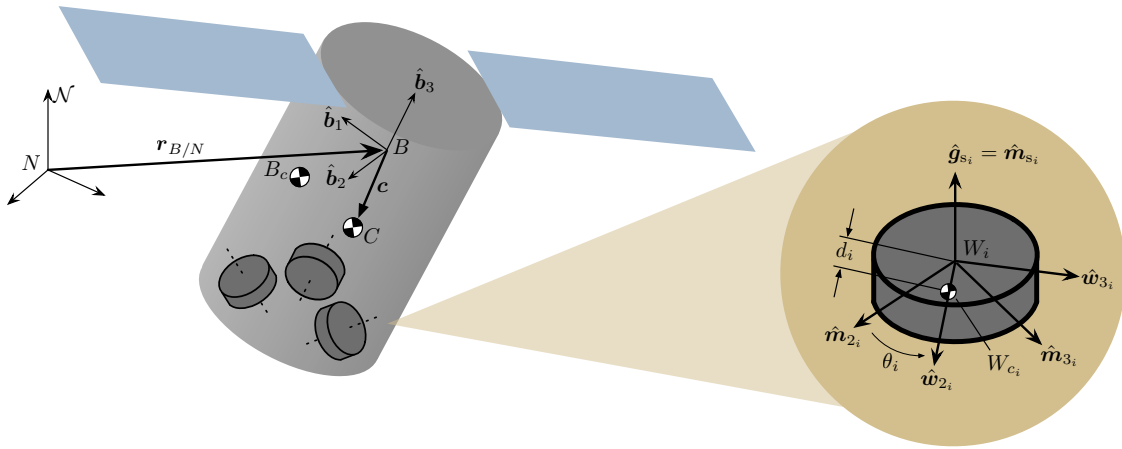


Figure 3.5: Reference frame and variable definitions.

Figure 3.5 shows the frame and variable definitions used for this problem. The formulation involves a rigid hub with its center of mass location labeled as point B_c , and N_{RW} RWs with their center of mass locations labeled as W_{c_i} . The frames being used for this formulation are the body-fixed frame, $\mathcal{B} : \{\hat{b}_1, \hat{b}_2, \hat{b}_3\}$, the motor frame of the i^{th} RW, $\mathcal{M}_i : \{\hat{m}_{s_i}, \hat{m}_{2_i}, \hat{m}_{3_i}\}$ which is also body-fixed, and the wheel-fixed frame of the i^{th} RW, $\mathcal{W}_i : \{\hat{g}_{s_i}, \hat{w}_{2_i}, \hat{w}_{3_i}\}$. The dynamics are modeled with respect to the \mathcal{B} frame which can be generally oriented. The \mathcal{W}_i frame is oriented such that the \hat{g}_{s_i} axis is aligned with the RW spin axis which is the same as the motor torque axis \hat{m}_{s_i} , the \hat{w}_{2_i} axis is perpendicular to \hat{g}_{s_i} and points in the direction towards the RW center of mass W_{c_i} . The \hat{w}_{3_i} completes the right hand rule. The \mathcal{M}_i frame is defined as being equal to the

\mathcal{W}_i frame at the beginning of the simulation and therefore the \mathcal{W}_i and \mathcal{M}_i frames are offset by an angle, θ_i , about the $\hat{\mathbf{m}}_{s_i} = \hat{\mathbf{g}}_{s_i}$ axes.

A few more key variables in Figure 3.5 need to be defined. The rigid spacecraft structure without the RWs is called the hub. Point B is the origin of the \mathcal{B} frame and is a general body-fixed point that does not have to be identical to the total spacecraft center of mass, nor the rigid hub center of mass B_c . Point W_i is the origin of the \mathcal{W}_i frame and can also have any location relative to point B . Point C is the center of mass of the total spacecraft system including the rigid hub and the RWs. Due to the RW imbalance, the vector \mathbf{c} , which points from point B to point C , will vary as seen by a body-fixed observer. The scalar variable d_i is the center of mass offset of the RW, or the distance from the spin axis, $\hat{\mathbf{g}}_{s_i}$ to W_{c_i} . Finally, the inertial frame orientation is defined through $\mathcal{N} : \{\hat{\mathbf{n}}_1, \hat{\mathbf{n}}_2, \hat{\mathbf{n}}_3\}$, while the origin of the inertial frame is labeled as N .

3.1.3.3 Balanced Reaction Wheel Discussion

Before showing the EOMs of a spacecraft with imbalanced reaction wheels, it is useful to explain how the commonly seen EOMs of balanced reaction wheels fit into the generalized EOM form and the back-substitution method. The equations of motion of a balanced reaction wheel are provided in Reference [39] and are slightly modified to adhere to the standard form seen in Section 2. Since a balanced reaction wheel does not change the center of mass location of the spacecraft, the translational equation of motion is not coupled with $\dot{\Omega}$ as shown below:

$$m_{sc}[I_{3 \times 3}]\ddot{\mathbf{r}}_{B/N} - m_{sc}[\tilde{\mathbf{c}}]\dot{\boldsymbol{\omega}}_{B/N} = \mathbf{F}_{ext} - 2m_{sc}[\tilde{\boldsymbol{\omega}}_{B/N}]\mathbf{c}' - m_{sc}[\tilde{\boldsymbol{\omega}}_{B/N}][\tilde{\boldsymbol{\omega}}_{B/N}]\mathbf{c} \quad (3.116)$$

The rotational equation of motion includes $\dot{\Omega}$ terms, and is thus coupled with the wheel motion as seen in the following equation:

$$m_{sc}[\tilde{\mathbf{c}}]\ddot{\mathbf{r}}_{B/N} + [I_{sc,B}]\dot{\boldsymbol{\omega}}_{B/N} + \sum_{i=1}^{N_{rw}} J_{s_i} \hat{\mathbf{g}}_{s_i} \dot{\Omega}_i = -[\tilde{\boldsymbol{\omega}}_{B/N}][I_{sc,B}]\boldsymbol{\omega}_{B/N} - \sum_{i=1}^{N_{rw}} (\boldsymbol{\omega}_{B/N} \times J_{s_i} \Omega_i \hat{\mathbf{g}}_{s_i}) + \mathbf{L}_B \quad (3.117)$$

The motor torque equation is coupled with $\dot{\boldsymbol{\omega}}_{\mathcal{B}/\mathcal{N}}$ as shown below.

$$\dot{\Omega}_i = \frac{u_{s_i}}{J_{s_i}} - \hat{\mathbf{g}}_{s_i}^T \dot{\boldsymbol{\omega}}_{\mathcal{B}/\mathcal{N}} \quad (3.118)$$

3.1.3.4 Back-Substitution Derivation

Since translation is not coupled with wheel speed, the back-substitution equation may be obtained readily following the same method used in the prior derivations:

$$m_{sc}[\tilde{\mathbf{c}}]\ddot{\mathbf{r}}_{\mathcal{B}/\mathcal{N}} + ([I_{sc,B}] - \sum_{i=1}^{N_{rw}} J_{s_i} \hat{\mathbf{g}}_{s_i} \hat{\mathbf{g}}_{s_i}^T) \dot{\boldsymbol{\omega}}_{\mathcal{B}/\mathcal{N}} = -[\tilde{\boldsymbol{\omega}}_{\mathcal{B}/\mathcal{N}}][I_{sc,B}]\boldsymbol{\omega}_{\mathcal{B}/\mathcal{N}} - \sum_{i=1}^{N_{rw}} (\hat{\mathbf{g}}_{s_i} u_{s_i} + \boldsymbol{\omega}_{\mathcal{B}/\mathcal{N}} \times J_{s_i} \Omega_i \hat{\mathbf{g}}_{s_i}) - [I'_{sc,B}]\boldsymbol{\omega}_{\mathcal{B}/\mathcal{N}} + \mathbf{L}_B \quad (3.119)$$

The back-substitution matrices can quickly be defined for balanced reaction wheels seen in the following equations:

$$[A] = m_{sc}[I_{3 \times 3}] \quad (3.120)$$

$$[B] = -m_{sc}[\tilde{\mathbf{c}}] \quad (3.121)$$

$$[C] = m_{sc}[\tilde{\mathbf{c}}] \quad (3.122)$$

$$[D] = [I_{sc,B}] - \sum_{i=1}^N J_{s_i} \hat{\mathbf{g}}_{s_i} \hat{\mathbf{g}}_{s_i}^T \quad (3.123)$$

$$\mathbf{v}_{trans} = \mathbf{F}_{ext} - 2m_{sc}[\tilde{\boldsymbol{\omega}}_{\mathcal{B}/\mathcal{N}}]\mathbf{c}' - m_{sc}[\tilde{\boldsymbol{\omega}}_{\mathcal{B}/\mathcal{N}}][\tilde{\boldsymbol{\omega}}_{\mathcal{B}/\mathcal{N}}]\mathbf{c} \quad (3.124)$$

$$\mathbf{v}_{rot} = -[\tilde{\boldsymbol{\omega}}_{\mathcal{B}/\mathcal{N}}][I_{sc,B}]\boldsymbol{\omega}_{\mathcal{B}/\mathcal{N}} - \sum_{i=1}^{N_{rw}} (\hat{\mathbf{g}}_{s_i} u_{s_i} + \boldsymbol{\omega}_{\mathcal{B}/\mathcal{N}} \times J_{s_i} \Omega_i \hat{\mathbf{g}}_{s_i}) - [I'_{sc,B}]\boldsymbol{\omega}_{\mathcal{B}/\mathcal{N}} + \mathbf{L}_B \quad (3.125)$$

This concludes the necessary definitions for balanced reaction wheels and shows that the only contributions from RWs to the back-substitution matrices are to the $[D]$ and \mathbf{v}_{rot} matrices. This agrees with intuition since balanced reaction wheels do not change the mass properties of the spacecraft and therefore only affect the rotational dynamics EOMs.

3.1.3.5 Imbalanced Reaction Wheel Back-Substitution

The derivation of equations of motion of an imbalanced reaction wheel can be seen in Reference [84], and the EOMs are repeated here for the reader's convenience. The translational equation

of motion is

$$\begin{aligned} \ddot{\mathbf{r}}_{B/N} - [\tilde{\mathbf{c}}]\dot{\boldsymbol{\omega}}_{B/N} + \frac{1}{m_{sc}} \sum_{i=1}^{N_{RW}} m_{r_{w_i}} d_i \hat{\mathbf{w}}_{3_i} \dot{\Omega}_i = \ddot{\mathbf{r}}_{C/N} - 2[\tilde{\boldsymbol{\omega}}_{B/N}]\mathbf{c}' - [\tilde{\boldsymbol{\omega}}_{B/N}][\tilde{\boldsymbol{\omega}}_{B/N}]\mathbf{c} \\ + \frac{1}{m_{sc}} \sum_{i=1}^{N_{RW}} m_{r_{w_i}} d_i \Omega_i^2 \hat{\mathbf{w}}_{2_i} \end{aligned} \quad (3.126)$$

The rotational equation of motion can be seen in the following equation:

$$\begin{aligned} m_{sc}[\tilde{\mathbf{c}}]\ddot{\mathbf{r}}_{B/N} + [I_{sc,B}]\dot{\boldsymbol{\omega}}_{B/N} + \sum_{i=1}^{N_{RW}} \left([I_{r_{w_i}, W_{c_i}}]\hat{\mathbf{g}}_{s_i} + m_{r_{w_i}} d_i [\tilde{\mathbf{r}}_{W_{c_i}/B}]\hat{\mathbf{w}}_{3_i} \right) \dot{\Omega}_i \\ = \sum_{i=1}^{N_{RW}} \left[m_{r_{w_i}} [\tilde{\mathbf{r}}_{W_{c_i}/B}] d_i \Omega_i^2 \hat{\mathbf{w}}_{2_i} - [I_{r_{w_i}, W_{c_i}}]' \Omega_i \hat{\mathbf{g}}_{s_i} - [\tilde{\boldsymbol{\omega}}_{B/N}] \left([I_{r_{w_i}, W_{c_i}}] \Omega_i \hat{\mathbf{g}}_{s_i} + m_{r_{w_i}} [\tilde{\mathbf{r}}_{W_{c_i}/B}] \mathbf{r}'_{W_{c_i}/B} \right) \right] \\ - [\tilde{\boldsymbol{\omega}}_{B/N}][I_{sc,B}]\boldsymbol{\omega}_{B/N} - [I_{sc,B}]\boldsymbol{\omega}_{B/N} + \mathbf{L}_B \end{aligned} \quad (3.127)$$

The motor torque equation is as follows

$$\begin{aligned} [m_{r_{w_i}} d_i \hat{\mathbf{w}}_{3_i}^T] \ddot{\mathbf{r}}_{B/N} + [(J_{11_i} + m_{r_{w_i}} d_i^2) \hat{\mathbf{g}}_{s_i}^T + J_{13_i} \hat{\mathbf{w}}_{3_i}^T - m_{r_{w_i}} d_i \hat{\mathbf{w}}_{3_i}^T [\tilde{\mathbf{r}}_{W_i/B}]] \dot{\boldsymbol{\omega}}_{B/N} + [J_{11_i} + m_{r_{w_i}} d_i^2] \dot{\Omega}_i \\ = -J_{13_i} \omega_{w_2} \omega_{s_i} + \omega_{w_2} \omega_{w_3} (J_{22_i} - J_{33_i} - m_{r_{w_i}} d_i^2) - m_{r_{w_i}} d_i \hat{\mathbf{w}}_{3_i}^T [\tilde{\boldsymbol{\omega}}_{B/N}] [\tilde{\boldsymbol{\omega}}_{B/N}] \mathbf{r}_{W_i/B} + u_{s_i} + \hat{\mathbf{g}}_{s_i}^T \boldsymbol{\tau}_{ext,i} \end{aligned} \quad (3.128)$$

These equations conform to the standard EOM form as seen in Section 2.

The back-substitution method derivation starts by solving for $\dot{\Omega}_i$ in the motor torque equation:

$$\begin{aligned} \dot{\Omega}_i = - \left(\frac{m_{r_{w_i}} d_i \hat{\mathbf{w}}_{3_i}^T}{J_{11_i} + m_{r_{w_i}} d_i^2} \right) \ddot{\mathbf{r}}_{B/N} - \frac{1}{J_{11_i} + m_{r_{w_i}} d_i^2} [(J_{11_i} + m_{r_{w_i}} d_i^2) \hat{\mathbf{g}}_{s_i}^T \\ + J_{13_i} \hat{\mathbf{w}}_{3_i}^T - m_{r_{w_i}} d_i \hat{\mathbf{w}}_{3_i}^T [\tilde{\mathbf{r}}_{W_i/B}]] \dot{\boldsymbol{\omega}}_{B/N} + \frac{1}{J_{11_i} + m_{r_{w_i}} d_i^2} \left(\omega_{w_2} \omega_{w_3} (J_{22_i} \right. \\ \left. - J_{33_i} - m_{r_{w_i}} d_i^2) - J_{13_i} \omega_{w_2} \omega_{s_i} - m_{r_{w_i}} d_i \hat{\mathbf{w}}_{3_i}^T [\tilde{\boldsymbol{\omega}}_{B/N}] [\tilde{\boldsymbol{\omega}}_{B/N}] \mathbf{r}_{W_i/B} + u_{s_i} \right) \end{aligned} \quad (3.129)$$

The following coefficients are defined and are used to de-clutter the final equations.

$$\mathbf{a}_{\Omega_i} = - \frac{m_{r_{w_i}} d_i}{J_{11_i} + m_{r_{w_i}} d_i^2} \hat{\mathbf{w}}_{3_i} \quad (3.130)$$

$$\mathbf{b}_{\Omega_i} = - \frac{1}{J_{11_i} + m_{r_{w_i}} d_i^2} [(J_{11_i} + m_{r_{w_i}} d_i^2) \hat{\mathbf{g}}_{s_i} + J_{13_i} \hat{\mathbf{w}}_{3_i} + m_{r_{w_i}} d_i [\tilde{\mathbf{r}}_{W_i/B}] \hat{\mathbf{w}}_{3_i}] \quad (3.131)$$

$$c_{\Omega_i} = \frac{1}{J_{11_i} + m_{r_{w_i}} d_i^2} \left(\omega_{w_{2_i}} \omega_{w_{3_i}} (J_{22_i} - J_{33_i} - m_{r_{w_i}} d_i^2) - J_{13_i} \omega_{w_{2_i}} \omega_{s_i} \right. \\ \left. - m_{r_{w_i}} d_i \hat{\boldsymbol{w}}_{3_i}^T [\tilde{\boldsymbol{\omega}}_{\mathcal{B}/\mathcal{N}}] [\tilde{\boldsymbol{\omega}}_{\mathcal{B}/\mathcal{N}}] \boldsymbol{r}_{W_i/B} + u_{s_i} + \hat{\boldsymbol{g}}_{s_i}^T \boldsymbol{\tau}_{ext,i} \right) \quad (3.132)$$

Writing the equation to fit the compact form seen in Eq 2.4 yields:

$$\dot{\Omega}_i = \boldsymbol{a}_{\Omega_i}^T \ddot{\boldsymbol{r}}_{B/N} + \boldsymbol{b}_{\Omega_i}^T \dot{\boldsymbol{\omega}}_{\mathcal{B}/\mathcal{N}} + c_{\Omega_i} \quad (3.133)$$

Plugging in the equation into the translational EOM, rearranging and multiplying both sides by m_{sc} yields:

$$\left[m_{sc} [I_{3 \times 3}] + \sum_{i=1}^{N_{RW}} m_{r_{w_i}} d_i \hat{\boldsymbol{w}}_{3_i} \boldsymbol{a}_{\Omega_i}^T \right] \ddot{\boldsymbol{r}}_{B/N} + \left[-m_{sc} [\tilde{\boldsymbol{c}}] + \sum_{i=1}^{N_{RW}} m_{r_{w_i}} d_i \hat{\boldsymbol{w}}_{3_i} \boldsymbol{b}_{\Omega_i}^T \right] \dot{\boldsymbol{\omega}}_{\mathcal{B}/\mathcal{N}} \\ = \boldsymbol{F}_{ext} - 2m_{sc} [\tilde{\boldsymbol{\omega}}_{\mathcal{B}/\mathcal{N}}] \boldsymbol{c}' - m_{sc} [\tilde{\boldsymbol{\omega}}_{\mathcal{B}/\mathcal{N}}] [\tilde{\boldsymbol{\omega}}_{\mathcal{B}/\mathcal{N}}] \boldsymbol{c} + \sum_{i=1}^{N_{RW}} \left[m_{r_{w_i}} d_i \Omega_i^2 \hat{\boldsymbol{w}}_{2_i} - m_{r_{w_i}} d_i c_{\Omega_i} \hat{\boldsymbol{w}}_{3_i} \right] \quad (3.134)$$

Eq. (3.134) is the de-coupled translational equation for the back-substitution method. Following the same steps as before, the de-coupled rotational EOM for imbalanced reaction wheels can be seen in the following equation.

$$\left[m_{sc} [\tilde{\boldsymbol{c}}] + \sum_{i=1}^{N_{RW}} \left([I_{r_{w_i}, W_{c_i}}] \hat{\boldsymbol{g}}_{s_i} + m_{r_{w_i}} d_i [\tilde{\boldsymbol{r}}_{W_{c_i}/B}] \hat{\boldsymbol{w}}_{3_i} \right) \boldsymbol{a}_{\Omega_i}^T \right] \ddot{\boldsymbol{r}}_{B/N} \\ + \left[[I_{sc,B}] + \sum_{i=1}^{N_{RW}} \left([I_{r_{w_i}, W_{c_i}}] \hat{\boldsymbol{g}}_{s_i} + m_{r_{w_i}} d_i [\tilde{\boldsymbol{r}}_{W_{c_i}/B}] \hat{\boldsymbol{w}}_{3_i} \right) \boldsymbol{b}_{\Omega_i}^T \right] \dot{\boldsymbol{\omega}}_{\mathcal{B}/\mathcal{N}} \\ = -[\tilde{\boldsymbol{\omega}}_{\mathcal{B}/\mathcal{N}}] [I_{sc,B}] \boldsymbol{\omega}_{\mathcal{B}/\mathcal{N}} - [I_{sc,B}]' \boldsymbol{\omega}_{\mathcal{B}/\mathcal{N}} + \boldsymbol{L}_B \\ + \sum_{i=1}^{N_{RW}} \left[m_{r_{w_i}} [\tilde{\boldsymbol{r}}_{W_{c_i}/B}] d_i \Omega_i^2 \hat{\boldsymbol{w}}_{2_i} - [I_{r_{w_i}, W_{c_i}}]' \Omega_i \hat{\boldsymbol{g}}_{s_i} - [\tilde{\boldsymbol{\omega}}_{\mathcal{B}/\mathcal{N}}] \left([I_{r_{w_i}, W_{c_i}}] \Omega_i \hat{\boldsymbol{g}}_{s_i} + m_{r_{w_i}} [\tilde{\boldsymbol{r}}_{W_{c_i}/B}] \boldsymbol{r}'_{W_{c_i}/B} \right) \right. \\ \left. - \left([I_{r_{w_i}, W_{c_i}}] \hat{\boldsymbol{g}}_{s_i} + m_{r_{w_i}} d_i [\tilde{\boldsymbol{r}}_{W_{c_i}/B}] \hat{\boldsymbol{w}}_{3_i} \right) c_{\Omega_i} \right] \quad (3.135)$$

All of the information needed to define the back-substitution matrices for imbalanced reaction wheels has been found. The imbalanced reaction wheel back-substitution matrices are given by,

$$[A] = m_{sc}[I_{3 \times 3}] + \sum_{i=1}^{N_{RW}} m_{rw_i} d_i \hat{\mathbf{w}}_{3_i} \mathbf{a}_{\Omega_i}^T \quad (3.136)$$

$$[B] = -m_{sc}[\tilde{\mathbf{c}}] + \sum_{i=1}^{N_{RW}} m_{rw_i} d_i \hat{\mathbf{w}}_{3_i} \mathbf{b}_{\Omega_i}^T \quad (3.137)$$

$$[C] = m_{sc}[\tilde{\mathbf{c}}] + \sum_{i=1}^{N_{RW}} \left([I_{rw_i, W_{c_i}}] \hat{\mathbf{g}}_{s_i} + m_{rw_i} d_i [\tilde{\mathbf{r}}_{W_{c_i}/B}] \hat{\mathbf{w}}_{3_i} \right) \mathbf{a}_{\Omega_i}^T \quad (3.138)$$

$$[D] = [I_{sc, B}] + \sum_{i=1}^{N_{RW}} \left([I_{rw_i, W_{c_i}}] \hat{\mathbf{g}}_{s_i} + m_{rw_i} d_i [\tilde{\mathbf{r}}_{W_{c_i}/B}] \hat{\mathbf{w}}_{3_i} \right) \mathbf{b}_{\Omega_i}^T \quad (3.139)$$

$$\mathbf{v}_{trans} = \mathbf{F}_{ext} - 2m_{sc}[\tilde{\boldsymbol{\omega}}_{\mathcal{B}/\mathcal{N}}] \mathbf{c}' - m_{sc}[\tilde{\boldsymbol{\omega}}_{\mathcal{B}/\mathcal{N}}][\tilde{\boldsymbol{\omega}}_{\mathcal{B}/\mathcal{N}}] \mathbf{c} + \sum_{i=1}^{N_{RW}} \left[m_{rw_i} d_i \Omega_i^2 \hat{\mathbf{w}}_{2_i} - m_{rw_i} d_i c_{\Omega_i} \hat{\mathbf{w}}_{3_i} \right] \quad (3.140)$$

$$\begin{aligned} \mathbf{v}_{rot} = & -[\tilde{\boldsymbol{\omega}}_{\mathcal{B}/\mathcal{N}}][I_{sc, B}] \boldsymbol{\omega}_{\mathcal{B}/\mathcal{N}} - [I_{sc, B}]' \boldsymbol{\omega}_{\mathcal{B}/\mathcal{N}} + \mathbf{L}_B \\ & + \sum_{i=1}^{N_{RW}} \left[m_{rw_i} [\tilde{\mathbf{r}}_{W_{c_i}/B}] d_i \Omega_i^2 \hat{\mathbf{w}}_{2_i} - [I_{rw_i, W_{c_i}}]' \Omega_i \hat{\mathbf{g}}_{s_i} - [\tilde{\boldsymbol{\omega}}_{\mathcal{B}/\mathcal{N}}] \left([I_{rw_i, W_{c_i}}] \Omega_i \hat{\mathbf{g}}_{s_i} + m_{rw_i} [\tilde{\mathbf{r}}_{W_{c_i}/B}] \mathbf{r}'_{W_{c_i}/B} \right) \right. \\ & \left. - \left([I_{rw_i, W_{c_i}}] \hat{\mathbf{g}}_{s_i} + m_{rw_i} d_i [\tilde{\mathbf{r}}_{W_{c_i}/B}] \hat{\mathbf{w}}_{3_i} \right) c_{\Omega_i} \right] \quad (3.141) \end{aligned}$$

This concludes the necessary definitions for balanced and imbalanced reaction wheels to fit the standard form for the EOMs introduced in Section 2.

3.1.4 Thruster Based Mass Depletion

3.1.4.1 Introduction

Another common physical phenomenon seen by spacecraft is thruster based mass depletion. Majority of spacecraft simulations assume that the only dynamical effect caused by thrusters is the well-known thruster force and the corresponding torque. However, when thrusters are ejecting mass out of the spacecraft, the spacecraft is changing its physical properties. Therefore, the resulting dynamics depends on the relative mass property change inside the fuel tanks compared to the mass that is being ejected at the thruster nozzle.

The simplest way to take into account the ejection of propellant is to use an “update-only” approach, thus updating the center of mass position and the inertia during the simulation in the

EOMs without considering the dynamical influences of the mass depletion. This results in a easy-to-implement model whose limitations consist in the lack of detailed attitude and translational motion prediction for high-fidelity purposes. A more accurate approach considers the spacecraft as an open system whose mass changes in accord with the fuel flows and, consequently, the dynamical variables are transported out of the system using the Reynolds theorem[85, 86, 87, 88, 89, 85]. Past works[90, 91, 92, 93] present the derivation of a variable mass rocket with an axial-symmetric design with a single axial-symmetric burn chamber and a circular nozzle. These assumptions decouple the rocket axial spin from the transverse angular velocity and results in a closed solution to the problem. Other works[94, 95] present the EOMs considering a system of coaxial bodies with different angular velocities. The studies present an analysis of the nutation angle in the case of a two-body satellite, like a spacecraft with a coaxial wheel. The equations must be specified accordingly with the number of interconnected bodies and this results in the need of re-derivation for a specific system of interconnected bodies and to take into account how particles leave the system. A more recent work[96] considers a body fixed reference origin and develops the translational and rotational EOM for a reentry module. The model lacks in a defined approach to connect the dynamical properties variation with the ejected mass characteristics.

In Reference [43], the fully-coupled dynamics is considered for this problem and the EOMs are developed using the standard from seen in Section 2.

3.1.4.2 Problem Statement

To help define the problem, Figure 3.6 is displayed. This problem involves a spacecraft consisting of a hub which is a rigid-body and has a center of mass location labeled as point B_c . The hub has T number of tanks and N number of thrusters attached to it. The figure only shows one tank and one thruster but the analytical development is general. The i_{th} tank has a center of mass location labeled as F_{c_i} and the j_{th} thruster is located at N_{c_j} . The body fixed reference frame \mathcal{B} : $\{\hat{b}_1, \hat{b}_2, \hat{b}_3\}$ with origin B can be oriented in any direction and point B can be located anywhere fixed to the hub. This means that point B and the center of mass location of the spacecraft, C ,

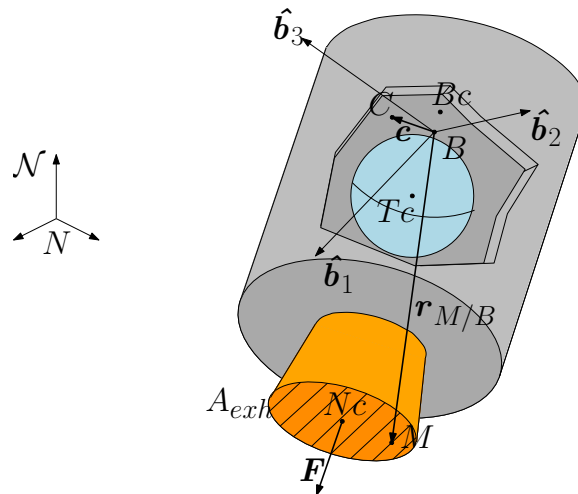


Figure 3.6: Thruster based mass depletion schematic

are not necessarily coincident. As a result, the vector \mathbf{c} defines the vector pointing from the body frame origin to the center of mass of the spacecraft. The inertial reference frame $\mathcal{N}: \{\hat{\mathbf{n}}_1, \hat{\mathbf{n}}_2, \hat{\mathbf{n}}_3\}$ is centered at N and is fixed in inertial space.

Another important description of this problem are the assumptions being used. The following list organizes the assumptions that are used for this formulation:

- The spacecraft hub is rigid and deformations are not considered
- The mass flow among the tanks, the thrusters and in the combustion chamber are considered to be second order effects and neglected
- The relative motion between the propellant and the fuel tanks is not considered in this present work
- The particles are accelerated instantaneously from the spacecraft velocity $\dot{\mathbf{r}}_{B/N}$ to the exhausted velocity \mathbf{v}_{exh} at the nozzle exit
- The particle exhausted velocity \mathbf{v}_{exh} is considered constant and parallel to the nozzle's normal $\hat{\mathbf{n}}$

3.1.4.3 Equations of Motion

The thorough development of the EOMs of a spacecraft with thrusters considering the fully-coupled problem can be seen in Reference [43]. The final form of the EOMs are included in the dissertation to show how the EOMs fit the standard form of the EOMs seen in Section 2. The translational EOM can be seen in the following equation:

$$\begin{aligned}
m_{sc}\ddot{\mathbf{r}}_{B/N} - m_{sc}[\tilde{\mathbf{c}}]\dot{\boldsymbol{\omega}}_{B/N} &= \mathbf{F}_{thr} - 2\dot{m}_{fuel}(\mathbf{c}' + [\tilde{\boldsymbol{\omega}}_{B/N}] \times \mathbf{c}) - m_{sc}\mathbf{c}'' - 2m_{sc}[\tilde{\boldsymbol{\omega}}_{B/N}]\mathbf{c}' \\
&- m_{sc}\ddot{m}_{fuel}\mathbf{c} - m_{sc}[\tilde{\boldsymbol{\omega}}_{B/N}][\tilde{\boldsymbol{\omega}}_{B/N}]\mathbf{c} + 2\sum_{j=1}^N\dot{m}_{noz_j}[\tilde{\boldsymbol{\omega}}_{B/N}]\mathbf{r}_{N_j/B} \\
&+ \sum_{j=1}^N\ddot{m}_{noz_j}\mathbf{r}_{F_{C_j}/B} + \mathbf{F}_{ext, vol} + \mathbf{F}_{ext, surf} \quad (3.142)
\end{aligned}$$

The rotational equation is also repeated here and is shown in Eq. (3.143).

$$\begin{aligned}
[I_{sc, B}]\dot{\boldsymbol{\omega}}_{B/N} + m_{sc}[\tilde{\mathbf{c}}]\ddot{\mathbf{r}}_{B/N} &= [\tilde{\boldsymbol{\omega}}_{B/N}]^T[I_{sc, B}]\boldsymbol{\omega}_{B/N} - [K]\boldsymbol{\omega}_{B/N} \\
&+ \sum_{i=1}^M\left(m_{fuel_i}[\tilde{\mathbf{r}}_{F_{C_i}/B}]^T\mathbf{r}''_{F_{C_i}/B} + m_{fuel_i}[\tilde{\boldsymbol{\omega}}_{B/N}]^T[\tilde{\mathbf{r}}_{F_{C_i}/B}]\mathbf{r}'_{F_{C_i}/B}\right. \\
&\quad \left.+ \dot{m}_{fuel_i}[\tilde{\mathbf{r}}_{F_{C_i}/B}]^T\mathbf{r}'_{F_{C_i}/B}\right) + \mathbf{L}_{B, vol} + \mathbf{L}_{B, surf} + \sum_{j=1}^N\mathbf{L}_{B_{thr_j}} \quad (3.143)
\end{aligned}$$

Looking at Equations (3.142)-(3.143), it is evident that thruster based mass depletion is unique to the models described up until this point because there are no second order state variables for this model. This is because thrusters do not add a degree of freedom to this system but rather act as an external force and torque on the system. However, this model does provide the fully-coupled solution to the problem and takes into account the dynamical effect of the changing mass properties of the spacecraft. Equations (3.142)-(3.143) fit the standard form introduced in Section 2 and provide another ready to implement solution into simulation software.

3.1.5 Dual-Hinged Rigid-Bodies

3.1.5.1 Introduction

The model described in Section 3.1.1 is a first order approximation to a flexing body attached to a spacecraft. That model is limited in that only one frequency can be present per appended body. For some analysis purposes, that model is sufficient, but in some case more flexibility is desired. In this section, a model is introduced that approximates a flexing body as two interconnected hinged rigid-bodies. This provides the ability to model two frequencies at a time and also model deployment of a set of two panels. This section provides the derivation of the EOMs for this system.

3.1.5.2 Problem Statement

This formulation assumes that there is a rigid hub, with N_S dual-linked solar panels (or appended rigid-bodies) and subscript i is used to indicate the i^{th} pair of solar panels. Figure 3.7 displays the frame and variable definitions used for this formulation.

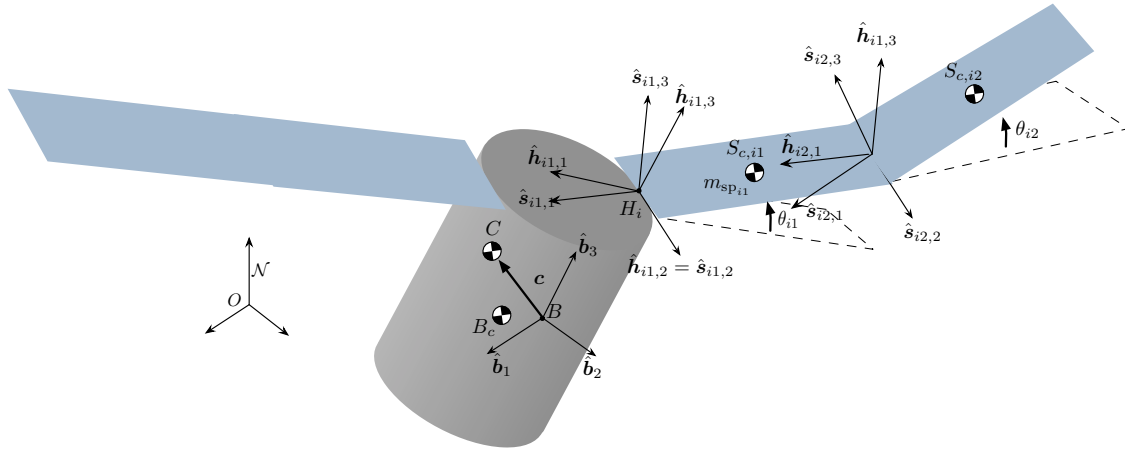


Figure 3.7: Frame and variable definitions used for dual-hinged rigid-bodies formulation

There are six coordinate frames defined for this formulation. The inertial reference frame is indicated by $\mathcal{N} : \{\hat{n}_1, \hat{n}_2, \hat{n}_3\}$. The body fixed coordinate frame, $\mathcal{B} : \{\hat{b}_1, \hat{b}_2, \hat{b}_3\}$, which is anchored to the hub and can be oriented in any direction. The first solar panel frame, $\mathcal{S}_{i1} : \{\hat{s}_{i1,1}, \hat{s}_{i1,2}, \hat{s}_{i1,3}\}$,

is a frame with its origin located at its corresponding hinge location, H_{i1} . The \mathcal{S}_{i1} frame is oriented such that $\hat{s}_{i1,1}$ points antiparallel to the center of mass of the first solar panel, $S_{c,i1}$. The $\hat{s}_{i1,2}$ axis is defined as the rotation axis that would yield a positive θ_{i1} using the right-hand rule. The distance from point H_{i1} to point $S_{c,i1}$ is defined as d_{i1} . The total length of the first panel is l_{i1} . The hinge frame, $\mathcal{H}_{i1} : \{\hat{h}_{i1,1}, \hat{h}_{i1,2}, \hat{h}_{i1,3}\}$, is a frame fixed with respect to the body frame, and is equivalent to the respective \mathcal{S}_{i1} frame when the corresponding solar panel is undeflected.

The other two frames \mathcal{S}_{i2} and \mathcal{H}_{i2} are frames attached to the second solar panel. The \mathcal{H}_{i2} frame is located at the joint between the two solar panels and $\hat{h}_{i1,2} = \hat{h}_{i2,2}$. The $\hat{h}_{i2,1}$ completes the definition of the \mathcal{H}_{i2} frame and can be oriented in any direction while orthogonal to the $\hat{h}_{i2,2}$ axis. This allows for the simulation to model undeployed solar panels, for example, and defines the undeflected direction of the second solar panel. The \mathcal{S}_{i2} frame is defined by being equal to the \mathcal{H}_{i2} when the second solar panel is undeflected from its equilibrium point and rotates about the $\hat{h}_{i2,2}$ axis.

There are a few more key locations that need to be defined. Point B is the origin of the body frame, and can have any location with respect to the hub. Point B_c is the location of the center of mass of the rigid hub. Using the variables and frames defined, the following section outlines the derivation of equations of motion for the spacecraft.

3.1.5.3 Rigid Spacecraft Hub Translational Motion

Following a similar derivation as in previous work [41], the derivation begins with Newton's first law for the center of mass of the spacecraft.

$$\ddot{\mathbf{r}}_{C/N} = \frac{\mathbf{F}}{m_{sc}} \quad (3.144)$$

Ultimately the acceleration of the body frame or point B is desired

$$\ddot{\mathbf{r}}_{B/N} = \ddot{\mathbf{r}}_{C/N} - \ddot{\mathbf{c}} \quad (3.145)$$

The definition of \mathbf{c} the location of the center of mass of the entire spacecraft, can be seen in Eq. (3.146).

$$\mathbf{c} = \frac{1}{m_{sc}} \left[m_{hub} \mathbf{r}_{B_c/B} + \sum_{i=1}^{N_S} (m_{sp_{i1}} \mathbf{r}_{S_{c,i1}/B} + m_{sp_{i2}} \mathbf{r}_{S_{c,i2}/B}) \right] \quad (3.146)$$

To find the inertial time derivative of \mathbf{c} , it is first necessary to find the time derivative of \mathbf{c} with respect to the body frame. A time derivative of any vector, \mathbf{v} , with respect to the body frame is denoted by \mathbf{v}' ; the inertial time derivative is labeled as $\dot{\mathbf{v}}$. The first and second body-relative time derivatives of \mathbf{c} can be seen in Eqs. (3.147) and (3.148).

$$\mathbf{c}' = \frac{1}{m_{sc}} \sum_{i=1}^{N_S} (m_{sp_{i1}} \mathbf{r}'_{S_{c,i1}/B} + m_{sp_{i2}} \mathbf{r}'_{S_{c,i2}/B}) \quad (3.147)$$

$$\mathbf{c}'' = \frac{1}{m_{sc}} \sum_{i=1}^{N_S} (m_{sp_{i1}} \mathbf{r}''_{S_{c,i1}/B} + m_{sp_{i2}} \mathbf{r}''_{S_{c,i2}/B}) \quad (3.148)$$

The vector $\mathbf{r}_{S_{c,i1}/B}$ is readily defined using the $\hat{\mathbf{s}}_{i,1}$ axis

$$\mathbf{r}_{S_{c,i1}/B} = \mathbf{r}_{H_{i1}/B} - d_{i1} \hat{\mathbf{s}}_{i1,1} \quad (3.149)$$

The vector $\mathbf{r}_{S_{c,i2}/B}$ is defined similarly

$$\mathbf{r}_{S_{c,i2}/B} = \mathbf{r}_{H_{i1}/B} - l_{i1} \hat{\mathbf{s}}_{i1,1} - d_{i2} \hat{\mathbf{s}}_{i2,1} \quad (3.150)$$

Now the first and second time derivatives with respect to the body frame of $\mathbf{r}_{S_{c,i1}/B}$ are taken

$$\mathbf{r}'_{S_{c,i1}/B} = d_{i1} \dot{\theta}_{i1} \hat{\mathbf{s}}_{i1,3} \quad (3.151)$$

$$\mathbf{r}''_{S_{c,i1}/B} = d_{i1} \hat{\mathbf{s}}_{i1,3} \ddot{\theta}_{i1} + d_{i1} \dot{\theta}_{i1}^2 \hat{\mathbf{s}}_{i1,1} \quad (3.152)$$

Similarly the body time derivatives of $\mathbf{r}_{S_{c,i2}/B}$ are defined in the following

$$\mathbf{r}'_{S_{c,i2}/B} = l_{i1} \dot{\theta}_{i1} \hat{\mathbf{s}}_{i1,3} + d_{i2} (\dot{\theta}_{i1} + \dot{\theta}_{i2}) \hat{\mathbf{s}}_{i2,3} \quad (3.153)$$

$$\mathbf{r}''_{S_{c,i2}/B} = (l_{i1} \hat{\mathbf{s}}_{i1,3} + d_{i2} \hat{\mathbf{s}}_{i2,3}) \ddot{\theta}_{i1} + d_{i2} \hat{\mathbf{s}}_{i2,3} \ddot{\theta}_{i2} + l_{i1} \dot{\theta}_{i1}^2 \hat{\mathbf{s}}_{i1,1} + d_{i2} (\dot{\theta}_{i1} + \dot{\theta}_{i2})^2 \hat{\mathbf{s}}_{i2,1} \quad (3.154)$$

Eqs. (3.147) and (3.148) are next reformulated to include these new definitions:

$$\mathbf{c}' = \frac{1}{m_{sc}} \sum_{i=1}^{N_S} \left(m_{sp_{i1}} \left[d_{i1} \dot{\theta}_{i1} \hat{\mathbf{s}}_{i1,3} \right] + m_{sp_{i2}} \left[l_{i1} \dot{\theta}_{i1} \hat{\mathbf{s}}_{i1,3} + d_{i2} (\dot{\theta}_{i1} + \dot{\theta}_{i2}) \hat{\mathbf{s}}_{i2,3} \right] \right) \quad (3.155)$$

$$\begin{aligned} \mathbf{c}'' = \frac{1}{m_{sc}} \sum_{i=1}^{N_S} \left(m_{sp_{i1}} d_{i1} (\ddot{\theta}_{i1} \hat{\mathbf{s}}_{i1,3} + \dot{\theta}_{i1}^2 \hat{\mathbf{s}}_{i1,1}) \right. \\ \left. + m_{sp_{i2}} \left[l_{i1} (\ddot{\theta}_{i1} \hat{\mathbf{s}}_{i1,3} + \dot{\theta}_{i1}^2 \hat{\mathbf{s}}_{i1,1}) + d_{i2} (\ddot{\theta}_{i1} + \ddot{\theta}_{i2}) \hat{\mathbf{s}}_{i2,3} + d_{i2} (\dot{\theta}_{i1} + \dot{\theta}_{i2})^2 \hat{\mathbf{s}}_{i2,1} \right] \right) \end{aligned} \quad (3.156)$$

Using the transport theorem[39] yields the following definition for $\ddot{\mathbf{c}}$

$$\ddot{\mathbf{c}} = \mathbf{c}'' + 2\boldsymbol{\omega}_{B/N} \times \mathbf{c}' + \dot{\boldsymbol{\omega}}_{B/N} \times \mathbf{c} + \boldsymbol{\omega}_{B/N} \times (\boldsymbol{\omega}_{B/N} \times \mathbf{c}) \quad (3.157)$$

Eq. (3.145) is updated to include Eq. (3.157)

$$\ddot{\mathbf{r}}_{B/N} = \ddot{\mathbf{r}}_{C/N} - \mathbf{c}'' - 2\boldsymbol{\omega}_{B/N} \times \mathbf{c}' - \dot{\boldsymbol{\omega}}_{B/N} \times \mathbf{c} - \boldsymbol{\omega}_{B/N} \times (\boldsymbol{\omega}_{B/N} \times \mathbf{c}) \quad (3.158)$$

Substituting Eq.(3.156) into Eq.(3.158) and moving the second order state variables to the left hand side results in

$$\begin{aligned} \ddot{\mathbf{r}}_{B/N} + \dot{\boldsymbol{\omega}}_{B/N} \times \mathbf{c} + \frac{1}{m_{sc}} \sum_{i=1}^{N_S} \left(\left[m_{sp_{i1}} d_{i1} \hat{\mathbf{s}}_{i1,3} + m_{sp_{i2}} l_{i1} \hat{\mathbf{s}}_{i1,3} + m_{sp_{i2}} d_{i2} \hat{\mathbf{s}}_{i2,3} \right] \ddot{\theta}_{i1} + m_{sp_{i2}} d_{i2} \hat{\mathbf{s}}_{i2,3} \ddot{\theta}_{i2} \right) \\ = \ddot{\mathbf{r}}_{C/N} - \frac{1}{m_{sc}} \sum_{i=1}^{N_S} \left(m_{sp_{i1}} d_{i1} \dot{\theta}_{i1}^2 \hat{\mathbf{s}}_{i1,1} + m_{sp_{i2}} \left[l_{i1} \dot{\theta}_{i1}^2 \hat{\mathbf{s}}_{i1,1} + d_{i2} (\dot{\theta}_{i1} + \dot{\theta}_{i2})^2 \hat{\mathbf{s}}_{i2,1} \right] \right) \\ - 2\boldsymbol{\omega}_{B/N} \times \mathbf{c}' - \boldsymbol{\omega}_{B/N} \times (\boldsymbol{\omega}_{B/N} \times \mathbf{c}) \end{aligned} \quad (3.159)$$

Introducing the tilde matrix[39] to replace the cross product operators and multiplying both sides by m_{sc} simplifies the equation to

$$\begin{aligned} m_{sc} \ddot{\mathbf{r}}_{B/N} - m_{sc} [\tilde{\mathbf{c}}] \dot{\boldsymbol{\omega}}_{B/N} + \sum_{i=1}^{N_S} \left(\left[m_{sp_{i1}} d_{i1} \hat{\mathbf{s}}_{i1,3} + m_{sp_{i2}} l_{i1} \hat{\mathbf{s}}_{i1,3} + m_{sp_{i2}} d_{i2} \hat{\mathbf{s}}_{i2,3} \right] \ddot{\theta}_{i1} + m_{sp_{i2}} d_{i2} \hat{\mathbf{s}}_{i2,3} \ddot{\theta}_{i2} \right) \\ = \mathbf{F} - 2m_{sc} [\tilde{\boldsymbol{\omega}}_{B/N}] \mathbf{c}' - m_{sc} [\tilde{\boldsymbol{\omega}}_{B/N}] [\tilde{\boldsymbol{\omega}}_{B/N}] \mathbf{c} \\ - \sum_{i=1}^{N_S} \left(m_{sp_{i1}} d_{i1} \dot{\theta}_{i1}^2 \hat{\mathbf{s}}_{i1,1} + m_{sp_{i2}} \left[l_{i1} \dot{\theta}_{i1}^2 \hat{\mathbf{s}}_{i1,1} + d_{i2} (\dot{\theta}_{i1} + \dot{\theta}_{i2})^2 \hat{\mathbf{s}}_{i2,1} \right] \right) \end{aligned} \quad (3.160)$$

Equation (3.160) is the translational motion equation and fits the standard form of the translational EOM introduced in Section 2.

3.1.5.4 Rigid Spacecraft Hub Rotational Motion

Starting with Euler's equation when the body fixed coordinate frame origin is not coincident with the center of mass of the body[39]

$$\dot{\mathbf{H}}_{sc,B} = \mathbf{L}_B + m_{sc}\ddot{\mathbf{r}}_{B/N} \times \mathbf{c} \quad (3.161)$$

where \mathbf{L}_B is the total external torque about point B . The definition of the angular momentum vector of the spacecraft about point B is

$$\begin{aligned} \mathbf{H}_{sc,B} = & [I_{hub,B_c}] \boldsymbol{\omega}_{B/N} + m_{hub} \mathbf{r}_{B_c/B} \times \dot{\mathbf{r}}_{B_c/B} \\ & + \sum_{i=1}^{N_S} \left([I_{sp_{i1},S_{c,i1}}] \boldsymbol{\omega}_{B/N} + \dot{\theta}_{i1} I_{s_{i1,2}} \hat{\mathbf{s}}_{i1,2} + m_{sp_{i1}} \mathbf{r}_{S_{c,i1}/B} \times \dot{\mathbf{r}}_{S_{c,i1}/B} \right. \\ & \left. + [I_{sp_{i2},S_{c,i2}}] \boldsymbol{\omega}_{B/N} + (\dot{\theta}_{i1} + \dot{\theta}_{i2}) I_{s_{i2,2}} \hat{\mathbf{s}}_{i2,2} + m_{sp_{i2}} \mathbf{r}_{S_{c,i2}/B} \times \dot{\mathbf{r}}_{S_{c,i2}/B} \right) \end{aligned} \quad (3.162)$$

Both solar panel inertia's about their center of masses' are assumed to be defined along principal inertia axes and are of the form

$$[I_{sp_{i1},S_{c,i1}}] = \begin{matrix} S_{i1} \\ \left[\begin{array}{ccc} I_{s_{i1,1}} & 0 & 0 \\ 0 & I_{s_{i1,2}} & 0 \\ 0 & 0 & I_{s_{i1,3}} \end{array} \right] \end{matrix} \quad (3.163)$$

$$[I_{sp_{i2},S_{c,i2}}] = \begin{matrix} S_{i2} \\ \left[\begin{array}{ccc} I_{s_{i2,1}} & 0 & 0 \\ 0 & I_{s_{i2,2}} & 0 \\ 0 & 0 & I_{s_{i2,3}} \end{array} \right] \end{matrix} \quad (3.164)$$

Now the inertial time derivative of Eq. (3.162) is taken and yields

$$\begin{aligned} \dot{\mathbf{H}}_{sc,B} = & [I_{hub,B_c}] \dot{\boldsymbol{\omega}}_{B/N} + \boldsymbol{\omega}_{B/N} \times [I_{hub,B_c}] \boldsymbol{\omega}_{B/N} + m_{hub} \mathbf{r}_{B_c/B} \times \ddot{\mathbf{r}}_{B_c/B} \\ & + \sum_{i=1}^{N_S} \left([I'_{sp_{i1},S_{c,i1}}] \boldsymbol{\omega}_{B/N} + [I_{sp_{i1},S_{c,i1}}] \dot{\boldsymbol{\omega}}_{B/N} + \boldsymbol{\omega}_{B/N} \times [I_{sp_{i1},S_{c,i1}}] \boldsymbol{\omega}_{B/N} \right. \\ & + \dot{\theta}_{i1} I_{s_{i1,2}} \hat{\mathbf{s}}_{i1,2} + \boldsymbol{\omega}_{B/N} \times \dot{\theta}_{i1} I_{s_{i1,2}} \hat{\mathbf{s}}_{i1,2} + m_{sp_{i1}} \mathbf{r}_{S_{c,i1}/B} \times \ddot{\mathbf{r}}_{S_{c,i1}/B} \\ & + [I'_{sp_{i2},S_{c,i2}}] \boldsymbol{\omega}_{B/N} + [I_{sp_{i2},S_{c,i2}}] \dot{\boldsymbol{\omega}}_{B/N} + \boldsymbol{\omega}_{B/N} \times [I_{sp_{i2},S_{c,i2}}] \boldsymbol{\omega}_{B/N} \\ & \left. + (\dot{\theta}_{i1} + \dot{\theta}_{i2}) I_{s_{i2,2}} \hat{\mathbf{s}}_{i2,2} + \boldsymbol{\omega}_{B/N} \times (\dot{\theta}_{i1} + \dot{\theta}_{i2}) I_{s_{i2,2}} \hat{\mathbf{s}}_{i2,2} + m_{sp_{i2}} \mathbf{r}_{S_{c,i2}/B} \times \ddot{\mathbf{r}}_{S_{c,i2}/B} \right) \end{aligned} \quad (3.165)$$

The terms $\ddot{\mathbf{r}}_{B_c/B}$, $\ddot{\mathbf{r}}_{S_{c,i1}/B}$ and $\ddot{\mathbf{r}}_{S_{c,i2}/B}$ are found using the transport theorem and knowing that $\mathbf{r}_{B_c/B}$ is fixed with respect to the body frame.

$$\ddot{\mathbf{r}}_{B_c/B} = \dot{\boldsymbol{\omega}}_{\mathcal{B}/\mathcal{N}} \times \mathbf{r}_{B_c/B} + \boldsymbol{\omega}_{\mathcal{B}/\mathcal{N}} \times (\boldsymbol{\omega}_{\mathcal{B}/\mathcal{N}} \times \mathbf{r}_{B_c/B}) \quad (3.166)$$

$$\ddot{\mathbf{r}}_{S_{c,i1}/B} = \mathbf{r}''_{S_{c,i1}/B} + 2\boldsymbol{\omega}_{\mathcal{B}/\mathcal{N}} \times \mathbf{r}'_{S_{c,i1}/B} + \dot{\boldsymbol{\omega}}_{\mathcal{B}/\mathcal{N}} \times \mathbf{r}_{S_{c,i1}/B} + \boldsymbol{\omega}_{\mathcal{B}/\mathcal{N}} \times (\boldsymbol{\omega}_{\mathcal{B}/\mathcal{N}} \times \mathbf{r}_{S_{c,i1}/B}) \quad (3.167)$$

$$\ddot{\mathbf{r}}_{S_{c,i2}/B} = \mathbf{r}''_{S_{c,i2}/B} + 2\boldsymbol{\omega}_{\mathcal{B}/\mathcal{N}} \times \mathbf{r}'_{S_{c,i2}/B} + \dot{\boldsymbol{\omega}}_{\mathcal{B}/\mathcal{N}} \times \mathbf{r}_{S_{c,i2}/B} + \boldsymbol{\omega}_{\mathcal{B}/\mathcal{N}} \times (\boldsymbol{\omega}_{\mathcal{B}/\mathcal{N}} \times \mathbf{r}_{S_{c,i2}/B}) \quad (3.168)$$

Incorporating Eqs. (3.166) - (3.168) into Eq. (3.165) results in

$$\begin{aligned} \dot{\mathbf{H}}_{sc,B} = & [I_{hub,B_c}] \dot{\boldsymbol{\omega}}_{\mathcal{B}/\mathcal{N}} + \boldsymbol{\omega}_{\mathcal{B}/\mathcal{N}} \times [I_{hub,B_c}] \boldsymbol{\omega}_{\mathcal{B}/\mathcal{N}} + m_{hub} \mathbf{r}_{B_c/B} \times (\dot{\boldsymbol{\omega}}_{\mathcal{B}/\mathcal{N}} \times \mathbf{r}_{B_c/B}) \\ & + m_{hub} \mathbf{r}_{B_c/B} \times [\boldsymbol{\omega}_{\mathcal{B}/\mathcal{N}} \times (\boldsymbol{\omega}_{\mathcal{B}/\mathcal{N}} \times \mathbf{r}_{B_c/B})] + \sum_{i=1}^{N_S} \left([I'_{sp_{i1},S_{c,i1}}] \boldsymbol{\omega}_{\mathcal{B}/\mathcal{N}} + [I_{sp_{i1},S_{c,i1}}] \dot{\boldsymbol{\omega}}_{\mathcal{B}/\mathcal{N}} \right. \\ & + \boldsymbol{\omega}_{\mathcal{B}/\mathcal{N}} \times [I_{sp_{i1},S_{c,i1}}] \boldsymbol{\omega}_{\mathcal{B}/\mathcal{N}} + \ddot{\theta}_{i1} I_{s_{i1,2}} \hat{\mathbf{s}}_{i1,2} + \boldsymbol{\omega}_{\mathcal{B}/\mathcal{N}} \times \dot{\theta}_{i1} I_{s_{i1,2}} \hat{\mathbf{s}}_{i1,2} + m_{sp_{i1}} \mathbf{r}_{S_{c,i1}/B} \times \mathbf{r}''_{S_{c,i1}/B} \\ & + 2m_{sp_{i1}} \mathbf{r}_{S_{c,i1}/B} \times (\boldsymbol{\omega}_{\mathcal{B}/\mathcal{N}} \times \mathbf{r}'_{S_{c,i1}/B}) + m_{sp_{i1}} \mathbf{r}_{S_{c,i1}/B} \times (\dot{\boldsymbol{\omega}}_{\mathcal{B}/\mathcal{N}} \times \mathbf{r}_{S_{c,i1}/B}) \\ & + m_{sp_{i1}} \mathbf{r}_{S_{c,i1}/B} \times [\boldsymbol{\omega}_{\mathcal{B}/\mathcal{N}} \times (\boldsymbol{\omega}_{\mathcal{B}/\mathcal{N}} \times \mathbf{r}_{S_{c,i1}/B})] + [I'_{sp_{i2},S_{c,i2}}] \boldsymbol{\omega}_{\mathcal{B}/\mathcal{N}} + [I_{sp_{i2},S_{c,i2}}] \dot{\boldsymbol{\omega}}_{\mathcal{B}/\mathcal{N}} \\ & + \boldsymbol{\omega}_{\mathcal{B}/\mathcal{N}} \times [I_{sp_{i2},S_{c,i2}}] \boldsymbol{\omega}_{\mathcal{B}/\mathcal{N}} + (\ddot{\theta}_{i1} + \ddot{\theta}_{i2}) I_{s_{i2,2}} \hat{\mathbf{s}}_{i2,2} + \boldsymbol{\omega}_{\mathcal{B}/\mathcal{N}} \times (\dot{\theta}_{i1} + \dot{\theta}_{i2}) I_{s_{i2,2}} \hat{\mathbf{s}}_{i2,2} \\ & + m_{sp_{i2}} \mathbf{r}_{S_{c,i2}/B} \times \mathbf{r}''_{S_{c,i2}/B} + 2m_{sp_{i2}} \mathbf{r}_{S_{c,i2}/B} \times (\boldsymbol{\omega}_{\mathcal{B}/\mathcal{N}} \times \mathbf{r}'_{S_{c,i2}/B}) \\ & \left. + m_{sp_{i2}} \mathbf{r}_{S_{c,i2}/B} \times (\dot{\boldsymbol{\omega}}_{\mathcal{B}/\mathcal{N}} \times \mathbf{r}_{S_{c,i2}/B}) + m_{sp_{i2}} \mathbf{r}_{S_{c,i2}/B} \times [\boldsymbol{\omega}_{\mathcal{B}/\mathcal{N}} \times (\boldsymbol{\omega}_{\mathcal{B}/\mathcal{N}} \times \mathbf{r}_{S_{c,i2}/B})] \right) \quad (3.169) \end{aligned}$$

Applying the parallel axis theorem the following inertia tensor terms are defined as

$$[I_{hub,B}] = [I_{hub,B_c}] + m_{hub} [\tilde{\mathbf{r}}_{B_c/B}] [\tilde{\mathbf{r}}_{B_c/B}]^T \quad (3.170)$$

$$[I_{sp_{i1},B}] = [I_{sp_{i1},S_{c,i1}}] + m_{sp_{i1}} [\tilde{\mathbf{r}}_{S_{c,i1}/B}] [\tilde{\mathbf{r}}_{S_{c,i1}/B}]^T \quad (3.171)$$

$$[I_{sp_{i2},B}] = [I_{sp_{i2},S_{c,i2}}] + m_{sp_{i2}} [\tilde{\mathbf{r}}_{S_{c,i2}/B}] [\tilde{\mathbf{r}}_{S_{c,i2}/B}]^T \quad (3.172)$$

$$[I_{sc,B}] = [I_{hub,B}] + \sum_{i=1}^{N_S} \left([I_{sp_{i1},B}] + [I_{sp_{i2},B}] \right) \quad (3.173)$$

Because the tilde matrices are skew-symmetric, taking the body-relative time derivative of Equa-

tion (3.173) yields

$$[I'_{sc,B}] = \sum_{i=1}^{N_S} \left[[I'_{sp_{i1},S_{c,i1}}] - m_{sp_{i1}} \left([\tilde{\mathbf{r}}'_{S_{c,i1}/B}] [\tilde{\mathbf{r}}_{S_{c,i1}/B}] + [\tilde{\mathbf{r}}_{S_{c,i1}/B}] [\tilde{\mathbf{r}}'_{S_{c,i1}/B}] \right) \right. \\ \left. + [I'_{sp_{i2},S_{c,i2}}] - m_{sp_{i2}} \left([\tilde{\mathbf{r}}'_{S_{c,i2}/B}] [\tilde{\mathbf{r}}_{S_{c,i2}/B}] + [\tilde{\mathbf{r}}_{S_{c,i2}/B}] [\tilde{\mathbf{r}}'_{S_{c,i2}/B}] \right) \right] \quad (3.174)$$

$[I'_{sp_{i1},S_{c,i1}}]$ needs to be defined and can be conveniently expressed by leveraging the assumption that the inertia matrix is diagonal (as seen in Eq. (3.163)) and is written in terms of its base vectors:

$$[I_{sp_{i1},S_{c,i1}}] = I_{s_{i1,1}} \hat{\mathbf{s}}_{i1,1} \hat{\mathbf{s}}_{i1,1}^T + I_{s_{i1,2}} \hat{\mathbf{s}}_{i1,2} \hat{\mathbf{s}}_{i1,2}^T + I_{s_{i1,3}} \hat{\mathbf{s}}_{i1,3} \hat{\mathbf{s}}_{i1,3}^T \quad (3.175)$$

Taking the body time derivative of Eq. (3.175) results in

$$[I'_{sp_{i1},S_{c,i1}}] = I_{s_{i1,1}} \hat{\mathbf{s}}'_{i1,1} \hat{\mathbf{s}}_{i1,1}^T + I_{s_{i1,1}} \hat{\mathbf{s}}_{i1,1} \hat{\mathbf{s}}_{i1,1}^{\prime T} + I_{s_{i1,2}} \hat{\mathbf{s}}'_{i1,2} \hat{\mathbf{s}}_{i1,2}^T \\ + I_{s_{i1,2}} \hat{\mathbf{s}}_{i1,2} \hat{\mathbf{s}}_{i1,2}^{\prime T} + I_{s_{i1,3}} \hat{\mathbf{s}}'_{i1,3} \hat{\mathbf{s}}_{i1,3}^T + I_{s_{i1,3}} \hat{\mathbf{s}}_{i1,3} \hat{\mathbf{s}}_{i1,3}^{\prime T} \quad (3.176)$$

Using the transport theorem for each basis vector in the frame: $\hat{\mathbf{s}}'_{i1,j} = \boldsymbol{\omega}_{S_{i1}/B} \times \hat{\mathbf{s}}_{i1,j} = \dot{\theta}_{i1} \hat{\mathbf{s}}_{i1,2} \times \hat{\mathbf{s}}_{i1,j}$, applying this to Eq. (3.176), evaluating the cross products, and simplifying results in

$$[I'_{sp_{i1},S_{c,i1}}] = \dot{\theta}_{i1} (I_{s_{i1,3}} - I_{s_{i1,1}}) (\hat{\mathbf{s}}_{i1,1} \hat{\mathbf{s}}_{i1,3}^T + \hat{\mathbf{s}}_{i1,3} \hat{\mathbf{s}}_{i1,1}^T) \quad (3.177)$$

Applying the same methodology for $[I'_{sp_{i2},S_{c,i2}}]$ and using the following definition: $\hat{\mathbf{s}}'_{i2,j} = \boldsymbol{\omega}_{S_{i2}/B} \times \hat{\mathbf{s}}_{i2,j} = (\dot{\theta}_{i1} + \dot{\theta}_{i2}) \hat{\mathbf{s}}_{i2,2} \times \hat{\mathbf{s}}_{i2,j}$ results in

$$[I'_{sp_{i2},S_{c,i2}}] = (\dot{\theta}_{i1} + \dot{\theta}_{i2}) (I_{s_{i2,3}} - I_{s_{i2,1}}) (\hat{\mathbf{s}}_{i2,1} \hat{\mathbf{s}}_{i2,3}^T + \hat{\mathbf{s}}_{i2,3} \hat{\mathbf{s}}_{i2,1}^T) \quad (3.178)$$

Substituting Eq. (3.177) and Eq. (3.178) into Eq. (3.169) and using Eq. (3.173) to simplify results in Eq. (3.179). The Jacobi Identity, $(\mathbf{a} \times \mathbf{b}) \times \mathbf{c} = \mathbf{a} \times (\mathbf{b} \times \mathbf{c}) - \mathbf{b} \times (\mathbf{a} \times \mathbf{c})$, is used to combine terms.

Factoring out $\dot{\boldsymbol{\omega}}_{B/N}$ and, selectively, $\boldsymbol{\omega}_{B/N}$ and utilizing the tilde matrix transforms Eq. 3.169 into

Eq.(3.179) so that $[I_{sc,B}]$ can be extracted.

$$\begin{aligned}
\dot{\mathbf{H}}_{sc,B} = & \left([I_{hub,B_c}] - m_{hub}[\tilde{\mathbf{r}}_{B_c/B}][\tilde{\mathbf{r}}_{B_c/B}] + \sum_{i=1}^{N_S} \left([I_{sp_{i1},S_{c,i1}}] + [I_{sp_{i2},S_{c,i2}}] - m_{sp_{i1}}[\tilde{\mathbf{r}}_{S_{c,i1}/B}][\tilde{\mathbf{r}}_{S_{c,i1}/B}] \right. \right. \\
& \left. \left. - m_{sp_{i2}}[\tilde{\mathbf{r}}_{S_{c,i2}/B}][\tilde{\mathbf{r}}_{S_{c,i2}/B}] \right) \right) \dot{\boldsymbol{\omega}}_{B/N} + \boldsymbol{\omega}_{B/N} \times \left([I_{hub,B_c}] - m_{hub}[\tilde{\mathbf{r}}_{B_c/B}][\tilde{\mathbf{r}}_{B_c/B}] + \right. \\
& \left. \sum_{i=1}^{N_S} \left([I_{sp_{i1},S_{c,i1}}] + [I_{sp_{i2},S_{c,i2}}] - m_{sp_{i1}}[\tilde{\mathbf{r}}_{S_{c,i1}/B}][\tilde{\mathbf{r}}_{S_{c,i1}/B}] - m_{sp_{i2}}[\tilde{\mathbf{r}}_{S_{c,i2}/B}][\tilde{\mathbf{r}}_{S_{c,i2}/B}] \right) \right) \boldsymbol{\omega}_{B/N} \\
& + \sum_{i=1}^{N_S} \left([I'_{sp_{i1},S_{c,i1}}] \boldsymbol{\omega}_{B/N} + \ddot{\theta}_{i1} I_{s_{i1,2}} \hat{\mathbf{s}}_{i1,2} + \boldsymbol{\omega}_{B/N} \times \dot{\theta}_{i1} I_{s_{i1,2}} \hat{\mathbf{s}}_{i1,2} + m_{sp_{i1}} \mathbf{r}_{S_{c,i1}/B} \times \mathbf{r}''_{S_{c,i1}/B} \right. \\
& \left. + 2m_{sp_{i1}} \mathbf{r}_{S_{c,i1}/B} \times \left(\boldsymbol{\omega}_{B/N} \times \mathbf{r}'_{S_{c,i1}/B} \right) + [I'_{sp_{i2},S_{c,i2}}] \boldsymbol{\omega}_{B/N} + (\ddot{\theta}_{i1} + \ddot{\theta}_{i2}) I_{s_{i2,2}} \hat{\mathbf{s}}_{i2,2} + \right. \\
& \left. \boldsymbol{\omega}_{B/N} \times (\dot{\theta}_{i1} + \dot{\theta}_{i2}) I_{s_{i2,2}} \hat{\mathbf{s}}_{i2,2} + m_{sp_{i2}} \mathbf{r}_{S_{c,i2}/B} \times \mathbf{r}''_{S_{c,i2}/B} + 2m_{sp_{i2}} \mathbf{r}_{S_{c,i2}/B} \times \left(\boldsymbol{\omega}_{B/N} \times \mathbf{r}'_{S_{c,i2}/B} \right) \right)
\end{aligned} \tag{3.179}$$

Eqs. (3.170)-(3.173) further simplify the equation to the following:

$$\begin{aligned}
\dot{\mathbf{H}}_{sc,B} = & [I_{sc,B}] \dot{\boldsymbol{\omega}}_{B/N} + \boldsymbol{\omega}_{B/N} \times [I_{sc,B}] \boldsymbol{\omega}_{B/N} \\
& + \sum_{i=1}^{N_S} \left([I'_{sp_{i1},S_{c,i1}}] \boldsymbol{\omega}_{B/N} + \ddot{\theta}_{i1} I_{s_{i1,2}} \hat{\mathbf{s}}_{i1,2} + \boldsymbol{\omega}_{B/N} \times \dot{\theta}_{i1} I_{s_{i1,2}} \hat{\mathbf{s}}_{i1,2} + m_{sp_{i1}} \mathbf{r}_{S_{c,i1}/B} \times \mathbf{r}''_{S_{c,i1}/B} \right. \\
& \left. + 2m_{sp_{i1}} \mathbf{r}_{S_{c,i1}/B} \times \left(\boldsymbol{\omega}_{B/N} \times \mathbf{r}'_{S_{c,i1}/B} \right) + [I'_{sp_{i2},S_{c,i2}}] \boldsymbol{\omega}_{B/N} + (\ddot{\theta}_{i1} + \ddot{\theta}_{i2}) I_{s_{i2,2}} \hat{\mathbf{s}}_{i2,2} + \right. \\
& \left. \boldsymbol{\omega}_{B/N} \times (\dot{\theta}_{i1} + \dot{\theta}_{i2}) I_{s_{i2,2}} \hat{\mathbf{s}}_{i2,2} + m_{sp_{i2}} \mathbf{r}_{S_{c,i2}/B} \times \mathbf{r}''_{S_{c,i2}/B} + 2m_{sp_{i2}} \mathbf{r}_{S_{c,i2}/B} \times \left(\boldsymbol{\omega}_{B/N} \times \mathbf{r}'_{S_{c,i2}/B} \right) \right)
\end{aligned} \tag{3.180}$$

Using the Jacobi Identity again, followed by tilde matrix substitution yields:

$$\begin{aligned}
\dot{\mathbf{H}}_{sc,B} = & [I_{sc,B}] \dot{\boldsymbol{\omega}}_{B/N} + \boldsymbol{\omega}_{B/N} \times [I_{sc,B}] \boldsymbol{\omega}_{B/N} \\
& + \sum_{i=1}^{N_S} \left([I'_{sp_{i1},S_{c,i1}}] \boldsymbol{\omega}_{B/N} - m_{sp_{i1}} \left([\tilde{\mathbf{r}}_{S_{c,i1}/B}][\tilde{\mathbf{r}}'_{S_{c,i1}/B}] + [\tilde{\mathbf{r}}'_{S_{c,i1}/B}][\tilde{\mathbf{r}}_{S_{c,i1}/B}] \right) \boldsymbol{\omega}_{B/N} + \ddot{\theta}_{i1} I_{s_{i1,2}} \hat{\mathbf{s}}_{i1,2} \right. \\
& \left. + \boldsymbol{\omega}_{B/N} \times \dot{\theta}_{i1} I_{s_{i1,2}} \hat{\mathbf{s}}_{i1,2} + m_{sp_{i1}} \mathbf{r}_{S_{c,i1}/B} \times \mathbf{r}''_{S_{c,i1}/B} + m_{sp_{i1}} \mathbf{r}_{S_{c,i1}/B} \times \left(\boldsymbol{\omega}_{B/N} \times \mathbf{r}'_{S_{c,i1}/B} \right) \right. \\
& \left. + [I'_{sp_{i2},S_{c,i2}}] \boldsymbol{\omega}_{B/N} - m_{sp_{i2}} \left([\tilde{\mathbf{r}}_{S_{c,i2}/B}][\tilde{\mathbf{r}}'_{S_{c,i2}/B}] + [\tilde{\mathbf{r}}'_{S_{c,i2}/B}][\tilde{\mathbf{r}}_{S_{c,i2}/B}] \right) \boldsymbol{\omega}_{B/N} + (\ddot{\theta}_{i1} + \ddot{\theta}_{i2}) I_{s_{i2,2}} \hat{\mathbf{s}}_{i2,2} \right. \\
& \left. + \boldsymbol{\omega}_{B/N} \times (\dot{\theta}_{i1} + \dot{\theta}_{i2}) I_{s_{i2,2}} \hat{\mathbf{s}}_{i2,2} + m_{sp_{i2}} \mathbf{r}_{S_{c,i2}/B} \times \mathbf{r}''_{S_{c,i2}/B} + m_{sp_{i2}} \mathbf{r}_{S_{c,i2}/B} \times \left(\boldsymbol{\omega}_{B/N} \times \mathbf{r}'_{S_{c,i2}/B} \right) \right)
\end{aligned} \tag{3.181}$$

Factoring out $\boldsymbol{\omega}_{\mathcal{B}/\mathcal{N}}$, and substituting in from Eq. (3.174) leaves:

$$\begin{aligned} \dot{\mathbf{H}}_{sc,B} = & [I_{sc,B}] \dot{\boldsymbol{\omega}}_{\mathcal{B}/\mathcal{N}} + \boldsymbol{\omega}_{\mathcal{B}/\mathcal{N}} \times [I_{sc,B}] \boldsymbol{\omega}_{\mathcal{B}/\mathcal{N}} + [I'_{sc,B}] \boldsymbol{\omega}_{\mathcal{B}/\mathcal{N}} + \sum_{i=1}^{N_S} \left[\ddot{\theta}_{i1} I_{s_{i1,2}} \hat{\mathbf{s}}_{i1,2} \right. \\ & + \boldsymbol{\omega}_{\mathcal{B}/\mathcal{N}} \times \dot{\theta}_{i1} I_{s_{i1,2}} \hat{\mathbf{s}}_{i1,2} + m_{sp_{i1}} \mathbf{r}_{S_{c,i1}/B} \times \mathbf{r}''_{S_{c,i1}/B} + m_{sp_{i1}} \boldsymbol{\omega}_{\mathcal{B}/\mathcal{N}} \times \left(\mathbf{r}_{S_{c,i1}/B} \times \mathbf{r}'_{S_{c,i1}/B} \right) \\ & + (\ddot{\theta}_{i1} + \ddot{\theta}_{i2}) I_{s_{i2,2}} \hat{\mathbf{s}}_{i2,2} + \boldsymbol{\omega}_{\mathcal{B}/\mathcal{N}} \times (\dot{\theta}_{i1} + \dot{\theta}_{i2}) I_{s_{i2,2}} \hat{\mathbf{s}}_{i2,2} \\ & \left. + m_{sp_{i2}} \mathbf{r}_{S_{c,i2}/B} \times \mathbf{r}''_{S_{c,i2}/B} + m_{sp_{i2}} \boldsymbol{\omega}_{\mathcal{B}/\mathcal{N}} \times \left(\mathbf{r}_{S_{c,i2}/B} \times \mathbf{r}'_{S_{c,i2}/B} \right) \right] \quad (3.182) \end{aligned}$$

Eqs. (3.161) and (3.182) are equated and yield

$$\begin{aligned} \mathbf{L}_B + m_{sc} \ddot{\mathbf{r}}_{B/\mathcal{N}} \times \mathbf{c} = & [I_{sc,B}] \dot{\boldsymbol{\omega}}_{\mathcal{B}/\mathcal{N}} + \boldsymbol{\omega}_{\mathcal{B}/\mathcal{N}} \times [I_{sc,B}] \boldsymbol{\omega}_{\mathcal{B}/\mathcal{N}} + [I'_{sc,B}] \boldsymbol{\omega}_{\mathcal{B}/\mathcal{N}} + \sum_{i=1}^{N_S} \left[\ddot{\theta}_{i1} I_{s_{i1,2}} \hat{\mathbf{s}}_{i1,2} \right. \\ & + \boldsymbol{\omega}_{\mathcal{B}/\mathcal{N}} \times \dot{\theta}_{i1} I_{s_{i1,2}} \hat{\mathbf{s}}_{i1,2} + m_{sp_{i1}} \mathbf{r}_{S_{c,i1}/B} \times \mathbf{r}''_{S_{c,i1}/B} + m_{sp_{i1}} \boldsymbol{\omega}_{\mathcal{B}/\mathcal{N}} \times \left(\mathbf{r}_{S_{c,i1}/B} \times \mathbf{r}'_{S_{c,i1}/B} \right) \\ & + (\ddot{\theta}_{i1} + \ddot{\theta}_{i2}) I_{s_{i2,2}} \hat{\mathbf{s}}_{i2,2} + \boldsymbol{\omega}_{\mathcal{B}/\mathcal{N}} \times (\dot{\theta}_{i1} + \dot{\theta}_{i2}) I_{s_{i2,2}} \hat{\mathbf{s}}_{i2,2} \\ & \left. + m_{sp_{i2}} \mathbf{r}_{S_{c,i2}/B} \times \mathbf{r}''_{S_{c,i2}/B} + m_{sp_{i2}} \boldsymbol{\omega}_{\mathcal{B}/\mathcal{N}} \times \left(\mathbf{r}_{S_{c,i2}/B} \times \mathbf{r}'_{S_{c,i2}/B} \right) \right] \quad (3.183) \end{aligned}$$

Finally, using tilde matrix and simplifying yields the modified Euler equation:

$$\begin{aligned} m_{sc} [\tilde{\mathbf{c}}] \ddot{\mathbf{r}}_{B/\mathcal{N}} + [I_{sc,B}] \dot{\boldsymbol{\omega}}_{\mathcal{B}/\mathcal{N}} + \sum_{i=1}^{N_S} \left[\ddot{\theta}_{i1} I_{s_{i1,2}} \hat{\mathbf{s}}_{i1,2} + m_{sp_{i1}} [\tilde{\mathbf{r}}_{S_{c,i1}/B}] \mathbf{r}''_{S_{c,i1}/B} \right. \\ \left. + (\ddot{\theta}_{i1} + \ddot{\theta}_{i2}) I_{s_{i2,2}} \hat{\mathbf{s}}_{i2,2} + m_{sp_{i2}} [\tilde{\mathbf{r}}_{S_{c,i2}/B}] \mathbf{r}''_{S_{c,i2}/B} \right] = -[\tilde{\boldsymbol{\omega}}_{\mathcal{B}/\mathcal{N}}] [I_{sc,B}] \boldsymbol{\omega}_{\mathcal{B}/\mathcal{N}} - [I'_{sc,B}] \boldsymbol{\omega}_{\mathcal{B}/\mathcal{N}} \\ - \sum_{i=1}^{N_S} \left[[\tilde{\boldsymbol{\omega}}_{\mathcal{B}/\mathcal{N}}] \dot{\theta}_{i1} I_{s_{i1,2}} \hat{\mathbf{s}}_{i1,2} + m_{sp_{i1}} [\tilde{\boldsymbol{\omega}}_{\mathcal{B}/\mathcal{N}}] [\tilde{\mathbf{r}}_{S_{c,i1}/B}] \mathbf{r}'_{S_{c,i1}/B} \right. \\ \left. + [\tilde{\boldsymbol{\omega}}_{\mathcal{B}/\mathcal{N}}] (\dot{\theta}_{i1} + \dot{\theta}_{i2}) I_{s_{i2,2}} \hat{\mathbf{s}}_{i2,2} + m_{sp_{i2}} [\tilde{\boldsymbol{\omega}}_{\mathcal{B}/\mathcal{N}}] [\tilde{\mathbf{r}}_{S_{c,i2}/B}] \mathbf{r}'_{S_{c,i2}/B} \right] + \mathbf{L}_B \quad (3.184) \end{aligned}$$

The second order terms need to be combined and results in:

$$\begin{aligned}
& m_{sc}[\tilde{\mathbf{c}}]\ddot{\mathbf{r}}_{B/N} + [I_{sc,B}]\dot{\boldsymbol{\omega}}_{B/N} + \sum_{i=1}^{N_S} \left[\left(I_{s_{i1,2}} \hat{\mathbf{s}}_{i1,2} + m_{sp_{i1}} d_{i1} [\tilde{\mathbf{r}}_{S_{c,i1}/B}] \hat{\mathbf{s}}_{i1,3} + I_{s_{i2,2}} \hat{\mathbf{s}}_{i2,2} \right. \right. \\
& \left. \left. + m_{sp_{i2}} l_{i1} [\tilde{\mathbf{r}}_{S_{c,i2}/B}] \hat{\mathbf{s}}_{i1,3} + m_{sp_{i2}} d_{i2} [\tilde{\mathbf{r}}_{S_{c,i2}/B}] \hat{\mathbf{s}}_{i2,3} \right) \ddot{\theta}_{i1} + \left(I_{s_{i2,2}} \hat{\mathbf{s}}_{i2,2} + m_{sp_{i2}} [\tilde{\mathbf{r}}_{S_{c,i2}/B}] d_{i2} \hat{\mathbf{s}}_{i2,3} \right) \ddot{\theta}_{i2} \right] \\
& = -[\tilde{\boldsymbol{\omega}}_{B/N}][I_{sc,B}]\boldsymbol{\omega}_{B/N} - [I'_{sc,B}]\boldsymbol{\omega}_{B/N} - \sum_{i=1}^{N_S} \left[[\tilde{\boldsymbol{\omega}}_{B/N}] \dot{\theta}_{i1} I_{s_{i1,2}} \hat{\mathbf{s}}_{i1,2} + m_{sp_{i1}} d_{i1} \dot{\theta}_{i1}^2 [\tilde{\mathbf{r}}_{S_{c,i1}/B}] \hat{\mathbf{s}}_{i1,1} \right. \\
& \left. + m_{sp_{i2}} l_{i1} \dot{\theta}_{i1}^2 [\tilde{\mathbf{r}}_{S_{c,i2}/B}] \hat{\mathbf{s}}_{i1,1} + m_{sp_{i1}} [\tilde{\boldsymbol{\omega}}_{B/N}] [\tilde{\mathbf{r}}_{S_{c,i1}/B}] \mathbf{r}'_{S_{c,i1}/B} + [\tilde{\boldsymbol{\omega}}_{B/N}] (\dot{\theta}_{i1} + \dot{\theta}_{i2}) I_{s_{i2,2}} \hat{\mathbf{s}}_{i2,2} \right. \\
& \left. + m_{sp_{i2}} d_{i2} (\dot{\theta}_{i1} + \dot{\theta}_{i2})^2 [\tilde{\mathbf{r}}_{S_{c,i2}/B}] \hat{\mathbf{s}}_{i2,1} + m_{sp_{i2}} [\tilde{\boldsymbol{\omega}}_{B/N}] [\tilde{\mathbf{r}}_{S_{c,i2}/B}] \mathbf{r}'_{S_{c,i2}/B} \right] + \mathbf{L}_B \quad (3.185)
\end{aligned}$$

The terms $\mathbf{r}''_{S_{c,i1}/B}$ and $\mathbf{r}''_{S_{c,i2}/B}$ contain second order state variables, therefore replacing their definition seen in Eqs. (3.152) and (3.154) and simplifying the expression yields

$$\begin{aligned}
& m_{sc}[\tilde{\mathbf{c}}]\ddot{\mathbf{r}}_{B/N} + [I_{sc,B}]\dot{\boldsymbol{\omega}}_{B/N} + \sum_{i=1}^{N_S} \left[\left(I_{s_{i1,2}} \hat{\mathbf{s}}_{i1,2} + m_{sp_{i1}} d_{i1} [\tilde{\mathbf{r}}_{S_{c,i1}/B}] \hat{\mathbf{s}}_{i1,3} + I_{s_{i2,2}} \hat{\mathbf{s}}_{i2,2} + m_{sp_{i2}} l_{i1} [\tilde{\mathbf{r}}_{S_{c,i2}/B}] \hat{\mathbf{s}}_{i1,3} \right. \right. \\
& \left. \left. + m_{sp_{i2}} d_{i2} [\tilde{\mathbf{r}}_{S_{c,i2}/B}] \hat{\mathbf{s}}_{i2,3} \right) \ddot{\theta}_{i1} + \left(I_{s_{i2,2}} \hat{\mathbf{s}}_{i2,2} + m_{sp_{i2}} d_{i2} [\tilde{\mathbf{r}}_{S_{c,i2}/B}] \hat{\mathbf{s}}_{i2,3} \right) \ddot{\theta}_{i2} \right] \\
& = -[\tilde{\boldsymbol{\omega}}_{B/N}][I_{sc,B}]\boldsymbol{\omega}_{B/N} - [I'_{sc,B}]\boldsymbol{\omega}_{B/N} - \sum_{i=1}^{N_S} \left[\dot{\theta}_{i1} I_{s_{i1,2}} [\tilde{\boldsymbol{\omega}}_{B/N}] \hat{\mathbf{s}}_{i1,2} + m_{sp_{i1}} [\tilde{\boldsymbol{\omega}}_{B/N}] [\tilde{\mathbf{r}}_{S_{c,i1}/B}] \mathbf{r}'_{S_{c,i1}/B} \right. \\
& \left. + m_{sp_{i1}} d_{i1} \dot{\theta}_{i1}^2 [\tilde{\mathbf{r}}_{S_{c,i1}/B}] \hat{\mathbf{s}}_{i1,1} + (\dot{\theta}_{i1} + \dot{\theta}_{i2}) I_{s_{i2,2}} [\tilde{\boldsymbol{\omega}}_{B/N}] \hat{\mathbf{s}}_{i2,2} + m_{sp_{i2}} [\tilde{\boldsymbol{\omega}}_{B/N}] [\tilde{\mathbf{r}}_{S_{c,i2}/B}] \mathbf{r}'_{S_{c,i2}/B} \right. \\
& \left. + m_{sp_{i2}} [\tilde{\mathbf{r}}_{S_{c,i2}/B}] (l_{i1} \dot{\theta}_{i1}^2 \hat{\mathbf{s}}_{i1,1} + d_{i2} (\dot{\theta}_{i1} + \dot{\theta}_{i2})^2 \hat{\mathbf{s}}_{i2,1}) \right] + \mathbf{L}_B \quad (3.186)
\end{aligned}$$

Equation (3.186) is the rotational motion equation for dual-hinged rigid-bodies and fits the standard form for the rotational EOM introduced in Section 2.

3.1.5.5 Dual Linked Solar Panel Motion

Let $\mathbf{L}_{H_{i1}} = L_{i1,1} \hat{\mathbf{s}}_{i1,1} + L_{i1,2} \hat{\mathbf{s}}_{i1,2} + L_{i1,3} \hat{\mathbf{s}}_{i1,3}$ be the total torque acting on the first solar panel at point H_{i1} . The corresponding hinge torque is given through

$$L_{i1,2} = -k_{i1} \theta_{i1} - c_{i1} \dot{\theta}_{i1} + k_{i2} \theta_{i2} + c_{i2} \dot{\theta}_{i2} + \hat{\mathbf{s}}_{i1,2} \cdot \boldsymbol{\tau}_{\text{ext}_{i1}, H_{i1}} + \hat{\mathbf{s}}_{i1,2} \cdot \mathbf{r}_{H_{i2}/H_{i1}} \times \mathbf{F}_{1/2i} \quad (3.187)$$

Where $\mathbf{F}_{1/2i}$ is the reaction of solar panel 2 acting on solar panel 1. It is important to point out that $\mathbf{F}_{1/2i} = -\mathbf{F}_{2/1i}$.

To define the $\mathbf{F}_{1/2i}$, $\mathbf{F}_{2/1i}$ needs to be defined. This is done performing the super particle theorem on the second solar panel:

$$\mathbf{F}_{2/1i} + \mathbf{F}_{\text{ext}_{i2}} = m_{sp_{i2}} \ddot{\mathbf{r}}_{S_{c,i2}/N} \quad (3.188)$$

The sum of the external forces on solar panel 2, $\mathbf{F}_{\text{ext}_{i2}}$, is separate because it does not contribute to the reaction force at the joint. With this definition $\mathbf{F}_{1/2i}$ is defined as

$$\mathbf{F}_{1/2i} = \mathbf{F}_{\text{ext}_{i2}} - m_{sp_{i2}} \ddot{\mathbf{r}}_{S_{c,i2}/N} \quad (3.189)$$

Plugging this definition into Eq. (3.187) yields

$$L_{i1,2} = -k_{i1}\theta_{i1} - c_{i1}\dot{\theta}_{i1} + k_{i2}\theta_{i2} + c_{i2}\dot{\theta}_{i2} + \hat{\mathbf{s}}_{i1,2} \cdot \boldsymbol{\tau}_{\text{ext}_{i1},H_{i1}} + \hat{\mathbf{s}}_{i1,2} \cdot \left[\mathbf{r}_{H_{i2}/H_{i1}} \times (\mathbf{F}_{\text{ext}_{i2}} - m_{sp_{i2}} \ddot{\mathbf{r}}_{S_{c,i2}/N}) \right] \quad (3.190)$$

The hinge structure produces the other two torques $L_{i1,1}$ and $L_{i1,3}$. $\boldsymbol{\tau}_{\text{ext}_{i1},H_{i1}}$ is the external torque on the solar panel and is projected onto the $\hat{\mathbf{s}}_{i,2}$ direction to find its contribution to $L_{i1,2}$. Gravity, for example would apply the following torque on the solar panel about point H_{i1}

$$\boldsymbol{\tau}_{g,H_{i1}} = \mathbf{r}_{S_{c,i1}/H_{i1}} \times \mathbf{F}_g \quad (3.191)$$

The inertial angular velocity vector for the solar panel frame is

$$\boldsymbol{\omega}_{S_{i1}/N} = \boldsymbol{\omega}_{S_{i1}/\mathcal{H}_{i1}} + \boldsymbol{\omega}_{\mathcal{H}_{i1}/\mathcal{B}} + \boldsymbol{\omega}_{\mathcal{B}/N} \quad (3.192)$$

where $\boldsymbol{\omega}_{S_{i1}/\mathcal{H}_{i1}} = \dot{\theta}_{i1} \hat{\mathbf{s}}_{i1,2}$. Because the hinge frame \mathcal{H}_{i1} is fixed relative to the body frame \mathcal{B} the relative angular velocity vector is $\boldsymbol{\omega}_{\mathcal{H}_{i1}/\mathcal{B}} = \mathbf{0}$. The body angular velocity vector is written in S_{i1} -frame components as

$$\boldsymbol{\omega}_{\mathcal{B}/N} = (\hat{\mathbf{s}}_{i1,1} \cdot \boldsymbol{\omega}_{\mathcal{B}/N}) \hat{\mathbf{s}}_{i1,1} + (\hat{\mathbf{s}}_{i1,2} \cdot \boldsymbol{\omega}_{\mathcal{B}/N}) \hat{\mathbf{s}}_{i1,2} + (\hat{\mathbf{s}}_{i1,3} \cdot \boldsymbol{\omega}_{\mathcal{B}/N}) \hat{\mathbf{s}}_{i1,3} \quad (3.193)$$

$$= \omega_{s_{i1,1}} \hat{\mathbf{s}}_{i1,1} + \omega_{s_{i1,2}} \hat{\mathbf{s}}_{i1,2} + \omega_{s_{i1,3}} \hat{\mathbf{s}}_{i1,3} \quad (3.194)$$

Using this definition greatly simplifies the following algebraic development. Finally, the inertial solar panel angular velocity vector is written as

$$\boldsymbol{\omega}_{S_{i1}/N} = \omega_{s_{i1,1}} \hat{\mathbf{s}}_{i1,1} + (\omega_{s_{i1,2}} + \dot{\theta}_{i1}) \hat{\mathbf{s}}_{i1,2} + \omega_{s_{i1,3}} \hat{\mathbf{s}}_{i1,3} \quad (3.195)$$

As $\hat{\mathbf{s}}_{i1,2}$ is a body-fixed vector, note that

$$\dot{\omega}_{s_{i1,2}} = \frac{\mathcal{B}_d}{dt} (\boldsymbol{\omega}_{\mathcal{B}/\mathcal{N}} \cdot \hat{\mathbf{s}}_{i1,2}) = \frac{\mathcal{B}_d}{dt} (\boldsymbol{\omega}_{\mathcal{B}/\mathcal{N}}) \cdot \hat{\mathbf{s}}_{i1,2} = \dot{\boldsymbol{\omega}}_{\mathcal{B}/\mathcal{N}} \cdot \hat{\mathbf{s}}_{i1,2} \quad (3.196)$$

Substituting these angular velocity components into the rotational equations of motion of a rigid-body with torques taken about its center of mass[39], the general solar panel equations of motion are written as

$$I_{s_{i1,1}} \dot{\omega}_{s_{i1,1}} = -(I_{s_{i1,3}} - I_{s_{i1,2}})(\omega_{s_{i1,2}} + \dot{\theta}_{i1})\omega_{s_{i1,3}} + L_{s_{i1,1}} \quad (3.197)$$

$$I_{s_{i1,2}}(\dot{\omega}_{s_{i1,2}} + \ddot{\theta}_{i1}) = -(I_{s_{i1,1}} - I_{s_{i1,3}})\omega_{s_{i1,3}}\omega_{s_{i1,1}} + L_{s_{i1,2}} \quad (3.198)$$

$$I_{s_{i1,3}} \dot{\omega}_{s_{i1,3}} = -(I_{s_{i1,2}} - I_{s_{i1,1}})\omega_{s_{i1,1}}(\omega_{s_{i1,2}} + \dot{\theta}_{i1}) + L_{s_{i1,3}} \quad (3.199)$$

where $\mathbf{L}_{S_{c,i1}} = L_{s_{i1,1}}\hat{\mathbf{s}}_{i1,1} + L_{s_{i1,2}}\hat{\mathbf{s}}_{i1,2} + L_{s_{i1,3}}\hat{\mathbf{s}}_{i1,3}$ is the net torque acting on the solar panel about its center of mass. The second differential equation is used to get the equations of motion of θ_{i1} . The first and third equation could be used to back-solve for the structural hinge torques embedded in $L_{s_{i1,1}}$ and $L_{s_{i1,3}}$ if needed.

Let $\mathbf{F}_{S_{c,i1}}$ be the net force acting on the first solar panel. Using the superparticle theorem[39] yields

$$\mathbf{F}_{S_{c,i1}} = m_{\text{sp}_{i1}} \ddot{\mathbf{r}}_{S_{c,i1}/N} \quad (3.200)$$

The torque about the solar panel center of mass can be related to the torque about the hinge point H_{i1} using

$$\mathbf{L}_{H_{i1}} = \mathbf{L}_{S_{c,i1}} + \mathbf{r}_{S_{c,i1}/H_{i1}} \times \mathbf{F}_{S_{c,i1}} \quad (3.201)$$

Solving for the torque about $S_{c,i1}$ yields

$$\mathbf{L}_{S_{c,i1}} = \mathbf{L}_{H_{i1}} - \mathbf{r}_{S_{c,i1}/H_{i1}} \times m_{\text{sp}_{i1}} \ddot{\mathbf{r}}_{S_{c,i1}/N} \quad (3.202)$$

Taking the vector dot product with $\hat{\mathbf{s}}_{i1,2}$ and using $\mathbf{r}_{S_{c,i1}/H_{i1}} = -d_{i1}\hat{\mathbf{s}}_{i1,1}$ results in

$$L_{s_{i1,2}} = \hat{\mathbf{s}}_{i1,2} \cdot \mathbf{L}_{S_{c,i1}} = \underbrace{\hat{\mathbf{s}}_{i1,2} \cdot \mathbf{L}_{H_{i1}}}_{L_{i1,2}} - \hat{\mathbf{s}}_{i1,2} \cdot \left(\mathbf{r}_{S_{c,i1}/H_{i1}} \times m_{\text{sp}_{i1}} \ddot{\mathbf{r}}_{S_{c,i1}/N} \right) \quad (3.203)$$

$$L_{s_{i1,2}} = -k_{i1}\theta_{i1} - c_{i1}\dot{\theta}_{i1} + k_{i2}\theta_{i2} + c_{i2}\dot{\theta}_{i2} + \hat{s}_{i1,2} \cdot \boldsymbol{\tau}_{\text{ext}_{i1}, H_{i1}} + \hat{s}_{i1,2} \cdot \left[\mathbf{r}_{H_{i2}/H_{i1}} \times (\mathbf{F}_{\text{ext}_{i2}} - m_{sp_{i2}} \ddot{\mathbf{r}}_{S_{c,i2}/N}) \right] + m_{sp_{i1}} d_{i1} \hat{s}_{i1,2} \cdot \left(\hat{s}_{i1,1} \times \ddot{\mathbf{r}}_{S_{c,i1}/N} \right) \quad (3.204)$$

Expanding a couple of definitions yields:

$$L_{s_{i1,2}} = -k_{i1}\theta_{i1} - c_{i1}\dot{\theta}_{i1} + k_{i2}\theta_{i2} + c_{i2}\dot{\theta}_{i2} + \hat{s}_{i1,2} \cdot \boldsymbol{\tau}_{\text{ext}_{i1}, H_{i1}} - l_{i1} \hat{s}_{i1,2} \cdot (\hat{s}_{i1,1} \times \mathbf{F}_{\text{ext}_{i2}}) + m_{sp_{i2}} l_{i1} \hat{s}_{i1,2} \cdot \left[\hat{s}_{i1,1} \times (\ddot{\mathbf{r}}_{S_{c,i2}/N}) \right] + m_{sp_{i1}} d_{i1} \hat{s}_{i1,2} \cdot \left(\hat{s}_{i1,1} \times \ddot{\mathbf{r}}_{S_{c,i1}/N} \right) \quad (3.205)$$

Using the double vector cross product identity results in:

$$L_{s_{i1,2}} = -k_{i1}\theta_{i1} - c_{i1}\dot{\theta}_{i1} + k_{i2}\theta_{i2} + c_{i2}\dot{\theta}_{i2} + \hat{s}_{i1,2} \cdot \boldsymbol{\tau}_{\text{ext}_{i1}, H_{i1}} + l_{i1} \hat{s}_{i1,3} \cdot \mathbf{F}_{\text{ext}_{i2}} - m_{sp_{i2}} l_{i1} \hat{s}_{i1,3} \cdot \ddot{\mathbf{r}}_{S_{c,i2}/N} - m_{sp_{i1}} d_{i1} \hat{s}_{i1,3} \cdot \ddot{\mathbf{r}}_{S_{c,i1}/N} \quad (3.206)$$

The following definitions need to be defined:

$$\begin{aligned} \ddot{\mathbf{r}}_{S_{c,i1}/N} &= \ddot{\mathbf{r}}_{B/N} + \ddot{\mathbf{r}}_{S_{c,i1}/B} \\ &= \ddot{\mathbf{r}}_{B/N} + \mathbf{r}''_{S_{c,i1}/B} + 2\boldsymbol{\omega}_{B/N} \times \mathbf{r}'_{S_{c,i1}/B} + \dot{\boldsymbol{\omega}}_{B/N} \times \mathbf{r}_{S_{c,i1}/B} + \boldsymbol{\omega}_{B/N} \times (\boldsymbol{\omega}_{B/N} \times \mathbf{r}_{S_{c,i1}/B}) \end{aligned} \quad (3.207)$$

$$\begin{aligned} \ddot{\mathbf{r}}_{S_{c,i2}/N} &= \ddot{\mathbf{r}}_{B/N} + \ddot{\mathbf{r}}_{S_{c,i2}/B} \\ &= \ddot{\mathbf{r}}_{B/N} + \mathbf{r}''_{S_{c,i2}/B} + 2\boldsymbol{\omega}_{B/N} \times \mathbf{r}'_{S_{c,i2}/B} + \dot{\boldsymbol{\omega}}_{B/N} \times \mathbf{r}_{S_{c,i2}/B} + \boldsymbol{\omega}_{B/N} \times (\boldsymbol{\omega}_{B/N} \times \mathbf{r}_{S_{c,i2}/B}) \end{aligned} \quad (3.208)$$

Substituting these definitions into the torque equation results in:

$$\begin{aligned} L_{s_{i1,2}} &= -k_{i1}\theta_{i1} - c_{i1}\dot{\theta}_{i1} + k_{i2}\theta_{i2} + c_{i2}\dot{\theta}_{i2} + \hat{s}_{i1,2} \cdot \boldsymbol{\tau}_{\text{ext}_{i1}, H_{i1}} + l_{i1} \hat{s}_{i1,3} \cdot \mathbf{F}_{\text{ext}_{i2}} - m_{sp_{i1}} d_{i1} \hat{s}_{i1,3} \cdot \left[\ddot{\mathbf{r}}_{B/N} \right. \\ &\quad \left. + \mathbf{r}''_{S_{c,i1}/B} + 2\boldsymbol{\omega}_{B/N} \times \mathbf{r}'_{S_{c,i1}/B} + \dot{\boldsymbol{\omega}}_{B/N} \times \mathbf{r}_{S_{c,i1}/B} + \boldsymbol{\omega}_{B/N} \times (\boldsymbol{\omega}_{B/N} \times \mathbf{r}_{S_{c,i1}/B}) \right] \\ &\quad - m_{sp_{i2}} l_{i1} \hat{s}_{i1,3} \cdot \left[\ddot{\mathbf{r}}_{B/N} + \mathbf{r}''_{S_{c,i2}/B} + 2\boldsymbol{\omega}_{B/N} \times \mathbf{r}'_{S_{c,i2}/B} + \dot{\boldsymbol{\omega}}_{B/N} \times \mathbf{r}_{S_{c,i2}/B} \right. \\ &\quad \left. + \boldsymbol{\omega}_{B/N} \times (\boldsymbol{\omega}_{B/N} \times \mathbf{r}_{S_{c,i2}/B}) \right] \end{aligned} \quad (3.209)$$

Substituting this torque into the earlier differential equation

$$I_{s_{i1,2}} (\dot{\omega}_{s_{i1,2}} + \ddot{\theta}_{i1}) = -(I_{s_{i1,1}} - I_{s_{i1,3}}) \omega_{s_{i1,3}} \omega_{s_{i1,1}} + L_{s_{i1,2}} \quad (3.210)$$

leads to the desired scalar hinged solar panel equation of motion

$$\begin{aligned}
I_{s_{i1,2}}(\hat{\mathbf{s}}_{i1,2}^T \dot{\boldsymbol{\omega}}_{\mathcal{B}/\mathcal{N}} + \ddot{\theta}_{i1}) &= -(I_{s_{i1,1}} - I_{s_{i1,3}})\omega_{s_{i1,3}}\omega_{s_{i1,1}} - k_{i1}\dot{\theta}_{i1} - c_{i1}\dot{\theta}_{i1} + k_{i2}\dot{\theta}_{i2} + c_{i2}\dot{\theta}_{i2} \\
&+ \hat{\mathbf{s}}_{i1,2} \cdot \boldsymbol{\tau}_{\text{ext}_{i1},H_{i1}} + l_{i1}\hat{\mathbf{s}}_{i1,3} \cdot \mathbf{F}_{\text{ext}_{i2}} - m_{\text{sp}_{i1}}d_{i1}\hat{\mathbf{s}}_{i1,3} \cdot \left[\ddot{\mathbf{r}}_{\mathcal{B}/\mathcal{N}} + \mathbf{r}''_{S_{c,i1}/\mathcal{B}} + 2\boldsymbol{\omega}_{\mathcal{B}/\mathcal{N}} \times \mathbf{r}'_{S_{c,i1}/\mathcal{B}} \right. \\
&+ \dot{\boldsymbol{\omega}}_{\mathcal{B}/\mathcal{N}} \times \mathbf{r}_{S_{c,i1}/\mathcal{B}} + \boldsymbol{\omega}_{\mathcal{B}/\mathcal{N}} \times (\boldsymbol{\omega}_{\mathcal{B}/\mathcal{N}} \times \mathbf{r}_{S_{c,i1}/\mathcal{B}}) \left. \right] - m_{\text{sp}_{i2}}l_{i1}\hat{\mathbf{s}}_{i1,3} \cdot \left[\ddot{\mathbf{r}}_{\mathcal{B}/\mathcal{N}} + \mathbf{r}''_{S_{c,i2}/\mathcal{B}} + 2\boldsymbol{\omega}_{\mathcal{B}/\mathcal{N}} \times \mathbf{r}'_{S_{c,i2}/\mathcal{B}} \right. \\
&\left. + \dot{\boldsymbol{\omega}}_{\mathcal{B}/\mathcal{N}} \times \mathbf{r}_{S_{c,i2}/\mathcal{B}} + \boldsymbol{\omega}_{\mathcal{B}/\mathcal{N}} \times (\boldsymbol{\omega}_{\mathcal{B}/\mathcal{N}} \times \mathbf{r}_{S_{c,i2}/\mathcal{B}}) \right] \quad (3.211)
\end{aligned}$$

Moving second order variables to the left hand side of the equation yields:

$$\begin{aligned}
&\left[m_{\text{sp}_{i1}}d_{i1}\hat{\mathbf{s}}_{i1,3}^T + m_{\text{sp}_{i2}}l_{i1}\hat{\mathbf{s}}_{i1,3}^T \right] \ddot{\mathbf{r}}_{\mathcal{B}/\mathcal{N}} + \left[I_{s_{i1,2}}\hat{\mathbf{s}}_{i1,2}^T - m_{\text{sp}_{i1}}d_{i1}\hat{\mathbf{s}}_{i1,3}^T[\tilde{\mathbf{r}}_{S_{c,i1}/\mathcal{B}}] - m_{\text{sp}_{i2}}l_{i1}\hat{\mathbf{s}}_{i1,3}^T[\tilde{\mathbf{r}}_{S_{c,i2}/\mathcal{B}}] \right] \dot{\boldsymbol{\omega}}_{\mathcal{B}/\mathcal{N}} \\
&+ I_{s_{i1,2}}\ddot{\theta}_{i1} + m_{\text{sp}_{i1}}d_{i1}\hat{\mathbf{s}}_{i1,3}^T \mathbf{r}''_{S_{c,i1}/\mathcal{B}} + m_{\text{sp}_{i2}}l_{i1}\hat{\mathbf{s}}_{i1,3}^T \mathbf{r}''_{S_{c,i2}/\mathcal{B}} = -(I_{s_{i1,1}} - I_{s_{i1,3}})\omega_{s_{i1,3}}\omega_{s_{i1,1}} - k_{i1}\dot{\theta}_{i1} - c_{i1}\dot{\theta}_{i1} \\
&+ k_{i2}\dot{\theta}_{i2} + c_{i2}\dot{\theta}_{i2} + \hat{\mathbf{s}}_{i1,2} \cdot \boldsymbol{\tau}_{\text{ext}_{i1},H_{i1}} + l_{i1}\hat{\mathbf{s}}_{i1,3} \cdot \mathbf{F}_{\text{ext}_{i2}} - m_{\text{sp}_{i1}}d_{i1}\hat{\mathbf{s}}_{i1,3} \cdot \left[2\boldsymbol{\omega}_{\mathcal{B}/\mathcal{N}} \times \mathbf{r}'_{S_{c,i1}/\mathcal{B}} \right. \\
&\left. + \boldsymbol{\omega}_{\mathcal{B}/\mathcal{N}} \times (\boldsymbol{\omega}_{\mathcal{B}/\mathcal{N}} \times \mathbf{r}_{S_{c,i1}/\mathcal{B}}) \right] - m_{\text{sp}_{i2}}l_{i1}\hat{\mathbf{s}}_{i1,3} \cdot \left[2\boldsymbol{\omega}_{\mathcal{B}/\mathcal{N}} \times \mathbf{r}'_{S_{c,i2}/\mathcal{B}} + \boldsymbol{\omega}_{\mathcal{B}/\mathcal{N}} \times (\boldsymbol{\omega}_{\mathcal{B}/\mathcal{N}} \times \mathbf{r}_{S_{c,i2}/\mathcal{B}}) \right] \quad (3.212)
\end{aligned}$$

Expanding the $\mathbf{r}''_{S_{c,i1}/\mathcal{B}}$ and $\mathbf{r}''_{S_{c,i2}/\mathcal{B}}$ terms, replacing cross products with the tilde matrix and again isolating the second order variables results in:

$$\begin{aligned}
&\left[m_{\text{sp}_{i1}}d_{i1}\hat{\mathbf{s}}_{i1,3}^T + m_{\text{sp}_{i2}}l_{i1}\hat{\mathbf{s}}_{i1,3}^T \right] \ddot{\mathbf{r}}_{\mathcal{B}/\mathcal{N}} + \left[I_{s_{i1,2}}\hat{\mathbf{s}}_{i1,2}^T - m_{\text{sp}_{i1}}d_{i1}\hat{\mathbf{s}}_{i1,3}^T[\tilde{\mathbf{r}}_{S_{c,i1}/\mathcal{B}}] - m_{\text{sp}_{i2}}l_{i1}\hat{\mathbf{s}}_{i1,3}^T[\tilde{\mathbf{r}}_{S_{c,i2}/\mathcal{B}}] \right] \dot{\boldsymbol{\omega}}_{\mathcal{B}/\mathcal{N}} \\
&+ \left[I_{s_{i1,2}} + m_{\text{sp}_{i1}}d_{i1}^2 + m_{\text{sp}_{i2}}l_{i1}^2 + m_{\text{sp}_{i2}}l_{i1}d_{i2}\hat{\mathbf{s}}_{i1,3}^T\hat{\mathbf{s}}_{i2,3} \right] \ddot{\theta}_{i1} + \left[m_{\text{sp}_{i2}}l_{i1}d_{i2}\hat{\mathbf{s}}_{i1,3}^T\hat{\mathbf{s}}_{i2,3} \right] \ddot{\theta}_{i2} \\
&= -(I_{s_{i1,1}} - I_{s_{i1,3}})\omega_{s_{i1,3}}\omega_{s_{i1,1}} - k_{i1}\dot{\theta}_{i1} - c_{i1}\dot{\theta}_{i1} + k_{i2}\dot{\theta}_{i2} + c_{i2}\dot{\theta}_{i2} + \hat{\mathbf{s}}_{i1,2}^T \boldsymbol{\tau}_{\text{ext}_{i1},H_{i1}} + l_{i1}\hat{\mathbf{s}}_{i1,3}^T \mathbf{F}_{\text{ext}_{i2}} \\
&\quad - m_{\text{sp}_{i1}}d_{i1}\hat{\mathbf{s}}_{i1,3}^T \left[2[\tilde{\boldsymbol{\omega}}_{\mathcal{B}/\mathcal{N}}]\mathbf{r}'_{S_{c,i1}/\mathcal{B}} + [\tilde{\boldsymbol{\omega}}_{\mathcal{B}/\mathcal{N}}][\tilde{\boldsymbol{\omega}}_{\mathcal{B}/\mathcal{N}}]\mathbf{r}_{S_{c,i1}/\mathcal{B}} \right] \\
&- m_{\text{sp}_{i2}}l_{i1}\hat{\mathbf{s}}_{i1,3}^T \left[2[\tilde{\boldsymbol{\omega}}_{\mathcal{B}/\mathcal{N}}]\mathbf{r}'_{S_{c,i2}/\mathcal{B}} + [\tilde{\boldsymbol{\omega}}_{\mathcal{B}/\mathcal{N}}][\tilde{\boldsymbol{\omega}}_{\mathcal{B}/\mathcal{N}}]\mathbf{r}_{S_{c,i2}/\mathcal{B}} + l_{i1}\dot{\theta}_{i1}^2\hat{\mathbf{s}}_{i1,1} + d_{i2}(\dot{\theta}_{i1} + \dot{\theta}_{i2})^2\hat{\mathbf{s}}_{i2,1} \right] \quad (3.213)
\end{aligned}$$

Eq. (3.213) is the EOM that describes the motion of the first solar panel with a linked secondary panel attached at the end. The final step is to find the EOM of the secondary panel. Following a similar pattern the EOM for the second panel is found. First the torque about point H_{i2} is defined as:

$$L_{i2,2} = -k_{i2}\dot{\theta}_{i2} - c_{i2}\dot{\theta}_{i2} + \hat{\mathbf{s}}_{i2,2} \cdot \boldsymbol{\tau}_{\text{ext}_{i2},H_{i2}} \quad (3.214)$$

The relationship between the torque about the center of mass of the solar panel and about the hinge point is defined as:

$$\mathbf{L}_{H_{i2}} = \mathbf{L}_{S_{c,i2}} + \mathbf{r}_{S_{c,i2}/H_{i2}} \times \mathbf{F}_{S_{c,i2}} \quad (3.215)$$

The torque about $\hat{\mathbf{s}}_{i2,2}$ is the only torque that is required:

$$L_{s_{i2,2}} = \hat{\mathbf{s}}_{i2,2} \cdot \mathbf{L}_{S_{c,i2}} = \underbrace{\hat{\mathbf{s}}_{i2,2} \cdot \mathbf{L}_{H_{i2}}}_{L_{i2,2}} - \hat{\mathbf{s}}_{i2,2} \cdot \left(\mathbf{r}_{S_{c,i2}/H_{i2}} \times m_{\text{sp}_{i2}} \ddot{\mathbf{r}}_{S_{c,i2}/N} \right) \quad (3.216)$$

Substituting Eq. (3.214) into the previous equation yields

$$L_{s_{i2,2}} = -k_{i2}\theta_{i2} - c_{i2}\dot{\theta}_{i2} + \hat{\mathbf{s}}_{i2,2} \cdot \boldsymbol{\tau}_{\text{ext}_{i2},H_{i2}} - m_{\text{sp}_{i2}} d_{i2} \hat{\mathbf{s}}_{i2,3} \cdot \ddot{\mathbf{r}}_{S_{c,i2}/N} \quad (3.217)$$

Substituting this torque into the modified Euler's equation for the second panel

$$I_{s_{i2,2}}(\dot{\omega}_{s_{i2,2}} + \ddot{\theta}_{i1} + \ddot{\theta}_{i2}) = -(I_{s_{i2,1}} - I_{s_{i2,3}})\omega_{s_{i2,3}}\omega_{s_{i2,1}} + L_{s_{i2,2}} \quad (3.218)$$

yields the following equation:

$$I_{s_{i2,2}}(\dot{\omega}_{s_{i2,2}} + \ddot{\theta}_{i1} + \ddot{\theta}_{i2}) = -(I_{s_{i2,1}} - I_{s_{i2,3}})\omega_{s_{i2,3}}\omega_{s_{i2,1}} - k_{i2}\theta_{i2} - c_{i2}\dot{\theta}_{i2} + \hat{\mathbf{s}}_{i2,2}^T \boldsymbol{\tau}_{\text{ext}_{i2},H_{i2}} - m_{\text{sp}_{i2}} d_{i2} \hat{\mathbf{s}}_{i2,3}^T \ddot{\mathbf{r}}_{S_{c,i2}/N} \quad (3.219)$$

Substituting the definition of $\ddot{\mathbf{r}}_{S_{c,i2}/N}$ into Eq (3.219) yields:

$$I_{s_{i2,2}}(\dot{\omega}_{s_{i2,2}} + \ddot{\theta}_{i1} + \ddot{\theta}_{i2}) = -(I_{s_{i2,1}} - I_{s_{i2,3}})\omega_{s_{i2,3}}\omega_{s_{i2,1}} - k_{i2}\theta_{i2} - c_{i2}\dot{\theta}_{i2} + \hat{\mathbf{s}}_{i2,2}^T \boldsymbol{\tau}_{\text{ext}_{i2},H_{i2}} - m_{\text{sp}_{i2}} d_{i2} \hat{\mathbf{s}}_{i2,3}^T \left[\ddot{\mathbf{r}}_{B/N} + \mathbf{r}_{S_{c,i2}/B}'' + 2\boldsymbol{\omega}_{B/N} \times \mathbf{r}_{S_{c,i2}/B}' + \dot{\boldsymbol{\omega}}_{B/N} \times \mathbf{r}_{S_{c,i2}/B} + \boldsymbol{\omega}_{B/N} \times (\boldsymbol{\omega}_{B/N} \times \mathbf{r}_{S_{c,i2}/B}) \right] \quad (3.220)$$

Expanding $\mathbf{r}_{S_{c,i2}/B}''$, isolating second order state variables to the left hand side and introducing the skew symmetric matrix:

$$\begin{aligned} & \left[m_{\text{sp}_{i2}} d_{i2} \hat{\mathbf{s}}_{i2,3}^T \right] \ddot{\mathbf{r}}_{B/N} + \left[I_{s_{i2,2}} \hat{\mathbf{s}}_{i2,2}^T - m_{\text{sp}_{i2}} d_{i2} \hat{\mathbf{s}}_{i2,3}^T [\tilde{\mathbf{r}}_{S_{c,i2}/B}] \right] \dot{\boldsymbol{\omega}}_{B/N} + \left[I_{s_{i2,2}} + m_{\text{sp}_{i2}} d_{i2}^2 \right. \\ & \left. + m_{\text{sp}_{i2}} l_{i1} d_{i2} \hat{\mathbf{s}}_{i2,3}^T \hat{\mathbf{s}}_{i1,3} \right] \ddot{\theta}_{i1} + \left[I_{s_{i2,2}} + m_{\text{sp}_{i2}} d_{i2}^2 \right] \ddot{\theta}_{i2} = -(I_{s_{i2,1}} - I_{s_{i2,3}})\omega_{s_{i2,3}}\omega_{s_{i2,1}} - k_{i2}\theta_{i2} - c_{i2}\dot{\theta}_{i2} \\ & \left. + \hat{\mathbf{s}}_{i2,2}^T \boldsymbol{\tau}_{\text{ext}_{i2},H_{i2}} - m_{\text{sp}_{i2}} d_{i2} \hat{\mathbf{s}}_{i2,3}^T \left[2[\tilde{\boldsymbol{\omega}}_{B/N}] \mathbf{r}_{S_{c,i2}/B}' + [\tilde{\boldsymbol{\omega}}_{B/N}] [\tilde{\boldsymbol{\omega}}_{B/N}] \mathbf{r}_{S_{c,i2}/B} + l_{i1} \dot{\theta}_{i1}^2 \hat{\mathbf{s}}_{i1,1} \right] \quad (3.221) \end{aligned}$$

Eq. (3.221) is the last EOM needed to describe the motion of the spacecraft. The dual-hinged rigid-body EOMs conform the generalized EOM form introduced in Section 2. The next section develops the back substitution method for interconnected panels and gives meaningful insight on how effectors connected to other effectors dynamically couple to the spacecraft.

3.1.5.6 Back Substitution Method

First, Eq. (3.213) and (3.221) are rearranged so that the second order state variables for the solar panel motions are isolated on the left hand side. This manipulation results in Eqs (3.222)-(3.223).

$$\begin{aligned}
& \left[I_{s_{i1,2}} + m_{sp_{i1}} d_{i1}^2 + m_{sp_{i2}} l_{i1}^2 + m_{sp_{i2}} l_{i1} d_{i2} \hat{s}_{i1,3}^T \hat{s}_{i2,3} \right] \ddot{\theta}_{i1} + \left[m_{sp_{i2}} l_{i1} d_{i2} \hat{s}_{i1,3}^T \hat{s}_{i2,3} \right] \ddot{\theta}_{i2} = \\
& - \left[m_{sp_{i1}} d_{i1} \hat{s}_{i1,3}^T + m_{sp_{i2}} l_{i1} \hat{s}_{i1,3}^T \right] \ddot{\mathbf{r}}_{B/N} - \left[I_{s_{i1,2}} \hat{s}_{i1,2}^T - m_{sp_{i1}} d_{i1} \hat{s}_{i1,3}^T [\tilde{\mathbf{r}}_{S_{c,i1}/B}] - m_{sp_{i2}} l_{i1} \hat{s}_{i1,3}^T [\tilde{\mathbf{r}}_{S_{c,i2}/B}] \right] \dot{\boldsymbol{\omega}}_{B/N} \\
& - (I_{s_{i1,1}} - I_{s_{i1,3}}) \omega_{s_{i1,3}} \omega_{s_{i1,1}} - k_{i1} \dot{\theta}_{i1} - c_{i1} \dot{\theta}_{i1} + k_{i2} \dot{\theta}_{i2} + c_{i2} \dot{\theta}_{i2} + \hat{s}_{i1,2}^T \boldsymbol{\tau}_{ext_{i1},H_{i1}} + l_{i1} \hat{s}_{i1,3}^T \mathbf{F}_{ext_{i2}} \\
& - m_{sp_{i1}} d_{i1} \hat{s}_{i1,3}^T \left[2[\tilde{\boldsymbol{\omega}}_{B/N}] \mathbf{r}'_{S_{c,i1}/B} + [\tilde{\boldsymbol{\omega}}_{B/N}] [\tilde{\boldsymbol{\omega}}_{B/N}] \mathbf{r}_{S_{c,i1}/B} \right] \\
& - m_{sp_{i2}} l_{i1} \hat{s}_{i1,3}^T \left[2[\tilde{\boldsymbol{\omega}}_{B/N}] \mathbf{r}'_{S_{c,i2}/B} + [\tilde{\boldsymbol{\omega}}_{B/N}] [\tilde{\boldsymbol{\omega}}_{B/N}] \mathbf{r}_{S_{c,i2}/B} + l_{i1} \dot{\theta}_{i1}^2 \hat{s}_{i1,1} + d_{i2} (\dot{\theta}_{i1} + \dot{\theta}_{i2})^2 \hat{s}_{i2,1} \right] \quad (3.222)
\end{aligned}$$

$$\begin{aligned}
& \left[I_{s_{i2,2}} + m_{sp_{i2}} d_{i2}^2 + m_{sp_{i2}} l_{i1} d_{i2} \hat{s}_{i2,3}^T \hat{s}_{i1,3} \right] \ddot{\theta}_{i1} + \left[I_{s_{i2,2}} + m_{sp_{i2}} d_{i2}^2 \right] \ddot{\theta}_{i2} = \\
& - \left[m_{sp_{i2}} d_{i2} \hat{s}_{i2,3}^T \right] \ddot{\mathbf{r}}_{B/N} - \left[I_{s_{i2,2}} \hat{s}_{i2,2}^T + m_{sp_{i2}} d_{i2} \hat{s}_{i2,3}^T [\tilde{\mathbf{r}}_{S_{c,i2}/B}] \right] \dot{\boldsymbol{\omega}}_{B/N} - (I_{s_{i2,1}} - I_{s_{i2,3}}) \omega_{s_{i2,3}} \omega_{s_{i2,1}} \\
& - k_{i2} \dot{\theta}_{i2} - c_{i2} \dot{\theta}_{i2} + \hat{s}_{i2,2}^T \boldsymbol{\tau}_{ext_{i2},H_{i2}} - m_{sp_{i2}} d_{i2} \hat{s}_{i2,3}^T \left[2[\tilde{\boldsymbol{\omega}}_{B/N}] \mathbf{r}'_{S_{c,i2}/B} \right. \\
& \left. + [\tilde{\boldsymbol{\omega}}_{B/N}] [\tilde{\boldsymbol{\omega}}_{B/N}] \mathbf{r}_{S_{c,i2}/B} + l_{i1} \dot{\theta}_{i1}^2 \hat{s}_{i1,1} \right] \quad (3.223)
\end{aligned}$$

Now, defining a matrix, $[A_i]$, with elements defined as:

$$a_{i1,1} = I_{s_{i1,2}} + m_{sp_{i1}} d_{i1}^2 + m_{sp_{i2}} l_{i1}^2 + m_{sp_{i2}} l_{i1} d_{i2} \hat{s}_{i1,3}^T \hat{s}_{i2,3} \quad (3.224a)$$

$$a_{i1,2} = m_{sp_{i2}} l_{i1} d_{i2} \hat{s}_{i1,3}^T \hat{s}_{i2,3} \quad (3.224b)$$

$$a_{i2,1} = I_{s_{i2,2}} + m_{sp_{i2}} d_{i2}^2 + m_{sp_{i2}} l_{i1} d_{i2} \hat{s}_{i2,3}^T \hat{s}_{i1,3} \quad (3.224c)$$

$$a_{i2,2} = I_{s_{i2,2}} + m_{sp_{i2}} d_{i2}^2 \quad (3.224d)$$

And defining the row elements of a matrix $[F_i]$ as:

$$\mathbf{f}_{i1} = -(m_{sp_{i2}}l_{i1} + m_{sp_{i1}}d_{i1})\hat{\mathbf{s}}_{i1,3}^T \quad (3.225a)$$

$$\mathbf{f}_{i2} = -m_{sp_{i2}}d_{i2}\hat{\mathbf{s}}_{i2,3}^T \quad (3.225b)$$

With a 2×3 matrix, $[G_i]$, which has row elements defined as the following:

$$\mathbf{g}_{i1} = -\left[I_{s_{i1,2}}\hat{\mathbf{s}}_{i1,2}^T - m_{sp_{i1}}d_{i1}\hat{\mathbf{s}}_{i1,3}^T[\tilde{\mathbf{r}}_{S_{c,i1}/B}] - m_{sp_{i2}}l_{i1}\hat{\mathbf{s}}_{i1,3}^T[\tilde{\mathbf{r}}_{S_{c,i2}/B}]\right]^T \quad (3.226a)$$

$$\mathbf{g}_{i2} = -\left[I_{s_{i2,2}}\hat{\mathbf{s}}_{i2,2}^T - m_{sp_{i2}}d_{i2}\hat{\mathbf{s}}_{i2,3}^T[\tilde{\mathbf{r}}_{S_{c,i2}/B}]\right]^T \quad (3.226b)$$

Also defining the vector \mathbf{v}_i as a 2×1 with the following components:

$$\begin{aligned} v_{i1} = & -(I_{s_{i1,1}} - I_{s_{i1,3}})\omega_{s_{i1,3}}\omega_{s_{i1,1}} - k_{i1}\theta_{i1} - c_{i1}\dot{\theta}_{i1} + k_{i2}\theta_{i2} + c_{i2}\dot{\theta}_{i2} + \hat{\mathbf{s}}_{i1,2}^T\boldsymbol{\tau}_{\text{ext}_{i1},H_{i1}} + l_{i1}\hat{\mathbf{s}}_{i1,3}^T\mathbf{F}_{\text{ext}_{i2}} \\ & - m_{sp_{i1}}d_{i1}\hat{\mathbf{s}}_{i1,3}^T\left[2[\tilde{\boldsymbol{\omega}}_{B/N}]\mathbf{r}'_{S_{c,i1}/B} + [\tilde{\boldsymbol{\omega}}_{B/N}][\tilde{\boldsymbol{\omega}}_{B/N}]\mathbf{r}_{S_{c,i1}/B}\right] \\ & - m_{sp_{i2}}l_{i1}\hat{\mathbf{s}}_{i1,3}^T\left[2[\tilde{\boldsymbol{\omega}}_{B/N}]\mathbf{r}'_{S_{c,i2}/B} + [\tilde{\boldsymbol{\omega}}_{B/N}][\tilde{\boldsymbol{\omega}}_{B/N}]\mathbf{r}_{S_{c,i2}/B} + l_{i1}\dot{\theta}_{i1}^2\hat{\mathbf{s}}_{i1,1} + d_{i2}(\dot{\theta}_{i1} + \dot{\theta}_{i2})^2\hat{\mathbf{s}}_{i2,1}\right] \end{aligned} \quad (3.227)$$

$$\begin{aligned} v_{i2} = & -(I_{s_{i2,1}} - I_{s_{i2,3}})\omega_{s_{i2,3}}\omega_{s_{i2,1}} - k_{i2}\theta_{i2} - c_{i2}\dot{\theta}_{i2} + \hat{\mathbf{s}}_{i2,2}^T\boldsymbol{\tau}_{\text{ext}_{i2},H_{i2}} \\ & - m_{sp_{i2}}d_{i2}\hat{\mathbf{s}}_{i2,3}^T\left[2[\tilde{\boldsymbol{\omega}}_{B/N}]\mathbf{r}'_{S_{c,i2}/B} + [\tilde{\boldsymbol{\omega}}_{B/N}][\tilde{\boldsymbol{\omega}}_{B/N}]\mathbf{r}_{S_{c,i2}/B} + l_{i1}\dot{\theta}_{i1}^2\hat{\mathbf{s}}_{i1,1}\right] \end{aligned} \quad (3.228)$$

Using all of the definitions just defined, Eqs. (3.222) and (3.223) can now be re-written as:

$$a_{i1,1}\ddot{\theta}_{i1} + a_{i1,2}\ddot{\theta}_{i2} = \mathbf{f}_{i1}\ddot{\mathbf{r}}_{B/N} + \mathbf{g}_{i1}\dot{\boldsymbol{\omega}}_{B/N} + v_{i1} \quad (3.229)$$

$$a_{i2,1}\ddot{\theta}_{i1} + a_{i2,2}\ddot{\theta}_{i2} = \mathbf{f}_{i2}\ddot{\mathbf{r}}_{B/N} + \mathbf{g}_{i2}\dot{\boldsymbol{\omega}}_{B/N} + v_{i2} \quad (3.230)$$

Eqs. (3.229) and (3.230) are combined and written in matrix form to utilize some linear algebra techniques.

$$[A_i] \begin{bmatrix} \ddot{\theta}_{i1} \\ \ddot{\theta}_{i2} \end{bmatrix} = [F_i]\ddot{\mathbf{r}}_{B/N} + [G_i]\dot{\boldsymbol{\omega}}_{B/N} + \mathbf{v}_i \quad (3.231)$$

Eq. (3.231) can now be solved by inverting matrix $[A_i]$. Note the definition $[E_i] = [A_i]^{-1}$.

$$\begin{bmatrix} \ddot{\theta}_{i1} \\ \ddot{\theta}_{i2} \end{bmatrix} = [E_i][F_i]\ddot{\mathbf{r}}_{B/N} + [E_i][G_i]\dot{\boldsymbol{\omega}}_{B/N} + [E_i]\mathbf{v}_i \quad (3.232)$$

And the subcomponents of $[E]$ are defined as

$$[E] = \begin{bmatrix} \mathbf{e}_{i1}^T \\ \mathbf{e}_{i2}^T \end{bmatrix} \quad (3.233)$$

Since the modified Euler's equation has $\ddot{\theta}_{i1}$ and $\ddot{\theta}_{i2}$ terms, it is more convenient to use the expression for $\ddot{\theta}_i$ as

$$\ddot{\theta}_{i1} = e_{i1}^T [F_i] \ddot{\mathbf{r}}_{B/N} + e_{i1}^T [G_i] \dot{\boldsymbol{\omega}}_{B/N} + e_{i1}^T \mathbf{v}_i \quad (3.234)$$

$$\ddot{\theta}_{i2} = e_{i2}^T [F_i] \ddot{\mathbf{r}}_{B/N} + e_{i2}^T [G_i] \dot{\boldsymbol{\omega}}_{B/N} + e_{i2}^T \mathbf{v}_i \quad (3.235)$$

The next step in the back substitution method is to analytically substitute Eqs. (3.234) and (3.235) into the translational and rotational EOMs. Performing this substitution for translation yields:

$$\begin{aligned} m_{sc} \ddot{\mathbf{r}}_{B/N} - m_{sc} [\tilde{\mathbf{c}}] \dot{\boldsymbol{\omega}}_{B/N} + \sum_{i=1}^{N_S} \left(\left[m_{sp_{i1}} d_{i1} \hat{\mathbf{s}}_{i1,3} + m_{sp_{i2}} l_{i1} \hat{\mathbf{s}}_{i1,3} + m_{sp_{i2}} d_{i2} \hat{\mathbf{s}}_{i2,3} \right] \left(e_{i1}^T [F_i] \ddot{\mathbf{r}}_{B/N} \right. \right. \\ \left. \left. + e_{i1}^T [G_i] \dot{\boldsymbol{\omega}}_{B/N} + e_{i1}^T \mathbf{v}_i \right) + m_{sp_{i2}} d_{i2} \hat{\mathbf{s}}_{i2,3} \left(e_{i2}^T [F_i] \ddot{\mathbf{r}}_{B/N} + e_{i2}^T [G_i] \dot{\boldsymbol{\omega}}_{B/N} + e_{i2}^T \mathbf{v}_i \right) \right) = \mathbf{F} - 2m_{sc} [\tilde{\boldsymbol{\omega}}_{B/N}] \mathbf{c}' \\ - m_{sc} [\tilde{\boldsymbol{\omega}}_{B/N}] [\tilde{\boldsymbol{\omega}}_{B/N}] \mathbf{c} - \sum_{i=1}^{N_S} \left(m_{sp_{i1}} d_{i1} \dot{\theta}_{i1}^2 \hat{\mathbf{s}}_{i1,1} + m_{sp_{i2}} \left[l_{i1} \dot{\theta}_{i1}^2 \hat{\mathbf{s}}_{i1,1} + d_{i2} (\dot{\theta}_{i1} + \dot{\theta}_{i2})^2 \hat{\mathbf{s}}_{i2,1} \right] \right) \end{aligned} \quad (3.236)$$

Combining like terms results in:

$$\begin{aligned} & \left\{ m_{sc} [I_{3 \times 3}] + \sum_{i=1}^{N_S} \left[\left(m_{sp_{i1}} d_{i1} \hat{\mathbf{s}}_{i1,3} + m_{sp_{i2}} l_{i1} \hat{\mathbf{s}}_{i1,3} + m_{sp_{i2}} d_{i2} \hat{\mathbf{s}}_{i2,3} \right) e_{i1}^T [F_i] + m_{sp_{i2}} d_{i2} \hat{\mathbf{s}}_{i2,3} e_{i2}^T [F_i] \right] \right\} \ddot{\mathbf{r}}_{B/N} \\ & + \left\{ -m_{sc} [\tilde{\mathbf{c}}] + \sum_{i=1}^{N_S} \left[\left(m_{sp_{i1}} d_{i1} \hat{\mathbf{s}}_{i1,3} + m_{sp_{i2}} l_{i1} \hat{\mathbf{s}}_{i1,3} + m_{sp_{i2}} d_{i2} \hat{\mathbf{s}}_{i2,3} \right) e_{i1}^T [G_i] + m_{sp_{i2}} d_{i2} \hat{\mathbf{s}}_{i2,3} e_{i2}^T [G_i] \right] \right\} \dot{\boldsymbol{\omega}}_{B/N} \\ & = \mathbf{F} - 2m_{sc} [\tilde{\boldsymbol{\omega}}_{B/N}] \mathbf{c}' - m_{sc} [\tilde{\boldsymbol{\omega}}_{B/N}] [\tilde{\boldsymbol{\omega}}_{B/N}] \mathbf{c} - \sum_{i=1}^{N_S} \left(m_{sp_{i1}} d_{i1} \dot{\theta}_{i1}^2 \hat{\mathbf{s}}_{i1,1} + m_{sp_{i2}} \left[l_{i1} \dot{\theta}_{i1}^2 \hat{\mathbf{s}}_{i1,1} + d_{i2} (\dot{\theta}_{i1} \right. \right. \\ & \left. \left. + \dot{\theta}_{i2})^2 \hat{\mathbf{s}}_{i2,1} \right] + \left[m_{sp_{i1}} d_{i1} \hat{\mathbf{s}}_{i1,3} + m_{sp_{i2}} l_{i1} \hat{\mathbf{s}}_{i1,3} + m_{sp_{i2}} d_{i2} \hat{\mathbf{s}}_{i2,3} \right] e_{i1}^T \mathbf{v}_i + m_{sp_{i2}} d_{i2} \hat{\mathbf{s}}_{i2,3} e_{i2}^T \mathbf{v}_i \right) \end{aligned} \quad (3.237)$$

Performing the same substitution into the rotational equation of motion and simplifying yields:

$$\begin{aligned}
& \left\{ m_{sc}[\tilde{\mathbf{c}}] + \sum_{i=1}^{N_S} \left[(I_{s_{i1,2}} \hat{\mathbf{s}}_{i1,2} + m_{sp_{i1}} d_{i1} [\tilde{\mathbf{r}}_{S_{c,i1}/B}] \hat{\mathbf{s}}_{i1,3} + I_{s_{i2,2}} \hat{\mathbf{s}}_{i2,2} + m_{sp_{i2}} l_{i1} [\tilde{\mathbf{r}}_{S_{c,i2}/B}] \hat{\mathbf{s}}_{i1,3} \right. \right. \\
& \quad \left. \left. + m_{sp_{i2}} d_{i2} [\tilde{\mathbf{r}}_{S_{c,i2}/B}] \hat{\mathbf{s}}_{i2,3} \right) e_{i1}^T [F_i] + (I_{s_{i2,2}} \hat{\mathbf{s}}_{i2,2} + m_{sp_{i2}} d_{i2} [\tilde{\mathbf{r}}_{S_{c,i2}/B}] \hat{\mathbf{s}}_{i2,3} \right) e_{i2}^T [F_i] \right\} \ddot{\mathbf{r}}_{B/N} \\
& + \left\{ [I_{sc,B}] + \sum_{i=1}^{N_S} \left[(I_{s_{i1,2}} \hat{\mathbf{s}}_{i1,2} + m_{sp_{i1}} d_{i1} [\tilde{\mathbf{r}}_{S_{c,i1}/B}] \hat{\mathbf{s}}_{i1,3} + I_{s_{i2,2}} \hat{\mathbf{s}}_{i2,2} + m_{sp_{i2}} l_{i1} [\tilde{\mathbf{r}}_{S_{c,i2}/B}] \hat{\mathbf{s}}_{i1,3} \right. \right. \\
& \quad \left. \left. + m_{sp_{i2}} d_{i2} [\tilde{\mathbf{r}}_{S_{c,i2}/B}] \hat{\mathbf{s}}_{i2,3} \right) e_{i1}^T [G_i] + (I_{s_{i2,2}} \hat{\mathbf{s}}_{i2,2} + m_{sp_{i2}} d_{i2} [\tilde{\mathbf{r}}_{S_{c,i2}/B}] \hat{\mathbf{s}}_{i2,3} \right) e_{i2}^T [G_i] \right\} \dot{\boldsymbol{\omega}}_{B/N} \\
& = -[\tilde{\boldsymbol{\omega}}_{B/N}] [I_{sc,B}] \boldsymbol{\omega}_{B/N} - [I'_{sc,B}] \boldsymbol{\omega}_{B/N} - \sum_{i=1}^{N_S} \left[\dot{\theta}_{i1} I_{s_{i1,2}} [\tilde{\boldsymbol{\omega}}_{B/N}] \hat{\mathbf{s}}_{i1,2} + m_{sp_{i1}} [\tilde{\boldsymbol{\omega}}_{B/N}] [\tilde{\mathbf{r}}_{S_{c,i1}/B}] \mathbf{r}'_{S_{c,i1}/B} \right. \\
& \quad \left. + m_{sp_{i1}} d_{i1} \dot{\theta}_{i1}^2 [\tilde{\mathbf{r}}_{S_{c,i1}/B}] \hat{\mathbf{s}}_{i1,1} + (\dot{\theta}_{i1} + \dot{\theta}_{i2}) I_{s_{i2,2}} [\tilde{\boldsymbol{\omega}}_{B/N}] \hat{\mathbf{s}}_{i2,2} + m_{sp_{i2}} [\tilde{\boldsymbol{\omega}}_{B/N}] [\tilde{\mathbf{r}}_{S_{c,i2}/B}] \mathbf{r}'_{S_{c,i2}/B} \right. \\
& \quad \left. + m_{sp_{i2}} [\tilde{\mathbf{r}}_{S_{c,i2}/B}] (l_{i1} \dot{\theta}_{i1}^2 \hat{\mathbf{s}}_{i1,1} + d_{i2} (\dot{\theta}_{i1} + \dot{\theta}_{i2})^2 \hat{\mathbf{s}}_{i2,1}) + (I_{s_{i1,2}} \hat{\mathbf{s}}_{i1,2} + m_{sp_{i1}} d_{i1} [\tilde{\mathbf{r}}_{S_{c,i1}/B}] \hat{\mathbf{s}}_{i1,3} + I_{s_{i2,2}} \hat{\mathbf{s}}_{i2,2} \right. \\
& \quad \left. + m_{sp_{i2}} l_{i1} [\tilde{\mathbf{r}}_{S_{c,i2}/B}] \hat{\mathbf{s}}_{i1,3} + m_{sp_{i2}} d_{i2} [\tilde{\mathbf{r}}_{S_{c,i2}/B}] \hat{\mathbf{s}}_{i2,3} \right) e_{i1}^T \mathbf{v}_i + (I_{s_{i2,2}} \hat{\mathbf{s}}_{i2,2} \\
& \quad \left. + m_{sp_{i2}} d_{i2} [\tilde{\mathbf{r}}_{S_{c,i2}/B}] \hat{\mathbf{s}}_{i2,3} \right) e_{i2}^T \mathbf{v}_i \Big] + \mathbf{L}_B \quad (3.238)
\end{aligned}$$

Now that the translational and rotational EOMs have been decoupled from the solar panel accelerations the back-substitution matrices can be defined. At this point it is useful to define the matrix contributions in a slightly different way than before by specifically the contributions from an effector. These modified definitions can be seen in following equations:

$$[A] = m_{sc} [I_{3 \times 3}] + [A_{\text{contr}}] \quad (3.239)$$

$$[B] = -m_{sc} [\tilde{\mathbf{c}}] + [B_{\text{contr}}] \quad (3.240)$$

$$\mathbf{v}_{\text{trans}} = \mathbf{F} - 2m_{sc} [\tilde{\boldsymbol{\omega}}_{B/N}] \mathbf{c}' - m_{sc} [\tilde{\boldsymbol{\omega}}_{B/N}] [\tilde{\boldsymbol{\omega}}_{B/N}] \mathbf{c} + \mathbf{v}_{\text{trans,contr}} \quad (3.241)$$

$$[C] = m_{sc} [\tilde{\mathbf{c}}] + [C_{\text{contr}}] \quad (3.242)$$

$$[D] = [I_{sc,B}] + [D_{contr}] \quad (3.243)$$

$$\mathbf{v}_{rot} = -[\tilde{\boldsymbol{\omega}}_{B/N}][I_{sc,B}]\boldsymbol{\omega}_{B/N} - [I'_{sc,B}]\boldsymbol{\omega}_{B/N} + \mathbf{L}_B + \mathbf{v}_{rot,contr} \quad (3.244)$$

Using these new definitions, the back-substitution matrices contributions for dual-hinged rigid-bodies are defined as:

$$[A_{contr}] = \sum_{i=1}^{N_S} \left[\left(m_{sp_{i1}} d_{i1} \hat{\mathbf{s}}_{i1,3} + m_{sp_{i2}} l_{i1} \hat{\mathbf{s}}_{i1,3} + m_{sp_{i2}} d_{i2} \hat{\mathbf{s}}_{i2,3} \right) e_{i1}^T [F_i] + m_{sp_{i2}} d_{i2} \hat{\mathbf{s}}_{i2,3} e_{i2}^T [F_i] \right] \quad (3.245)$$

$$[B_{contr}] = \sum_{i=1}^{N_S} \left[\left(m_{sp_{i1}} d_{i1} \hat{\mathbf{s}}_{i1,3} + m_{sp_{i2}} l_{i1} \hat{\mathbf{s}}_{i1,3} + m_{sp_{i2}} d_{i2} \hat{\mathbf{s}}_{i2,3} \right) e_{i1}^T [G_i] + m_{sp_{i2}} d_{i2} \hat{\mathbf{s}}_{i2,3} e_{i2}^T [G_i] \right] \quad (3.246)$$

$$\begin{aligned} \mathbf{v}_{trans,contr} = & - \sum_{i=1}^{N_S} \left(m_{sp_{i1}} d_{i1} \dot{\theta}_{i1}^2 \hat{\mathbf{s}}_{i1,1} + m_{sp_{i2}} \left[l_{i1} \dot{\theta}_{i1}^2 \hat{\mathbf{s}}_{i1,1} + d_{i2} (\dot{\theta}_{i1} + \dot{\theta}_{i2})^2 \hat{\mathbf{s}}_{i2,1} \right] \right. \\ & \left. + \left[m_{sp_{i1}} d_{i1} \hat{\mathbf{s}}_{i1,3} + m_{sp_{i2}} l_{i1} \hat{\mathbf{s}}_{i1,3} + m_{sp_{i2}} d_{i2} \hat{\mathbf{s}}_{i2,3} \right] e_{i1}^T \mathbf{v}_i + m_{sp_{i2}} d_{i2} \hat{\mathbf{s}}_{i2,3} e_{i2}^T \mathbf{v}_i \right) \end{aligned} \quad (3.247)$$

$$\begin{aligned} [C_{contr}] = & \sum_{i=1}^{N_S} \left[\left(I_{s_{i1,2}} \hat{\mathbf{s}}_{i1,2} + m_{sp_{i1}} d_{i1} [\tilde{\mathbf{r}}_{S_{c,i1}/B}] \hat{\mathbf{s}}_{i1,3} + I_{s_{i2,2}} \hat{\mathbf{s}}_{i2,2} + m_{sp_{i2}} l_{i1} [\tilde{\mathbf{r}}_{S_{c,i2}/B}] \hat{\mathbf{s}}_{i1,3} \right. \right. \\ & \left. \left. + m_{sp_{i2}} d_{i2} [\tilde{\mathbf{r}}_{S_{c,i2}/B}] \hat{\mathbf{s}}_{i2,3} \right) e_{i1}^T [F_i] + \left(I_{s_{i2,2}} \hat{\mathbf{s}}_{i2,2} + m_{sp_{i2}} d_{i2} [\tilde{\mathbf{r}}_{S_{c,i2}/B}] \hat{\mathbf{s}}_{i2,3} \right) e_{i2}^T [F_i] \right] \end{aligned} \quad (3.248)$$

$$\begin{aligned} [D_{contr}] = & \sum_{i=1}^{N_S} \left[\left(I_{s_{i1,2}} \hat{\mathbf{s}}_{i1,2} + m_{sp_{i1}} d_{i1} [\tilde{\mathbf{r}}_{S_{c,i1}/B}] \hat{\mathbf{s}}_{i1,3} + I_{s_{i2,2}} \hat{\mathbf{s}}_{i2,2} + m_{sp_{i2}} l_{i1} [\tilde{\mathbf{r}}_{S_{c,i2}/B}] \hat{\mathbf{s}}_{i1,3} \right. \right. \\ & \left. \left. + m_{sp_{i2}} d_{i2} [\tilde{\mathbf{r}}_{S_{c,i2}/B}] \hat{\mathbf{s}}_{i2,3} \right) e_{i1}^T [G_i] + \left(I_{s_{i2,2}} \hat{\mathbf{s}}_{i2,2} + m_{sp_{i2}} d_{i2} [\tilde{\mathbf{r}}_{S_{c,i2}/B}] \hat{\mathbf{s}}_{i2,3} \right) e_{i2}^T [G_i] \right] \end{aligned} \quad (3.249)$$

$$\begin{aligned} [v_{rot,contr}] = & - \sum_{i=1}^{N_S} \left[\dot{\theta}_{i1} I_{s_{i1,2}} [\tilde{\boldsymbol{\omega}}_{B/N}] \hat{\mathbf{s}}_{i1,2} + m_{sp_{i1}} [\tilde{\boldsymbol{\omega}}_{B/N}] [\tilde{\mathbf{r}}_{S_{c,i1}/B}] \mathbf{r}'_{S_{c,i1}/B} + m_{sp_{i1}} d_{i1} \dot{\theta}_{i1}^2 [\tilde{\mathbf{r}}_{S_{c,i1}/B}] \hat{\mathbf{s}}_{i1,1} \right. \\ & \left. + (\dot{\theta}_{i1} + \dot{\theta}_{i2}) I_{s_{i2,2}} [\tilde{\boldsymbol{\omega}}_{B/N}] \hat{\mathbf{s}}_{i2,2} + m_{sp_{i2}} [\tilde{\boldsymbol{\omega}}_{B/N}] [\tilde{\mathbf{r}}_{S_{c,i2}/B}] \mathbf{r}'_{S_{c,i2}/B} + m_{sp_{i2}} [\tilde{\mathbf{r}}_{S_{c,i2}/B}] (l_{i1} \dot{\theta}_{i1}^2 \hat{\mathbf{s}}_{i1,1} \right. \\ & \left. + d_{i2} (\dot{\theta}_{i1} + \dot{\theta}_{i2})^2 \hat{\mathbf{s}}_{i2,1}) + \left(I_{s_{i1,2}} \hat{\mathbf{s}}_{i1,2} + m_{sp_{i1}} d_{i1} [\tilde{\mathbf{r}}_{S_{c,i1}/B}] \hat{\mathbf{s}}_{i1,3} + I_{s_{i2,2}} \hat{\mathbf{s}}_{i2,2} + m_{sp_{i2}} l_{i1} [\tilde{\mathbf{r}}_{S_{c,i2}/B}] \hat{\mathbf{s}}_{i1,3} \right. \right. \\ & \left. \left. + m_{sp_{i2}} d_{i2} [\tilde{\mathbf{r}}_{S_{c,i2}/B}] \hat{\mathbf{s}}_{i2,3} \right) e_{i1}^T \mathbf{v}_i + \left(I_{s_{i2,2}} \hat{\mathbf{s}}_{i2,2} + m_{sp_{i2}} d_{i2} [\tilde{\mathbf{r}}_{S_{c,i2}/B}] \hat{\mathbf{s}}_{i2,3} \right) e_{i2}^T \mathbf{v}_i \right] \end{aligned} \quad (3.250)$$

This concludes the derivation of EOMs for dual-hinged rigid-bodies conforming to both the generalized EOM form and the back-substitution method seen in Section 2.

3.1.6 Imbalanced Variable Speed Control Moment Gyroscopes

3.1.6.1 Introduction

Similar to reaction wheels, variable speed control moment gyroscopes (VSCMGs) are also susceptible to jitter disturbances. In Reference [45], a dynamics model is developed using the standard EOM form and back-substitution method introduced in this dissertation. This work is summarized in this section to show conformity with these equations.

3.1.6.2 Problem Statement

The problem consists of modeling static and dynamic imbalance of any number of wheel + gimbal assemblies attached to a rigid spacecraft. In order to develop the equations of motion in a general way, arbitrary locations, inertia tensors, and center of mass locations for the spacecraft hub, gimbal, and wheels are considered. Additionally, the wheel center of mass is not assumed to lie on the gimbal axis of the VSCMG, and the wheel frame origin and gimbal frame origin are not assumed to coincide.

The development considers the body frame and N gimbal and wheel frames as well as the inertial frame. The body frame is denoted \mathcal{B} . The basis vectors of the body frame are

$$\mathcal{B} : \{B, \hat{\mathbf{b}}_1, \hat{\mathbf{b}}_2, \hat{\mathbf{b}}_3\} \quad (3.251)$$

The i^{th} gimbal and wheel frames are denoted \mathcal{G}_i and \mathcal{W}_i , respectively. The basis vectors of \mathcal{G}_i and \mathcal{W}_i are defined as

$$\mathcal{G}_i : \{G_i, \hat{\mathbf{g}}_{s_i}, \hat{\mathbf{g}}_{t_i}, \hat{\mathbf{g}}_{g_i}\} \quad (3.252)$$

$$\mathcal{W}_i : \{W_i, \hat{\mathbf{g}}_{s_i}, \hat{\mathbf{w}}_{2_i}, \hat{\mathbf{w}}_{3_i}\} \quad (3.253)$$

It is assumed that the $\hat{\mathbf{g}}_{s_i}$ vectors of the \mathcal{G}_i and \mathcal{W}_i frames are always parallel.

Parameters relating to the spacecraft hub are denoted with a subscript text B. Parameters relating to the i^{th} gimbal and wheel are denoted with subscripts text G_i and W_i , respectively. The hub, gimbal, and wheel each are allowed center of mass offsets from their respective coordinate frame origins. The hub's center of mass location is labeled as B_c . This location is described with respect to the body frame origin as $\mathbf{r}_{B_c/B}$. The gimbal is also allowed a general center of mass offset from the gimbal frame origin. This location is labeled as G_{c_i} and is located with respect to the gimbal frame origin as $\mathbf{r}_{G_{c_i}/G_i}$. The wheel's center of mass location is labeled somewhat differently. The wheel center of mass is assumed to lie on the $\hat{\mathbf{w}}_{2_i}$ axis a length d_i from the wheel frame origin. This does not result in loss of generality since the parameters L_i and ℓ_i describe the axial and transverse offset, respectively, of the wheel origin. Thus, the wheel center of mass location is allowed to vary in three dimensions with respect to the gimbal frame (and thus the body frame as well, since the gimbal origin location does not vary with respect to the body). Since the gimbal and wheel centers of mass change with time, so does the overall spacecraft center of mass. The time-varying center of mass of the entire system is denoted c .

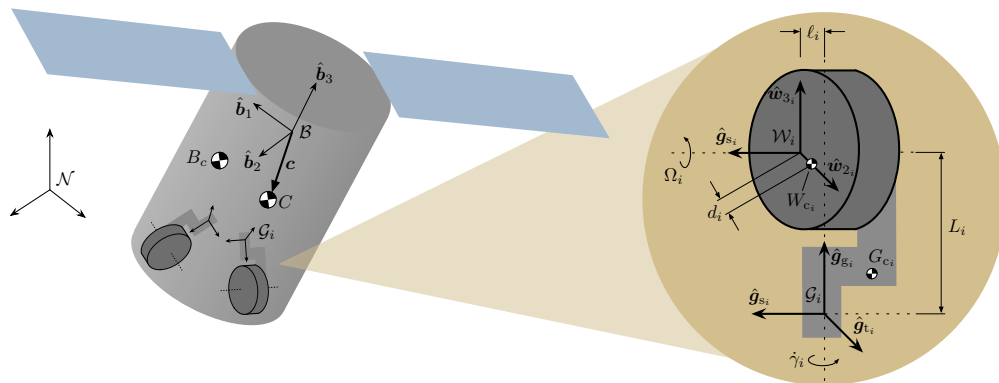


Figure 3.8: Reference frame setup and variable definitions for the spacecraft + VSCMG problem.

3.1.6.3 Balanced VSCMG Back-Substitution

The balanced VSCMG equations of motion are reproduced here for the reader's convenience. The balanced translational equation of motion is given below. Note that translation is not coupled with $\dot{\Omega}$ or $\ddot{\gamma}_i$.

$$m_{sc}\ddot{\mathbf{r}}_{B/N} - m_{sc}[\tilde{\mathbf{c}}]\dot{\boldsymbol{\omega}} = \mathbf{F} - 2m_{sc}[\tilde{\boldsymbol{\omega}}]\mathbf{c}' - m_{sc}[\tilde{\boldsymbol{\omega}}]^2\mathbf{c}$$

The rotational equation of motion includes $\dot{\Omega}_i$ and $\ddot{\gamma}_i$ terms, and is thus coupled with VSCMG motion as seen below.

$$\begin{aligned} m_{sc}[\tilde{\mathbf{c}}]\ddot{\mathbf{r}}_{B/N} + [I_{sc,B}]\dot{\boldsymbol{\omega}} + \sum_{i=1}^N I_{V_{g_i}}\hat{\mathbf{g}}_{g_i}\ddot{\gamma}_i + \sum_{i=1}^N I_{W_{s_i}}\hat{\mathbf{g}}_{s_i}\dot{\Omega}_i \\ = \mathbf{L}_B - [I_{sc,B}]\boldsymbol{\omega} - [\tilde{\boldsymbol{\omega}}][I_{sc,B}]\boldsymbol{\omega} - \sum_{i=1}^N \left[+ I_{W_{t_i}}\Omega\dot{\gamma}\hat{\mathbf{g}}_{t_i} + \Omega_i\dot{\gamma}_i(I_{W_{s_i}} - I_{W_{t_i}})\hat{\mathbf{g}}_{t_i} \right. \\ \left. + [\tilde{\boldsymbol{\omega}}][I_{G_i,G_{c_i}}]\dot{\gamma}_i\hat{\mathbf{g}}_{g_i} + [\tilde{\boldsymbol{\omega}}][I_{W_i,W_{c_i}}]\boldsymbol{\omega}_{W_i/B} \right] \end{aligned}$$

The gimbal torque equation can be seen in the following equation.

$$I_{V_{g_i}}(\hat{\mathbf{g}}_{g_i}^T\dot{\boldsymbol{\omega}} + \ddot{\gamma}_i) = u_{g_i} + (I_{V_{s_i}} - I_{V_{t_i}})\omega_s\omega_t + I_{W_{s_i}}\Omega_i\omega_t$$

The wheel torque equation is described below.

$$I_{W_{s_i}}(\hat{\mathbf{g}}_{s_i}^T\dot{\boldsymbol{\omega}} + \dot{\Omega}_i) = -I_{W_{s_i}}\omega_t\dot{\gamma}_i + u_{s_i}$$

For the back-substitution method, first the gimbal torque equation is solved for $\ddot{\gamma}_i$ in terms of $\dot{\boldsymbol{\omega}}_{B/N}$.

$$\ddot{\gamma}_i = \frac{1}{I_{V_{g_i}}} \left(u_{g_i} + (I_{V_{s_i}} - I_{V_{t_i}})\omega_s\omega_t + I_{W_{s_i}}\Omega_i\omega_t - I_{V_{g_i}}\hat{\mathbf{g}}_{g_i}^T\dot{\boldsymbol{\omega}} \right) \quad (3.254)$$

Additionally, the wheel torque equation is solved for $\dot{\Omega}_i$ in terms of $\dot{\boldsymbol{\omega}}_{B/N}$

$$\dot{\Omega}_i = -\omega_t\dot{\gamma}_i - \hat{\mathbf{g}}_{s_i}^T\dot{\boldsymbol{\omega}} + \frac{u_{s_i}}{I_{W_{s_i}}} \quad (3.255)$$

Plugging into the rotational equation of motion and group like terms.

$$\begin{aligned}
m_{sc}[\tilde{\mathbf{c}}]\ddot{\mathbf{r}}_{B/N} + \left[[I_{sc,B}] - \sum_{i=1}^N (I_{V_{g_i}} \hat{\mathbf{g}}_{g_i} \hat{\mathbf{g}}_{g_i}^T \dot{\boldsymbol{\omega}} + I_{W_{s_i}} \hat{\mathbf{g}}_{s_i} \hat{\mathbf{g}}_{s_i}^T) \right] \dot{\boldsymbol{\omega}} \\
= \mathbf{L}_B - [I_{sc,B}]' \boldsymbol{\omega} - [\tilde{\boldsymbol{\omega}}][I_{sc,B}] \boldsymbol{\omega} - \sum_{i=1}^N \left[(u_{s_i} - I_{W_{s_i}} \omega_t \dot{\gamma}_i) \hat{\mathbf{g}}_{s_i} + I_{W_{s_i}} \Omega \dot{\gamma}_i \hat{\mathbf{g}}_{t_i} \right. \\
\left. + (u_{g_i} + (I_{V_{s_i}} - I_{V_{t_i}}) \omega_s \omega_t + I_{W_{s_i}} \Omega_i \omega_t) \hat{\mathbf{g}}_{g_i} + [\tilde{\boldsymbol{\omega}}][I_{G_i, G_{c_i}}] \dot{\gamma}_i \hat{\mathbf{g}}_{g_i} + [\tilde{\boldsymbol{\omega}}][I_{W_i, W_{c_i}}] \boldsymbol{\omega}_{\mathcal{W}_i/B} \right] \quad (3.256)
\end{aligned}$$

All of the information needed to define the back-substitution contribution matrices for a balanced VSCMG is defined. The balanced VSCMG back-substitution contribution matrices are given by:

$$[A_{\text{contr}}] = [0_{3 \times 3}] \quad (3.257)$$

$$[B_{\text{contr}}] = [0_{3 \times 3}] \quad (3.258)$$

$$[C_{\text{contr}}] = [0_{3 \times 3}] \quad (3.259)$$

$$[D_{\text{contr}}] = - \sum_{i=1}^N [I_{V_{g_i}} \hat{\mathbf{g}}_{g_i} \hat{\mathbf{g}}_{g_i}^T + I_{W_{s_i}} \hat{\mathbf{g}}_{s_i} \hat{\mathbf{g}}_{s_i}^T] \quad (3.260)$$

$$\mathbf{v}_{\text{trans,contr}} = \mathbf{0} \quad (3.261)$$

$$\begin{aligned}
\mathbf{v}_{\text{rot,contr}} = - \sum_{i=1}^N \left[(u_{s_i} - I_{W_{s_i}} \omega_t \dot{\gamma}_i) \hat{\mathbf{g}}_{s_i} + I_{W_{s_i}} \Omega \dot{\gamma}_i \hat{\mathbf{g}}_{t_i} + (u_{g_i} + (I_{V_{s_i}} - I_{V_{t_i}}) \omega_s \omega_t + I_{W_{s_i}} \Omega_i \omega_t) \hat{\mathbf{g}}_{g_i} \right. \\
\left. + [\tilde{\boldsymbol{\omega}}][I_{G_i, G_{c_i}}] \dot{\gamma}_i \hat{\mathbf{g}}_{g_i} + [\tilde{\boldsymbol{\omega}}][I_{W_i, W_{c_i}}] \boldsymbol{\omega}_{\mathcal{W}_i/B} \right] \quad (3.262)
\end{aligned}$$

3.1.6.4 Imbalanced VSCMG Back-Substitution

The EOMs representing a spacecraft with N imbalanced VSCMGs were derived in Reference [45] and are repeated here to show conformity between the EOMs and the generalized EOMs provided in this dissertation. The first step is to rewrite the translational equation of motion in a

convenient form. The original equation is,

$$\begin{aligned} \ddot{\mathbf{r}}_{B/N} - [\tilde{\mathbf{c}}]\dot{\boldsymbol{\omega}} + \frac{1}{m_{sc}} \sum_{i=1}^N \left[m_{G_i} [\tilde{\mathbf{g}}_{g_i}] \mathbf{r}_{G_{c_i}/G_i} - m_{W_i} d_i c \theta_i \hat{\mathbf{g}}_{s_i} + m_{W_i} \ell_i \hat{\mathbf{g}}_{t_i} \right] \ddot{\gamma}_i + \frac{1}{m_{sc}} \sum_{i=1}^N [m_{W_i} d_i \hat{\boldsymbol{\omega}}_{3_i}] \dot{\Omega}_i \\ = \ddot{\mathbf{r}}_{C/N} - 2[\tilde{\boldsymbol{\omega}}]\mathbf{c}' - [\tilde{\boldsymbol{\omega}}][\tilde{\boldsymbol{\omega}}]\mathbf{c} - \frac{1}{m_{sc}} \sum_{i=1}^N \left[m_{G_i} \dot{\gamma}_i [\tilde{\mathbf{g}}_{g_i}] \mathbf{r}'_{G_{c_i}/B} \right. \\ \left. + m_{W_i} [(2d_i \dot{\gamma}_i \Omega_i s \theta_i - \ell_i \dot{\gamma}_i^2) \hat{\mathbf{g}}_{s_i} - d_i \dot{\gamma}_i^2 c \theta_i \hat{\mathbf{g}}_{t_i} - d_i \Omega_i^2 \hat{\boldsymbol{\omega}}_{2_i}] \right] \end{aligned} \quad (3.263)$$

This equation may be abbreviated as,

$$\ddot{\mathbf{r}}_{B/N} - [\tilde{\mathbf{c}}]\dot{\boldsymbol{\omega}} + \frac{1}{m_{sc}} \sum_{i=1}^N \mathbf{u}_{r_i} \ddot{\gamma}_i + \frac{1}{m_{sc}} \sum_{i=1}^N \mathbf{v}_{r_i} \dot{\Omega}_i = \ddot{\mathbf{r}}_{C/N} - 2[\tilde{\boldsymbol{\omega}}]\mathbf{c}' - [\tilde{\boldsymbol{\omega}}]^2 \mathbf{c} - \frac{1}{m_{sc}} \sum_{i=1}^N \mathbf{k}_{r_i} \quad (3.264)$$

where,

$$\mathbf{u}_{r_i} = m_{G_i} [\tilde{\mathbf{g}}_{g_i}] \mathbf{r}_{G_{c_i}/G_i} - m_{W_i} d_i c \theta_i \hat{\mathbf{g}}_{s_i} + m_{W_i} \ell_i \hat{\mathbf{g}}_{t_i} \quad (3.265)$$

$$\mathbf{v}_{r_i} = m_{W_i} d_i \hat{\boldsymbol{\omega}}_{3_i} \quad (3.266)$$

$$\mathbf{k}_{r_i} = m_{G_i} \dot{\gamma}_i [\tilde{\mathbf{g}}_{g_i}] \mathbf{r}'_{G_{c_i}/B} + m_{W_i} [(2d_i \dot{\gamma}_i \Omega_i s \theta_i - \ell_i \dot{\gamma}_i^2) \hat{\mathbf{g}}_{s_i} - d_i \dot{\gamma}_i^2 c \theta_i \hat{\mathbf{g}}_{t_i} - d_i \Omega_i^2 \hat{\boldsymbol{\omega}}_{2_i}] \quad (3.267)$$

The next step is to rewrite the rotational equation of motion in a convenient form. The original equation is,

$$\begin{aligned} m_{sc} [\tilde{\mathbf{c}}] \ddot{\mathbf{r}}_{B/N} + [I_{sc,B}] \dot{\boldsymbol{\omega}} + \sum_{i=1}^N \left[[I_{G_i, G_{c_i}}] \hat{\mathbf{g}}_{g_i} + m_{G_i} [\tilde{\mathbf{r}}_{G_{c_i}/B}] [\tilde{\mathbf{g}}_{g_i}] \mathbf{r}_{G_{c_i}/G_i} + [I_{W_i, W_{c_i}}] \hat{\mathbf{g}}_{g_i} \right. \\ \left. + m_{W_i} [\tilde{\mathbf{r}}_{W_{c_i}/B}] (\ell_i \hat{\mathbf{g}}_{t_i} - d_i c \theta_i \hat{\mathbf{g}}_{s_i}) \right] \ddot{\gamma}_i + \sum_{i=1}^N \left[[I_{W_i, W_{c_i}}] \hat{\mathbf{g}}_{s_i} + m_{W_i} d_i [\tilde{\mathbf{r}}_{W_{c_i}/B}] \hat{\boldsymbol{\omega}}_{3_i} \right] \dot{\Omega}_i \\ = \mathbf{L}_B - [I_{sc,B}]' \boldsymbol{\omega} - [\tilde{\boldsymbol{\omega}}] [I_{sc,B}] \boldsymbol{\omega} - \sum_{i=1}^N \left[[I_{G_i, G_{c_i}}]' \dot{\gamma}_i \hat{\mathbf{g}}_{g_i} + [\tilde{\boldsymbol{\omega}}] [I_{G_i, G_{c_i}}] \dot{\gamma}_i \hat{\mathbf{g}}_{g_i} + m_{G_i} [\tilde{\boldsymbol{\omega}}] [\tilde{\mathbf{r}}_{G_{c_i}/B}] \mathbf{r}'_{G_{c_i}/B} \right. \\ \left. + m_{G_i} \dot{\gamma}_i [\tilde{\mathbf{r}}_{G_{c_i}/B}] [\tilde{\mathbf{g}}_{g_i}] \mathbf{r}'_{G_{c_i}/G_i} + [I_{W_i, W_{c_i}}] \Omega_i \dot{\gamma}_i \hat{\mathbf{g}}_{t_i} + [I_{W_i, W_{c_i}}]' \boldsymbol{\omega}_{W_i/B} + [\tilde{\boldsymbol{\omega}}] [I_{W_i, W_{c_i}}] \boldsymbol{\omega}_{W_i/B} \right. \\ \left. + m_{W_i} [\tilde{\boldsymbol{\omega}}] [\tilde{\mathbf{r}}_{W_{c_i}/B}] \mathbf{r}'_{W_{c_i}/B} + m_{W_i} [\tilde{\mathbf{r}}_{W_{c_i}/B}] [(2d_i \dot{\gamma}_i \Omega_i s \theta_i - \ell_i \dot{\gamma}_i^2) \hat{\mathbf{g}}_{s_i} - d_i \dot{\gamma}_i^2 c \theta_i \hat{\mathbf{g}}_{t_i} - d_i \Omega_i^2 \hat{\boldsymbol{\omega}}_{2_i}] \right] \end{aligned}$$

This equation may be abbreviated as,

$$\begin{aligned} m_{sc} [\tilde{\mathbf{c}}] \ddot{\mathbf{r}}_{B/N} + [I_{sc,B}] \dot{\boldsymbol{\omega}} + \sum_{i=1}^N \mathbf{u}_{\omega_i} \ddot{\gamma}_i + \sum_{i=1}^N \mathbf{v}_{\omega_i} \dot{\Omega}_i \\ = \mathbf{L}_B - [I_{sc,B}]' \boldsymbol{\omega} - [\tilde{\boldsymbol{\omega}}] [I_{sc,B}] \boldsymbol{\omega} - \sum_{i=1}^N \mathbf{k}_{\omega_i} \end{aligned} \quad (3.268)$$

where,

$$\begin{aligned} \mathbf{u}_{\omega_i} = & [I_{G_i, G_{c_i}}] \hat{\mathbf{g}}_{g_i} + m_{G_i} [\tilde{\mathbf{r}}_{G_{c_i}/B}] [\tilde{\hat{\mathbf{g}}}_{g_i}] \mathbf{r}_{G_{c_i}/G_i} + [I_{W_i, W_{c_i}}] \hat{\mathbf{g}}_{g_i} \\ & + m_{W_i} [\tilde{\mathbf{r}}_{W_{c_i}/B}] (\ell_i \hat{\mathbf{g}}_{t_i} - d_i c \theta_i \hat{\mathbf{g}}_{s_i}) \end{aligned} \quad (3.269)$$

$$\mathbf{v}_{\omega_i} = [I_{W_i, W_{c_i}}] \hat{\mathbf{g}}_{s_i} + m_{W_i} d_i [\tilde{\mathbf{r}}_{W_{c_i}/B}] \hat{\mathbf{w}}_{3_i} \quad (3.270)$$

$$\begin{aligned} \mathbf{k}_{\omega_i} = & [I_{G_i, G_{c_i}}]' \dot{\gamma}_i \hat{\mathbf{g}}_{g_i} + [\tilde{\omega}][I_{G_i, G_{c_i}}] \dot{\gamma}_i \hat{\mathbf{g}}_{g_i} + m_{G_i} [\tilde{\omega}] [\tilde{\mathbf{r}}_{G_{c_i}/B}] \mathbf{r}'_{G_{c_i}/B} + m_{G_i} \dot{\gamma}_i [\tilde{\mathbf{r}}_{G_{c_i}/B}] [\tilde{\hat{\mathbf{g}}}_{g_i}] \mathbf{r}'_{G_{c_i}/G_i} \\ & + [I_{W_i, W_{c_i}}] \Omega \dot{\gamma} \hat{\mathbf{g}}_{t_i} + [I_{W_i, W_{c_i}}]' \omega_{\mathcal{W}_i/B} + [\tilde{\omega}] [I_{W_i, W_{c_i}}] \omega_{\mathcal{W}_i/B} + m_{W_i} [\tilde{\omega}] [\tilde{\mathbf{r}}_{W_{c_i}/B}] \mathbf{r}'_{W_{c_i}/B} \\ & + m_{W_i} [\tilde{\mathbf{r}}_{W_{c_i}/B}] [(2d_i \dot{\gamma}_i \Omega_i s \theta_i - \ell_i \dot{\gamma}_i^2) \hat{\mathbf{g}}_{s_i} - d_i \dot{\gamma}_i^2 c \theta_i \hat{\mathbf{g}}_{t_i} - d_i \Omega_i^2 \hat{\mathbf{w}}_{2_i}] \end{aligned} \quad (3.271)$$

Again, including the equations from Reference [45], the gimbal torque equation is:

$$\begin{aligned} & \hat{\mathbf{g}}_{g_i}^T \left[m_{V_i} [\tilde{\mathbf{r}}_{V_{c_i}/G_i}] \right] \ddot{\mathbf{r}}_{B/N} + \hat{\mathbf{g}}_{g_i}^T \left[[I_{V_i, V_{c_i}}] + m_{V_i} [\tilde{\mathbf{r}}_{V_{c_i}/G_i}] [\tilde{\mathbf{r}}_{V_{c_i}/B}]^T \right] \dot{\omega} + \hat{\mathbf{g}}_{g_i}^T \left[[I_{G_i, G_{c_i}}] \hat{\mathbf{g}}_{g_i} \right. \\ & + [I_{W_i, W_{c_i}}] \hat{\mathbf{g}}_{g_i} + [P_i] (\ell_i \hat{\mathbf{g}}_{t_i} - d_i c \theta_i \hat{\mathbf{g}}_{s_i}) + [Q_i] [\tilde{\hat{\mathbf{g}}}_{g_i}] \mathbf{r}_{G_{c_i}/G_i} \left. \right] \ddot{\gamma}_i + \hat{\mathbf{g}}_{g_i}^T \left[[I_{W_i, W_{c_i}}] \hat{\mathbf{g}}_{s_i} + [P_i] d_i \hat{\mathbf{w}}_{3_i} \right] \dot{\Omega}_i \\ & = -\hat{\mathbf{g}}_{g_i}^T \left[\dot{\gamma}_i [Q_i] [\tilde{\hat{\mathbf{g}}}_{g_i}] \mathbf{r}'_{G_{c_i}/G_i} + [P_i] [(2d_i \dot{\gamma}_i \Omega_i s \theta_i - \ell_i \dot{\gamma}_i^2) \hat{\mathbf{g}}_{s_i} - d_i \dot{\gamma}_i^2 c \theta_i \hat{\mathbf{g}}_{t_i} - d_i \Omega_i^2 \hat{\mathbf{w}}_{2_i}] \right. \\ & + [I_{G_i, G_{c_i}}]' \omega_{G_i/N} + [\tilde{\omega}] [I_{G_i, G_{c_i}}] \omega_{G_i/N} + [I_{W_i, W_{c_i}}] \Omega \dot{\gamma} \hat{\mathbf{g}}_{t_i} + [I_{W_i, W_{c_i}}]' \omega_{\mathcal{W}_i/N} + [\tilde{\omega}] [I_{W_i, W_{c_i}}] \omega_{\mathcal{W}_i/N} \\ & + m_{G_i} [\tilde{\mathbf{r}}_{G_{c_i}/V_{c_i}}] (2[\tilde{\omega}] \mathbf{r}'_{G_{c_i}/V_{c_i}} + [\tilde{\omega}]^2 \mathbf{r}_{G_{c_i}/V_{c_i}}) + m_{W_i} [\tilde{\mathbf{r}}_{W_{c_i}/V_{c_i}}] (2[\tilde{\omega}] \mathbf{r}'_{W_{c_i}/V_{c_i}} \\ & \left. + [\tilde{\omega}]^2 \mathbf{r}_{W_{c_i}/V_{c_i}}) + m_{V_i} [\tilde{\mathbf{r}}_{V_{c_i}/G_i}] (2[\tilde{\omega}] \mathbf{r}'_{V_{c_i}/B} + [\tilde{\omega}]^2 \mathbf{r}_{V_{c_i}/B}) \right] + u_{g_i} \end{aligned} \quad (3.272)$$

where,

$$[I_{V_i, V_{c_i}}] = [I_{G_i, V_{c_i}}] + [I_{W_i, V_{c_i}}] \quad (3.273)$$

$$[I_{G_i, V_{c_i}}] = [I_{G_i, G_i}] + m_{G_i} [\tilde{\mathbf{r}}_{G_{c_i}/V_{c_i}}] [\tilde{\mathbf{r}}_{G_{c_i}/V_{c_i}}]^T \quad (3.274)$$

$$[I_{W_i, V_{c_i}}] = [I_{W_i, W_{c_i}}] + m_{W_i} [\tilde{\mathbf{r}}_{W_{c_i}/V_{c_i}}] [\tilde{\mathbf{r}}_{W_{c_i}/V_{c_i}}]^T \quad (3.275)$$

$$[P_i] = m_{W_i} \rho_{G_i} [\tilde{\mathbf{r}}_{W_{c_i}/V_{c_i}}] - m_{G_i} \rho_{W_i} [\tilde{\mathbf{r}}_{G_{c_i}/V_{c_i}}] + m_{W_i} [\tilde{\mathbf{r}}_{V_{c_i}/G_i}] \quad (3.276)$$

$$[Q_i] = m_{G_i} \rho_{W_i} [\tilde{\mathbf{r}}_{G_{c_i}/V_{c_i}}] - m_{W_i} \rho_{G_i} [\tilde{\mathbf{r}}_{W_{c_i}/V_{c_i}}] + m_{G_i} [\tilde{\mathbf{r}}_{V_{c_i}/G_i}] \quad (3.277)$$

$$[\tilde{\omega}]^2 = [\tilde{\omega}] [\tilde{\omega}] \quad (3.278)$$

Finally, the wheel torque equation is defined as:

$$\begin{aligned} & [m_{W_i} d_i \hat{\omega}_{3_i}^T] \ddot{\mathbf{r}}_{B/N} + \left[\hat{\mathbf{g}}_{s_i}^T [I_{W_i, W_{c_i}}] + m_{W_i} d_i \hat{\mathbf{g}}_{s_i}^T [\tilde{\omega}_{2_i}] [\tilde{\mathbf{r}}_{W_{c_i}/B}]^T \right] \dot{\omega} \\ & \quad + [J_{12_i} s \theta_i + J_{13_i} c \theta_i - m_{W_i} d_i \ell_i s \theta_i] \ddot{\gamma}_i + [J_{11_i} + m_{W_i} d_i^2] \dot{\Omega}_i \\ & = -\hat{\mathbf{g}}_{s_i}^T \left[[I_{W_i, W_{c_i}}]' \omega_{W_i/N} + [\tilde{\omega}] [I_{W_i, W_{c_i}}] \omega_{W_i/N} + m_{W_i} d_i [\tilde{\omega}_{2_i}] \left[2[\tilde{\mathbf{r}}'_{W_{c_i}/B}]^T \omega + [\tilde{\omega}] [\tilde{\omega}] \mathbf{r}_{W_{c_i}/B} \right] \right] \\ & \quad + (J_{13_i} s \theta_i - J_{12_i} c \theta_i) \Omega \dot{\gamma} - m_{W_i} d_i^2 \dot{\gamma}_i^2 c \theta_i s \theta_i + u_{s_i} \quad (3.279) \end{aligned}$$

To begin the back-substitution method, first the gimbal torque equation is solved for $\ddot{\gamma}_i$ in terms of $\ddot{\mathbf{r}}_{B/N}$ and $\dot{\omega}_{B/N}$ and $\dot{\Omega}_i$

$$\ddot{\gamma}_i = \mathbf{a}_{\gamma_i}^T \ddot{\mathbf{r}}_{B/N} + \mathbf{b}_{\gamma_i}^T \dot{\omega} + c_{\gamma_i} \dot{\Omega}_i + d_{\gamma_i} \quad (3.280)$$

where,

$$\mathbf{a}_{\gamma_i} = e^{-1} m_{V_i} [\tilde{\mathbf{r}}_{V_{c_i}/G_i}] \hat{\mathbf{g}}_{g_i} \quad (3.281)$$

$$\mathbf{b}_{\gamma_i} = -e^{-1} \left([I_{V_i, V_{c_i}}]^T \hat{\mathbf{g}}_{g_i} - m_{V_i} [\tilde{\mathbf{r}}_{V_{c_i}/B}] [\tilde{\mathbf{r}}_{V_{c_i}/G_i}] \hat{\mathbf{g}}_{g_i} \right) \quad (3.282)$$

$$c_{\gamma_i} = -e^{-1} \left(\hat{\mathbf{g}}_{g_i}^T [I_{W_i, W_{c_i}}] \hat{\mathbf{g}}_{s_i} + d_i \hat{\mathbf{g}}_{g_i}^T [P_i] \hat{\omega}_{3_i} \right) \quad (3.283)$$

$$\begin{aligned}
d_{\gamma_i} = & -e_{\gamma_i}^{-1} \hat{\mathbf{g}}_{\mathbf{g}_i}^T \left[\dot{\gamma}_i [Q_i] [\tilde{\mathbf{g}}_{\mathbf{g}_i}] \mathbf{r}'_{G_{c_i}/G_i} + [P_i] \left[(2d_i \dot{\gamma}_i \Omega_i s \theta_i - \ell_i \dot{\gamma}_i^2) \hat{\mathbf{g}}_{s_i} - d_i \dot{\gamma}_i^2 c \theta_i \hat{\mathbf{g}}_{t_i} - d_i \Omega_i^2 \hat{\mathbf{w}}_{2_i} \right] \right. \\
& + [I_{G_i, G_{c_i}}]' \boldsymbol{\omega}_{G_i/N} + [\tilde{\boldsymbol{\omega}}] [I_{G_i, G_{c_i}}] \boldsymbol{\omega}_{G_i/N} + [I_{W_i, W_{c_i}}] \Omega \dot{\gamma} \hat{\mathbf{g}}_{t_i} + [I_{W_i, W_{c_i}}]' \boldsymbol{\omega}_{W_i/N} + [\tilde{\boldsymbol{\omega}}] [I_{W_i, W_{c_i}}] \boldsymbol{\omega}_{W_i/N} \\
& + m_{G_i} [\tilde{\mathbf{r}}_{G_{c_i}/V_{c_i}}] (2[\tilde{\boldsymbol{\omega}}] \mathbf{r}'_{G_{c_i}/V_{c_i}} + [\tilde{\boldsymbol{\omega}}]^2 \mathbf{r}_{G_{c_i}/V_{c_i}}) + m_{W_i} [\tilde{\mathbf{r}}_{W_{c_i}/V_{c_i}}] (2[\tilde{\boldsymbol{\omega}}] \mathbf{r}'_{W_{c_i}/V_{c_i}} + [\tilde{\boldsymbol{\omega}}]^2 \mathbf{r}_{W_{c_i}/V_{c_i}}) \\
& \left. + m_{V_i} [\tilde{\mathbf{r}}_{V_{c_i}/G_i}] (2[\tilde{\boldsymbol{\omega}}] \mathbf{r}'_{V_{c_i}/B} + [\tilde{\boldsymbol{\omega}}]^2 \mathbf{r}_{V_{c_i}/B}) \right] + e_{\gamma_i}^{-1} u_{\mathbf{g}_i} \quad (3.284)
\end{aligned}$$

$$e_{\gamma_i} = \hat{\mathbf{g}}_{\mathbf{g}_i}^T \left[[I_{G_i, G_{c_i}}] \hat{\mathbf{g}}_{\mathbf{g}_i} + [I_{W_i, W_{c_i}}] \hat{\mathbf{g}}_{\mathbf{g}_i} + [P_i] (\ell_i \hat{\mathbf{g}}_{t_i} - d_i c \theta_i \hat{\mathbf{g}}_{s_i}) + [Q_i] [\tilde{\mathbf{g}}_{\mathbf{g}_i}] \mathbf{r}_{G_{c_i}/G_i} \right] \quad (3.285)$$

Next, the wheel torque equation is solved for $\dot{\Omega}_i$ in terms of $\ddot{\mathbf{r}}_{B/N}$ and $\dot{\boldsymbol{\omega}}_{B/N}$ and $\ddot{\gamma}_i$

$$\dot{\Omega}_i = \mathbf{a}_{\Omega_i}^T \ddot{\mathbf{r}}_{B/N} + \mathbf{b}_{\Omega_i}^T \dot{\boldsymbol{\omega}}_{B/N} + c_{\Omega_i} \ddot{\gamma}_i + d_{\Omega_i} \quad (3.286)$$

where

$$\mathbf{a}_{\Omega_i} = -e_{\Omega_i}^{-1} m_{W_i} d_i \hat{\mathbf{w}}_{3_i} \quad (3.287)$$

$$\mathbf{b}_{\Omega_i} = -e_{\Omega_i}^{-1} \left([I_{W_i, W_{c_i}}]^T \hat{\mathbf{g}}_{s_i} - m_{W_i} d_i [\tilde{\mathbf{r}}_{W_{c_i}/B}] [\tilde{\mathbf{w}}_{2_i}] \hat{\mathbf{g}}_{s_i} \right) \quad (3.288)$$

$$c_{\Omega_i} = -e_{\Omega_i}^{-1} (J_{12_i} s \theta_i + J_{13_i} c \theta_i - m_{W_i} d_i \ell_i s \theta_i) \quad (3.289)$$

$$\begin{aligned}
d_{\Omega_i} = & -e_{\Omega_i}^{-1} \left[\hat{\mathbf{g}}_{s_i}^T [I_{W_i, W_{c_i}}]' \boldsymbol{\omega}_{W_i/N} + \hat{\mathbf{g}}_{s_i}^T [\tilde{\boldsymbol{\omega}}] [I_{W_i, W_{c_i}}] \boldsymbol{\omega}_{W_i/N} + m_{W_i} d_i \hat{\mathbf{g}}_{s_i}^T [\tilde{\mathbf{w}}_{2_i}] \left[2[\tilde{\mathbf{r}}'_{W_{c_i}/B}]^T \boldsymbol{\omega} \right. \right. \\
& \left. \left. + [\tilde{\boldsymbol{\omega}}] [\tilde{\boldsymbol{\omega}}] \mathbf{r}_{W_{c_i}/B} \right] + (J_{13_i} s \theta_i - J_{12_i} c \theta_i) \Omega \dot{\gamma} - m_{W_i} d_i^2 \dot{\gamma}_i^2 c \theta_i s \theta_i + u_{s_i} \right] \quad (3.290)
\end{aligned}$$

$$e_{\Omega_i} = J_{11_i} + m_{W_i} d_i^2 \quad (3.291)$$

Substituting Eq. (3.280) into Eq. (3.286) decouples the gimbal and motor torque equations and yields:

$$\begin{aligned}
\dot{\Omega}_i = & \mathbf{a}_{\Omega_i}^T \ddot{\mathbf{r}}_{B/N} + \mathbf{b}_{\Omega_i}^T \dot{\boldsymbol{\omega}}_{B/N} + c_{\Omega_i} \left[\mathbf{a}_{\gamma_i}^T \ddot{\mathbf{r}}_{B/N} + \mathbf{b}_{\gamma_i}^T \dot{\boldsymbol{\omega}} + c_{\gamma_i} \dot{\Omega}_i + d_{\gamma_i} \right] + d_{\Omega_i} \\
= & \frac{\mathbf{a}_{\Omega_i}^T + c_{\Omega_i} \mathbf{a}_{\gamma_i}^T}{1 - c_{\Omega_i} c_{\gamma_i}} \ddot{\mathbf{r}}_{B/N} + \frac{\mathbf{b}_{\Omega_i}^T + c_{\Omega_i} \mathbf{b}_{\gamma_i}^T}{1 - c_{\Omega_i} c_{\gamma_i}} \dot{\boldsymbol{\omega}} + \frac{d_{\Omega_i} + c_{\Omega_i} d_{\gamma_i}}{1 - c_{\Omega_i} c_{\gamma_i}} \\
= & \mathbf{p}_i^T \ddot{\mathbf{r}}_{B/N} + \mathbf{q}_i^T \dot{\boldsymbol{\omega}} + s_i \quad (3.292)
\end{aligned}$$

where,

$$\mathbf{p}_i = \frac{\mathbf{a}_{\Omega_i} + c_{\Omega_i} \mathbf{a}_{\gamma_i}}{1 - c_{\Omega_i} c_{\gamma_i}} \quad (3.293)$$

$$\mathbf{q}_i = \frac{\mathbf{b}_{\Omega_i} + c_{\Omega_i} \mathbf{b}_{\gamma_i}}{1 - c_{\Omega_i} c_{\gamma_i}} \quad (3.294)$$

$$s_i = \frac{d_{\Omega_i} + c_{\Omega_i} d_{\gamma_i}}{1 - c_{\Omega_i} c_{\gamma_i}} \quad (3.295)$$

Similar to prior back-substitution methods, Eq. (3.280) is substituted into the translational equation of motion Eq. (3.264).

$$\begin{aligned} \ddot{\mathbf{r}}_{B/N} - [\tilde{\mathbf{c}}] \dot{\boldsymbol{\omega}} + \frac{1}{m_{sc}} \sum_{i=1}^N \mathbf{u}_{r_i} \left[\mathbf{a}_{\gamma_i}^T \ddot{\mathbf{r}}_{B/N} + \mathbf{b}_{\gamma_i}^T \dot{\boldsymbol{\omega}} + c_{\gamma_i} \dot{\Omega}_i + d_{\gamma_i} \right] + \frac{1}{m_{sc}} \sum_{i=1}^N \mathbf{v}_{r_i} \dot{\Omega}_i \\ = \ddot{\mathbf{r}}_{C/N} - 2[\tilde{\boldsymbol{\omega}}] \mathbf{c}' - [\tilde{\boldsymbol{\omega}}]^2 \mathbf{c} - \frac{1}{m_{sc}} \sum_{i=1}^N \mathbf{k}_{r_i} \end{aligned} \quad (3.296)$$

Substituting Eq. (3.292) and grouping like terms, and multiplying each side of the equation by m_{sc} results in:

$$\begin{aligned} \left[m_{sc} [I_{3 \times 3}] + \sum_{i=1}^N \left(\mathbf{u}_{r_i} \mathbf{a}_{\gamma_i}^T + \frac{(\mathbf{v}_{r_i} + \mathbf{u}_{r_i} c_{\gamma_i})(\mathbf{a}_{\Omega_i}^T + c_{\Omega_i} \mathbf{a}_{\gamma_i}^T)}{1 - c_{\Omega_i} c_{\gamma_i}} \right) \right] \ddot{\mathbf{r}}_{B/N} \\ + \left[-m_{sc} [\tilde{\mathbf{c}}] + \sum_{i=1}^N \left(\mathbf{u}_{r_i} \mathbf{b}_{\gamma_i}^T + \frac{(\mathbf{v}_{r_i} + \mathbf{u}_{r_i} c_{\gamma_i})(\mathbf{b}_{\Omega_i}^T + c_{\Omega_i} \mathbf{b}_{\gamma_i}^T)}{1 - c_{\Omega_i} c_{\gamma_i}} \right) \right] \dot{\boldsymbol{\omega}} \\ = \mathbf{F} - 2m_{sc} [\tilde{\boldsymbol{\omega}}] \mathbf{c}' - m_{sc} [\tilde{\boldsymbol{\omega}}]^2 \mathbf{c} - \sum_{i=1}^N \left(\mathbf{k}_{r_i} + \mathbf{u}_{r_i} d_{\gamma_i} + \frac{(\mathbf{v}_{r_i} + \mathbf{u}_{r_i} c_{\gamma_i})(c_{\Omega_i} d_{\gamma_i} + d_{\Omega_i})}{1 - c_{\Omega_i} c_{\gamma_i}} \right) \end{aligned} \quad (3.297)$$

The translational EOM is now decoupled from the other second order state variables. The rotational EOM needs to be decoupled in a similar manner and is completed by substituting Eq. (3.280) into the rotational equation of motion Eq. (3.268):

$$\begin{aligned} \left[m_{sc} [\tilde{\mathbf{c}}] + \sum_{i=1}^N \mathbf{u}_{\omega_i} \mathbf{a}_{\gamma_i}^T \right] \ddot{\mathbf{r}}_{B/N} + \left[[I_{sc,B}] + \sum_{i=1}^N \mathbf{u}_{\omega_i} \mathbf{b}_{\gamma_i}^T \right] \dot{\boldsymbol{\omega}} + \sum_{i=1}^N (\mathbf{v}_{\omega_i} + \mathbf{u}_{\omega_i} c_{\gamma_i}) \dot{\Omega}_i \\ = \mathbf{L}_B - [I_{sc,B}]' \boldsymbol{\omega} - [\tilde{\boldsymbol{\omega}}] [I_{sc,B}] \boldsymbol{\omega} - \frac{1}{m_{sc}} \sum_{i=1}^N (\mathbf{k}_{\omega_i} + \mathbf{u}_{\omega_i} d_{\gamma_i}) \end{aligned} \quad (3.298)$$

The final step is to substitute Eq. (3.292) into Eq. (3.298) and group like terms. This yields:

$$\begin{aligned}
& \left[m_{sc}[\tilde{\mathbf{c}}] + \sum_{i=1}^N \left(\mathbf{u}_{\omega_i} \mathbf{a}_{\gamma_i}^T + \frac{(\mathbf{v}_{\omega_i} + \mathbf{u}_{\omega_i} c_{\gamma_i})(\mathbf{a}_{\Omega_i}^T + c_{\Omega_i} \mathbf{a}_{\gamma_i}^T)}{1 - c_{\Omega_i} c_{\gamma_i}} \right) \right] \ddot{\mathbf{r}}_{B/N} \\
& + \left[[I_{sc,B}] + \sum_{i=1}^N \left(\mathbf{u}_{\omega_i} \mathbf{b}_{\gamma_i}^T + \frac{(\mathbf{v}_{\omega_i} + \mathbf{u}_{\omega_i} c_{\gamma_i})(\mathbf{b}_{\Omega_i}^T + c_{\Omega_i} \mathbf{b}_{\gamma_i}^T)}{1 - c_{\Omega_i} c_{\gamma_i}} \right) \right] \dot{\boldsymbol{\omega}} \quad (3.299) \\
& = \mathbf{L}_B - [I_{sc,B}]' \boldsymbol{\omega} - [\tilde{\boldsymbol{\omega}}][I_{sc,B}] \boldsymbol{\omega} - \sum_{i=1}^N \left(\mathbf{k}_{\omega_i} + \mathbf{u}_{\omega_i} d_{\gamma_i} + \frac{(\mathbf{v}_{\omega_i} + \mathbf{u}_{\omega_i} c_{\gamma_i})(c_{\Omega_i} d_{\gamma_i} + d_{\Omega_i})}{1 - c_{\Omega_i} c_{\gamma_i}} \right)
\end{aligned}$$

Now that the analytical back-substitution method has been performed on the EOMs, the back-substitution matrices contributions can be defined. The contributions are:

$$[A_{\text{contr}}] = \sum_{i=1}^N \left[\mathbf{u}_{r_i} \mathbf{a}_{\gamma_i}^T + (\mathbf{v}_{r_i} + \mathbf{u}_{r_i} c_{\gamma_i}) \mathbf{p}_i^T \right] \quad (3.300)$$

$$[B_{\text{contr}}] = \sum_{i=1}^N \left[\mathbf{u}_{r_i} \mathbf{b}_{\gamma_i}^T + (\mathbf{v}_{r_i} + \mathbf{u}_{r_i} c_{\gamma_i}) \mathbf{q}_i^T \right] \quad (3.301)$$

$$[C_{\text{contr}}] = \sum_{i=1}^N \left[\mathbf{u}_{\omega_i} \mathbf{a}_{\gamma_i}^T + (\mathbf{v}_{\omega_i} + \mathbf{u}_{\omega_i} c_{\gamma_i}) \mathbf{p}_i^T \right] \quad (3.302)$$

$$[D_{\text{contr}}] = \sum_{i=1}^N \left[\mathbf{u}_{\omega_i} \mathbf{b}_{\gamma_i}^T + (\mathbf{v}_{\omega_i} + \mathbf{u}_{\omega_i} c_{\gamma_i}) \mathbf{q}_i^T \right] \quad (3.303)$$

$$\mathbf{v}_{\text{trans,contr}} = - \sum_{i=1}^N \left[\mathbf{k}_{r_i} + \mathbf{u}_{r_i} d_{\gamma_i} + (\mathbf{v}_{r_i} + \mathbf{u}_{r_i} c_{\gamma_i}) s_i \right] \quad (3.304)$$

$$\mathbf{v}_{\text{rot,contr}} = - \sum_{i=1}^N \left[\mathbf{k}_{\omega_i} + \mathbf{u}_{\omega_i} d_{\gamma_i} + (\mathbf{v}_{\omega_i} + \mathbf{u}_{\omega_i} c_{\gamma_i}) s_i \right] \quad (3.305)$$

This development confirms that the model for both the balanced and imbalanced VSCMGs conform to the standard EOM form introduced in this dissertation and a ready to be implemented model into software simulation.

3.1.7 Fuel Slosh - Pendulum Based Model

3.1.7.1 Introduction

Fuel slosh is a complicated phenomenon that sometimes requires multiple models to bound the dynamical behavior. The spring mass damper model introduced earlier is a good model when

dealing with translational movement, but does not cover all of the dynamical behavior when performing rotational maneuvers. In contrast, a spherical pendulum model does perform better with rotational maneuvers. This section describes the EOM and back-substitution method for a spherical pendulum model representing fuel slosh. This work was completed with collaborator Paolo Cappuccio of La Sapienza University of Rome during July - September of 2017.

3.1.7.2 Problem Statement

The spacecraft model is composed by a rigid hub, a fuel tank and N_P lumped masses simulating the propellant. Subscript j indicates the j_{th} propellant slosh mass, m_j . Figure 3.9 shows reference frame and key point definitions used for this formulation.

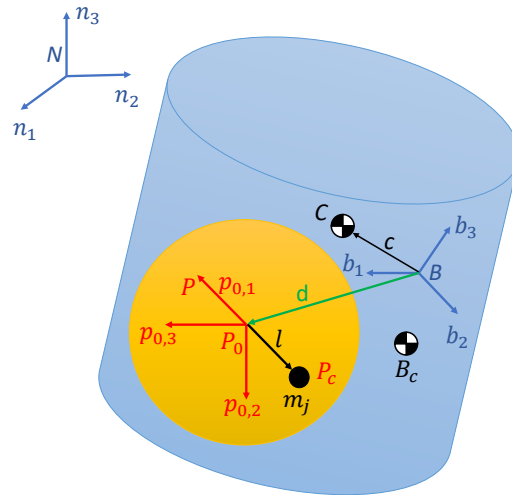


Figure 3.9: Frame and variable definitions used for formulation

Four coordinate frames are defined for this formulation. The inertial reference frame is indicated by $\mathcal{N} : \{\hat{n}_1, \hat{n}_2, \hat{n}_3\}$. The body fixed coordinate frame, $\mathcal{B} : \{\hat{b}_1, \hat{b}_2, \hat{b}_3\}$, which is fixed with respect to the hub and can be oriented in any direction. Point B indicates the origin of the body fixed reference frame, which can be any point fixed with respect to the hub. The initial pendulum frame, $\mathcal{P}_{0,j} : \{\hat{p}_{0,j,1}, \hat{p}_{0,j,2}, \hat{p}_{0,j,3}\}$, is a frame with its origin located at the tank geometrical center, T . The $\mathcal{P}_{0,j}$ frame is a fixed frame with respect to the body frame, oriented such that $\hat{p}_{0,j,1}$

points to the propellant slosh mass in its initial position, P_j . The constant distance from point T to point P_j is defined as l_j , while with \mathbf{l}_j is indicated the vector from T to $P_{c,j}$.

The remaining key points to be defined are: point B_c is the location of the center of mass of the rigid hub and point $P_{c,j}$ is the instantaneous position of the propellant slosh mass m_j . \mathbf{d} is vector from the center of the body reference system to the tank geometrical center.

Figure 3.10 provides further detail of the propellant slosh parameters and reference frames. As seen in Figure 3.9, an individual slosh particle is free to move in every direction while connected by rigid weightless rod to the geometrical center of the tank. A linear damper effect is considered using a damping matrix, D . The variables, φ_j and ϑ_j are state variables and quantify the angular displacement from initial position for the corresponding slosh mass.

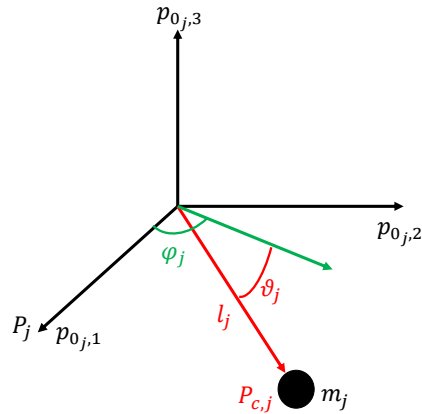


Figure 3.10: Further detail of propellant slosh and reference frames

Using the variables and frames defined, the following section outlines the equations of motion for the spacecraft.

3.1.7.3 Equation of Motion

The translational EOM was found to fit the standard form seen in Section 2 and can be seen in the following equation:

$$\begin{aligned}
\ddot{\mathbf{r}}_{B/N} - [\tilde{\mathbf{c}}]\dot{\boldsymbol{\omega}}_{B/N} - \frac{1}{m_{sc}} \sum_{j=1}^{N_P} m_j l_j \left[\left(\sin(\varphi_j) \cos(\vartheta_j) \hat{\mathbf{p}}_{0,j,1} - \cos(\varphi_j) \cos(\vartheta_j) \hat{\mathbf{p}}_{0,j,2} \right) \ddot{\varphi}_j \right. \\
+ \left. \left(\cos(\varphi_j) \sin(\vartheta_j) \hat{\mathbf{p}}_{0,j,1} + \sin(\varphi_j) \sin(\vartheta_j) \hat{\mathbf{p}}_{0,j,2} + \cos(\vartheta_j) \hat{\mathbf{p}}_{0,j,3} \right) \ddot{\vartheta}_j \right] = \ddot{\mathbf{r}}_{C/N} - 2[\tilde{\boldsymbol{\omega}}_{B/N}]\mathbf{c}' \\
- [\tilde{\boldsymbol{\omega}}_{B/N}][\tilde{\boldsymbol{\omega}}_{B/N}]\mathbf{c} - \frac{1}{m_{sc}} \sum_{j=1}^{N_P} m_j l_j \left[\left(-\cos(\varphi_j) \cos(\vartheta_j) \hat{\mathbf{p}}_{0,j,1} - \sin(\varphi_j) \cos(\vartheta_j) \hat{\mathbf{p}}_{0,j,2} \right) \dot{\varphi}_j^2 \right. \\
+ \left. \left(-\cos(\varphi_j) \cos(\vartheta_j) \hat{\mathbf{p}}_{0,j,1} - \sin(\varphi_j) \cos(\vartheta_j) \hat{\mathbf{p}}_{0,j,2} + \sin(\vartheta_j) \hat{\mathbf{p}}_{0,j,3} \right) \dot{\vartheta}_j^2 \right. \\
\left. + \left(2 \sin(\varphi_j) \sin(\vartheta_j) \hat{\mathbf{p}}_{0,j,1} - 2 \cos(\varphi_j) \sin(\vartheta_j) \hat{\mathbf{p}}_{0,j,2} \right) \dot{\varphi}_j \dot{\vartheta}_j \right] \quad (3.306)
\end{aligned}$$

Similarly, the rotational EOM was developed and yields:

$$\begin{aligned}
m_{sc}[\tilde{\mathbf{c}}]\ddot{\mathbf{r}}_{B/N} + [I_{sc,B}]\dot{\boldsymbol{\omega}}_{B/N} - \sum_{j=1}^{N_P} m_j l_j [\tilde{\mathbf{r}}_{P_{c,j}/B}] \left[\left(\sin(\varphi_j) \cos(\vartheta_j) \hat{\mathbf{p}}_{0,j,1} - \cos(\varphi_j) \cos(\vartheta_j) \hat{\mathbf{p}}_{0,j,2} \right) \ddot{\varphi}_j \right. \\
+ \left. \left(\cos(\varphi_j) \sin(\vartheta_j) \hat{\mathbf{p}}_{0,j,1} + \sin(\varphi_j) \sin(\vartheta_j) \hat{\mathbf{p}}_{0,j,2} + \cos(\vartheta_j) \hat{\mathbf{p}}_{0,j,3} \right) \ddot{\vartheta}_j \right] = \mathbf{L}_B - [\tilde{\boldsymbol{\omega}}_{B/N}][I_{sc,B}]\boldsymbol{\omega}_{B/N} \\
- [I'_{sc,B}]\boldsymbol{\omega}_{B/N} - \sum_{j=1}^{N_P} m_j \left\{ [\tilde{\boldsymbol{\omega}}_{B/N}][\tilde{\mathbf{r}}_{P_{c,j}/B}]\mathbf{r}'_{P_{c,j}/B} + l_j [\tilde{\mathbf{r}}_{P_{c,j}/B}] \left[\left(-\cos(\varphi_j) \cos(\vartheta_j) \hat{\mathbf{p}}_{0,j,1} \right. \right. \right. \\
- \left. \left. \sin(\varphi_j) \cos(\vartheta_j) \hat{\mathbf{p}}_{0,j,2} \right) \dot{\varphi}_j^2 + \left(-\cos(\varphi_j) \cos(\vartheta_j) \hat{\mathbf{p}}_{0,j,1} - \sin(\varphi_j) \cos(\vartheta_j) \hat{\mathbf{p}}_{0,j,2} + \sin(\vartheta_j) \hat{\mathbf{p}}_{0,j,3} \right) \dot{\vartheta}_j^2 \right. \\
\left. \left. + \left(2 \sin(\varphi_j) \sin(\vartheta_j) \hat{\mathbf{p}}_{0,j,1} - 2 \cos(\varphi_j) \sin(\vartheta_j) \hat{\mathbf{p}}_{0,j,2} \right) \dot{\varphi}_j \dot{\vartheta}_j \right] \right\} \quad (3.307)
\end{aligned}$$

To help define the sloshing equation, \mathbf{l}_j from Figure 3.10 is defined in Eq. (3.308).

$$\mathbf{l}_j = l_j \begin{matrix} \mathcal{P}_{0,j} \\ \left[\begin{array}{c} \cos(\varphi_j) \cos(\vartheta_j) \\ \sin(\varphi_j) \cos(\vartheta_j) \\ -\sin(\vartheta_j) \end{array} \right] \end{matrix} \quad (3.308)$$

The body frame relative first and second time derivatives of \mathbf{l}_j also need to be defined and can be seen in the following equations:

$$\mathbf{l}'_j = l_j \begin{matrix} \mathcal{P}_{0,j} \\ \left[\begin{array}{c} -\dot{\varphi}_j \sin(\varphi_j) \cos(\vartheta_j) - \dot{\vartheta}_j \cos(\varphi_j) \sin(\vartheta_j) \\ \dot{\varphi}_j \cos(\varphi_j) \cos(\vartheta_j) - \dot{\vartheta}_j \sin(\varphi_j) \sin(\vartheta_j) \\ -\dot{\vartheta}_j \cos(\vartheta_j) \end{array} \right] \end{matrix} \quad (3.309)$$

$$\mathbf{l}''_j = l_j \begin{matrix} \mathcal{P}_{0,j} \\ \left[\begin{array}{c} -\ddot{\varphi}_j \sin(\varphi_j) \cos(\vartheta_j) - \ddot{\vartheta}_j \cos(\varphi_j) \sin(\vartheta_j) - \dot{\varphi}_j^2 \cos(\varphi_j) \cos(\vartheta_j) \\ -\dot{\vartheta}_j^2 \cos(\varphi_j) \cos(\vartheta_j) + 2\dot{\varphi}_j \dot{\vartheta}_j \sin(\varphi_j) \sin(\vartheta_j) \\ \ddot{\varphi}_j \cos(\varphi_j) \cos(\vartheta_j) - \ddot{\vartheta}_j \sin(\varphi_j) \sin(\vartheta_j) - \dot{\varphi}_j^2 \sin(\varphi_j) \cos(\vartheta_j) \\ -\dot{\vartheta}_j^2 \sin(\varphi_j) \cos(\vartheta_j) - 2\dot{\varphi}_j \dot{\vartheta}_j \cos(\varphi_j) \sin(\vartheta_j) \\ -\ddot{\vartheta}_j \cos(\vartheta_j) + \dot{\vartheta}_j^2 \sin(\vartheta_j) \end{array} \right] \end{matrix} \quad (3.310)$$

Using these definitions, the sloshing equations were found and can be seen in Eqs (3.311)- (3.312).

$$\begin{aligned} m_j l_j^2 \ddot{\varphi}_j \cos^2(\vartheta_j) - m_j \hat{\mathbf{p}}_{0,j,3}^T [\tilde{\mathbf{l}}_j] ([\tilde{\mathbf{l}}_j] + [\tilde{\mathbf{d}}]) \tilde{\boldsymbol{\omega}}_{B/N} + m_j \hat{\mathbf{p}}_{0,j,3}^T [\tilde{\mathbf{l}}_j] \ddot{\mathbf{r}}_{B/N} = -m_j \hat{\mathbf{p}}_{0,j,3}^T [\tilde{\mathbf{l}}_j] [\tilde{\boldsymbol{\omega}}_{B/N}] [\tilde{\boldsymbol{\omega}}_{B/N}] \mathbf{d} \\ + \hat{\mathbf{p}}_{0,j,3}^T \mathbf{L}_{T,j} + 2m_j l_j^2 \dot{\varphi}_j \dot{\vartheta}_j \cos(\vartheta_j) \sin(\vartheta_j) - m_j \hat{\mathbf{p}}_{0,j,3}^T [\tilde{\mathbf{l}}_j] \left[2[\tilde{\boldsymbol{\omega}}_{B/N}] \mathbf{l}'_j + [\tilde{\boldsymbol{\omega}}_{B/N}] [\tilde{\boldsymbol{\omega}}_{B/N}] \mathbf{l}_j \right] \end{aligned} \quad (3.311)$$

$$\begin{aligned} m_j l_j^2 \ddot{\vartheta}_j - m_j \hat{\mathbf{p}}_{0,j,2}^T [\tilde{\mathbf{l}}_j] ([\tilde{\mathbf{l}}_j] + [\tilde{\mathbf{d}}]) \tilde{\boldsymbol{\omega}}_{B/N} + m_j \hat{\mathbf{p}}_{0,j,2}^T [\tilde{\mathbf{l}}_j] \ddot{\mathbf{r}}_{B/N} = -m_j \hat{\mathbf{p}}_{0,j,2}^T [\tilde{\mathbf{l}}_j] [\tilde{\boldsymbol{\omega}}_{B/N}] [\tilde{\boldsymbol{\omega}}_{B/N}] \mathbf{d} \\ + \hat{\mathbf{p}}_{0,j,2}^T \mathbf{L}_{T,j} - m_j l_j^2 \dot{\varphi}_j^2 \cos(\vartheta_j) \sin(\vartheta_j) - m_j \hat{\mathbf{p}}_{0,j,2}^T [\tilde{\mathbf{l}}_j] \left[2[\tilde{\boldsymbol{\omega}}_{B/N}] \mathbf{l}'_j + [\tilde{\boldsymbol{\omega}}_{B/N}] [\tilde{\boldsymbol{\omega}}_{B/N}] \mathbf{l}_j \right] \end{aligned} \quad (3.312)$$

3.1.7.4 Back-substitution Method

A step-by-step derivation of the back-substitution method is presented in the following section. Starting from Eq. (3.311), the $\ddot{\varphi}_j$ is isolated on the left hand side of the equation

$$\begin{aligned} \ddot{\varphi}_j = \frac{1}{m_j l_j^2 \cos^2(\vartheta_j)} \left\{ m_j \hat{\mathbf{p}}_{0j,3}^T [\tilde{\mathbf{l}}_j] ([\tilde{\mathbf{l}}_j] + [\tilde{\mathbf{d}}]) \dot{\boldsymbol{\omega}}_{B/N} - m_j \hat{\mathbf{p}}_{0j,3}^T [\tilde{\mathbf{l}}_j] \ddot{\mathbf{r}}_{B/N} - m_j \hat{\mathbf{p}}_{0j,3}^T [\tilde{\mathbf{l}}_j] [\tilde{\boldsymbol{\omega}}_{B/N}] [\tilde{\boldsymbol{\omega}}_{B/N}] \mathbf{d} \right. \\ \left. + \hat{\mathbf{p}}_{0j,3}^T \mathbf{L}_{T,j} + 2m_j l_j^2 \dot{\varphi}_j \dot{\vartheta} \cos(\vartheta_j) \sin(\vartheta_j) - m_j \hat{\mathbf{p}}_{0j,3}^T [\tilde{\mathbf{l}}_j] \left[2[\tilde{\boldsymbol{\omega}}_{B/N}] \mathbf{l}'_j + [\tilde{\boldsymbol{\omega}}_{B/N}] [\tilde{\boldsymbol{\omega}}_{B/N}] \mathbf{l}_j \right] \right\} \quad (3.313) \end{aligned}$$

and is simplified to a simpler form:

$$\ddot{\varphi}_j = \frac{1}{m_j l_j^2 \cos^2(\vartheta_j)} \left(m_j \hat{\mathbf{p}}_{0j,3}^T [\tilde{\mathbf{l}}_j] ([\tilde{\mathbf{l}}_j] + [\tilde{\mathbf{d}}]) \dot{\boldsymbol{\omega}}_{B/N} - m_j \hat{\mathbf{p}}_{0j,3}^T [\tilde{\mathbf{l}}_j] \ddot{\mathbf{r}}_{B/N} + a_{\varphi_j} \right) \quad (3.314)$$

Further simplification yields a familiar form

$$\ddot{\varphi}_j = \mathbf{a}_{\varphi_j}^T \ddot{\mathbf{r}}_{B/N} + \mathbf{b}_{\varphi_j}^T \dot{\boldsymbol{\omega}}_{B/N} + c_{\varphi_j} \quad (3.315)$$

using the following definitions:

$$\mathbf{a}_{\varphi_j}^T = -\frac{\hat{\mathbf{p}}_{0j,3}^T [\tilde{\mathbf{l}}_j]}{l_j^2 \cos^2(\vartheta_j)} \quad (3.316)$$

$$\mathbf{b}_{\varphi_j}^T = \frac{\hat{\mathbf{p}}_{0j,3}^T [\tilde{\mathbf{l}}_j] ([\tilde{\mathbf{l}}_j] + [\tilde{\mathbf{d}}])}{l_j^2 \cos^2(\vartheta_j)} \quad (3.317)$$

$$\begin{aligned} c_{\varphi_j} = \frac{1}{m_j l_j^2 \cos^2(\vartheta_j)} \left\{ -m_j \hat{\mathbf{p}}_{0j,3}^T [\tilde{\mathbf{l}}_j] [\tilde{\boldsymbol{\omega}}_{B/N}] [\tilde{\boldsymbol{\omega}}_{B/N}] \mathbf{d} + \hat{\mathbf{p}}_{0j,3}^T \mathbf{L}_{T,j} \right. \\ \left. + 2m_j l_j^2 \dot{\varphi}_j \dot{\vartheta} \cos(\vartheta_j) \sin(\vartheta_j) - m_j \hat{\mathbf{p}}_{0j,3}^T [\tilde{\mathbf{l}}_j] \left[2[\tilde{\boldsymbol{\omega}}_{B/N}] \mathbf{l}'_j + [\tilde{\boldsymbol{\omega}}_{B/N}] [\tilde{\boldsymbol{\omega}}_{B/N}] \mathbf{l}_j \right] \right\} \quad (3.318) \end{aligned}$$

Following a similar process for Eq. (3.312)

$$\begin{aligned} \ddot{\vartheta}_j = \frac{1}{m_j l_j^2} \left\{ m_j \hat{\mathbf{p}}_{0j,2}^T [\tilde{\mathbf{l}}_j] ([\tilde{\mathbf{l}}_j] + [\tilde{\mathbf{d}}]) \dot{\boldsymbol{\omega}}_{B/N} - m_j \hat{\mathbf{p}}_{0j,2}^T [\tilde{\mathbf{l}}_j] \ddot{\mathbf{r}}_{B/N} - m_j \hat{\mathbf{p}}_{0j,2}^T [\tilde{\mathbf{l}}_j] [\tilde{\boldsymbol{\omega}}_{B/N}] [\tilde{\boldsymbol{\omega}}_{B/N}] \mathbf{d} \right. \\ \left. + \hat{\mathbf{p}}_{0j,2}^T \mathbf{L}_{T,j} - m_j l_j^2 \dot{\varphi}_j^2 \cos(\vartheta_j) \sin(\vartheta_j) - m_j \hat{\mathbf{p}}_{0j,2}^T [\tilde{\mathbf{l}}_j] \left[2[\tilde{\boldsymbol{\omega}}_{B/N}] \mathbf{l}'_j + [\tilde{\boldsymbol{\omega}}_{B/N}] [\tilde{\boldsymbol{\omega}}_{B/N}] \mathbf{l}_j \right] \right\} \quad (3.319) \end{aligned}$$

which results in a simpler form:

$$\ddot{\vartheta}_j = \frac{1}{m_j l_j^2} \left(m_j \hat{\mathbf{p}}_{0j,2}^T [\tilde{\mathbf{l}}_j] ([\tilde{\mathbf{l}}_j] + [\tilde{\mathbf{d}}]) \dot{\boldsymbol{\omega}}_{B/N} - m_j \hat{\mathbf{p}}_{0j,2}^T [\tilde{\mathbf{l}}_j] \ddot{\mathbf{r}}_{B/N} + a_{\vartheta_j} \right) \quad (3.320)$$

Modifying to the equation to be consistent with the standard form:

$$\ddot{\vartheta}_j = \mathbf{a}_{\vartheta_j}^T \ddot{\mathbf{r}}_{B/N} + \mathbf{b}_{\vartheta_j}^T \dot{\boldsymbol{\omega}}_{B/N} + c_{\vartheta_j} \quad (3.321)$$

using the following definitions:

$$\mathbf{a}_{\vartheta_j}^T = -\frac{\hat{\mathbf{p}}_{0j,2}'^T[\tilde{\mathbf{l}}_j]}{l_j^2} \quad (3.322)$$

$$\mathbf{b}_{\vartheta_j}^T = \frac{\hat{\mathbf{p}}_{0j,2}'^T[\tilde{\mathbf{l}}_j](\tilde{\mathbf{l}}_j + [\tilde{\mathbf{d}}])}{l_j^2} \quad (3.323)$$

$$c_{\vartheta_j} = \frac{1}{m_j l_j^2} \left\{ -m_j \hat{\mathbf{p}}_{0j,2}'^T[\tilde{\mathbf{l}}_j][\tilde{\boldsymbol{\omega}}_{B/N}][\tilde{\boldsymbol{\omega}}_{B/N}]\mathbf{d} + \hat{\mathbf{p}}_{0j,2}'^T \mathbf{L}_{T,j} - m_j l_j^2 \dot{\varphi}_j^2 \cos(\vartheta_j) \sin(\vartheta_j) \right. \\ \left. - m_j \hat{\mathbf{p}}_{0j,2}'^T[\tilde{\mathbf{l}}_j] \left[2[\tilde{\boldsymbol{\omega}}_{B/N}]\mathbf{l}'_j + [\tilde{\boldsymbol{\omega}}_{B/N}][\tilde{\boldsymbol{\omega}}_{B/N}]\mathbf{l}_j \right] \right\} \quad (3.324)$$

The next step of the back-substitution method is to decouple the translational EOM:

$$\ddot{\mathbf{r}}_{B/N} - [\tilde{\mathbf{c}}]\dot{\boldsymbol{\omega}}_{B/N} - \frac{1}{m_{sc}} \sum_{j=1}^{N_P} m_j l_j \left[\left(\sin(\varphi_j) \cos(\vartheta_j) \hat{\mathbf{p}}_{0j,1} - \cos(\varphi_j) \cos(\vartheta_j) \hat{\mathbf{p}}_{0j,2} \right) (\mathbf{a}_{\varphi_j}^T \ddot{\mathbf{r}}_{B/N} \right. \\ \left. + \mathbf{b}_{\varphi_j}^T \dot{\boldsymbol{\omega}}_{B/N} + c_{\varphi_j} \right) + \left(\cos(\varphi_j) \sin(\vartheta_j) \hat{\mathbf{p}}_{0j,1} + \sin(\varphi_j) \sin(\vartheta_j) \hat{\mathbf{p}}_{0j,2} + \cos(\vartheta_j) \hat{\mathbf{p}}_{0j,3} \right) (\mathbf{a}_{\vartheta_j}^T \ddot{\mathbf{r}}_{B/N} \\ \left. + \mathbf{b}_{\vartheta_j}^T \dot{\boldsymbol{\omega}}_{B/N} + c_{\vartheta_j} \right) \right] = \ddot{\mathbf{r}}_{C/N} - 2[\tilde{\boldsymbol{\omega}}_{B/N}]\mathbf{c}' - [\tilde{\boldsymbol{\omega}}_{B/N}][\tilde{\boldsymbol{\omega}}_{B/N}]\mathbf{c} - \frac{1}{m_{sc}} \sum_{j=1}^{N_P} m_j l_j \left[\left(-\cos(\varphi_j) \cos(\vartheta_j) \hat{\mathbf{p}}_{0j,1} \right. \right. \\ \left. \left. - \sin(\varphi_j) \cos(\vartheta_j) \hat{\mathbf{p}}_{0j,2} \right) \dot{\varphi}_j^2 + \left(-\cos(\varphi_j) \cos(\vartheta_j) \hat{\mathbf{p}}_{0j,1} - \sin(\varphi_j) \cos(\vartheta_j) \hat{\mathbf{p}}_{0j,2} + \sin(\vartheta_j) \hat{\mathbf{p}}_{0j,3} \right) \dot{\vartheta}_j^2 \right. \\ \left. + \left(2 \sin(\varphi_j) \sin(\vartheta_j) \hat{\mathbf{p}}_{0j,1} - 2 \cos(\varphi_j) \sin(\vartheta_j) \hat{\mathbf{p}}_{0j,2} \right) \dot{\varphi}_j \dot{\vartheta}_j \right] \quad (3.325)$$

Simplifying this result and combining like terms the final decoupled translational equation is:

$$\begin{aligned}
& \left\{ m_{sc}[I_{3 \times 3}] - \sum_{j=1}^{N_P} m_j l_j \left[\left(\sin(\varphi_j) \cos(\vartheta_j) \hat{\mathbf{p}}_{0,j,1} - \cos(\varphi_j) \cos(\vartheta_j) \hat{\mathbf{p}}_{0,j,2} \right) \mathbf{a}_{\varphi_j}^T + \left(\cos(\varphi_j) \sin(\vartheta_j) \hat{\mathbf{p}}_{0,j,1} \right. \right. \right. \\
& \left. \left. \left. + \sin(\varphi_j) \sin(\vartheta_j) \hat{\mathbf{p}}_{0,j,2} + \cos(\vartheta_j) \hat{\mathbf{p}}_{0,j,3} \right) \mathbf{a}_{\vartheta_j}^T \right] \right\} \ddot{\mathbf{r}}_{B/N} + \left\{ -m_{sc}[\tilde{\mathbf{c}}] - \sum_{j=1}^{N_P} m_j l_j \left[\left(\sin(\varphi_j) \cos(\vartheta_j) \hat{\mathbf{p}}_{0,j,1} \right. \right. \right. \\
& \left. \left. \left. - \cos(\varphi_j) \cos(\vartheta_j) \hat{\mathbf{p}}_{0,j,2} \right) \mathbf{b}_{\varphi_j}^T + \left(\cos(\varphi_j) \sin(\vartheta_j) \hat{\mathbf{p}}_{0,j,1} + \sin(\varphi_j) \sin(\vartheta_j) \hat{\mathbf{p}}_{0,j,2} + \cos(\vartheta_j) \hat{\mathbf{p}}_{0,j,3} \right) \mathbf{b}_{\vartheta_j}^T \right] \right\} \dot{\boldsymbol{\omega}}_{B/N} \\
& = m_{sc} \ddot{\mathbf{r}}_{C/N} - 2m_{sc}[\tilde{\boldsymbol{\omega}}_{B/N}] \mathbf{c}' - m_{sc}[\tilde{\boldsymbol{\omega}}_{B/N}][\tilde{\boldsymbol{\omega}}_{B/N}] \mathbf{c} - \sum_{j=1}^{N_P} m_j l_j \left[\left(-\cos(\varphi_j) \cos(\vartheta_j) \hat{\mathbf{p}}_{0,j,1} \right. \right. \\
& \left. \left. - \sin(\varphi_j) \cos(\vartheta_j) \hat{\mathbf{p}}_{0,j,2} \right) \dot{\varphi}_j^2 + \left(-\cos(\varphi_j) \cos(\vartheta_j) \hat{\mathbf{p}}_{0,j,1} - \sin(\varphi_j) \cos(\vartheta_j) \hat{\mathbf{p}}_{0,j,2} + \sin(\vartheta_j) \hat{\mathbf{p}}_{0,j,3} \right) \dot{\vartheta}_j^2 \right. \\
& \quad \left. + \left(2 \sin(\varphi_j) \sin(\vartheta_j) \hat{\mathbf{p}}_{0,j,1} - 2 \cos(\varphi_j) \sin(\vartheta_j) \hat{\mathbf{p}}_{0,j,2} \right) \dot{\varphi}_j \dot{\vartheta}_j - \left(\sin(\varphi_j) \cos(\vartheta_j) \hat{\mathbf{p}}_{0,j,1} \right. \right. \\
& \quad \left. \left. - \cos(\varphi_j) \cos(\vartheta_j) \hat{\mathbf{p}}_{0,j,2} \right) c_{\varphi_j} - \left(\cos(\varphi_j) \sin(\vartheta_j) \hat{\mathbf{p}}_{0,j,1} + \sin(\varphi_j) \sin(\vartheta_j) \hat{\mathbf{p}}_{0,j,2} + \cos(\vartheta_j) \hat{\mathbf{p}}_{0,j,3} \right) c_{\vartheta_j} \right] \\
& \tag{3.326}
\end{aligned}$$

The final step of the back-substitution method is to decoupled the rotational EOM. Following a similar pattern to the translational EOM, the substitution results in:

$$\begin{aligned}
& m_{sc}[\tilde{\mathbf{c}}] \ddot{\mathbf{r}}_{B/N} + [I_{sc,B}] \dot{\boldsymbol{\omega}}_{B/N} - \sum_{j=1}^{N_P} m_j l_j [\tilde{\mathbf{r}}_{P_{c,j}/B}] \left[\left(\sin(\varphi_j) \cos(\vartheta_j) \hat{\mathbf{p}}_{0,j,1} \right. \right. \\
& \left. \left. - \cos(\varphi_j) \cos(\vartheta_j) \hat{\mathbf{p}}_{0,j,2} \right) \left(\mathbf{a}_{\varphi_j}^T \ddot{\mathbf{r}}_{B/N} + \mathbf{b}_{\varphi_j}^T \dot{\boldsymbol{\omega}}_{B/N} + c_{\varphi_j} \right) + \left(\cos(\varphi_j) \sin(\vartheta_j) \hat{\mathbf{p}}_{0,j,1} + \sin(\varphi_j) \sin(\vartheta_j) \hat{\mathbf{p}}_{0,j,2} \right. \right. \\
& \quad \left. \left. + \cos(\vartheta_j) \hat{\mathbf{p}}_{0,j,3} \right) \left(\mathbf{a}_{\vartheta_j}^T \ddot{\mathbf{r}}_{B/N} + \mathbf{b}_{\vartheta_j}^T \dot{\boldsymbol{\omega}}_{B/N} + c_{\vartheta_j} \right) \right] = \\
& \quad \mathbf{L}_B - [\tilde{\boldsymbol{\omega}}_{B/N}][I_{sc,B}] \boldsymbol{\omega}_{B/N} - [I'_{sc,B}] \boldsymbol{\omega}_{B/N} - \sum_{j=1}^{N_P} m_j \left\{ [\tilde{\boldsymbol{\omega}}_{B/N}][\tilde{\mathbf{r}}_{P_{c,j}/B}] \mathbf{r}'_{P_{c,j}/B} \right. \\
& \quad \left. + l_j [\tilde{\mathbf{r}}_{P_{c,j}/B}] \left[\left(-\cos(\varphi_j) \cos(\vartheta_j) \hat{\mathbf{p}}_{0,j,1} - \sin(\varphi_j) \cos(\vartheta_j) \hat{\mathbf{p}}_{0,j,2} \right) \dot{\varphi}_j^2 + \left(-\cos(\varphi_j) \cos(\vartheta_j) \hat{\mathbf{p}}_{0,j,1} \right. \right. \right. \\
& \quad \left. \left. - \sin(\varphi_j) \cos(\vartheta_j) \hat{\mathbf{p}}_{0,j,2} + \sin(\vartheta_j) \hat{\mathbf{p}}_{0,j,3} \right) \dot{\vartheta}_j^2 + \left(2 \sin(\varphi_j) \sin(\vartheta_j) \hat{\mathbf{p}}_{0,j,1} - 2 \cos(\varphi_j) \sin(\vartheta_j) \hat{\mathbf{p}}_{0,j,2} \right) \dot{\varphi}_j \dot{\vartheta}_j \right] \right\} \\
& \tag{3.327}
\end{aligned}$$

Simplifying and combining like terms yields the desired decoupled rotational EOM:

$$\begin{aligned}
& \left\{ m_{sc}[\tilde{\mathbf{c}}] - \sum_{j=1}^{N_P} m_j l_j [\tilde{\mathbf{r}}_{P_{c,j}/B}] \left[\left(\sin(\varphi_j) \cos(\vartheta_j) \hat{\mathbf{p}}_{0,j,1} - \cos(\varphi_j) \cos(\vartheta_j) \hat{\mathbf{p}}_{0,j,2} \right) \mathbf{a}_{\varphi_j}^T \right. \right. \\
& \quad \left. \left. + \left(\cos(\varphi_j) \sin(\vartheta_j) \hat{\mathbf{p}}_{0,j,1} + \sin(\varphi_j) \sin(\vartheta_j) \hat{\mathbf{p}}_{0,j,2} + \cos(\vartheta_j) \hat{\mathbf{p}}_{0,j,3} \right) \mathbf{a}_{\vartheta_j}^T \right] \right\} \ddot{\mathbf{r}}_{B/N} + \left\{ [I_{sc,B}] \right. \\
& \quad \left. - \sum_{j=1}^{N_P} m_j l_j [\tilde{\mathbf{r}}_{P_{c,j}/B}] \left[\left(\sin(\varphi_j) \cos(\vartheta_j) \hat{\mathbf{p}}_{0,j,1} - \cos(\varphi_j) \cos(\vartheta_j) \hat{\mathbf{p}}_{0,j,2} \right) \mathbf{b}_{\varphi_j}^T + \left(\cos(\varphi_j) \sin(\vartheta_j) \hat{\mathbf{p}}_{0,j,1} \right. \right. \right. \\
& \quad \left. \left. + \sin(\varphi_j) \sin(\vartheta_j) \hat{\mathbf{p}}_{0,j,2} + \cos(\vartheta_j) \hat{\mathbf{p}}_{0,j,3} \right) \mathbf{b}_{\vartheta_j}^T \right] \right\} \dot{\boldsymbol{\omega}}_{B/N} = \mathbf{L}_B - [\tilde{\boldsymbol{\omega}}_{B/N}] [I_{sc,B}] \boldsymbol{\omega}_{B/N} - [I'_{sc,B}] \boldsymbol{\omega}_{B/N} \\
& \quad - \sum_{j=1}^{N_P} m_j \left\{ [\tilde{\boldsymbol{\omega}}_{B/N}] [\tilde{\mathbf{r}}_{P_{c,j}/B}] \mathbf{r}'_{P_{c,j}/B} + l_j [\tilde{\mathbf{r}}_{P_{c,j}/B}] \left[\left(-\cos(\varphi_j) \cos(\vartheta_j) \hat{\mathbf{p}}_{0,j,1} - \sin(\varphi_j) \cos(\vartheta_j) \hat{\mathbf{p}}_{0,j,2} \right) \dot{\varphi}_j^2 \right. \right. \\
& \quad \left. \left. + \left(-\cos(\varphi_j) \cos(\vartheta_j) \hat{\mathbf{p}}_{0,j,1} - \sin(\varphi_j) \cos(\vartheta_j) \hat{\mathbf{p}}_{0,j,2} + \sin(\vartheta_j) \hat{\mathbf{p}}_{0,j,3} \right) \dot{\vartheta}_j^2 + \left(2 \sin(\varphi_j) \sin(\vartheta_j) \hat{\mathbf{p}}_{0,j,1} \right. \right. \right. \\
& \quad \left. \left. - 2 \cos(\varphi_j) \sin(\vartheta_j) \hat{\mathbf{p}}_{0,j,2} \right) \dot{\varphi}_j \dot{\vartheta}_j - \left(\sin(\varphi_j) \cos(\vartheta_j) \hat{\mathbf{p}}_{0,j,1} - \cos(\varphi_j) \cos(\vartheta_j) \hat{\mathbf{p}}_{0,j,2} \right) c_{\varphi_j} \right. \\
& \quad \left. \left. - \left(\cos(\varphi_j) \sin(\vartheta_j) \hat{\mathbf{p}}_{0,j,1} + \sin(\varphi_j) \sin(\vartheta_j) \hat{\mathbf{p}}_{0,j,2} + \cos(\vartheta_j) \hat{\mathbf{p}}_{0,j,3} \right) c_{\vartheta_j} \right] \right\} \quad (3.328)
\end{aligned}$$

The back-substitution analytical method steps have now been completed and the following back-substitution matrices definitions are defined:

$$\begin{aligned}
[A] = & \left\{ m_{sc} [I_{3 \times 3}] - \sum_{j=1}^{N_P} m_j l_j \left[\left(\sin(\varphi_j) \cos(\vartheta_j) \hat{\mathbf{p}}_{0,j,1} - \cos(\varphi_j) \cos(\vartheta_j) \hat{\mathbf{p}}_{0,j,2} \right) \mathbf{a}_{\varphi_j}^T \right. \right. \\
& \quad \left. \left. + \left(\cos(\varphi_j) \sin(\vartheta_j) \hat{\mathbf{p}}_{0,j,1} + \sin(\varphi_j) \sin(\vartheta_j) \hat{\mathbf{p}}_{0,j,2} + \cos(\vartheta_j) \hat{\mathbf{p}}_{0,j,3} \right) \mathbf{a}_{\vartheta_j}^T \right] \right\} \quad (3.329)
\end{aligned}$$

$$\begin{aligned}
[B] = & \left\{ -m_{sc} [\tilde{\mathbf{c}}] - \sum_{j=1}^{N_P} m_j l_j \left[\left(\sin(\varphi_j) \cos(\vartheta_j) \hat{\mathbf{p}}_{0,j,1} - \cos(\varphi_j) \cos(\vartheta_j) \hat{\mathbf{p}}_{0,j,2} \right) \mathbf{b}_{\varphi_j}^T \right. \right. \\
& \quad \left. \left. + \left(\cos(\varphi_j) \sin(\vartheta_j) \hat{\mathbf{p}}_{0,j,1} + \sin(\varphi_j) \sin(\vartheta_j) \hat{\mathbf{p}}_{0,j,2} + \cos(\vartheta_j) \hat{\mathbf{p}}_{0,j,3} \right) \mathbf{b}_{\vartheta_j}^T \right] \right\} \quad (3.330)
\end{aligned}$$

$$\begin{aligned}
[C] = & \left\{ m_{sc} [\tilde{\mathbf{c}}] - \sum_{j=1}^{N_P} m_j l_j [\tilde{\mathbf{r}}_{P_{c,j}/B}] \left[\left(\sin(\varphi_j) \cos(\vartheta_j) \hat{\mathbf{p}}_{0,j,1} - \cos(\varphi_j) \cos(\vartheta_j) \hat{\mathbf{p}}_{0,j,2} \right) \mathbf{a}_{\varphi_j}^T \right. \right. \\
& \quad \left. \left. + \left(\cos(\varphi_j) \sin(\vartheta_j) \hat{\mathbf{p}}_{0,j,1} + \sin(\varphi_j) \sin(\vartheta_j) \hat{\mathbf{p}}_{0,j,2} + \cos(\vartheta_j) \hat{\mathbf{p}}_{0,j,3} \right) \mathbf{a}_{\vartheta_j}^T \right] \right\} \quad (3.331)
\end{aligned}$$

$$\begin{aligned}
[D] = & \left\{ [I_{sc,B}] - \sum_{j=1}^{N_P} m_j l_j [\tilde{\mathbf{r}}_{P_{c,j}/B}] \left[\left(\sin(\varphi_j) \cos(\vartheta_j) \hat{\mathbf{p}}_{0,j,1} - \cos(\varphi_j) \cos(\vartheta_j) \hat{\mathbf{p}}_{0,j,2} \right) \mathbf{b}_{\varphi_j}^T \right. \right. \\
& \left. \left. + \left(\cos(\varphi_j) \sin(\vartheta_j) \hat{\mathbf{p}}_{0,j,1} + \sin(\varphi_j) \sin(\vartheta_j) \hat{\mathbf{p}}_{0,j,2} + \cos(\vartheta_j) \hat{\mathbf{p}}_{0,j,3} \right) \mathbf{b}_{\vartheta_j}^T \right] \right\} \quad (3.332)
\end{aligned}$$

$$\begin{aligned}
\mathbf{v}_{\text{trans}} = & m_{sc} \ddot{\mathbf{r}}_{C/N} - 2m_{sc} [\tilde{\boldsymbol{\omega}}_{B/N}] \mathbf{c}' - m_{sc} [\tilde{\boldsymbol{\omega}}_{B/N}] [\tilde{\boldsymbol{\omega}}_{B/N}] \mathbf{c} \\
& - \sum_{j=1}^{N_P} m_j l_j \left[\left(-\cos(\varphi_j) \cos(\vartheta_j) \hat{\mathbf{p}}_{0,j,1} - \sin(\varphi_j) \cos(\vartheta_j) \hat{\mathbf{p}}_{0,j,2} \right) \dot{\varphi}_j^2 + \left(-\cos(\varphi_j) \cos(\vartheta_j) \hat{\mathbf{p}}_{0,j,1} \right. \right. \\
& \quad \left. \left. - \sin(\varphi_j) \cos(\vartheta_j) \hat{\mathbf{p}}_{0,j,2} + \sin(\vartheta_j) \hat{\mathbf{p}}_{0,j,3} \right) \dot{\vartheta}_j^2 + \left(2 \sin(\varphi_j) \sin(\vartheta_j) \hat{\mathbf{p}}_{0,j,1} \right. \right. \\
& \quad \left. \left. - 2 \cos(\varphi_j) \sin(\vartheta_j) \hat{\mathbf{p}}_{0,j,2} \right) \dot{\varphi}_j \dot{\vartheta}_j - \left(\sin(\varphi_j) \cos(\vartheta_j) \hat{\mathbf{p}}_{0,j,1} - \cos(\varphi_j) \cos(\vartheta_j) \hat{\mathbf{p}}_{0,j,2} \right) c_{\varphi_j} \right. \\
& \quad \left. - \left(\cos(\varphi_j) \sin(\vartheta_j) \hat{\mathbf{p}}_{0,j,1} + \sin(\varphi_j) \sin(\vartheta_j) \hat{\mathbf{p}}_{0,j,2} + \cos(\vartheta_j) \hat{\mathbf{p}}_{0,j,3} \right) c_{\vartheta_j} \right] \quad (3.333)
\end{aligned}$$

$$\begin{aligned}
\mathbf{v}_{\text{rot}} = & \mathbf{L}_B - [\tilde{\boldsymbol{\omega}}_{B/N}] [I_{sc,B}] \boldsymbol{\omega}_{B/N} - [I'_{sc,B}] \boldsymbol{\omega}_{B/N} \\
& - \sum_{j=1}^{N_P} m_j \left\{ [\tilde{\boldsymbol{\omega}}_{B/N}] [\tilde{\mathbf{r}}_{P_{c,j}/B}] \mathbf{r}'_{P_{c,j}/B} + l_j [\tilde{\mathbf{r}}_{P_{c,j}/B}] \left[\left(-\cos(\varphi_j) \cos(\vartheta_j) \hat{\mathbf{p}}_{0,j,1} - \sin(\varphi_j) \cos(\vartheta_j) \hat{\mathbf{p}}_{0,j,2} \right) \dot{\varphi}_j^2 \right. \right. \\
& \quad \left. \left. + \left(-\cos(\varphi_j) \cos(\vartheta_j) \hat{\mathbf{p}}_{0,j,1} - \sin(\varphi_j) \cos(\vartheta_j) \hat{\mathbf{p}}_{0,j,2} + \sin(\vartheta_j) \hat{\mathbf{p}}_{0,j,3} \right) \dot{\vartheta}_j^2 + \left(2 \sin(\varphi_j) \sin(\vartheta_j) \hat{\mathbf{p}}_{0,j,1} \right. \right. \right. \\
& \quad \left. \left. - 2 \cos(\varphi_j) \sin(\vartheta_j) \hat{\mathbf{p}}_{0,j,2} \right) \dot{\varphi}_j \dot{\vartheta}_j - \left(\sin(\varphi_j) \cos(\vartheta_j) \hat{\mathbf{p}}_{0,j,1} - \cos(\varphi_j) \cos(\vartheta_j) \hat{\mathbf{p}}_{0,j,2} \right) c_{\varphi_j} \right. \\
& \quad \left. \left. - \left(\cos(\varphi_j) \sin(\vartheta_j) \hat{\mathbf{p}}_{0,j,1} + \sin(\varphi_j) \sin(\vartheta_j) \hat{\mathbf{p}}_{0,j,2} + \cos(\vartheta_j) \hat{\mathbf{p}}_{0,j,3} \right) c_{\vartheta_j} \right] \right\} \quad (3.334)
\end{aligned}$$

These equations conclude the necessary steps required for the fuel slosh spherical pendulum model. These equations conform with the standard form of the EOMs and the back-substitution method introduced in Section 2.

3.1.8 N-Connected Hinged Rigid-Bodies

3.1.8.1 Introduction

The last model included in the examples of fully-coupled spacecraft dynamics problems is the extension of hinged rigid-bodies to N-Connected hinged rigid-bodies. This extension allows for general number of interconnected panels to be connected to the spacecraft and retains the standard

EOM form introduced in this dissertation. This work was completed with collaborator Iosto Fodde of Delft University of Technology during August - December of 2017.

Figure 3.11 shows a schematic of N-connected hinged rigid bodies and follows a similar definition of the panels as seen in the dual-hinged rigid-bodies formulation and the single hinged rigid-bodies formulation.

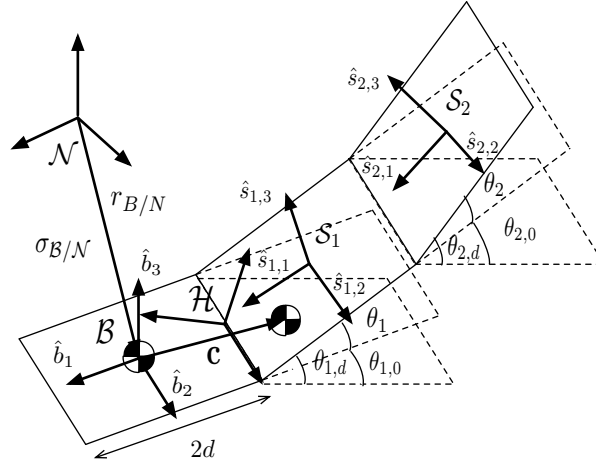


Figure 3.11: Frame and variable definitions for the system discussed here, where $N_p = 2$.

3.1.8.2 Equations of Motion

The translational equation has been developed and results in the following equation:

$$\begin{aligned}
 m_{sc} \ddot{\mathbf{r}}_{B/N} - m_{sc} [\ddot{\mathbf{c}}] \dot{\boldsymbol{\omega}}_{B/N} + \sum_{i=1}^{N_p} \left[\sum_{k=i}^{N_p} (2[N_p - k] + 1) dm_p \hat{\mathbf{s}}_{k,3} \right] \ddot{\theta}_i &= \mathbf{F}_{ext} - 2m_{sc} [\tilde{\boldsymbol{\omega}}_{B/N}] \mathbf{c}' \\
 - m_{sc} [\tilde{\boldsymbol{\omega}}_{B/N}] [\tilde{\boldsymbol{\omega}}_{B/N}] \mathbf{c} - \sum_{i=1}^{N_p} \left[\left(\sum_{k=1}^i \dot{\theta}_k \right)^2 (2[N_p - i] + 1) dm_p \hat{\mathbf{s}}_{i,1} \right] & \quad (3.335)
 \end{aligned}$$

Similarly the rotational equation of motion can be seen in Eq. (3.336) and fits the familiar form throughout this dissertation.

$$\begin{aligned}
m_{sc}[\tilde{\mathbf{c}}]\ddot{\mathbf{r}}_{B/N} + [I_{sc,B}]\dot{\boldsymbol{\omega}}_{B/N} + \sum_{i=1}^{N_p} \left[\sum_{k=i}^{N_p} I_{s_{k,2}} \hat{\mathbf{s}}_{k,2} + \sum_{k=i}^{N_p} \left[\tilde{\mathbf{r}}_{S_k/B} \right] + \sum_{n=k+1}^{N_p} 2[\tilde{\mathbf{r}}_{S_n/B}] \right] m_p d\hat{\mathbf{s}}_{k,3} \ddot{\theta}_i \\
= -[\tilde{\boldsymbol{\omega}}_{B/N}][I_{sc,B}]\boldsymbol{\omega}_{B/N} - [I'_{sc,B}]\boldsymbol{\omega}_{B/N} - \sum_{i=1}^{N_p} \left(m_p [\tilde{\boldsymbol{\omega}}_{B/N}] [\tilde{\mathbf{r}}_{S_i/B}] \mathbf{r}'_{S_i/B} \right. \\
\left. + \left(\sum_{k=1}^i \dot{\theta}_k \right)^2 \left[\tilde{\mathbf{r}}_{S_i/B} \right] + \sum_{n=i+1}^{N_p} 2[\tilde{\mathbf{r}}_{S_n/B}] \right] m_p d\hat{\mathbf{s}}_{i,1} + I_{s_{i,2}} \left(\sum_{k=1}^i \dot{\theta}_k \right) [\tilde{\boldsymbol{\omega}}_{B/N}] \hat{\mathbf{s}}_{i,2} \Big) + \mathbf{L}_B \quad (3.336)
\end{aligned}$$

The N hinged rigid-body equation of motion is:

$$\begin{aligned}
\left[dm_p \hat{\mathbf{s}}_{j,3}^T + \sum_{i=j+1}^{N_p} 2dm_p \hat{\mathbf{s}}_{j,3}^T \right] \ddot{\mathbf{r}}_{B/N} + \left[I_{s_{j,2}} \hat{\mathbf{s}}_{j,2}^T - m_p d\hat{\mathbf{s}}_{j,3}^T [\tilde{\mathbf{r}}_{S_i/B}] - \sum_{i=j+1}^{N_p} 2m_p d\hat{\mathbf{s}}_{j,3}^T [\tilde{\mathbf{r}}_{S_i/B}] \right] \dot{\boldsymbol{\omega}}_{B/N} + \\
\sum_{i=1}^{N_p} \left[I_{s_{j,2}} H[j-i] + m_p d^2 \hat{\mathbf{s}}_{j,3}^T \sum_{k=i}^{N_p} (2\hat{\mathbf{s}}_{k,3} + 4\hat{\mathbf{s}}_{k,3}(N_p-j) - H[k-j]4\hat{\mathbf{s}}_{k,3}(k-j)) - H[j-i]\hat{\mathbf{s}}_{j,3} \right] \ddot{\theta}_i \\
= K + 2d\hat{\mathbf{s}}_{j,3}^T \mathbf{F}_{ext,j+1} - (I_{s_{j,1}} - I_{s_{j,3}}) \omega_{s_{j,3}} \omega_{s_{j,1}} - m_p d\hat{\mathbf{s}}_{j,3}^T \left[2[\tilde{\boldsymbol{\omega}}_{B/N}] \mathbf{r}'_{S_j/B} + [\tilde{\boldsymbol{\omega}}_{B/N}] [\tilde{\boldsymbol{\omega}}_{B/N}] \mathbf{r}_{S_j/B} + \right. \\
\left. \sum_{i=j+1}^{N_p} \left(4[\tilde{\boldsymbol{\omega}}_{B/N}] \mathbf{r}'_{S_j/B} + 2[\tilde{\boldsymbol{\omega}}_{B/N}] [\tilde{\boldsymbol{\omega}}_{B/N}] \mathbf{r}_{S_j/B} \right) \right. \\
\left. + \left(\sum_{n=1}^i \dot{\theta}_n \right)^2 (2\hat{\mathbf{s}}_{i,1} + 4\hat{\mathbf{s}}_{i,1}(N_p-j) - H[i-j]4\hat{\mathbf{s}}_{i,1}(i-j) - \left(\sum_{n=1}^i \dot{\theta}_n \right)^2 \hat{\mathbf{s}}_{j,1}) \right] \quad (3.337)
\end{aligned}$$

where $H[x]$ is the Heaviside function. It has been verified that when $N_p = 1$, Eq. (3.337) matches Eq. (3.56) and similarly for the dual-hinged rigid-body equations.

3.1.8.3 Back Substitution Method

The back substitution method is used to gain a simpler expression that combines the three equations of motion. First, Eq. (3.337) is rearranged so that the second order state variables for

the panel motions are isolated on the left hand side:

$$\begin{aligned}
& \sum_{i=1}^{N_p} \left[I_{s_j,2} H[j-i] + m_p d^2 \hat{s}_{j,3}^T \sum_{k=i}^{N_p} (2\hat{s}_{k,3} + 4\hat{s}_{k,3}(N_p-j) - H[k-j]4\hat{s}_{k,3}(k-j)) - H[j-i]\hat{s}_{j,3} \right] \ddot{\theta}_i \\
&= - \left[dm_p \hat{s}_{j,3}^T + \sum_{i=j+1}^{N_p} 2dm_p \hat{s}_{j,3}^T \right] \ddot{\mathbf{r}}_{B/N} - \left[I_{s_j,2} \hat{s}_{j,2}^T - m_p d \hat{s}_{j,3}^T [\tilde{\mathbf{r}}_{S_i/B}] - \sum_{i=j+1}^{N_p} 2m_p d \hat{s}_{j,3}^T [\tilde{\mathbf{r}}_{S_i/B}] \right] \dot{\boldsymbol{\omega}}_{B/N} \\
&+ K + 2d \hat{s}_{j,3}^T \mathbf{F}_{ext,j+1} - (I_{s_{j,1}} - I_{s_{j,3}}) \omega_{s_{j,3}} \omega_{s_{j,1}} - m_p d \hat{s}_{j,3}^T \left[2[\tilde{\boldsymbol{\omega}}_{B/N}] \mathbf{r}'_{S_j/B} + [\tilde{\boldsymbol{\omega}}_{B/N}] [\tilde{\boldsymbol{\omega}}_{B/N}] \mathbf{r}_{S_j/B} \right. \\
&\quad \left. + \sum_{i=j+1}^{N_p} \left(4[\tilde{\boldsymbol{\omega}}_{B/N}] \mathbf{r}'_{S_j/B} + 2[\tilde{\boldsymbol{\omega}}_{B/N}] [\tilde{\boldsymbol{\omega}}_{B/N}] \mathbf{r}_{S_j/B} \right) \right. \\
&\quad \left. + \left(\sum_{n=1}^i \dot{\theta}_i \right)^2 (2\hat{s}_{i,1} + 4\hat{s}_{i,1}(N_p-j) - H[i-j]4\hat{s}_{i,1}(i-j) - \left(\sum_{n=1}^i \dot{\theta}_i \right)^2 \hat{s}_{j,1}) \right] \quad (3.338)
\end{aligned}$$

Now, defining the elements of a matrix $[A]$ as:

$$a_{j,i} = I_{s_j,2} H[j-i] + m_p d^2 \hat{s}_{j,3}^T \sum_{k=i}^{N_p} (2\hat{s}_{k,3} + 4\hat{s}_{k,3}(N_p-j) - H[k-j]4\hat{s}_{k,3}(k-j)) - H[j-i]\hat{s}_{j,3} \quad (3.339)$$

And defining the row elements of a matrix $[F]$ as:

$$\mathbf{f}_{j,1} = - \left[dm_p \hat{s}_{j,3}^T + \sum_{i=j+1}^{N_p} 2dm_p \hat{s}_{j,3}^T \right] \quad (3.340)$$

with a matrix $[G]$ which has row elements defined as:

$$\mathbf{g}_{j,1} = - \left[I_{s_j,2} \hat{s}_{j,2}^T - m_p d \hat{s}_{j,3}^T [\tilde{\mathbf{r}}_{S_i/B}] - \sum_{i=j+1}^{N_p} 2m_p d \hat{s}_{j,3}^T [\tilde{\mathbf{r}}_{S_i/B}] \right] \quad (3.341)$$

Also by defining the vector \mathbf{v}

$$\begin{aligned}
\mathbf{v}_{j,1} &= K + 2d \hat{s}_{j,3}^T \mathbf{F}_{ext,j+1} - (I_{s_{j,1}} - I_{s_{j,3}}) \omega_{s_{j,3}} \omega_{s_{j,1}} - m_p d \hat{s}_{j,3}^T \left[2[\tilde{\boldsymbol{\omega}}_{B/N}] \mathbf{r}'_{S_j/B} + [\tilde{\boldsymbol{\omega}}_{B/N}] [\tilde{\boldsymbol{\omega}}_{B/N}] \mathbf{r}_{S_j/B} \right. \\
&\quad \left. + \sum_{i=j+1}^{N_p} \left(4[\tilde{\boldsymbol{\omega}}_{B/N}] \mathbf{r}'_{S_j/B} + 2[\tilde{\boldsymbol{\omega}}_{B/N}] [\tilde{\boldsymbol{\omega}}_{B/N}] \mathbf{r}_{S_j/B} \right) \right. \\
&\quad \left. + \left(\sum_{n=1}^i \dot{\theta}_i \right)^2 (2\hat{s}_{i,1} + 4\hat{s}_{i,1}(N_p-j) - H[i-j]4\hat{s}_{i,1}(i-j) - \left(\sum_{n=1}^i \dot{\theta}_i \right)^2 \hat{s}_{j,1}) \right] \quad (3.342)
\end{aligned}$$

Equation (3.338) can then be written in matrix form to utilize some linear algebra techniques.

$$[A] \begin{bmatrix} \ddot{\theta}_1 \\ \vdots \\ \ddot{\theta}_{N_p} \end{bmatrix} = [F] \ddot{\mathbf{r}}_{B/N} + [G] \dot{\boldsymbol{\omega}}_{B/N} + \mathbf{v} \quad (3.343)$$

Eq. (3.343) can now be solved by inverting matrix $[A]$. Note the definition $[E] = [A]^{-1}$.

$$\begin{bmatrix} \ddot{\theta}_1 \\ \vdots \\ \ddot{\theta}_{N_p} \end{bmatrix} = [E][F]\ddot{\mathbf{r}}_{B/N} + [E][G]\dot{\boldsymbol{\omega}}_{B/N} + [E]\mathbf{v} \quad (3.344)$$

And the subcomponents of $[E]$ are defined as

$$[E] = \begin{bmatrix} \mathbf{e}_1^T \\ \vdots \\ \mathbf{e}_{N_p}^T \end{bmatrix} \quad (3.345)$$

Since the modified Euler's equation, Eq. (3.336), has $\ddot{\theta}_i$ terms, it is more convenient to use the expression for $\ddot{\theta}_i$ as

$$\ddot{\theta}_i = \mathbf{e}_i^T [F]\ddot{\mathbf{r}}_{B/N} + \mathbf{e}_i^T [G]\dot{\boldsymbol{\omega}}_{B/N} + \mathbf{e}_i^T \mathbf{v} \quad (3.346)$$

The next step in the back substitution method is to analytically substitute Eq. (3.346) into the translational and rotational EOMs. Performing this substitution for translation yields:

$$\begin{aligned} m_{sc}\ddot{\mathbf{r}}_{B/N} - m_{sc}[\tilde{\mathbf{c}}]\dot{\boldsymbol{\omega}}_{B/N} + \sum_{i=1}^{N_p} \left[\sum_{k=i}^{N_p} (2[N_p - k] + 1) dm_p \hat{\mathbf{s}}_{k,3} [\mathbf{e}_i^T [F]\ddot{\mathbf{r}}_{B/N} + \mathbf{e}_i^T [G]\dot{\boldsymbol{\omega}}_{B/N} + \mathbf{e}_i^T \mathbf{v}] \right] \\ = \mathbf{F}_{ext} - 2m_{sc}[\tilde{\boldsymbol{\omega}}_{B/N}]\mathbf{c}' - m_{sc}[\tilde{\boldsymbol{\omega}}_{B/N}][\tilde{\boldsymbol{\omega}}_{B/N}]\mathbf{c} - \sum_{i=1}^{N_p} \left[\left(\sum_{k=1}^i \dot{\theta}_k \right)^2 (2[N_p - i] + 1) dm_p \hat{\mathbf{s}}_{i,1} \right] \end{aligned} \quad (3.347)$$

Combining like terms yields:

$$\begin{aligned}
& \left\{ m_{sc}[I_{3 \times 3}] + \sum_{i=1}^{N_p} \left[\sum_{k=i}^{N_p} (2[N_p - k] + 1) dm_p \hat{\mathbf{s}}_{k,3} \right] e_i^T [F] \right\} \ddot{\mathbf{r}}_{B/N} \\
& + \left\{ -m_{sc}[\tilde{\mathbf{c}}] + \sum_{i=1}^{N_p} \left[\sum_{k=i}^{N_p} (2[N_p - k] + 1) dm_p \hat{\mathbf{s}}_{k,3} \right] e_i^T [G] \right\} \dot{\boldsymbol{\omega}}_{B/N} \\
& = \mathbf{F}_{\text{ext}} - 2m_{sc}[\tilde{\boldsymbol{\omega}}_{B/N}] \mathbf{c}' - m_{sc}[\tilde{\boldsymbol{\omega}}_{B/N}][\tilde{\boldsymbol{\omega}}_{B/N}] \mathbf{c} - \sum_{i=1}^{N_p} \left[\left(\sum_{k=1}^i \dot{\theta}_k \right)^2 (2[N_p - i] + 1) dm_p \hat{\mathbf{s}}_{i,1} \right] \\
& \quad - \sum_{i=1}^{N_p} \left[\sum_{k=i}^{N_p} (2[N_p - k] + 1) dm_p \hat{\mathbf{s}}_{k,3} e_i^T \mathbf{v} \right] \quad (3.348)
\end{aligned}$$

Substitution into the rotational equation of motion:

$$\begin{aligned}
& m_{sc}[\tilde{\mathbf{c}}] \ddot{\mathbf{r}}_{B/N} + [I_{sc,B}] \dot{\boldsymbol{\omega}}_{B/N} + \sum_{i=1}^{N_p} \left[\sum_{k=i}^{N_p} (I_{s_{k,2}} \hat{\mathbf{s}}_{k,2} + [\tilde{\mathbf{r}}_{S_k/B}] \right. \\
& + \left. \sum_{n=k+1}^{N_p} 2[\tilde{\mathbf{r}}_{S_n/B}] \right] m_p d\hat{\mathbf{s}}_{k,3} [e_i^T [F] \ddot{\mathbf{r}}_{B/N} + e_i^T [G] \dot{\boldsymbol{\omega}}_{B/N} + e_i^T \mathbf{v}] = -[\tilde{\boldsymbol{\omega}}_{B/N}] [I_{sc,B}] \boldsymbol{\omega}_{B/N} - [I'_{sc,B}] \boldsymbol{\omega}_{B/N} \\
& \quad - \sum_{i=1}^{N_p} \left(m_p [\tilde{\boldsymbol{\omega}}_{B/N}] [\tilde{\mathbf{r}}_{S_i/B}] \mathbf{r}'_{S_i/B} + \left(\sum_{k=1}^i \dot{\theta}_k \right)^2 \left[[\tilde{\mathbf{r}}_{S_i/B}] + \sum_{n=i+1}^{N_p} 2[\tilde{\mathbf{r}}_{S_n/B}] \right] m_p d\hat{\mathbf{s}}_{i,1} \right. \\
& \quad \left. + I_{s_{i,2}} \left(\sum_{k=1}^i \dot{\theta}_k \right) [\tilde{\boldsymbol{\omega}}_{B/N}] \hat{\mathbf{s}}_{i,2} \right) + \mathbf{L}_B \quad (3.349)
\end{aligned}$$

Combining like terms yields:

$$\begin{aligned}
& \left\{ m_{sc}[\tilde{\mathbf{c}}] + \sum_{i=1}^{N_p} \left[\sum_{k=i}^{N_p} (I_{s_{k,2}} \hat{\mathbf{s}}_{k,2} + [\tilde{\mathbf{r}}_{S_k/B}] + \sum_{n=k+1}^{N_p} 2[\tilde{\mathbf{r}}_{S_n/B}] \right] m_p d\hat{\mathbf{s}}_{k,3} e_i^T [F] \right\} \ddot{\mathbf{r}}_{B/N} \\
& + \left\{ [I_{sc,B}] + \sum_{i=1}^{N_p} \left[\sum_{k=i}^{N_p} (I_{s_{k,2}} \hat{\mathbf{s}}_{k,2} + [\tilde{\mathbf{r}}_{S_k/B}] + \sum_{n=k+1}^{N_p} 2[\tilde{\mathbf{r}}_{S_n/B}] \right] m_p d\hat{\mathbf{s}}_{k,3} e_i^T [G] \right\} \dot{\boldsymbol{\omega}}_{B/N} \\
& = -[\tilde{\boldsymbol{\omega}}_{B/N}] [I_{sc,B}] \boldsymbol{\omega}_{B/N} - [I'_{sc,B}] \boldsymbol{\omega}_{B/N} - \sum_{i=1}^{N_p} \left(m_p [\tilde{\boldsymbol{\omega}}_{B/N}] [\tilde{\mathbf{r}}_{S_i/B}] \mathbf{r}'_{S_i/B} + \left(\sum_{k=1}^i \dot{\theta}_k \right)^2 \left[[\tilde{\mathbf{r}}_{S_i/B}] \right. \right. \\
& \quad \left. \left. + \sum_{n=i+1}^{N_p} 2[\tilde{\mathbf{r}}_{S_n/B}] \right] m_p d\hat{\mathbf{s}}_{i,1} + I_{s_{i,2}} \left(\sum_{k=1}^i \dot{\theta}_k \right) [\tilde{\boldsymbol{\omega}}_{B/N}] \hat{\mathbf{s}}_{i,2} \right) + \mathbf{L}_B - \sum_{i=1}^{N_p} \left[\sum_{k=i}^{N_p} (I_{s_{k,2}} \hat{\mathbf{s}}_{k,2} \right. \\
& \quad \left. + [\tilde{\mathbf{r}}_{S_k/B}] + \sum_{n=k+1}^{N_p} 2[\tilde{\mathbf{r}}_{S_n/B}] \right] m_p d\hat{\mathbf{s}}_{k,3} e_i^T \mathbf{v} \quad (3.350)
\end{aligned}$$

Now, the analytical steps have been completed for the back-substitution method and the matrices contributions for the N-Connected hinged rigid-bodies can be seen in the following equations:

$$[A_{\text{contr}}] = \sum_{i=1}^{N_p} \left[\sum_{k=i}^{N_p} (2[N_p - k] + 1) dm_p \hat{\mathbf{s}}_{k,3} \right] e_i^T [F] \quad (3.351)$$

$$[B_{\text{contr}}] = \sum_{i=1}^{N_p} \left[\sum_{k=i}^{N_p} (2[N_p - k] + 1) dm_p \hat{\mathbf{s}}_{k,3} \right] e_i^T [G] \quad (3.352)$$

$$\mathbf{v}_{\text{trans,contr}} = - \sum_{i=1}^{N_p} \left[\left(\sum_{k=1}^i \dot{\theta}_k \right)^2 (2[N_p - i] + 1) dm_p \hat{\mathbf{s}}_{i,1} \right] - \sum_{i=1}^{N_p} \left[\sum_{k=i}^{N_p} (2[N_p - k] + 1) dm_p \hat{\mathbf{s}}_{k,3} e_i^T \mathbf{v} \right] \quad (3.353)$$

$$[C_{\text{contr}}] = \sum_{i=1}^{N_p} \left[\sum_{k=i}^{N_p} (I_{s_{k,2}} \hat{\mathbf{s}}_{k,2} + [\tilde{\mathbf{r}}_{S_k/B}] + \sum_{n=k+1}^{N_p} 2[\tilde{\mathbf{r}}_{S_n/B}]) m_p d\hat{\mathbf{s}}_{k,3} \right] e_i^T [F] \quad (3.354)$$

$$[D_{\text{contr}}] = \sum_{i=1}^{N_p} \left[\sum_{k=i}^{N_p} (I_{s_{k,2}} \hat{\mathbf{s}}_{k,2} + [\tilde{\mathbf{r}}_{S_k/B}] + \sum_{n=k+1}^{N_p} 2[\tilde{\mathbf{r}}_{S_n/B}]) m_p d\hat{\mathbf{s}}_{k,3} \right] e_i^T [G] \quad (3.355)$$

$$\begin{aligned} [v_{\text{rot,contr}}] = & - \sum_{i=1}^{N_p} \left(m_p [\tilde{\omega}_{B/N}] [\tilde{\mathbf{r}}_{S_i/B}] \mathbf{r}'_{S_i/B} + \left(\sum_{k=1}^i \dot{\theta}_k \right)^2 \left[[\tilde{\mathbf{r}}_{S_i/B}] + \sum_{n=i+1}^{N_p} 2[\tilde{\mathbf{r}}_{S_n/B}] \right] m_p d\hat{\mathbf{s}}_{i,1} \right. \\ & \left. + I_{s_{i,2}} \left(\sum_{k=1}^i \dot{\theta}_k \right) [\tilde{\omega}_{B/N}] \hat{\mathbf{s}}_{i,2} \right) - \sum_{i=1}^{N_p} \left[\sum_{k=i}^{N_p} (I_{s_{k,2}} \hat{\mathbf{s}}_{k,2} + [\tilde{\mathbf{r}}_{S_k/B}] + \sum_{n=k+1}^{N_p} 2[\tilde{\mathbf{r}}_{S_n/B}]) m_p d\hat{\mathbf{s}}_{k,3} \right] e_i^T \mathbf{v} \end{aligned} \quad (3.356)$$

These equations conclude the necessary steps for the N-Connected hinged rigid-body model and confirms that the model agrees with the standardized EOM form and the back-substitution method introduced in this dissertation.

It should be noted here before the section pertaining to Kane's method development that the derivation of equations of motion for N-Hinged rigid-bodies was actually completed solely using Kane's Method. This gives further validation of the systematic approach to developing the EOMs using both Newtonian/Eulerian mechanics and Kane's method.

3.2 Kane's Method Derivation Comparisons

In Section 1.2.1, it is explained that the final form of the equations of motion can depend on the method used to derive the EOMs. The equations of motion solutions provided in the prior

sections used Newtonian and Eulerian mechanics to derive solutions. This section is provided to show that Kane's method [2] can be used to derive the EOMs and still arrive at the introduced standardized EOM form. This is an important result because Kane's method is a very powerful method in developing dynamics solutions particularly involving multi-body applications. [2].

3.2.1 Hinged Rigid-Bodies

The first step in Kane's Method is to define the state variables and their respective chosen generalized speeds. A powerful attribute of Kane's method is the generalized speeds do not have to be the direct time derivative of the generalized coordinates [18]. For hinged rigid-bodies the states and generalized speeds are defined in the following equation:

$$\mathbf{X} = \begin{bmatrix} \mathbf{r}_{B/N} \\ \boldsymbol{\sigma}_{B/N} \\ \theta_1 \\ \cdot \\ \theta_{N_S} \end{bmatrix} \quad \mathbf{u} = \begin{bmatrix} \dot{\mathbf{r}}_{B/N} \\ \boldsymbol{\omega}_{B/N} \\ \dot{\theta}_1 \\ \cdot \\ \dot{\theta}_{N_S} \end{bmatrix} \quad (3.357)$$

Next, the velocities of the center of mass of all of the bodies and the angular velocities of the rigid bodies need to be defined and can be seen in the following equations:

$$\dot{\mathbf{r}}_{B_c/N} = \dot{\mathbf{r}}_{B/N} + \boldsymbol{\omega}_{B/N} \times \mathbf{r}_{B_c/B} = \dot{\mathbf{r}}_{B/N} - [\tilde{\mathbf{r}}_{B_c/B}] \boldsymbol{\omega}_{B/N} \quad (3.358)$$

$$\dot{\mathbf{r}}_{C/N} = \dot{\mathbf{r}}_{B/N} + \dot{\mathbf{c}} \quad (3.359)$$

$$\dot{\mathbf{r}}_{S_i/N} = \dot{\mathbf{r}}_{B/N} + \mathbf{r}'_{S_i/B} + \boldsymbol{\omega}_{B/N} \times \mathbf{r}_{S_i/B} = \dot{\mathbf{r}}_{B/N} + d_i \dot{\theta}_i \hat{\mathbf{s}}_{i,3} - [\tilde{\mathbf{r}}_{S_i/B}] \boldsymbol{\omega}_{B/N} \quad (3.360)$$

$$\boldsymbol{\omega}_{S/N} = \boldsymbol{\omega}_{B/N} + \dot{\theta}_i \hat{\mathbf{s}}_{i,2} \quad (3.361)$$

Next, the following partial velocity table is created:

Table 3.1: Partial velocity table for hinged rigid-bodies

r	$\mathbf{v}_r^{B_c}$	$\boldsymbol{\omega}_r^B$	$\mathbf{v}_r^{S_i}$	$\boldsymbol{\omega}_r^{S_i}$
1 – 3	$[I_{3 \times 3}]$	$[0_{3 \times 3}]$	$[I_{3 \times 3}]$	$[0_{3 \times 3}]$
4 – 6	$-\tilde{\mathbf{r}}_{B_c/B}$	$[I_{3 \times 3}]$	$-\tilde{\mathbf{r}}_{S_i/B}$	$[I_{3 \times 3}]$
7 – N_S	$[0_{3 \times 1}]$	$[0_{3 \times 1}]$	$d_i \hat{\mathbf{s}}_{i,3}$	$\hat{\mathbf{s}}_{i,2}$

Using these partial velocity definitions, the follow sections will step through the formulation for the translational EOM development using Kane's Method.

3.2.1.1 Rigid Spacecraft Hub Translational Motion

The definition of a generalized force is [2]:

$$F_r = \sum_r^N \mathbf{v}_r^T \cdot \mathbf{F} \quad (3.362)$$

Using this definition the external force applied on the spacecraft for the translational equations is defined as:

$$\mathbf{F}_{1-3} = [\mathbf{v}_{1-3}^C]^T \mathbf{F}_{\text{ext}} = \mathbf{F}_{\text{ext}} \quad (3.363)$$

Using the definition of generalized inertia forces [2],

$$F_r^* = \sum_r^N \left[\boldsymbol{\omega}_r^T \mathbf{T}^* + \mathbf{v}_r^T (-m_r \mathbf{a}_r) \right] \quad (3.364)$$

the inertia forces for the hub translational motion are defined as

$$\mathbf{F}_{1-3}^* = [\mathbf{v}_{1-3}^{B_c}]^T (-m_{\text{hub}} \ddot{\mathbf{r}}_{B_c/N}) + \sum_i^{N_S} [\mathbf{v}_{1-3}^{S_i}]^T (-m_{\text{sp}_i} \ddot{\mathbf{r}}_{S_i/N}) = -m_{\text{hub}} \ddot{\mathbf{r}}_{B_c/N} + \sum_i^{N_S} -m_{\text{sp}_i} \ddot{\mathbf{r}}_{S_i/N} \quad (3.365)$$

Finally, Kane's equation is defined as

$$F_r + F_r^* = 0; \quad r = 1, 2, \dots, N \quad (3.366)$$

therefore,

$$\mathbf{F}_{\text{ext}} - m_{\text{hub}} \ddot{\mathbf{r}}_{B_c/N} + \sum_i^{N_P} -m_{\text{sp}_i} \ddot{\mathbf{r}}_{S_i/N} = 0 \quad (3.367)$$

Expanding and rearranging results in

$$m_{\text{hub}} (\ddot{\mathbf{r}}_{B/N} + \ddot{\mathbf{r}}_{B_c/B}) + \sum_i^{N_S} m_{\text{sp}_i} (\ddot{\mathbf{r}}_{B/N} + \ddot{\mathbf{r}}_{S_i/B}) = \mathbf{F}_{\text{ext}} \quad (3.368)$$

Plugging in definitions, combining like terms and rearranging yields the final equation:

$$m_{sc}\ddot{\mathbf{r}}_{B/N} - m_{sc}[\tilde{\mathbf{c}}]\dot{\boldsymbol{\omega}}_{B/N} + \sum_i^{N_s} m_{sp_i} d_i \hat{\mathbf{s}}_{i,3} \ddot{\theta}_i = \mathbf{F}_{ext} - 2m_{sc}[\tilde{\boldsymbol{\omega}}_{B/N}]\mathbf{c}' - m_{sc}[\tilde{\boldsymbol{\omega}}_{B/N}][\tilde{\boldsymbol{\omega}}_{B/N}]\mathbf{c} - \sum_i^{N_s} m_{sp_i} d_i \dot{\theta}_i^2 \hat{\mathbf{s}}_{i,1} \quad (3.369)$$

Equation (3.369) is identical to Eq. (3.15) found using Newtonian mechanics, which confidence in both the solution to the dynamics problem and the applicability of the generalized EOM form.

3.2.1.2 Rigid Spacecraft Hub Rotational Motion

To begin the rotational dynamics formulation, the torque acting on the spacecraft, \mathbf{L}_B needs to be defined as a general active force. This definition can be seen in the following equation:

$$\mathbf{F}_{4-6} = [\boldsymbol{\omega}_{4-6}^B]^T \mathbf{L}_B = \mathbf{L}_B \quad (3.370)$$

To define the generalized inertia forces, the definition of \mathbf{T}^* needs to be defined for a rigid-body [18]:

$$\mathbf{T}^* = -[I_c]\dot{\boldsymbol{\omega}} - [\tilde{\boldsymbol{\omega}}][I_c]\boldsymbol{\omega} \quad (3.371)$$

Using this definition, the generalized inertia forces for the rotational dynamics equation is

$$\begin{aligned} \mathbf{F}_{4-6}^* &= [\boldsymbol{\omega}_{4-6}^B]^T \mathbf{T}_{hub}^* + [\mathbf{v}_{4-6}^{B_c}]^T (-m_{hub} \ddot{\mathbf{r}}_{B_c/N}) + \sum_i^{N_s} \left([\mathbf{v}_{4-6}^{S_i}]^T (-m_{sp_i} \ddot{\mathbf{r}}_{S_i/N}) + [\boldsymbol{\omega}_{4-6}^{S_i}]^T \mathbf{T}_{sp_i}^* \right) \\ &= -[I_{hub,B}]\dot{\boldsymbol{\omega}}_{B/N} - [\tilde{\boldsymbol{\omega}}_{B/N}][I_{hub,B}]\boldsymbol{\omega}_{B/N} - m_{hub}[\tilde{\mathbf{r}}_{B_c/B}]\ddot{\mathbf{r}}_{B_c/N} \\ &\quad + \sum_i^{N_s} \left(-m_{sp_i}[\tilde{\mathbf{r}}_{S_i/B}]\ddot{\mathbf{r}}_{S_i/N} - [I_{sp_i,S_i}]\dot{\boldsymbol{\omega}}_{S_i/N} - [\tilde{\boldsymbol{\omega}}_{S_i/N}][I_{sp_i,S_i}]\boldsymbol{\omega}_{S_i/N} \right) \end{aligned} \quad (3.372)$$

Using Kane's equation, the following equation of motion for the rotational dynamics is defined:

$$\begin{aligned} \mathbf{L}_B - [I_{hub,B}]\dot{\boldsymbol{\omega}}_{B/N} - [\tilde{\boldsymbol{\omega}}_{B/N}][I_{hub,B}]\boldsymbol{\omega}_{B/N} - m_{hub}[\tilde{\mathbf{r}}_{B_c/B}]\ddot{\mathbf{r}}_{B_c/N} \\ + \sum_i^{N_s} \left(-m_{sp_i}[\tilde{\mathbf{r}}_{S_i/B}]\ddot{\mathbf{r}}_{S_i/N} - [I_{sp_i,S_i}]\dot{\boldsymbol{\omega}}_{S_i/N} - [\tilde{\boldsymbol{\omega}}_{S_i/N}][I_{sp_i,S_i}]\boldsymbol{\omega}_{S_i/N} \right) = 0 \end{aligned} \quad (3.373)$$

Since the hinged rigid-body formulation has been developed in detail earlier in the dissertation, the intermediate steps are chosen to not be included. Expanding and combining like terms yields the following final rotational EOM:

$$\begin{aligned}
m_{sc}[\tilde{\mathbf{c}}]\ddot{\mathbf{r}}_{B/N} + [I_{sc,B}]\dot{\boldsymbol{\omega}}_{B/N} + \sum_i^{N_S} \left[I_{s_{i,2}}\hat{\mathbf{s}}_{i,2} + m_{sp_i}d_i[\tilde{\mathbf{r}}_{S_i/B}]\hat{\mathbf{s}}_{i,3} \right] \ddot{\theta}_i = -[\tilde{\boldsymbol{\omega}}_{B/N}][I_{sc,B}]\boldsymbol{\omega}_{B/N} \\
- [I'_{sc,B}]\boldsymbol{\omega}_{B/N} - \sum_i^{N_S} \left(m_{sp_i}[\tilde{\boldsymbol{\omega}}_{B/N}][\tilde{\mathbf{r}}_{S_i/B}]\mathbf{r}'_{S_i/B} + m_{sp_i}d_i\dot{\theta}_i^2[\tilde{\mathbf{r}}_{S_i/B}]\hat{\mathbf{s}}_{i,1} \right. \\
\left. + I_{s_{i,2}}\dot{\theta}_i[\tilde{\boldsymbol{\omega}}_{B/N}]\hat{\mathbf{s}}_{i,2} \right) + \mathbf{L}_B \quad (3.374)
\end{aligned}$$

This final equation is the same equation developed for hinged rigid-bodies using Newtonian/Eulerian mechanics. The last EOM to check is the flexing equation of motion.

3.2.1.3 Flexing Equation of Motion

Following the similar pattern for translational and rotational equations, the generalized active forces are defined:

$$F_7 = \boldsymbol{\omega}_r^{S_i} \cdot (-k_i\theta_i\hat{\mathbf{s}}_{i,2} - c_i\dot{\theta}_i\hat{\mathbf{s}}_{i,2}) = \hat{\mathbf{s}}_{i,2} \cdot (-k_i\theta_i\hat{\mathbf{s}}_{i,2} - c_i\dot{\theta}_i\hat{\mathbf{s}}_{i,2}) = -k_i\theta_i - c_i\dot{\theta}_i \quad (3.375)$$

The generalized inertia forces are defined as:

$$F_7^* = \boldsymbol{\omega}_r^{S_i} \cdot \mathbf{T}_{sp_i}^* + \mathbf{v}_r^{S_i} \cdot (-m_{sp_i}\ddot{\mathbf{r}}_{S_i/N}) = \boldsymbol{\omega}_r^{S_i} \cdot \left[-[I_{sp_i,S_i}]\dot{\boldsymbol{\omega}}_{S_i/N} - [\tilde{\boldsymbol{\omega}}_{S_i/N}][I_{sp_i,S_i}]\boldsymbol{\omega}_{S_i/N} \right] + \mathbf{v}_r^{S_i} \cdot (-m_{sp_i}\ddot{\mathbf{r}}_{S_i/N}) \quad (3.376)$$

Using Kane's equation the following EOM is defined:

$$-k_i\theta_i - c_i\dot{\theta}_i + \hat{\mathbf{s}}_{i,2} \cdot \left[-[I_{sp_i,S_i}]\dot{\boldsymbol{\omega}}_{S_i/N} - [\tilde{\boldsymbol{\omega}}_{S_i/N}][I_{sp_i,S_i}]\boldsymbol{\omega}_{S_i/N} \right] + d_i\hat{\mathbf{s}}_{i,3} \cdot (-m_{sp_i}\ddot{\mathbf{r}}_{S_i/N}) = 0 \quad (3.377)$$

Omitting some analytical steps to the final solution:

$$\begin{aligned}
m_{sp_i}d_i\hat{\mathbf{s}}_{i,3}^T\ddot{\mathbf{r}}_{B/N} + \left[I_{s_{i,2}}\hat{\mathbf{s}}_{i,2}^T - m_{sp_i}d_i\hat{\mathbf{s}}_{i,3}^T[\tilde{\mathbf{r}}_{S_i/B}] \right] \dot{\boldsymbol{\omega}}_{B/N} + \left[I_{s_{i,2}} + m_{sp_i}d_i^2 \right] \ddot{\theta}_i \\
= -k_i\theta_i - c_i\dot{\theta}_i + (I_{s_{i,3}} - I_{s_{i,1}})\omega_{s_{i,3}}\omega_{s_{i,1}} - m_{sp_i}d_i\hat{\mathbf{s}}_{i,3}^T[\tilde{\boldsymbol{\omega}}_{B/N}][\tilde{\boldsymbol{\omega}}_{B/N}]\mathbf{r}_{S_i/B} = 0 \quad (3.378)
\end{aligned}$$

This equation concludes the Kane's Method derivation of hinged rigid-bodies and confirms that both Newtonian/Eulerian mechanics and Kane's Method can be used to derive the EOMs and still arrive at the standardized EOM form. This a promising result because Kane's Method is a powerful tool in developing EOMs for multi-body dynamics.

3.2.2 Fuel Slosh - Lumped Mass Spring Mass Damper Model

This section re-derives the EOMs for the spring mass damper based fuel slosh model that was derived earlier using Newtonian/Eulerian mechanics. Starting with the definition of the generalized coordinates and their respective generalized speeds are:

$$\mathbf{q} = \begin{bmatrix} \mathbf{r}_{B/N} \\ \boldsymbol{\sigma}_{B/N} \\ \rho_1 \\ \cdot \\ \rho_{NP} \end{bmatrix} \quad \mathbf{u} = \begin{bmatrix} \dot{\mathbf{r}}_{B/N} \\ \boldsymbol{\omega}_{B/N} \\ \dot{\rho}_1 \\ \cdot \\ \dot{\rho}_{NP} \end{bmatrix} \quad (3.379)$$

The necessary velocities and angular velocities needed to be defined can be seen in the following equations:

$$\dot{\mathbf{r}}_{B/N} = \dot{\mathbf{r}}_{B/N} \quad (3.380)$$

$$\dot{\mathbf{r}}_{C/N} = \dot{\mathbf{r}}_{B/N} + \dot{\mathbf{c}} \quad (3.381)$$

$$\dot{\mathbf{r}}_{P_{c,j}/N} = \dot{\mathbf{r}}_{B/N} + \mathbf{r}'_{P_{c,j}/B} + \boldsymbol{\omega}_{B/N} \times \mathbf{r}_{P_{c,j}/B} = \dot{\mathbf{r}}_{B/N} + \dot{\rho}_j \hat{\mathbf{p}}_j - [\tilde{\mathbf{r}}_{P_{c,j}/B}] \boldsymbol{\omega}_{B/N} \quad (3.382)$$

Now the following partial velocity table used heavily in Kane's Method is created and can be seen in Table 3.2.

Using these partial velocity definitions, the follow sections will step through the formulation for the translational, rotational and slosh EOMs developed using Kane's method.

Table 3.2: Partial velocity table for fuel slosh

r	\mathbf{v}_r^B	$\boldsymbol{\omega}_r^B$	$\mathbf{v}_r^{P_c}$
1 - 3	$[I_{3 \times 3}]$	$[0_{3 \times 3}]$	$[I_{3 \times 3}]$
4 - 6	$[0_{3 \times 3}]$	$[I_{3 \times 3}]$	$-[\tilde{\mathbf{r}}_{P_{c,j}/B}]$
7 - N_P	$[0_{3 \times 1}]$	$[0_{3 \times 1}]$	$\hat{\mathbf{p}}_j$

3.2.2.1 Rigid Spacecraft Hub Translational Motion

Using the definition of the external force applied on the spacecraft for the translational equation, the general active force is:

$$\mathbf{F}_{1-3} = [\mathbf{v}_{1-3}^C]^T \mathbf{F}_{\text{ext}} = \mathbf{F}_{\text{ext}} \quad (3.383)$$

Using the definition of the generalized inertia forces, the inertia forces for the hub translational motion can be seen in the following equation.

$$\mathbf{F}_{1-3}^* = [\mathbf{v}_{1-3}^B]^T (-m_{\text{hub}} \ddot{\mathbf{r}}_{B/N}) + \sum_j^{N_P} [\mathbf{v}_{1-3}^{P_c}]^T (-m_j \ddot{\mathbf{r}}_{P_{c,j}/N}) = -m_{\text{hub}} \ddot{\mathbf{r}}_{B/N} + \sum_j^{N_P} -m_j \ddot{\mathbf{r}}_{P_{c,j}/N} \quad (3.384)$$

Finally, using Kane's equation, the initial form of the EOM is:

$$\mathbf{F}_{\text{ext}} - m_{\text{hub}} \ddot{\mathbf{r}}_{B/N} + \sum_j^{N_P} -m_j \ddot{\mathbf{r}}_{P_{c,j}/N} = 0 \quad (3.385)$$

Expanding and rearranging results in

$$m_{\text{hub}} \ddot{\mathbf{r}}_{B/N} + \sum_j^{N_P} m_j (\ddot{\mathbf{r}}_{B/N} + \ddot{\mathbf{r}}_{P_{c,j}/B}) = \mathbf{F}_{\text{ext}} \quad (3.386)$$

Plugging Eq. (3.87) into Eq. (3.407) results in

$$m_{\text{hub}} \ddot{\mathbf{r}}_{B/N} + \sum_j^{N_P} m_j \left[\ddot{\mathbf{r}}_{B/N} + \ddot{\rho}_j \hat{\mathbf{p}}_j + 2\boldsymbol{\omega}_{B/N} \times \mathbf{r}'_{P_{c,j}/B} + \dot{\boldsymbol{\omega}}_{B/N} \times \mathbf{r}_{P_{c,j}/B} + \boldsymbol{\omega}_{B/N} \times (\boldsymbol{\omega}_{B/N} \times \mathbf{r}_{P_{c,j}/B}) \right] = \mathbf{F}_{\text{ext}} \quad (3.387)$$

Combining like terms and rearranging yields

$$m_{\text{sc}} \ddot{\mathbf{r}}_{B/N} - m_{\text{sc}} [\tilde{\mathbf{c}}] \dot{\boldsymbol{\omega}}_{B/N} + \sum_{j=1}^{N_P} m_j \hat{\mathbf{p}}_j \ddot{\rho}_j = \mathbf{F}_{\text{ext}} - 2m_{\text{sc}} [\tilde{\boldsymbol{\omega}}_{B/N}] \mathbf{c}' - m_{\text{sc}} [\tilde{\boldsymbol{\omega}}_{B/N}] [\tilde{\boldsymbol{\omega}}_{B/N}] \mathbf{c} \quad (3.388)$$

which is identical to Eq. (3.82) found using Newtonian mechanics.

3.2.2.2 Rigid Spacecraft Hub Rotational Motion

The general active forces acting on the spacecraft for the rotational equations is defined as:

$$\mathbf{F}_{4-6} = [\boldsymbol{\omega}_{4-6}^{\mathcal{B}}]^T \mathbf{L}_B = \mathbf{L}_B \quad (3.389)$$

Similar to the hinged rigid-body development the generalized inertia forces for the rotational equations in the fuel slosh model is:

$$\begin{aligned} \mathbf{F}_{4-6}^* &= [\boldsymbol{\omega}_{4-6}^{\mathcal{B}}]^T \mathbf{T}^* + \sum_j^{N_P} [\mathbf{v}_{4-6}^{P_c}]^T (-m_j \ddot{\mathbf{r}}_{P_{c,j}/N}) \\ &= -[I_{\text{hub},B}] \dot{\boldsymbol{\omega}}_{\mathcal{B}/N} - [\tilde{\boldsymbol{\omega}}_{\mathcal{B}/N}] [I_{\text{hub},B}] \boldsymbol{\omega}_{\mathcal{B}/N} + \sum_j^{N_P} -[\tilde{\mathbf{r}}_{P_{c,j}/B}]^T (-m_j \ddot{\mathbf{r}}_{P_{c,j}/N}) \end{aligned} \quad (3.390)$$

Using Kane's equation, the form of the rotational dynamics equation is defined in the following equation:

$$\mathbf{L}_B - [I_{\text{hub},B}] \dot{\boldsymbol{\omega}}_{\mathcal{B}/N} - [\tilde{\boldsymbol{\omega}}_{\mathcal{B}/N}] [I_{\text{hub},B}] \boldsymbol{\omega}_{\mathcal{B}/N} + \sum_j^{N_P} -[\tilde{\mathbf{r}}_{P_{c,j}/B}] (m_j \ddot{\mathbf{r}}_{P_{c,j}/N}) = 0 \quad (3.391)$$

Plugging in definitions and combining like terms results in the same equation seen in Eq. (3.95) found using Newtonian mechanics.

$$\begin{aligned} m_{\text{sc}} [\tilde{\mathbf{c}}] \ddot{\mathbf{r}}_{\mathcal{B}/N} + [I_{\text{sc},B}] \dot{\boldsymbol{\omega}}_{\mathcal{B}/N} + \sum_{j=1}^{N_P} m_j [\tilde{\mathbf{r}}_{P_{c,j}/B}] \hat{\mathbf{p}}_j \ddot{\rho}_j = \\ - [\tilde{\boldsymbol{\omega}}_{\mathcal{B}/N}] [I_{\text{sc},B}] \boldsymbol{\omega}_{\mathcal{B}/N} - [I'_{\text{sc},B}] \boldsymbol{\omega}_{\mathcal{B}/N} - \sum_{j=1}^{N_P} m_j [\tilde{\boldsymbol{\omega}}_{\mathcal{B}/N}] [\tilde{\mathbf{r}}_{P_{c,j}/B}] \mathbf{r}'_{P_{c,j}/B} + \mathbf{L}_B \end{aligned} \quad (3.392)$$

3.2.2.3 Fuel Slosh Motion

Following the similar pattern for translational and rotational equations the generalized active forces are defined for fuel slosh motion equation:

$$\mathbf{F}_7 = \mathbf{v}_r^{P_c} \cdot (-k \rho_j \hat{\mathbf{p}}_j - c \dot{\rho}_j \hat{\mathbf{p}}_j) = -k \rho_j - c \dot{\rho}_j \quad (3.393)$$

The generalized inertia forces are defined as:

$$\mathbf{F}_7^* = \mathbf{v}_r^{P_c} \cdot (-m_j \ddot{\mathbf{r}}_{P_{c,j}/N}) = \hat{\mathbf{p}}_j^T (-m_j \ddot{\mathbf{r}}_{P_{c,j}/N}) \quad (3.394)$$

Using Kane's equation the following equations of motion are defined:

$$-k\rho_j - c\dot{\rho} - m_j \hat{\mathbf{p}}_j^T \left[\ddot{\mathbf{r}}_{B/N} + \ddot{\rho}_j \hat{\mathbf{p}}_j + 2\boldsymbol{\omega}_{B/N} \times \mathbf{r}'_{P_{c,j}/B} + \dot{\boldsymbol{\omega}}_{B/N} \times \mathbf{r}_{P_{c,j}/B} + \boldsymbol{\omega}_{B/N} \times (\boldsymbol{\omega}_{B/N} \times \mathbf{r}_{P_{c,j}/B}) \right] = 0 \quad (3.395)$$

Rearranging and combining like terms results in:

$$m_j \hat{\mathbf{p}}_j^T \ddot{\mathbf{r}}_{B/N} - m_j \hat{\mathbf{p}}_j^T [\tilde{\mathbf{r}}_{P_{c,j}/B}] \dot{\boldsymbol{\omega}}_{B/N} + m_j \ddot{\rho}_j = -k_j \rho_j - c_j \dot{\rho}_j - 2m_j \hat{\mathbf{p}}_j^T [\tilde{\boldsymbol{\omega}}_{B/N}] \mathbf{r}'_{P_{c,j}/B} - m_j \hat{\mathbf{p}}_j^T [\tilde{\boldsymbol{\omega}}_{B/N}] [\tilde{\boldsymbol{\omega}}_{B/N}] \mathbf{r}_{P_{c,j}/B} \quad (3.396)$$

which is identical to Eq. (3.100). This result finalizes the agreement between the Newtonian/Eulerian mechanics development and the Kane's method derivation for the fuel slosh model.

3.2.3 Dual-Hinged Rigid-Bodies

Another model chosen to derive the EOMs using Kane's method is the dual-hinged rigid-body model. Similar to the first derivations, the derivation begins defining the state variables and generalized speeds. The choice of state variables and their respective chosen generalized speeds for the dual-hinged rigid body model are:

$$\mathbf{X} = \begin{bmatrix} \mathbf{r}_{B/N} \\ \boldsymbol{\sigma}_{B/N} \\ \theta_{1,1} \\ \theta_{1,2} \\ \cdot \\ \theta_{N_S,1} \\ \theta_{N_S,2} \end{bmatrix} \quad \mathbf{u} = \begin{bmatrix} \dot{\mathbf{r}}_{B/N} \\ \boldsymbol{\omega}_{B/N} \\ \dot{\theta}_{1,1} \\ \dot{\theta}_{1,2} \\ \cdot \\ \dot{\theta}_{N_S,1} \\ \dot{\theta}_{N_S,2} \end{bmatrix} \quad (3.397)$$

The necessary velocities and angular velocities needed to be defined can be seen in the following equations:

$$\dot{\mathbf{r}}_{B_c/N} = \dot{\mathbf{r}}_{B/N} + \boldsymbol{\omega}_{B/N} \times \mathbf{r}_{B_c/B} = \dot{\mathbf{r}}_{B/N} - [\tilde{\mathbf{r}}_{B_c/B}] \boldsymbol{\omega}_{B/N} \quad (3.398)$$

$$\dot{\mathbf{r}}_{S_{c,i1}/B} = \dot{\mathbf{r}}_{B/N} + \mathbf{r}'_{S_{c,i1}/B} + \boldsymbol{\omega}_{B/N} \times \mathbf{r}_{S_{c,i1}/B} = \dot{\mathbf{r}}_{B/N} + d_{i1}\dot{\theta}_{i1}\hat{\mathbf{s}}_{i1,3} - [\tilde{\mathbf{r}}_{S_{c,i1}/B}]\boldsymbol{\omega}_{B/N} \quad (3.399)$$

$$\begin{aligned} \dot{\mathbf{r}}_{S_{c,i2}/B} &= \dot{\mathbf{r}}_{B/N} + \mathbf{r}'_{S_{c,i2}/B} + \boldsymbol{\omega}_{B/N} \times \mathbf{r}_{S_{c,i2}/B} \\ &= \dot{\mathbf{r}}_{B/N} + l_{i1}\dot{\theta}_{i1}\hat{\mathbf{s}}_{i1,3} + d_{i2}(\dot{\theta}_{i1} + \dot{\theta}_{i2})\hat{\mathbf{s}}_{i2,3} - [\tilde{\mathbf{r}}_{S_{c,i2}/B}]\boldsymbol{\omega}_{B/N} \end{aligned} \quad (3.400)$$

$$\boldsymbol{\omega}_{S_{i1}/N} = \boldsymbol{\omega}_{B/N} + \dot{\theta}_{i1}\hat{\mathbf{s}}_{i1,2} \quad (3.401)$$

$$\boldsymbol{\omega}_{S_{i2}/N} = \boldsymbol{\omega}_{B/N} + (\dot{\theta}_{i1} + \dot{\theta}_{i2})\hat{\mathbf{s}}_{i2,2} \quad (3.402)$$

$$\dot{\mathbf{r}}_{C/N} = \dot{\mathbf{r}}_{B/N} + \dot{\mathbf{c}} \quad (3.403)$$

Now the following partial velocity table can be created using the velocities defined. This table can be seen in Table 3.3.

Table 3.3: Partial velocity table for dual-hinged rigid-bodies

r	$\mathbf{v}_r^{B_c}$	$\boldsymbol{\omega}_r^B$	$\mathbf{v}_r^{S_{c,i1}}$	$\boldsymbol{\omega}_r^{S_{i1}}$	$\mathbf{v}_r^{S_{c,i2}}$	$\boldsymbol{\omega}_r^{S_{i2}}$
1 – 3	$[I_{3 \times 3}]$	$[0_{3 \times 3}]$	$[I_{3 \times 3}]$	$[0_{3 \times 3}]$	$[I_{3 \times 3}]$	$[0_{3 \times 3}]$
4 – 6	$-\tilde{\mathbf{r}}_{B_c/B}$	$[I_{3 \times 3}]$	$-\tilde{\mathbf{r}}_{S_{c,i1}/B}$	$[I_{3 \times 3}]$	$-\tilde{\mathbf{r}}_{S_{c,i2}/B}$	$[I_{3 \times 3}]$
7	$[0_{3 \times 1}]$	$[0_{3 \times 1}]$	$d_{i1}\hat{\mathbf{s}}_{i1,3}$	$\hat{\mathbf{s}}_{i1,2}$	$l_{i1}\hat{\mathbf{s}}_{i1,3} + d_{i2}\hat{\mathbf{s}}_{i2,3}$	$\hat{\mathbf{s}}_{i2,2}$
8	$[0_{3 \times 1}]$	$[0_{3 \times 1}]$	$[0_{3 \times 1}]$	$[0_{3 \times 1}]$	$d_{i2}\hat{\mathbf{s}}_{i2,3}$	$\hat{\mathbf{s}}_{i2,2}$

Using these partial velocity definitions, the follow sections will step through the formulation for the translational, rotational and flexing EOMs developed using Kane's method.

3.2.3.1 Rigid Spacecraft Hub Translational Motion

The translational generalized active force can be seen in the following equation:

$$\mathbf{F}_{1-3} = [\mathbf{v}_{1-3}^C]^T \mathbf{F}_{\text{ext}} = \mathbf{F}_{\text{ext}} \quad (3.404)$$

Similarly, the inertia forces for the hub translational motion are defined as

$$\begin{aligned}\mathbf{F}_{1-3}^* &= [\mathbf{v}_{1-3}^{B_c}]^T (-m_{\text{hub}} \ddot{\mathbf{r}}_{B_c/N}) + \sum_i^{N_S} \left([\mathbf{v}_{1-3}^{S_{c,i1}}]^T (-m_{\text{sp}i1} \ddot{\mathbf{r}}_{S_{c,i1}/N}) + [\mathbf{v}_{1-3}^{S_{c,i2}}]^T (-m_{\text{sp}i2} \ddot{\mathbf{r}}_{S_{c,i2}/N}) \right) \\ &= -m_{\text{hub}} \ddot{\mathbf{r}}_{B_c/N} + \sum_i^{N_S} \left(-m_{\text{sp}i1} \ddot{\mathbf{r}}_{S_{c,i1}/N} - m_{\text{sp}i2} \ddot{\mathbf{r}}_{S_{c,i2}/N} \right)\end{aligned}\quad (3.405)$$

Using Kane's equation the initial form of the translational EOM is

$$\mathbf{F}_{\text{ext}} - m_{\text{hub}} \ddot{\mathbf{r}}_{B_c/N} + \sum_i^{N_S} \left(-m_{\text{sp}i1} \ddot{\mathbf{r}}_{S_{c,i1}/N} - m_{\text{sp}i2} \ddot{\mathbf{r}}_{S_{c,i2}/N} \right) = 0 \quad (3.406)$$

Expanding and rearranging results in

$$m_{\text{hub}} (\ddot{\mathbf{r}}_{B/N} + \ddot{\mathbf{r}}_{B_c/B}) + \sum_i^{N_S} \left[m_{\text{sp}i1} (\ddot{\mathbf{r}}_{B/N} + \ddot{\mathbf{r}}_{S_{c,i1}/B}) + m_{\text{sp}i2} (\ddot{\mathbf{r}}_{B/N} + \ddot{\mathbf{r}}_{S_{c,i2}/B}) \right] = \mathbf{F}_{\text{ext}} \quad (3.407)$$

Plugging Eq. (3.167) into Eq. (3.407) results in

$$\begin{aligned}m_{\text{hub}} \ddot{\mathbf{r}}_{B/N} + m_{\text{hub}} \left[\dot{\boldsymbol{\omega}}_{B/N} \times \mathbf{r}_{B_c/B} + \boldsymbol{\omega}_{B/N} \times (\boldsymbol{\omega}_{B/N} \times \mathbf{r}_{B_c/B}) \right] + \sum_i^{N_S} \left(m_{\text{sp}i1} \left[\ddot{\mathbf{r}}_{B/N} + \mathbf{r}_{S_{c,i1}/B}'' \right. \right. \\ \left. \left. + 2\boldsymbol{\omega}_{B/N} \times \mathbf{r}_{S_{c,i1}/B}' + \dot{\boldsymbol{\omega}}_{B/N} \times \mathbf{r}_{S_{c,i1}/B} + \boldsymbol{\omega}_{B/N} \times (\boldsymbol{\omega}_{B/N} \times \mathbf{r}_{S_{c,i1}/B}) \right] + m_{\text{sp}i2} \left[\ddot{\mathbf{r}}_{B/N} \right. \right. \\ \left. \left. + \mathbf{r}_{S_{c,i2}/B}'' + 2\boldsymbol{\omega}_{B/N} \times \mathbf{r}_{S_{c,i2}/B}' + \dot{\boldsymbol{\omega}}_{B/N} \times \mathbf{r}_{S_{c,i2}/B} + \boldsymbol{\omega}_{B/N} \times (\boldsymbol{\omega}_{B/N} \times \mathbf{r}_{S_{c,i2}/B}) \right] \right) = \mathbf{F}_{\text{ext}}\end{aligned}\quad (3.408)$$

Combining like terms results in:

$$\begin{aligned}m_{\text{sc}} \ddot{\mathbf{r}}_{B/N} - m_{\text{sc}} [\tilde{\mathbf{c}}] \dot{\boldsymbol{\omega}}_{B/N} + \sum_i^{N_S} \left(m_{\text{sp}i1} \left[d_{i1} \hat{\mathbf{s}}_{i1,3} \ddot{\theta}_{i1} + d_{i1} \dot{\theta}_{i1}^2 \hat{\mathbf{s}}_{i1,1} \right] \right. \\ \left. + m_{\text{sp}i2} \left[(l_{i1} \hat{\mathbf{s}}_{i1,3} + d_{i2} \hat{\mathbf{s}}_{i2,3}) \ddot{\theta}_{i1} + d_{i2} \hat{\mathbf{s}}_{i2,3} \ddot{\theta}_{i2} + l_{i1} \dot{\theta}_{i1}^2 \hat{\mathbf{s}}_{i1,1} + d_{i2} (\dot{\theta}_{i1} + \dot{\theta}_{i2})^2 \hat{\mathbf{s}}_{i2,1} \right] \right) \\ = \mathbf{F}_{\text{ext}} - 2m_{\text{sc}} [\tilde{\boldsymbol{\omega}}_{B/N}] \mathbf{c}' - m_{\text{sc}} [\tilde{\boldsymbol{\omega}}_{B/N}] [\tilde{\boldsymbol{\omega}}_{B/N}] \mathbf{c}\end{aligned}\quad (3.409)$$

Rearranging and putting in final form:

$$\begin{aligned}m_{\text{sc}} \ddot{\mathbf{r}}_{B/N} - m_{\text{sc}} [\tilde{\mathbf{c}}] \dot{\boldsymbol{\omega}}_{B/N} + \sum_i^{N_S} \left(\left[m_{\text{sp}i1} d_{i1} \hat{\mathbf{s}}_{i1,3} + m_{\text{sp}i2} l_{i1} \hat{\mathbf{s}}_{i1,3} + m_{\text{sp}i2} d_{i2} \hat{\mathbf{s}}_{i2,3} \right] \ddot{\theta}_{i1} + m_{\text{sp}i2} d_{i2} \hat{\mathbf{s}}_{i2,3} \ddot{\theta}_{i2} \right) \\ = \mathbf{F}_{\text{ext}} - 2m_{\text{sc}} [\tilde{\boldsymbol{\omega}}_{B/N}] \mathbf{c}' - m_{\text{sc}} [\tilde{\boldsymbol{\omega}}_{B/N}] [\tilde{\boldsymbol{\omega}}_{B/N}] \mathbf{c} \\ - \sum_i^{N_S} \left(m_{\text{sp}i1} d_{i1} \dot{\theta}_{i1}^2 \hat{\mathbf{s}}_{i1,1} + m_{\text{sp}i2} \left[(l_{i1} \dot{\theta}_{i1}^2 \hat{\mathbf{s}}_{i1,1} + d_{i2} (\dot{\theta}_{i1} + \dot{\theta}_{i2})^2 \hat{\mathbf{s}}_{i2,1}) \right] \right)\end{aligned}\quad (3.410)$$

which is identical to Eq. (3.160) found using Newtonian mechanics.

3.2.3.2 Rigid Spacecraft Hub Rotational Motion

The torque acting on the spacecraft, \mathbf{L}_B needs to be defined as a general active force. Using Eq. (3.362), active forces acting on the spacecraft for the rotational equations can be defined as:

$$\mathbf{F}_{4-6} = [\boldsymbol{\omega}_{4-6}^{\mathcal{B}}]^T \mathbf{L}_B = \mathbf{L}_B \quad (3.411)$$

The generalized inertia forces for the rotational motion equation for dual-hinged rigid-bodies can be seen in Eq. (3.412).

$$\begin{aligned} \mathbf{F}_{4-6}^* &= [\boldsymbol{\omega}_{4-6}^{\mathcal{B}}]^T \mathbf{T}_{\text{hub}}^* + [\mathbf{v}_{4-6}^{B_c}]^T (-m_{\text{hub}} \ddot{\mathbf{r}}_{B_c/N}) + \sum_i^{N_S} \left([\mathbf{v}_{4-6}^{S_{c,i1}}]^T (-m_{\text{sp}_{i1}} \ddot{\mathbf{r}}_{S_{c,i1}/N}) + [\boldsymbol{\omega}_{4-6}^{S_{i1}}]^T \mathbf{T}_{\text{sp}_{i1}}^* \right. \\ &\quad \left. + [\mathbf{v}_{4-6}^{S_{c,i1}}]^T (-m_{\text{sp}_{i1}} \ddot{\mathbf{r}}_{S_{c,i1}/N}) + [\boldsymbol{\omega}_{4-6}^{S_{i1}}]^T \mathbf{T}_{\text{sp}_{i1}}^* \right) = -[I_{\text{hub},B}] \dot{\boldsymbol{\omega}}_{\mathcal{B}/N} - [\tilde{\boldsymbol{\omega}}_{\mathcal{B}/N}] [I_{\text{hub},B}] \boldsymbol{\omega}_{\mathcal{B}/N} \\ &\quad - m_{\text{hub}} [\tilde{\mathbf{r}}_{B_c/B}] \ddot{\mathbf{r}}_{B_c/N} + \sum_i^{N_S} \left(-m_{\text{sp}_{i1}} [\tilde{\mathbf{r}}_{S_{c,i1}/B}] \ddot{\mathbf{r}}_{S_{c,i1}/N} - [I_{\text{sp}_{i1},S_{c,i1}}] \dot{\boldsymbol{\omega}}_{S_{i1}/N} - [\tilde{\boldsymbol{\omega}}_{S_{i1}/N}] [I_{\text{sp}_{i1},S_{c,i1}}] \boldsymbol{\omega}_{S_{i1}/N} \right. \\ &\quad \left. - m_{\text{sp}_{i2}} [\tilde{\mathbf{r}}_{S_{c,i2}/B}] \ddot{\mathbf{r}}_{S_{c,i2}/N} - [I_{\text{sp}_{i2},S_{c,i2}}] \dot{\boldsymbol{\omega}}_{S_{i2}/N} - [\tilde{\boldsymbol{\omega}}_{S_{i2}/N}] [I_{\text{sp}_{i2},S_{c,i2}}] \boldsymbol{\omega}_{S_{i2}/N} \right) \quad (3.412) \end{aligned}$$

Using Kane's equation, Eq. (3.366), the following equations of motion for the rotational dynamics are defined:

$$\begin{aligned} \mathbf{L}_B - [I_{\text{hub},B}] \dot{\boldsymbol{\omega}}_{\mathcal{B}/N} - [\tilde{\boldsymbol{\omega}}_{\mathcal{B}/N}] [I_{\text{hub},B}] \boldsymbol{\omega}_{\mathcal{B}/N} - m_{\text{hub}} [\tilde{\mathbf{r}}_{B_c/B}] \ddot{\mathbf{r}}_{B_c/N} \\ + \sum_i^{N_S} \left(-m_{\text{sp}_{i1}} [\tilde{\mathbf{r}}_{S_{c,i1}/B}] \ddot{\mathbf{r}}_{S_{c,i1}/N} - [I_{\text{sp}_{i1},S_{c,i1}}] \dot{\boldsymbol{\omega}}_{S_{i1}/N} - [\tilde{\boldsymbol{\omega}}_{S_{i1}/N}] [I_{\text{sp}_{i1},S_{c,i1}}] \boldsymbol{\omega}_{S_{i1}/N} \right. \\ \left. - m_{\text{sp}_{i2}} [\tilde{\mathbf{r}}_{S_{c,i2}/B}] \ddot{\mathbf{r}}_{S_{c,i2}/N} - [I_{\text{sp}_{i2},S_{c,i2}}] \dot{\boldsymbol{\omega}}_{S_{i2}/N} - [\tilde{\boldsymbol{\omega}}_{S_{i2}/N}] [I_{\text{sp}_{i2},S_{c,i2}}] \boldsymbol{\omega}_{S_{i2}/N} \right) = 0 \quad (3.413) \end{aligned}$$

Some analytical development is omitted since a thorough derivation has already been included for dual-hinged rigid bodies. Expanding, simplifying, and moving the second order state derivatives

to the left hand side:

$$\begin{aligned}
& m_{sc}[\tilde{\mathbf{c}}]\ddot{\mathbf{r}}_{B/N} + [I_{sc,B}]\dot{\boldsymbol{\omega}}_{B/N} + \sum_i^{N_S} \left([I_{s_{i1,2}}]\hat{\mathbf{s}}_{i1,2} + m_{sp_{i1}}d_{i1}[\tilde{\mathbf{r}}_{S_{c,i1}/B}]\hat{\mathbf{s}}_{i1,3} + I_{s_{i2,2}}\hat{\mathbf{s}}_{i2,2} \right. \\
& \left. + m_{sp_{i2}}[\tilde{\mathbf{r}}_{S_{c,i2}/B}](l_{i1}\hat{\mathbf{s}}_{i1,3} + d_{i2}\hat{\mathbf{s}}_{i2,3}) \right] \ddot{\theta}_{i1} + I_{s_{i2,2}}\hat{\mathbf{s}}_{i2,2} + m_{sp_{i2}}d_{i2}[\tilde{\mathbf{r}}_{S_{c,i2}/B}]\hat{\mathbf{s}}_{i2,3}\ddot{\theta}_{i2} \Big) = -[\tilde{\boldsymbol{\omega}}_{B/N}][I_{sc,B}]\boldsymbol{\omega}_{B/N} \\
& - [I'_{sc,B}]\boldsymbol{\omega}_{B/N} - \sum_i^{N_S} \left(m_{sp_{i1}}d_{i1}\dot{\theta}_{i1}^2[\tilde{\mathbf{r}}_{S_{c,i1}/B}]\hat{\mathbf{s}}_{i1,1} + I_{s_{i1,2}}\dot{\theta}_{i1}[\tilde{\boldsymbol{\omega}}_{B/N}]\hat{\mathbf{s}}_{i1,2} + m_{sp_{i1}}[\tilde{\boldsymbol{\omega}}_{B/N}][\tilde{\mathbf{r}}_{S_{c,i1}/B}]\mathbf{r}'_{S_{c,i1}/B} \right. \\
& \quad \left. + m_{sp_{i2}}[\tilde{\mathbf{r}}_{S_{c,i2}/B}][l_{i1}\dot{\theta}_{i1}^2\hat{\mathbf{s}}_{i1,1} + d_{i2}(\dot{\theta}_{i1} + \dot{\theta}_{i2})^2\hat{\mathbf{s}}_{i2,1}] + I_{s_{i2,2}}(\dot{\theta}_{i1} + \dot{\theta}_{i2})[\tilde{\boldsymbol{\omega}}_{B/N}]\hat{\mathbf{s}}_{i2,2} \right. \\
& \quad \left. + m_{sp_{i2}}[\tilde{\boldsymbol{\omega}}_{B/N}][\tilde{\mathbf{r}}_{S_{c,i2}/B}]\mathbf{r}'_{S_{c,i2}/B} \right) + \mathbf{L}_B \quad (3.414)
\end{aligned}$$

which is the same solution as the one which used Newtonian/Eulerian mechanics.

3.2.3.3 Panel 1 Flexing Equation

Following the similar pattern for translational and rotational equations the generalized active forces are defined for the first interconnected panel:

$$F_7 = \boldsymbol{\omega}_7^{S_{i1}} \cdot \left[(-k_{i1}\theta_{i1} - c_{i1}\dot{\theta}_{i1})\hat{\mathbf{s}}_{i1,2} + (k_{i2}\theta_{i2} + c_{i2}\dot{\theta}_{i2})\hat{\mathbf{s}}_{i2,2} + \boldsymbol{\tau}_{\text{ext}_{i1},H_{i1}} \right] + \mathbf{v}_7^{H_{i2}} \cdot \mathbf{F}_{1/2i} \quad (3.415)$$

Expanding the terms in the generalized active forces for panel 1 results in:

$$F_7 = \hat{\mathbf{s}}_{i1,2} \cdot \left[(-k_{i1}\theta_{i1} - c_{i1}\dot{\theta}_{i1})\hat{\mathbf{s}}_{i1,2} + (k_{i2}\theta_{i2} + c_{i2}\dot{\theta}_{i2})\hat{\mathbf{s}}_{i2,2} + \boldsymbol{\tau}_{\text{ext}_{i1},H_{i1}} \right] + l_{i1}\hat{\mathbf{s}}_{i1,3} \cdot \left[\mathbf{F}_{\text{ext}_{i2}} - m_{sp_{i2}}\ddot{\mathbf{r}}_{S_{c,i2}/N} \right] \quad (3.416)$$

Further simplification yields:

$$F_7 = -k_{i1}\theta_{i1} - c_{i1}\dot{\theta}_{i1} + k_{i2}\theta_{i2} + c_{i2}\dot{\theta}_{i2} + \hat{\mathbf{s}}_{i1,2} \cdot \boldsymbol{\tau}_{\text{ext}_{i1},H_{i1}} + l_{i1}\hat{\mathbf{s}}_{i1,3} \cdot \mathbf{F}_{\text{ext}_{i2}} - m_{sp_{i2}}l_{i1}\hat{\mathbf{s}}_{i1,3} \cdot \ddot{\mathbf{r}}_{S_{c,i2}/N} \quad (3.417)$$

The generalized inertia forces are defined as:

$$\begin{aligned}
F_7^* &= \boldsymbol{\omega}_7^{S_{i1}} \cdot \mathbf{T}_{sp_{i1}}^* + \mathbf{v}_7^{S_{c,i1}} \cdot (-m_{sp_{i1}}\ddot{\mathbf{r}}_{S_{c,i1}/N}) \\
&= \hat{\mathbf{s}}_{i1,2} \cdot \left[-[I_{sp_{i1},S_{c,i1}}]\dot{\boldsymbol{\omega}}_{S_{i1}/N} - [\tilde{\boldsymbol{\omega}}_{S_{i1}/N}][I_{sp_{i1},S_{c,i1}}]\boldsymbol{\omega}_{S_{i1}/N} \right] + d_{i1}\hat{\mathbf{s}}_{i1,3} \cdot (-m_{sp_{i1}}\ddot{\mathbf{r}}_{S_{c,i1}/N}) \quad (3.418)
\end{aligned}$$

Using Kane's equation the first form of the EOM is defined as:

$$\begin{aligned}
& -k_{i1}\theta_{i1} - c_{i1}\dot{\theta}_{i1} + k_{i2}\theta_{i2} + c_{i2}\dot{\theta}_{i2} + \hat{\mathbf{s}}_{i1,2} \cdot \boldsymbol{\tau}_{\text{ext}_{i1},H_{i1}} + l_{i1}\hat{\mathbf{s}}_{i1,3} \cdot \mathbf{F}_{\text{ext}_{i2}} - m_{sp_{i2}}l_{i1}\hat{\mathbf{s}}_{i1,3} \cdot \ddot{\mathbf{r}}_{S_{c,i2}/N} \\
& + \hat{\mathbf{s}}_{i1,2} \cdot \left[-[I_{sp_{i1},S_{c,i1}}]\dot{\boldsymbol{\omega}}_{S_{i1}/N} - [\tilde{\boldsymbol{\omega}}_{S_{i1}/N}][I_{sp_{i1},S_{c,i1}}]\boldsymbol{\omega}_{S_{i1}/N} \right] - m_{sp_{i1}}d_{i1}\hat{\mathbf{s}}_{i1,3} \cdot \ddot{\mathbf{r}}_{S_{c,i1}/N} = 0 \quad (3.419)
\end{aligned}$$

Omitting some analytical development, the equation further simplifies to:

$$\begin{aligned}
& \left[m_{sp_{i1}}d_{i1}\hat{\mathbf{s}}_{i1,3}^T + m_{sp_{i2}}l_{i1}\hat{\mathbf{s}}_{i1,3}^T \right] \ddot{\mathbf{r}}_{B/N} + \left[I_{s_{i1,2}}\hat{\mathbf{s}}_{i1,2}^T - m_{sp_{i1}}d_{i1}\hat{\mathbf{s}}_{i1,3}^T[\tilde{\mathbf{r}}_{S_{c,i1}/B}] - m_{sp_{i2}}l_{i1}\hat{\mathbf{s}}_{i1,3}^T[\tilde{\mathbf{r}}_{S_{c,i2}/B}] \right] \dot{\boldsymbol{\omega}}_{B/N} \\
& + \left[I_{s_{i1,2}} + m_{sp_{i1}}d_{i1}^2 + m_{sp_{i2}}l_{i1}^2 + m_{sp_{i2}}l_{i1}d_{i2}\hat{\mathbf{s}}_{i1,3}^T\hat{\mathbf{s}}_{i2,3} \right] \ddot{\theta}_{i1} + \left[m_{sp_{i2}}l_{i1}d_{i2}\hat{\mathbf{s}}_{i1,3}^T\hat{\mathbf{s}}_{i2,3} \right] \ddot{\theta}_{i2} \\
& = -(I_{s_{i1,1}} - I_{s_{i1,3}})\omega_{s_{i1,3}}\omega_{s_{i1,1}} - k_{i1}\theta_{i1} - c_{i1}\dot{\theta}_{i1} + k_{i2}\theta_{i2} + c_{i2}\dot{\theta}_{i2} + \hat{\mathbf{s}}_{i1,2}^T\boldsymbol{\tau}_{\text{ext}_{i1},H_{i1}} + l_{i1}\hat{\mathbf{s}}_{i1,3}^T\mathbf{F}_{\text{ext}_{i2}} \\
& - m_{sp_{i1}}d_{i1}\hat{\mathbf{s}}_{i1,3}^T[\tilde{\boldsymbol{\omega}}_{B/N}][\tilde{\boldsymbol{\omega}}_{B/N}]\mathbf{r}_{S_{c,i1}/B} - m_{sp_{i2}}l_{i1}\hat{\mathbf{s}}_{i1,3}^T \left[2[\tilde{\boldsymbol{\omega}}_{B/N}]\mathbf{r}'_{S_{c,i2}/B} + [\tilde{\boldsymbol{\omega}}_{B/N}][\tilde{\boldsymbol{\omega}}_{B/N}]\mathbf{r}_{S_{c,i2}/B} \right. \\
& \quad \left. + d_{i2}(\dot{\theta}_{i1} + \dot{\theta}_{i2})^2\hat{\mathbf{s}}_{i2,1} \right] \quad (3.420)
\end{aligned}$$

This equation is the same equation found using Newtonian/Eulerian mechanics.

3.2.3.4 Panel 2 Flexing Equation

The generalized active forces are defined for the second interconnected panel in the following equation:

$$F_8 = \boldsymbol{\omega}_8^{S_{i2}} \cdot \left[(-k_{i2}\theta_{i2} - c_{i2}\dot{\theta}_{i2})\hat{\mathbf{s}}_{i2,2} + \boldsymbol{\tau}_{\text{ext}_{i2},H_{i2}} \right] \quad (3.421)$$

Simplifying this result yields:

$$F_8 = \hat{\mathbf{s}}_{i2,2} \cdot \left[(-k_{i2}\theta_{i2} - c_{i2}\dot{\theta}_{i2})\hat{\mathbf{s}}_{i2,2} + \boldsymbol{\tau}_{\text{ext}_{i2},H_{i2}} \right] = -k_{i2}\theta_{i2} - c_{i2}\dot{\theta}_{i2} + \hat{\mathbf{s}}_{i2,2} \cdot \boldsymbol{\tau}_{\text{ext}_{i2},H_{i2}} \quad (3.422)$$

The generalized inertia forces are defined as:

$$\begin{aligned}
F_8^* & = \boldsymbol{\omega}_8^{S_{i2}} \cdot \mathbf{T}_{sp_{i2}}^* + \mathbf{v}_8^{S_{c,i2}} \cdot (-m_{sp_{i2}}\ddot{\mathbf{r}}_{S_{c,i2}/N}) \\
& = \hat{\mathbf{s}}_{i2,2} \cdot \left[-[I_{sp_{i2},S_{c,i2}}]\dot{\boldsymbol{\omega}}_{S_{i2}/N} - [\tilde{\boldsymbol{\omega}}_{S_{i2}/N}][I_{sp_{i2},S_{c,i2}}]\boldsymbol{\omega}_{S_{i2}/N} \right] + d_{i2}\hat{\mathbf{s}}_{i2,3} \cdot (-m_{sp_{i2}}\ddot{\mathbf{r}}_{S_{c,i2}/N}) \quad (3.423)
\end{aligned}$$

Using Kane's equation the first form of the EOM can be seen in the following equation:

$$\begin{aligned}
& -k_{i2}\theta_{i2} - c_{i2}\dot{\theta}_{i2} + \hat{\mathbf{s}}_{i2,2} \cdot \boldsymbol{\tau}_{\text{ext}_{i2},H_{i2}} + \hat{\mathbf{s}}_{i2,2} \cdot \left[-[I_{sp_{i2},S_{c,i2}}]\dot{\boldsymbol{\omega}}_{S_{i2}/N} - [\tilde{\boldsymbol{\omega}}_{S_{i2}/N}][I_{sp_{i2},S_{c,i2}}]\boldsymbol{\omega}_{S_{i2}/N} \right] \\
& \quad - m_{sp_{i2}}d_{i2}\hat{\mathbf{s}}_{i2,3}^T\ddot{\mathbf{r}}_{S_{c,i2}/N} = 0 \quad (3.424)
\end{aligned}$$

Expanding and simplifying results in the final form of the equation:

$$\begin{aligned}
& \left[m_{\text{sp}_{i2}} d_{i2} \hat{\mathbf{s}}_{i2,3}^T \right] \ddot{\mathbf{r}}_{B/N} + \left[I_{s_{i2,2}} \hat{\mathbf{s}}_{i2,2}^T - m_{\text{sp}_{i2}} d_{i2} \hat{\mathbf{s}}_{i2,3}^T [\tilde{\mathbf{r}}_{S_{c,i2}/B}] \right] \dot{\boldsymbol{\omega}}_{\mathcal{B}/\mathcal{N}} + \left[I_{s_{i2,2}} + m_{\text{sp}_{i2}} d_{i2}^2 \right. \\
& \left. + m_{\text{sp}_{i2}} l_{i1} d_{i2} \hat{\mathbf{s}}_{i2,3}^T \hat{\mathbf{s}}_{i1,3} \right] \ddot{\theta}_{i1} + \left[I_{s_{i2,2}} + m_{\text{sp}_{i2}} d_{i2}^2 \right] \ddot{\theta}_{i2} = -(I_{s_{i2,1}} - I_{s_{i2,3}}) \omega_{s_{i2,3}} \omega_{s_{i2,1}} - k_{i2} \theta_{i2} - c_{i2} \dot{\theta}_{i2} \\
& \quad + \hat{\mathbf{s}}_{i2,2} \cdot \boldsymbol{\tau}_{\text{ext}_{i2}, H_{i2}} - m_{\text{sp}_{i2}} d_{i2} \hat{\mathbf{s}}_{i2,3}^T \left[2[\tilde{\boldsymbol{\omega}}_{\mathcal{B}/\mathcal{N}}] \mathbf{r}'_{S_{c,i2}/B} + [\tilde{\boldsymbol{\omega}}_{\mathcal{B}/\mathcal{N}}][\tilde{\boldsymbol{\omega}}_{\mathcal{B}/\mathcal{N}}] \mathbf{r}_{S_{c,i2}/B} + l_{i1} \dot{\theta}_{i1}^2 \hat{\mathbf{s}}_{i1,1} \right] \quad (3.425)
\end{aligned}$$

This concludes the necessary Kane's Method development that confirms the arrival at the same equations previously found using Newtonian/Eulerian mechanics.

Chapter 4

Modular Software Architecture for Spacecraft Dynamics Simulations

The final research goal of this proposed research is to design a software architecture that will utilize the common structure of the generalized EOM form and the modularization of the coupled EOMs from the back-substitution method. As mentioned before, multi-body dynamics simulations can result in disorganized and massive software implementations or a complex interrelation between the effectors and a system mass matrix. The proposed design alleviates this complicated interaction while retaining the fully-coupled nature of the problem. Additionally the proposed research will develop a modular architecture for multi-rigidly connected spacecraft that allows for deployment and docking of the spacecraft.

4.1 Single Spacecraft Architecture

Figure 4.1 shows the Unified Modeling Language (UML) class diagram for object oriented computer programming languages proposed in this dissertation. This is the design that allows complex fully-coupled dynamics to be implemented in software while retaining a modular architecture. Additionally, it aims to solve the issues of testability, maintainability, and scalability that fully-coupled dynamics problems pose.

The `dynamicObject` seen in Figure 4.1 is a parent class or abstract class that defines the base functionality of the object that will control the calculation of the system EOMs and essentially solve for the well-known state derivative vector $\dot{\mathbf{X}} = \mathbf{f}(\mathbf{X}, t)$. However, the term state vector is used loosely here because the `stateManager` organizes, stores, and controls all states of the system.

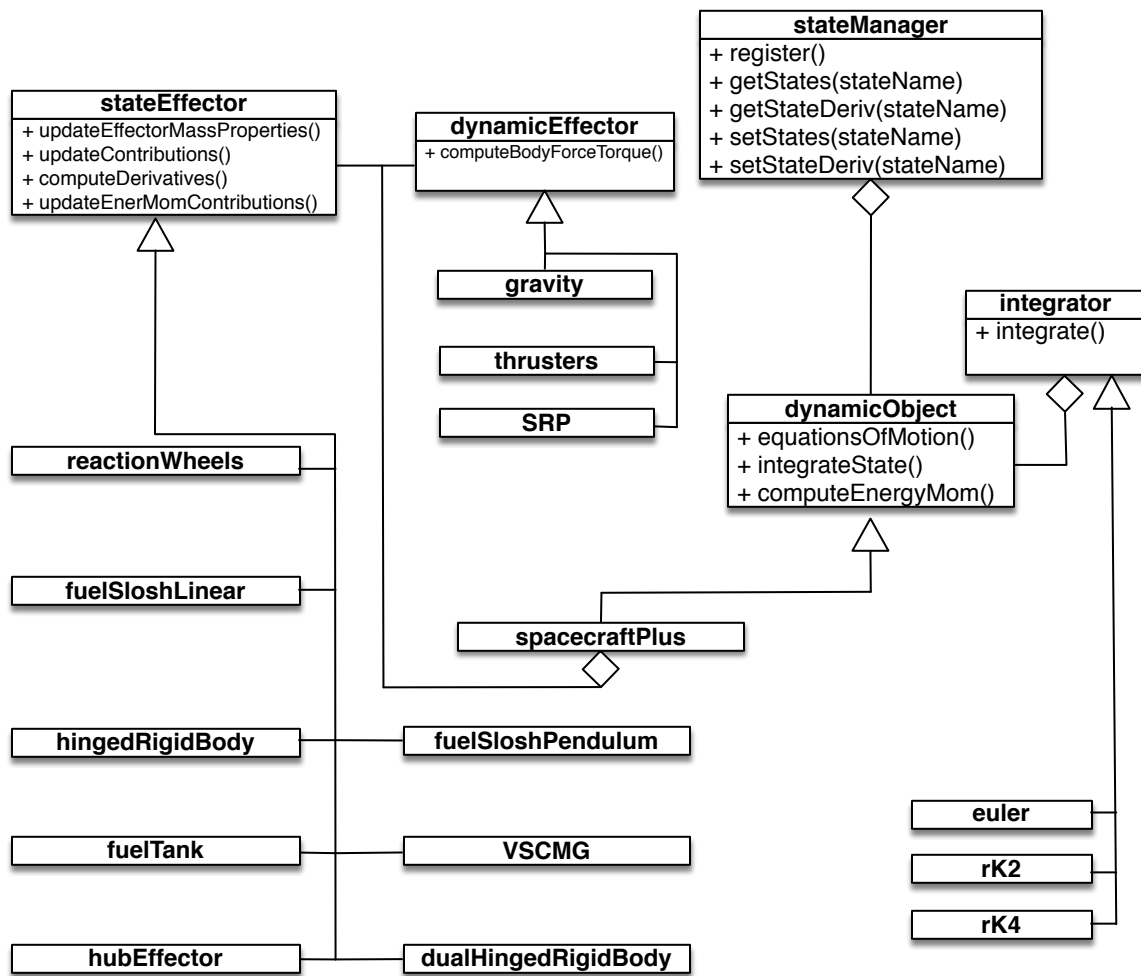


Figure 4.1: UML Diagram for Modular Architecture.

The `dynamicObject` is an abstract or parent class because this would allow for different types of systems to be implemented in the future which are not necessarily using the proposed back-substitution method in this dissertation. Therefore, the `spacecraftPlus` is an instantiation of the `dynamicObject` and is the class that is implementing the back-substitution method.

In the generalized EOMs introduced earlier in this dissertation, the term “effectors” is used to define objects that are attached to the spacecraft and have dynamic states that need to be integrated. Some examples are: reaction wheels, flexing solar arrays, fuel slosh, etc. In this modular software architecture, those effectors are called `stateEffectors` and are illustrated in Figure 4.1. In contrast, `dynamicEffectors` are phenomena that result in an external forces or torques being

applied to the spacecraft. Examples of these include: gravity, thrusters, SRP, etc.

The `stateEffector` abstract or parent class is the class that defines the necessary methods (and variables) needed for each effector to provide contributions to the spacecrafts mass properties (m_{sc} , $[I_{sc,B}]$, \mathbf{c} , etc.) using the method `updateEffectorMassProperties` and contributions to the back substitution matrices ($[A]$, $[B]$... \mathbf{v}_{Trans} , etc.) using the method `updateContributions`. Each effector needs to be able to compute their derivatives using the method `computeDerivatives`. Finally, the method `computeEnerMomContributions` is the method that enables effectors add their contributions to the energy and momentum of the system for verification purposes. Additionally, it should be noted that in Figure 4.1 it shows that both `stateEffectors` and `dynamicEffectors` are aggregated in `spacecraftPlus`. This allows for the modularity of the dynamics because `spacecraftPlus` does not know the type of effectors attached to it, but rather has an array of `stateEffectors` or `dynamicEffectors` which makes it general.

Another important aspect of the software architecture is the `hubEffector` instantiation of `stateEffector`. The `hubEffector` is representing the rigid body hub defined in the generalized EOM form and has translational and attitude states associated with it. The `hubEffector` is unique to all of the `stateEffectors` because it is not included in the array of `stateEffectors` that are looped over in `spacecraftPlus` but rather defined as an object in `spacecraftPlus` and its methods are always called in `equationsOfMotion()`. This is because the assumption for the back-substitution method and the generalized EOM form is that the spacecraft will always have a rigid body hub with a body frame, \mathcal{B} , attached and with the corresponding states: $\mathbf{r}_{B/N}$, $\dot{\mathbf{r}}_{B/N}$, $\boldsymbol{\sigma}_{B/N}$ and $\boldsymbol{\omega}_{B/N}$.

Since `spacecraftPlus` is an instantiation of `dynamicObject`, it inherits the methods that are defined in Figure 4.1. The method `equationsOfMotion()` is the method that solves for all of the state derivatives of the spacecraft system. To explain this method in more detail, Figure 4.2 is included to show the flow in pseudo code. The spacecraft mass properties need to be calculated first because in Eqs. (2.1) and (2.2) the total spacecraft mass, m_{sc} , inertia, $[I_{sc,B}]$ and other parameters are needed. Next, the `gravityEffector` class is called to compute the gravity acting on the

spacecraft. This is done at this location because some `stateEffectors` might need to know the gravitational acceleration. Following this step, the `stateEffectors` are looped over to find their contributions to the back-substitution matrices and the `dynamicEffectors` are looped over to get their contributions to \mathbf{F}_{ext} and \mathbf{L}_B . Now, all of the necessary values have been computed for the hub state derivatives to be calculated using Eq. 2.19, which is computed in the `hubEffector`'s `computeDerivatives`. Finally, the `stateEffectors` are looped over to compute their derivatives using $\ddot{\mathbf{r}}_{B/N}$ and $\dot{\boldsymbol{\omega}}_{B/N}$.

```

spacecraftPlus
equationsOfMotion()
    hubEffector.updateEffectorMassProperties()
    for(effector in stateEffectors)
        effector.updateEffectorMassProperties()
    end

    gravityEffector.computeGravField()

    for(effector in stateEffectors)
        effector.updateContributions()
    end

    for(effector in dynEffectors)
        effector.computeBodyForceTorque()
    end

    hubEffector.computeDerivatives()
    for(effector in stateEffectors)
        effector.computeDerivatives()
    end
end

```

Figure 4.2: Pseudo code for the `equationsOfMotion()` method within `spacecraftPlus`

Since the `hubEffector`'s derivative calculation is so vital in this structure, Figure 4.3 is shown to explain the calculations needed for this step. Again, this is shown using pseudo code. Additionally, this method shows the interaction between the `stateManager` and the rest of the system. The `stateManager` stores the states of the system in individual objects. These objects can be accessed using a string and once the object has been accessed, the methods seen in Figure 4.1 under the `stateManager` class are available. For example, the `getState` method delivers the current

value of the state stored in that state object. In Figure 4.3, the hub effector uses those methods to retrieve the desired information from the `stateManager`. Ultimately setting the derivative values for the `hubEffector` is the goal of the `computeDerivatives` method and does so by using `setStateDeriv` for both $\ddot{\mathbf{r}}_{B/N}$ and $\dot{\boldsymbol{\omega}}_{B/N}$.

```

hubEffector
computeDerivatives()

rBN_NState = stateManager.getStateObject('hubPosition')
rBNDot_NState = stateManager.getStateObject('hubVelocity')
sigmaBN_State = stateManager.getStateObject('hubRotPosition')
omegaBN_BState = stateManager.getStateObject('hubRotVelocity')

rBNDot_N = rBNDot_NState.getState()
rBN_NState.setStateDeriv(rBNDot_N)

sigmaBNDot = omegaToSigmaDot(omegaBN_BState.getState())
sigmaBN_State.setStateDeriv(sigmaBNDot)


$$\dot{\boldsymbol{\omega}}_{B/N} = \left( [D] - [C][A]^{-1}[B] \right)^{-1} (\mathbf{v}_2 - [C][A]^{-1}\mathbf{v}_1)$$



$$\ddot{\mathbf{r}}_{B/N} = [A]^{-1}(\mathbf{v}_1 - [B]\dot{\boldsymbol{\omega}}_{B/N})$$


omegaBN_BState.setStateDeriv(omegaBN_Dot)
rBNDot_NState.setStateDeriv(rBNDot_N)

end

```

Figure 4.3: Pseudo code for `hubEffector computeDerivatives()` method

Another important method in this architecture is the `computeDerivatives` method for a generic `stateEffector`. To highlight this method, the hinged rigid bodies example introduced in this dissertation is used. Figure 4.4 shows the pseudo code for the `computeDerivatives` method of a hinged rigid body effector. When this method is being computed, $\ddot{\mathbf{r}}_{B/N}$ and $\dot{\boldsymbol{\omega}}_{B/N}$ have already been calculated, therefore the hinged rigid body effector can use the state manager's method called `getStateDeriv` which gives access to those pre-computed values. Looking at Eq. (3.58), the hinged rigid body effector utilizes $\ddot{\mathbf{r}}_{B/N}$ and $\dot{\boldsymbol{\omega}}_{B/N}$ in its calculation, and utilized saved variables for faster

results and is a benefit of the back-substitution method.

```

hingedRigidBody
computeDerivatives()
    theta_State = stateManager.getStateObject('panelTheta')
    thetaDot_State = stateManager.getStateObject('panelThetaDot')
    hubVelocity_State = stateManager.getStateObject('hubVelocity')
    hubRotVelocity_State = stateManager.getStateObject('hubRotVelocity')

    thetaDot = thetaDot_State.getState()
    theta_State.setStateDeriv(thetaDot)

    rBNDDot_N = hubVelocity_State.getStateDeriv()
    omegaDotBN_B = hubRotVelocity_State.getStateDeriv()

    
$$\ddot{\theta}_i = \mathbf{a}_{\theta_i}^T \ddot{\mathbf{r}}_{B/N} + \mathbf{b}_{\theta_i}^T \dot{\boldsymbol{\omega}}_{B/N} + c_{\theta_i}$$


    thetaDot_State.setStateDeriv(thetaDDot)
end

```

Figure 4.4: Pseudo code for `hingedRigidBody computeDerivatives()` method

The power of this design is that `stateEffectors` can just be attached to the spacecraft in no particular order and the scalability of this design is unconstrained. Adding another effector does not depend on any other effectors even though the fully-coupled nature is still retained. All of the coupling is through the rigid body hub and the analytical form of the back-substitution method allows for this modularity. Additionally, a fixed size system mass matrix is inverted as opposed to a dynamically allocated matrix of varying size which is common in fully-coupled dynamics simulations.

4.2 Multiple Spacecraft Architecture

A goal of this dissertation is to expand the modular software architecture to allow for multiple spacecraft to be simulated at a time and allow for docking and detachment. Figure 2.2 shows a diagram of the desired ability of this architecture with multiple spacecraft that can either be docked

to the primary spacecraft or unattached. However, the architecture should allow for spacecraft to dock and detach as much as desired throughout the link of the simulation.

Further description is needed for this multi-spacecraft architecture. For the purposes of this dissertation the attached spacecraft must include the primary spacecraft. In other words, the primary spacecraft must always be included in the docked spacecraft (its valid if there are no docked spacecraft) throughout the length of the simulation. For example, if the rocket problem was to be simulated, the primary spacecraft would need to be defined as one of the last spacecraft to stay attached. Using Figure 2.2 as an example, if the primary spacecraft were to detach from the spacecraft with the flexing solar arrays, the other smaller spacecraft could not connect directly to the flexing solar array spacecraft. However, if the flexing solar array spacecraft re-attached to the primary spacecraft, the smaller spacecraft could choose to dock with either spacecraft. Additionally, closed chain docking is not allowed. This architecture could be easily expanded to allow for multiple primary spacecraft, but the current formulation does not allow for that for sake of simplicity.

Another assumption is that contact physics between docking spacecraft is not being discussed in this architecture, therefore the docking between spacecraft is assumed to be “soft docks”. In other works, the exchange of momentum between docking spacecraft is not being considered. However, this architecture is not limited by this assumption. Contact physics and the exchange of momentum between docking spacecraft could be implemented using this architecture but it is beyond the scope of this dissertation.

In Section 2.2, the EOMs that describe the motion of a spacecraft system is introduced. Using those equations and leveraging the software architecture designed for a single spacecraft, the UML class diagram that can be used to develop a simulation with multiple spacecraft can be seen in Figure 4.5. This architecture is meant to replace the single spacecraft architecture if multi-spacecraft is desired. Therefore all of the `stateEffectors` `dynamicEffectors` defined from the prior class diagram can be re-used. The class diagram is very similar to the class diagram for single spacecraft simulations. One main difference is the class change from `spacecraftPlus` to `spacecraft`. This change is more than a name change because as it can be seen, the new `spacecraft` class is no longer

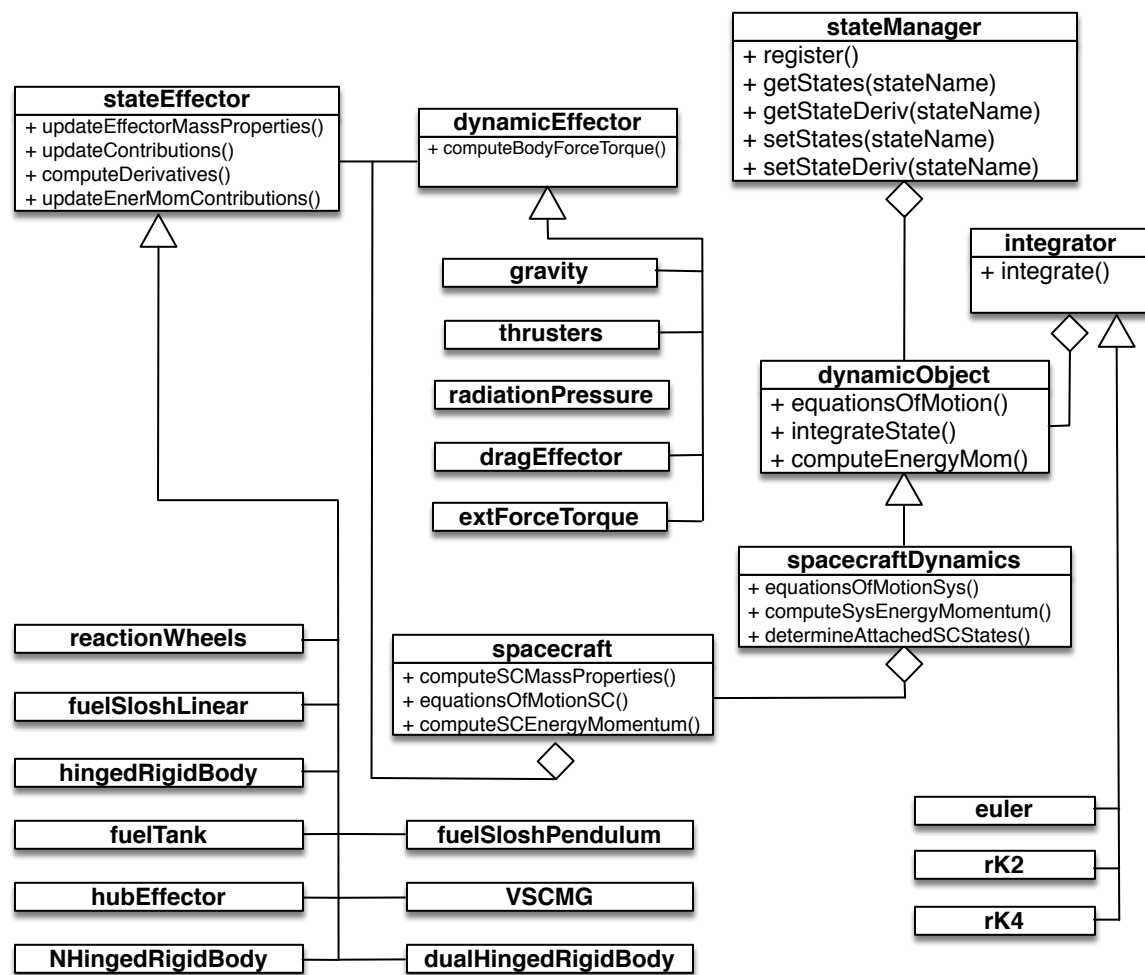


Figure 4.5: UML diagram for multi-spacecraft modular architecture

inheriting from the `dynamicObject` class. This is a key change because now the `spacecraft` class is an object that defines a total spacecraft with `stateEffectors` and `dynamicEffectors` attached to it but no longer has the job of controlling the integration and equation of motion generation as `spacecraftPlus` does in the single spacecraft architecture. However, each spacecraft has very similar mathematics to calculate and so retaining an object that essentially defines a spacecraft is very useful.

The `spacecraftDynamics` class is the new class in Figure 4.5 and is the class that inherits from the `dynamicObject`. With that, comes the responsibility of controlling the integration with the `integrateState` method, and the logic required to do both the multi-spacecraft simulation

```

spacecraftDynamics
equationsOfMotionSys()
    primarySC.hubEffector.updateEffectorMassProperties()
    for(effector in primarySC.stateEffectors)
        effector.updateEffectorMassProperties()
    end

    for(attachedSC in vectorOfAttachedSC)
        attachedSC.hubEffector.updateEffectorMassProperties()
        for(effector in attachedSC.stateEffectors)
            effector.updateEffectorMassProperties()
        end
    end

    primarySC.gravityEffector.computeGravField()

    for(effector in primarySC.stateEffectors)
        effector.updateContributions()
    end

    for(attachedSC in vectorOfAttachedSC)
        for(effector in attachedSC.stateEffectors)
            effector.updateContributions()
        end
    end

    for(effector in primarySC.dynEffectors)
        effector.computeBodyForceTorque()
    end

    for(attachedSC in vectorOfAttachedSC)
        for(effector in attachedSC.stateEffectors)
            effector.computeBodyForceTorque()
        end
    end

    primarySC.hubEffector.computeDerivatives()
    for(effector in stateEffectors)
        effector.computeDerivatives()
    end

    for(attachedSC in vectorOfAttachedSC)
        for(effector in attachedSC.stateEffectors)
            effector.computeDerivatives()
        end
    end
end

```

Figure 4.6: Pseudo code for the `equationsOfMotionSys()` method within `spacecraftDynamics`

and back-substitution in the `equationsOfMotion` method. Since the back-substitution method was already implemented in the `spacecraftPlus` `equationsOfMotion` method, this calculation is

stored in the new `spacecraft` class under its `equationsOfMotion` method. However this method is now only applicable to spacecraft that are unattached from the primary spacecraft.

There are three additional methods that the `spacecraftDynamics` class defines and the first one is the `equationsOfMotionsSys` method. This method controls the logic of the primary spacecraft computing the acceleration of the state variables of the primary spacecraft hub and getting contributions from the other spacecraft. However, as seen in Figure 4.6, all other attached spacecraft to the primary spacecraft do not calculate their own hub derivatives. This is key feature because it removes unnecessary math being calculated and relies on the fact that all of the other connected spacecraft hub states can be found from the kinematic relationships between the primary hub and the attached spacecraft hubs.

```

spacecraftDynamics
equationsOfMotion()
    equationsOfMotionSys()
    for(unAttachedSC in vectorOfUnAttachedSC)
        unAttachedSC.equationsOfMotionSC()
    end
end

```

Figure 4.7: Pseudo code for the `equationsOfMotion()` method within `spacecraftDynamics`

Now that both the `spacecraftDynamics` class `equationsOfMotionSys` and the `spacecraft` class `equationsOfMotion` methods have been described, the final method that needs to be described related to the dynamics calculations is the `spacecraftDynamics` `equationsOfMotion` method that it inherits from the `dynamicsObject` class. This simple pseudo code seen in Figure 4.7 shows how the calculations for the equations can be separated into the connected system of spacecraft and the unattached independent spacecraft equations. This again is leveraging the modularity of the equations developed in Section 2.

The final method that needs to be described for this multi-spacecraft architecture is the `integrateState` method in the `spacecraftDynamics` class seen in Figure 4.8. This shows that

```

spacecraftDynamics
integrateState()
    integrate()
    determineAttachedSCStates()
    computeEnergyMomentumSys()
    for(unAttachedSC in vectorOfUnAttachedSC)
        unAttachedSC.computeEnergyMomentumSC()
    end
end

```

Figure 4.8: Pseudo code for the `integrateState()` method within `spacecraftDynamics`

the `integrate` method is called to step the states one step forward in time but after this call the spacecraft attached to the primary spacecraft have not had their hub states updated. This is the job of the `determineAttachedSCState` method in the `spacecraftDynamics` class. This method uses the primary hub's states and the kinematic relationships to find the other attached spacecraft states. After these methods have been computed, the `computeEnergyMomentumSys` method which computes the attached spacecraft system energy and momentum is called. Finally, the unattached independent spacecraft have the opportunity to calculate their energy and momentum with `computeEnergyMomentumSC` calls.

Both the single spacecraft and multi-spacecraft software architectures described utilize the back-substitution method and the generalized EOM form introduced in Section 2. These architectures could be implemented in any object oriented language and result in elegant modular software implementations that solve the problems of maintainability, testability, and scalability for multi-body spacecraft dynamics problems.

Chapter 5

Basilisk Astrodynamics Software Package Validation and Verification

The Basilisk Astrodynamics Software Package is chosen as the implementation code base for the modular software dynamics architecture. However, this validation and verification section and the rest of the dissertation is not dependent on the chosen software package. This software architecture could be implemented in any object oriented language. Every dynamics model that has been introduced in this dissertation has been implemented in Basilisk and this section explains some of the methods used to validate and verify both the EOMs and the software implementation of the equations.

The terms validation and verification can have different meanings depending on the application. The validation and verification process used in this dissertation is similar to the formal spacecraft validation and verification (V&V) process that many spacecraft missions utilize. The process is meant to determine whether the functions of the software are meeting the desired capability, also known as validation. Verification is ensuring that the actual implementation of the software is properly performing the previously described functions. This process can be performed on any software, but the most common portions of code from a spacecraft mission perspective that involve V&V related tasks, are flight software algorithms and the simulation models. The details of the actual V&V process can depend on the resources and time available for the project. For example, in this dissertation, it is known it is not an exhaustive validation and verification procedure and does not involve comparison to experimental data. However, the procedure for validating and verifying the software is rigorous and gives confidence in both the equations motion developed and

the implementation of the equations in software.

5.1 Validation Examples

Validation of analytical development of spacecraft EOMs and software implementation can be a difficult task, especially when experimentation is not available. To validate dynamics models, one method is to define tests that might simplify the complicated problem to something simpler and that can confirm the software is providing the expected results. Additionally, writing out the expected functions and assumptions/limitations of each model will ensure that the developer is aware of all of the expected functionality of the code. From a validation perspective, the process is typically not exhaustive without doing experimental comparisons. However, for this dissertation the validation examples coupled with verification effort discussed in this chapter is sufficient to ensuring expected results and validating/verifying the models.

5.1.1 SpacecraftPlus

5.1.1.1 Introduction

`spacecraftPlus` is an instantiation of the `dynamicObject` abstract class. This abstract class is representing systems that have equations of motion that need to be integrated and therefore the main goal of this dynamic object is finding the state derivatives and interfacing with the integrator to integrate the state forward in time. `spacecraftPlus` is representing a spacecraft that can be simulating only the translational movement which would mean the spacecraft only has mass (for gravity only simulations, setting the mass is not necessary), it could be simulating only rotational dynamics which would result in the spacecraft only having inertia, and finally both translational and rotational dynamics can be simulated at a time which results in the spacecraft having mass, inertia and center of mass offset.

`spacecraftPlus` is the module where the equations of motion of the spacecraft are computed including the interaction between the `hubEffector`, `stateEffectors` and `dynamicEffectors`. The

hubEffector is where the translational and rotational derivatives are computed, the stateEffectors give contributions to spacecraftPlus and computes their derivatives and the dynamicEffectors provide force and torque contributions to spacecraftPlus.

5.1.1.2 Model Functions

This module is intended to be used as a model to represent a spacecraft that can be decomposed into a rigid body hub and has the ability to model state effectors such as reactions wheels, and flexing solar panels, etc attached to the hub. The following is a list of functions that this model should achieve.

- Updates the mass properties of the spacecraft by adding up all of the contributions to the mass properties from the hubEffector and the stateEffectors
- Adds up all of the matrix contributions from the hubEffector and stateEffectors for the back substitution method and gives this information to the hub effector
- Adds up the force and torque contributions from dynamicEffectors and gravityEffector
- Calls all of the computeDerivatives methods for the hub and all of the state effectors which is essentially solving $\dot{\mathbf{X}} = \mathbf{f}(\mathbf{X}, t)$
- Integrates the states forward one time step using the selected integrator
- Calculates the total energy and momentum of the spacecraft by adding up contributions from the hub and the state effectors

5.1.1.3 Model Assumptions and Limitations

Outlining the assumptions and limitations of a module can give perspective on how the simulation was meant to be designed. Below is a summary of the assumptions/limitations:

- stateEffectors that are changing the mass properties of the spacecraft are considered new bodies that are added to the mass properties of the spacecraft

- The limitations of the simulation are primarily based on what configuration are set for the spacecraft in (i.e. what state effectors and dynamic effectors that are attached to the spacecraft). Additionally it is limited to the current capability of the models in regards to state effectors and dynamic effectors.
- The accuracy of the simulation is based upon the integrator and integrator step size
- As discussed in the description section, the body fixed frame \mathcal{B} can be oriented generally and the origin of the \mathcal{B} frame can be placed anywhere as long as it is fixed with respect to the body. This means that there are no limitations from the rigid body hub perspective.

5.1.1.4 MRP switching test

An important aspect of spacecraft dynamics simulations involving MRPs are the ability to switch to the shadow set of the MRPs to avoid singularities [39]. In Basilisk the MRPs are switched to the shadow set in `hubEffector` after one step of the integration using the method `modifyStates()` which is available to all `stateEffectors` that need to change their states to a different but equivalent form. The MRP switching adheres to the following equation[39]:

$$\begin{aligned}
 &\mathbf{if} \quad [s = |\boldsymbol{\sigma}(t + dt)|] > 1 \quad \mathbf{then} \\
 &\quad \boldsymbol{\sigma}(t + dt) = -\frac{\boldsymbol{\sigma}(t + dt)}{s^2} \\
 &\quad \mathbf{end \ if}
 \end{aligned} \tag{5.1}$$

To check that the switch in the simulation is behaving the way it should, the following check was developed. If the switch happened at time t_s , then there are two variables from the sim that will be used: $\boldsymbol{\sigma}(t_{s-1})$ and $\boldsymbol{\sigma}(t_s)$. The intermediate MRP that is switched in the simulation is not an output of the simulation, but needs to be defined: $\boldsymbol{\sigma}_0(t_s)$. To check the switching the following math occurs:

$$\boldsymbol{\sigma}_0(t_s) \approx \boldsymbol{\sigma}(t_{s-1}) + \frac{\boldsymbol{\sigma}(t_{s-1}) - \boldsymbol{\sigma}(t_{s-2})}{\Delta t} \Delta t \tag{5.2}$$

where this is an Euler approximation to the intermediate MRP before the switch occurs. Now using Eq. (5.1) the following definition is made:

$$\sigma_{\text{ch}}(t_s) = -\frac{\sigma_0(t_s)}{|\sigma_0(t_s)|^2} \quad (5.3)$$

Where $\sigma_{\text{ch}}(t_s)$ is the MRP to check vs. the simulation MRP. Therefore, in this test, it is making sure that $\sigma(t_s) \approx \sigma_{\text{ch}}(t_s)$.

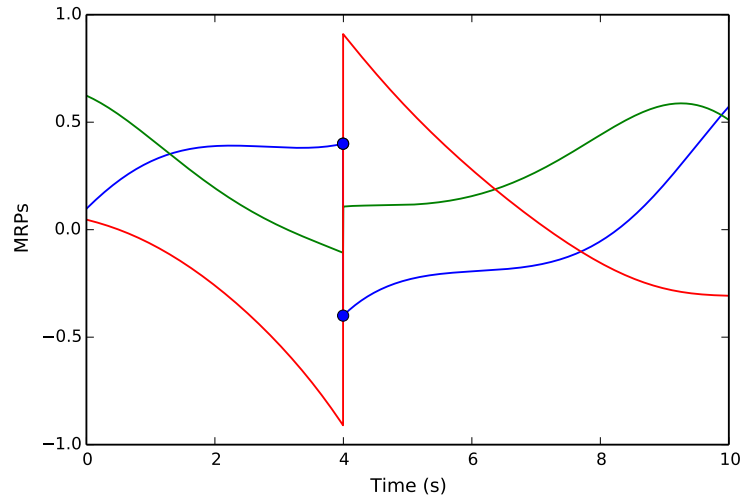


Figure 5.1: Attitude of Spacecraft in MRPs

Figure 5.1 shows the MRPs over the simulation time of the test and it shows that the switch occurs at around 4 seconds. Figure 5.2 shows the values being saved from Basilisk at the time of switching. The results of the test confirm that the switching is being computed properly because with a time step of 0.01 the relative accuracy of $\sigma(t_s) \approx \sigma_{\text{ch}}(t_s)$ is 10^{-6} . Additionally, the results are dependent on the time step because of the Euler approximation used in the test. As the time step goes down the accuracy approaches zero with agrees with intuition. This test gives validation in the analytical development and software implementation.

5.1.1.5 Rotational Dynamics Validation Test

To validate the rotational dynamics, a relationship that involves both the attitude and attitude rate was chosen. The following calculation is a modified example from Reference[39] and

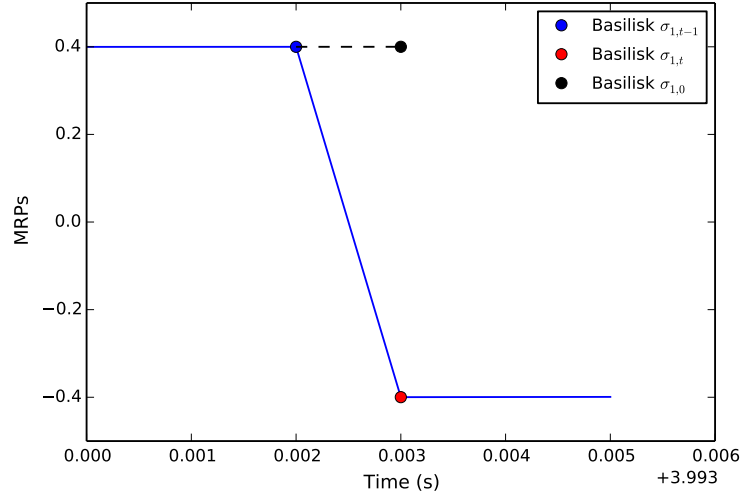


Figure 5.2: MRP Switching

repeated here for convenience. To begin this example, the angular momentum vector is chosen to be aligned with the inertial frame:

$${}^{\mathcal{N}}\mathbf{H} = -H\hat{\mathbf{n}}_3 = \begin{bmatrix} 0 \\ 0 \\ -H \end{bmatrix} \quad (5.4)$$

The following relationship is written:

$${}^B\mathbf{H} = [BN]{}^{\mathcal{N}}\mathbf{H} \quad (5.5)$$

Since MRPs are the attitude parameterization chosen for Basilisk, then the direction cosine matrix $[BN]$ is written in terms of the current MRPs. If there are no external torque's acting on the spacecraft, then the angular momentum vector will be conserved in the inertial frame. Therefore, using the definition of transformation from MRPs to the direction cosine matrix[39], the following relationship will always hold:

$${}^B \begin{bmatrix} H_1 \\ H_2 \\ H_3 \end{bmatrix} = -H \begin{bmatrix} 8\sigma_1\sigma_3 - 4\sigma_2(1 - \sigma^2) \\ 8\sigma_2\sigma_3 + 4\sigma_1(1 - \sigma^2) \\ 4(-\sigma_1^2 - \sigma_2^2 + \sigma_3^2) + (1 - \sigma^2)^2 \end{bmatrix} = \begin{bmatrix} I_1\omega_1 \\ I_2\omega_2 \\ I_3\omega_3 \end{bmatrix} \quad (5.6)$$

Finally, the current angular velocity components in the body frame can be found from the current MRPs using the following relationship:

$$\omega_1 = -\frac{H}{I_1} \left[8\sigma_1\sigma_3 - 4\sigma_2(1 - \sigma^2) \right] \quad (5.7)$$

$$\omega_2 = -\frac{H}{I_2} \left[8\sigma_2\sigma_3 + 4\sigma_1(1 - \sigma^2) \right] \quad (5.8)$$

$$\omega_3 = -\frac{H}{I_3} \left[4(-\sigma_1^2 - \sigma_2^2 + \sigma_3^2) + (1 - \sigma^2)^2 \right] \quad (5.9)$$

This gives a closed form solution between the current MRPs and the angular velocity of the

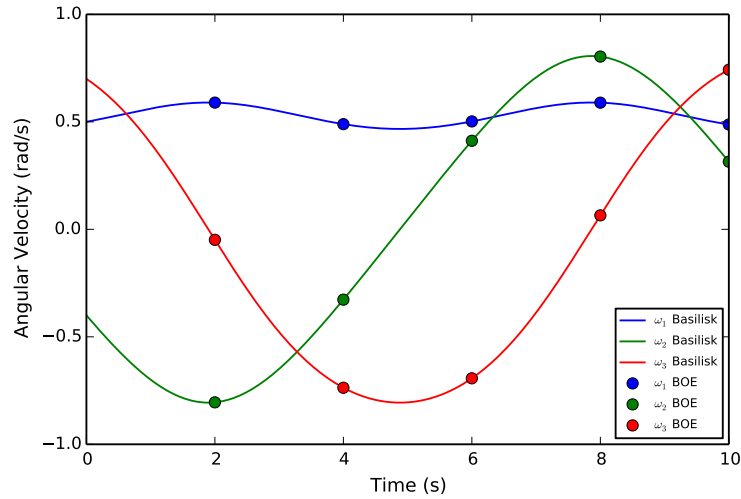


Figure 5.3: Basilisk vs Validation Test Calculation For Rotation

spacecraft. The test picks 5 points during a simulation and verifies that this relationship holds true.

Figure 5.3 shows the results of this test which gives validation for both the analytical development and the software implementation. With a time step of 0.01, Basilisk provides a relative accuracy of 10^{-10} . Again, these results are dependent on the time step of the simulation but as the time step goes down, the relative accuracy approaches zero.

5.1.1.6 Translational Validation Calculation Scenario

The translational BOE calculation can be seen in Figure 5.4. In this test a positive force is placed on the hub in the \hat{b}_1 direction with no torque and no initial rotation of the spacecraft. This results in a one degree of freedom problem as seen in Figure 5.4. The force is applied for some length of time, left off for another length of time, and then a negative force is applied to the system for an additional length of time. The test is ensuring that Basilisk is giving the same results as the analytical development described below.

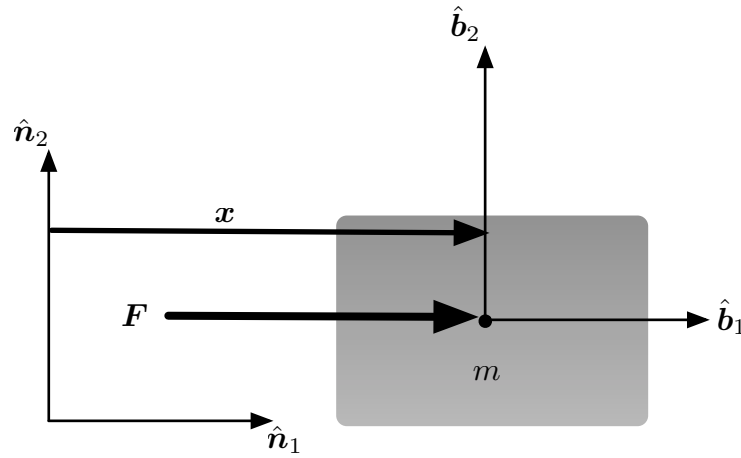


Figure 5.4: Schematic of translational validation example

Figure 5.5 shows that there is a closed form solution to both the position and velocity of the block in Figure 5.4 with respect to time. These values can be described with the following equations. The acceleration during the first length of time that the force is applied is

$$a_1 = \frac{F_1}{m} \quad (5.10)$$

and when the negative second force is applied the acceleration is

$$a_2 = -\frac{F_1}{m} \quad (5.11)$$

The velocity at t_1 as seen in Figure 5.5 is described in the following equation:

$$v_1 = a_1 t_1 \quad (5.12)$$

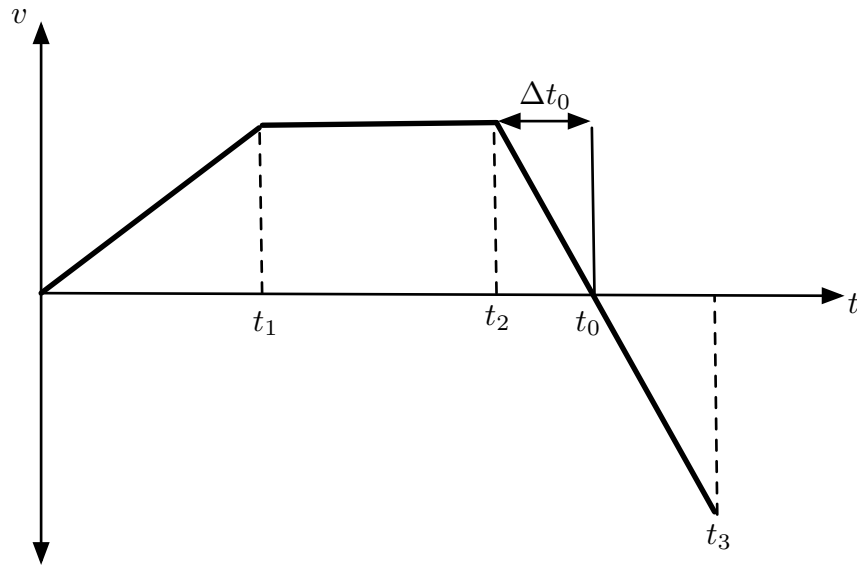


Figure 5.5: Velocity vs time curve for translational validation example

Using v_1 , v_2 can be found simply:

$$v_2 = v_1 \quad (5.13)$$

Finally, v_3 can be found using v_2 as seen in the following equation:

$$v_3 = v_2 + a_2(t_3 - t_2) \quad (5.14)$$

Like the velocities, there is a closed form solution for each position using the common relationship between position and velocity for constant acceleration problems. These values can be seen in the following equations.

$$x_1 = \frac{1}{2}v_1t_1 \quad (5.15)$$

$$x_2 = x_1 + v_2(t_2 - t_1) \quad (5.16)$$

$$x_3 = x_2 + \frac{1}{2}v_2(t_0 - t_2) + \frac{1}{2}v_3(t_3 - t_0) \quad (5.17)$$

t_0 and Δt_0 are two values that need to be found. First, Δt_0 , can be found using the following equations.

$$0 = v_2 + a_2(\Delta t_0) \quad (5.18)$$

$$\Delta t_0 = -\frac{v_2}{a_2} \quad (5.19)$$

Next, the relationship between t_0 , t_2 and Δt_0 can be used to define t_0 :

$$t_0 = t_2 + \Delta t_0 \quad (5.20)$$

Now that all of the necessary variables have been defined the translational validation test can be implemented. The results from this validation test can be seen in Figures 5.6-5.7. The position and velocity curve of the spacecraft from Basilisk was plotted against each of the three position and velocity points that come from the analytical development. The results confirm that Basilisk is giving expected results with regard to the simple translational example and providing an relative accuracy of 10^{-10} with a time step of 0.01 seconds. This provides validation of the model and gives confidence in both the analytical development of the model and the software implementation of the model.

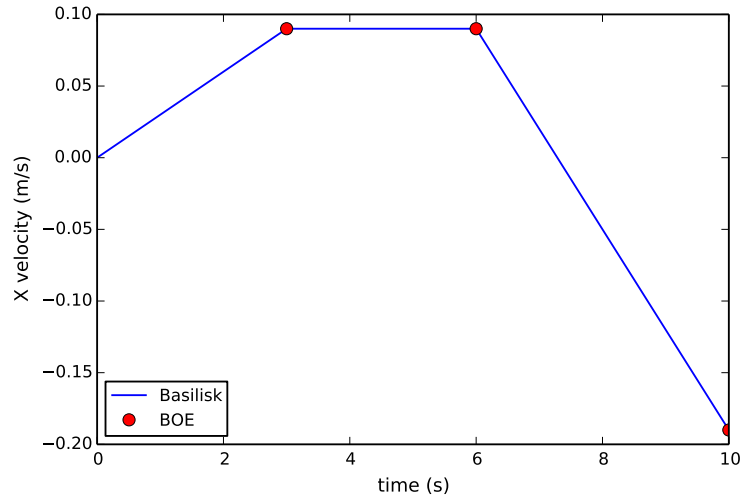


Figure 5.6: Translation Velocity Validation Test

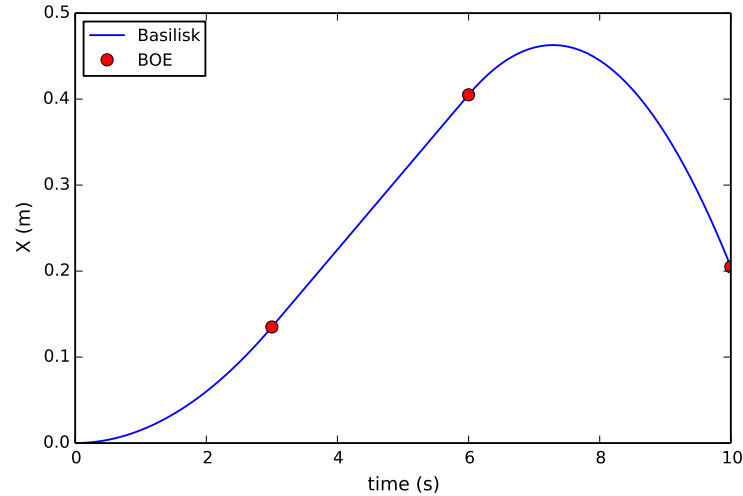


Figure 5.7: Translation Position Validation Test

5.1.1.7 Dynamics Calculated About Point B Validation Test

The dynamics for the spacecraft have been derived in relation to the body frame origin, point B , which is not necessarily coincident with point C . Therefore the `dynamicEffectors` and `stateEffectors` define their torques about point B as oppose to about point C . This allows the simulation to have multi-body dynamics where the center of mass of the spacecraft can move with respect to the body frame. However, in rigid body dynamics it is very common to have the body frame origin coincident with the center of mass of the spacecraft. Therefore, to confirm that the dynamics has been developed correctly to handle this torque mapping a test has been created.

The test runs two simulations: one with the body frame origin defined at the center of mass of the spacecraft, and one with the body frame origin not coincident with the center of mass. An external force and corresponding torque is applied to the spacecraft in both cases: in the first case the torque is being defined about point $B = C$, and in the second case the torque is being defined about point $B \neq C$. Both simulations are given identical initial conditions and the expectation is that the simulations should give identical results. The following parameters describe the success criteria.

- Agreement between both simulations for the translational states
- Agreement between both simulations for the attitude states

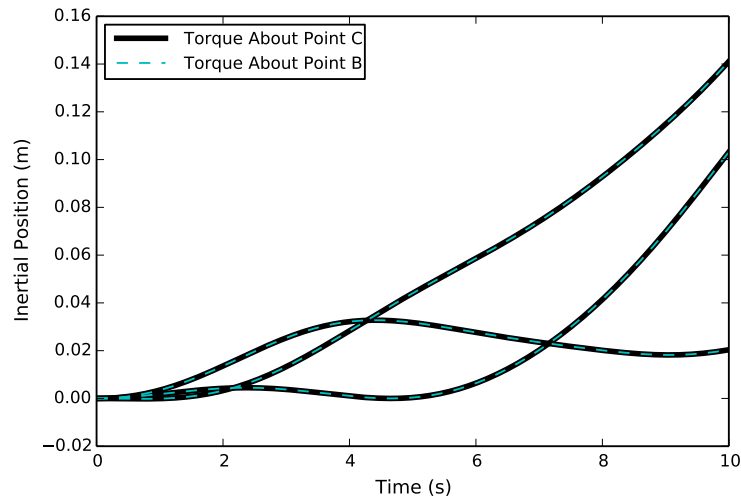


Figure 5.8: PointB vs PointC Translation

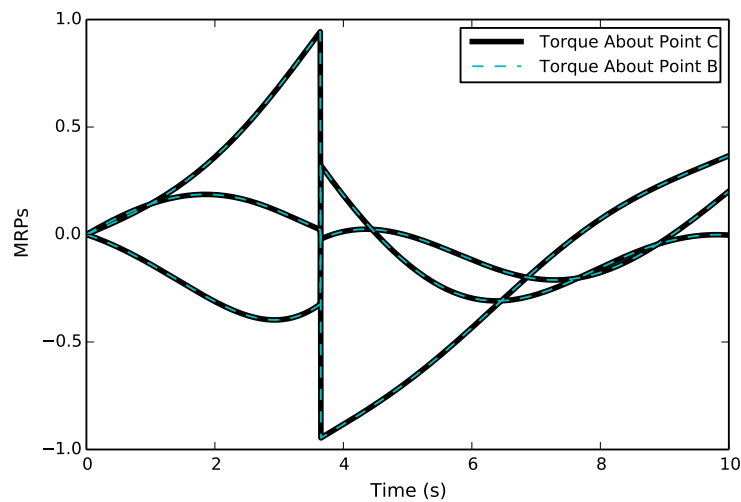


Figure 5.9: PointB vs PointC Attitude

The results from this test can be seen in Figures 5.8-5.9. The results show that the test is working and Basilisk is giving an agreement between the two data sets of about 10^{-15} which is right

around machine precision. This gives validation in the formulation, the software implementation, and gives further confidence in the results.

5.1.2 HingedRigidBodyStateEffector

The `hingedRigidBodyStateEffector` class is an instantiation of the `stateEffector` abstract class. The `stateEffector` abstract class is a base class for modules that have dynamic states or degrees of freedom with respect to the rigid body hub. Examples of these would be reaction wheels, variable speed control moment gyroscopes, fuel slosh particles, etc. Since the `stateEffectors` are attached to the hub, the state effectors are directly affecting the hub as well as the hub is back affecting the state effectors.

Specifically, a hinged rigid body state effector is a rigid body that has a diagonal inertia with respect to its \mathcal{S}_i frame as seen in Figure 6.1. It is attached to the hub through a hinge with a linear torsional spring and linear damping term.

5.1.2.1 Model Functions

This module is intended to be used as an approximation to a flexing body attached to the spacecraft. Examples include solar arrays, antennas, and other appended bodies that would exhibit flexing behavior. Below is a list of functions that this model performs:

- Compute its contributions to the mass properties of the spacecraft
- Provides matrix contributions for the back substitution method
- Compute its derivatives for θ and $\dot{\theta}$
- Adds energy and momentum contributions to the spacecraft

5.1.2.2 Model Assumptions and Limitations

The `hingedRigidBodyStateEffector` is designed in Basilisk with the following assumptions/limitations:

- Is a first-order approximation to a flexing body
- Is developed in such a way that does not require constraints to be met
- The hinged rigid body must have a diagonal inertia tensor with respect the \mathcal{S}_i frame
- Only linear spring and damping terms
- Will only approximate one flexing mode at a time
- Cannot simulate multiple interconnected panels
- The hinged rigid body will always stay attached to the hub (the hinge does not have torque limits)
- The hinge does not have travel limits, therefore if the spring is not stiff enough it will unrealistically travel through bounds such as running into the spacecraft hub
- The EOMs are nonlinear equations of motion, therefore there can be inaccuracies (and divergence) that result from integration. Having a time step of ≤ 0.10 sec is recommended, but this also depends on the natural frequency of the system
- When trying to match the frequency of a physical appended body, note that the natural frequency of the coupled system will be different than the appending body flexing by itself: use eigenvalues to find the coupled frequency

5.1.2.3 Steady State Deflection Validation Test

The validation calculation for the steady state deflection can be seen in Fig. 5.10(a). This test involves an initially at rest spacecraft, and a constant external force is applied to the rigid-body hub for the length of the simulation. There is damping in the torsional joints of each panel and the spacecraft is symmetrical. With these descriptions the spacecraft should only move in the direction of the applied force and the spacecraft should not rotate. Initially there will be a transient of the deflection of the solar panels but they will eventually dampen to the steady-state value, θ_{ss} .

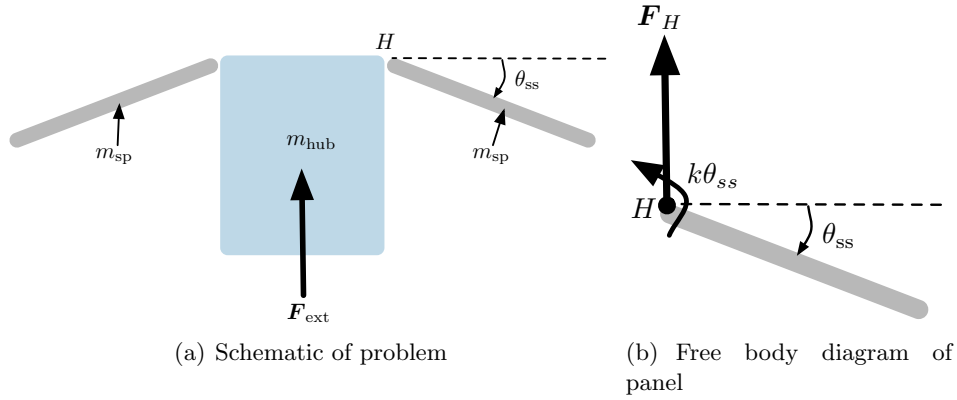


Figure 5.10: Steady state deflection validation problem description

To find the steady-state value first the sum of the forces acting on the solar panel using Figure 5.10(b) as reference for the free body diagram is found:

$$\sum F = F_H = m_{sp}a_{ss} \quad (5.21)$$

where m_{sp} is the mass of each solar panel, and a_{ss} is the steady state acceleration of the panel. Since the force is being applied continuously, once the transient dies out, the acceleration of the solar panel is

$$a_{ss} = \frac{F_{ext}}{m_{sc}} \quad (5.22)$$

The mass of the spacecraft, m_{sc} is

$$m_{sc} = m_{hub} + 2m_{sp} \quad (5.23)$$

Performing the sum of the torques about point H at steady state results in

$$\sum \tau = -k\theta_{ss} - F_h d \cos(\theta_{ss}) = 0 \quad (5.24)$$

Using these definitions and manipulating the equations the resulting steady state deflection does not have a closed form solution. Therefore, the function

$$f(\theta_{ss}) = k\theta_{ss} + \frac{1}{m_{sc}} m_{sp} F d \cos(\theta_{ss}) \quad (5.25)$$

defines the root function that must be solved. A Newton-Raphson method was chosen and the success criteria for this test is whether Basilisk gives the same results as this calculation within a certain tolerance.

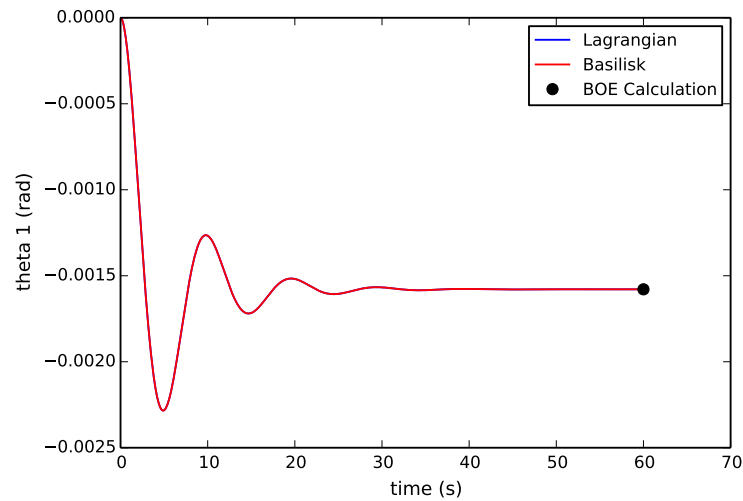


Figure 5.11: Validation Test Calculation for Steady State Theta 1 Deflection vs Simulation

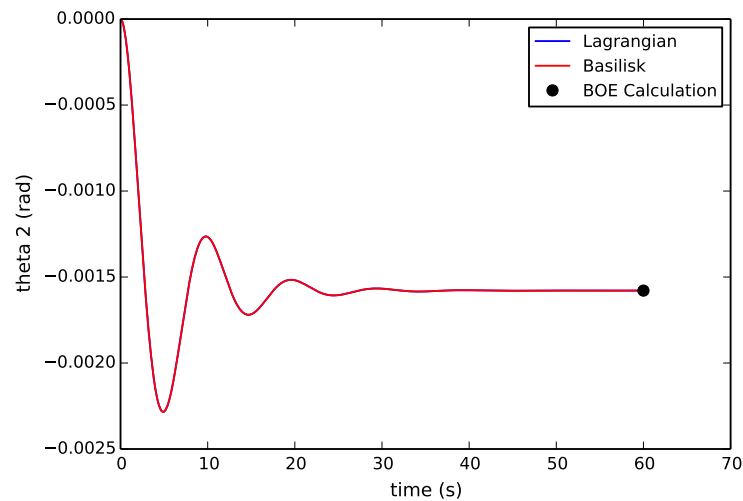


Figure 5.12: Validation Test Calculation for Steady State Theta 2 Deflection vs Simulation

The results seen in Figures 5.11-5.12 show that the test working Basilisk is achieving the expected results with respect to the analytical development. This gives validation in the model.

5.1.2.4 Frequency and Max Deflection Validation Test Description

The validation calculation for the frequency of oscillation of flexing hinged rigid bodies when a constant force is being applied to the spacecraft is done by making the following assumptions:

- The force is being directed through the center of mass of the spacecraft, along the $\hat{\mathbf{b}}_2$ direction
- The panels are initially undeflected and they are symmetric therefore the body will not rotate
- Rotation is no longer apart of the equations so the translation and solar panel equations are the only equations needed
- $\hat{\mathbf{s}}_{i,3}$ is assumed to be equal to $\hat{\mathbf{h}}_{i,3}$ in the equations of motion
- No external torque is being applied directly to the hinged rigid bodies
- Non-linear terms are neglected

Using the third assumption from above, the rotational motion is taken out of the equations of motion:

$$m_{sc}\ddot{\mathbf{r}}_{B/N} + \sum_i^N m_{sp_i} d_i \hat{\mathbf{s}}_{i,3} \ddot{\theta}_i = \mathbf{F}_{ext} - \sum_i^N m_{sp_i} d_i \dot{\theta}_i^2 \hat{\mathbf{s}}_{i,1} \quad (5.26)$$

$$m_{sp_i} d_i \hat{\mathbf{s}}_{i,3}^T \ddot{\mathbf{r}}_{B/N} + (I_{s_{i,2}} + m_{sp_i} d_i^2) \ddot{\theta}_i = -k_i \theta_i - c_i \dot{\theta}_i + \hat{\mathbf{s}}_{i,2}^T \boldsymbol{\tau}_{ext, H_i} \quad (5.27)$$

Next, assumptions 4-6 are applied:

$$m_{sc}\ddot{\mathbf{r}}_{B/N} + \sum_i^N m_{sp_i} d_i \hat{\mathbf{h}}_{i,3} \ddot{\theta}_i = \mathbf{F}_{ext} \quad (5.28)$$

$$m_{sp_i} d_i \hat{\mathbf{h}}_{i,3}^T \ddot{\mathbf{r}}_{B/N} + (I_{s_{i,2}} + m_{sp_i} d_i^2) \ddot{\theta}_i = -k_i \theta_i - c_i \dot{\theta}_i \quad (5.29)$$

Finally, knowing that the force is being directed along the $\hat{\mathbf{b}}_2$ axis and that the spacecraft will not rotate, the equations simplify to:

$$m_{sc}\ddot{y}_{B/N} + \sum_i^N m_{sp_i} d_i \ddot{\theta}_i = F_y \quad (5.30)$$

$$m_{sp_i} d_i \ddot{y}_{B/N} + (I_{s_{i,2}} + m_{sp_i} d_i^2) \ddot{\theta}_i = -k_i \theta_i - c_i \dot{\theta}_i \quad (5.31)$$

Converting these equations to State Space Representation [3]:

$$\begin{bmatrix} 1 & 0 & 0 & 0 & 0 & 0 \\ 0 & m_{sc} & 0 & m_{sp_1} d_1 & 0 & m_{sp_2} d_2 \\ 0 & 0 & 1 & 0 & 0 & 0 \\ 0 & m_{sp_1} d_1 & 0 & I_{s_{1,2}} + m_{sp_1} d_1^2 & 0 & 0 \\ 0 & 0 & 0 & 0 & 1 & 0 \\ 0 & m_{sp_2} d_2 & 0 & 0 & 0 & I_{s_{2,2}} + m_{sp_2} d_2^2 \end{bmatrix} \begin{bmatrix} \dot{y}_{B/N} \\ \ddot{y}_{B/N} \\ \dot{\theta}_1 \\ \ddot{\theta}_1 \\ \dot{\theta}_2 \\ \ddot{\theta}_2 \end{bmatrix} = \begin{bmatrix} 0 & 1 & 0 & 0 & 0 & 0 \\ 0 & 0 & 0 & 0 & 0 & 0 \\ 0 & 0 & 0 & 1 & 0 & 0 \\ 0 & 0 & -k_1 & -c_1 & 0 & 0 \\ 0 & 0 & 0 & 0 & 0 & 1 \\ 0 & 0 & 0 & 0 & -k_2 & -c_2 \end{bmatrix} \begin{bmatrix} y_{B/N} \\ \dot{y}_{B/N} \\ \theta_1 \\ \dot{\theta}_1 \\ \theta_2 \\ \dot{\theta}_2 \end{bmatrix} + \begin{bmatrix} 0 \\ F_y \\ 0 \\ 0 \\ 0 \\ 0 \end{bmatrix} \quad (5.32)$$

Equation (5.32) is written in a more compact form:

$$[M]\dot{\mathbf{X}} = [A]\mathbf{X} + \mathbf{F} \quad (5.33)$$

The equivalent dynamics matrix for this coupled system is:

$$[\tilde{A}] = [M][A] \quad (5.34)$$

Finding the eigenvalues of $[\tilde{A}]$ will describe the coupled natural frequencies of the combined system. The integrated test for this scenario ensures that the analytical coupled frequency of oscillation matches the frequency obtained from the simulation.

The next validation calculation that is needed is to find the maximum deflection while the force is being applied and when the force is not being applied (with the assumption that there is no damping). When the force is being applied the following max deflection can be seen in the following equation:

$$\theta_{\max} = 2\theta_{SS} \quad (5.35)$$

which uses the definition of θ_{SS} from Fig. 5.10.

Finally, the maximum deflection when the force is not being applied uses energy techniques. Once the force is no longer being applied, energy is conserved and the velocity of the center of mass is constant. The energy when the force is turned off is represented in the following equation:

$$E_0 = \frac{1}{2}m_{\text{hub}}\dot{y}_{B/N}^2 + 2\left[\frac{1}{2}m_{\text{sp}}\dot{\mathbf{r}}_{\text{sp}} \cdot \dot{\mathbf{r}}_{\text{sp}} + \frac{1}{2}I_{\text{sp}}\dot{\theta}^2 + \frac{1}{2}k\theta^2\right] \quad (5.36)$$

Where $\dot{\mathbf{r}}_{\text{sp}}$ is

$$\dot{\mathbf{r}}_{\text{sp}} = \begin{bmatrix} -d\dot{\theta} \sin(\theta) \\ \dot{y}_{B/N} + d\dot{\theta} \cos(\theta) \end{bmatrix} \quad (5.37)$$

Next, the velocity of the center of mass of the system is defined in the following equation:

$$v_{\text{CoM}} = \frac{1}{m_{\text{tot}}}(m_{\text{hub}}\dot{y}_{B/N} + 2m_{\text{sp}}\dot{r}_{\text{sp},y}) \quad (5.38)$$

This value can be computed from the values at the time the force is shut off and is a conserved quantity.

When the panels are deflected at max deflection, $\dot{\theta} = 0$. Leveraging this assumption the final energy is defined as follows:

$$E_F = \frac{1}{2}m_{\text{tot}}v_{\text{CoM}}^2 + 2\left[\frac{1}{2}k\theta_{\max}^2\right] \quad (5.39)$$

Conservation of energy states

$$E_0 = \frac{1}{2}m_{\text{tot}}v_{\text{CoM}}^2 + k\theta_{\max}^2 \quad (5.40)$$

Therefore, θ_{\max} is found using the following equation:

$$\theta_{\max} = \sqrt{\frac{E_0 - \frac{1}{2}m_{\text{tot}}v_{\text{CoM}}^2}{k}} \quad (5.41)$$

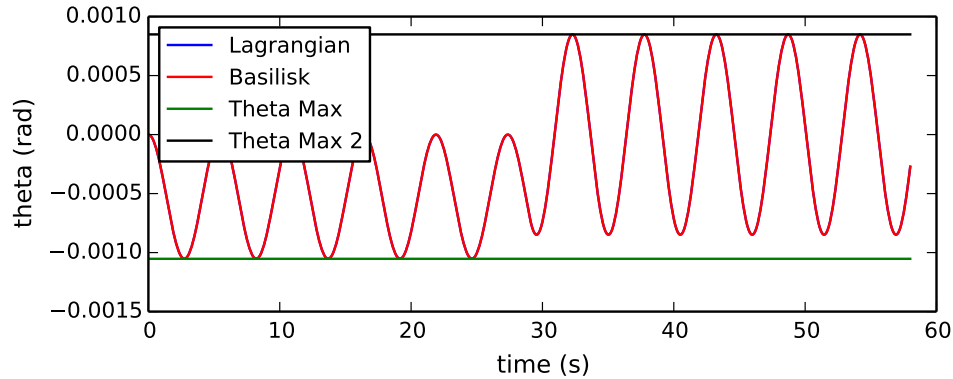


Figure 5.13: Max Theta While Forcing

Table 5.1: Frequency and amplitude test results for hinged rigid-bodies

Name	Calculation	Basilisk Results	Relative Error
Frequency	0.182710919651	0.183486238532	0.00424341841673
Theta Max 1	-0.00105263143315	-0.00105259806106	3.17034890432e-05
Theta Max 2	0.000848883927341	0.000848853165165	3.62383770165e-05

The test results for this validation test can be seen in Figure 5.13 and Table 5.1. Both of these results give confidence in the analytical development of the EOMs and the software implementation of the code.

5.1.2.5 Lagrangian vs Basilisk Scenario

In this scenario the equations of motion for a planar simulation of a spacecraft hub and two hinged rigid bodies using Lagrangian mechanics was developed using Mathematica. This simulation is ran independently in the validation test and the results are compared vs Basilisk results. A force and torque is applied for a certain amount of time, then turned off. Then another pulse of a force and torque is applied and turn off and the simulation runs for another few seconds. The results can be seen in Figures 5.14-5.18. The results show that Basilisk and the Lagrangian formulation give identical results and they actually agree down to approximately machine precision. This test gives further validation of system and gives confidence in both the analytical development and the software implementation.

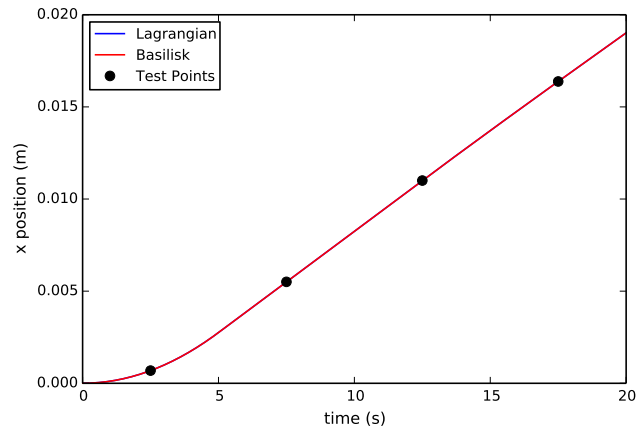


Figure 5.14: X Position Lagrangian Vs Basilisk

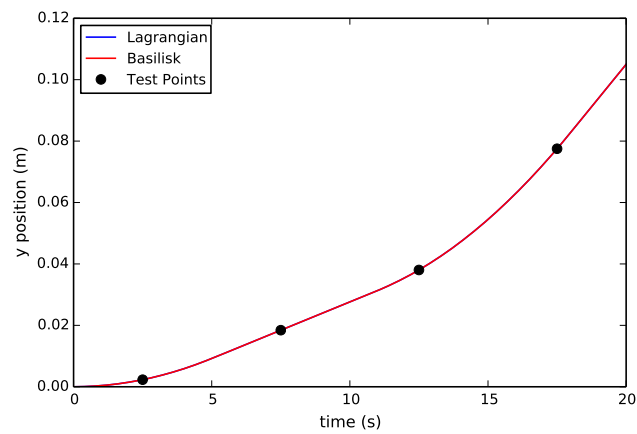


Figure 5.15: Y Position Lagrangian Vs Basilisk

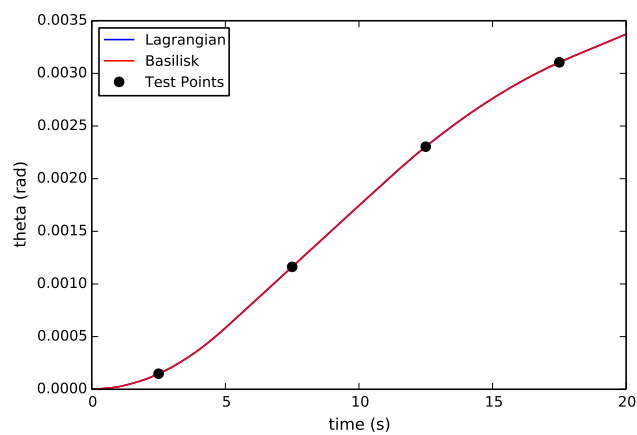


Figure 5.16: Theta Lagrangian Vs Basilisk

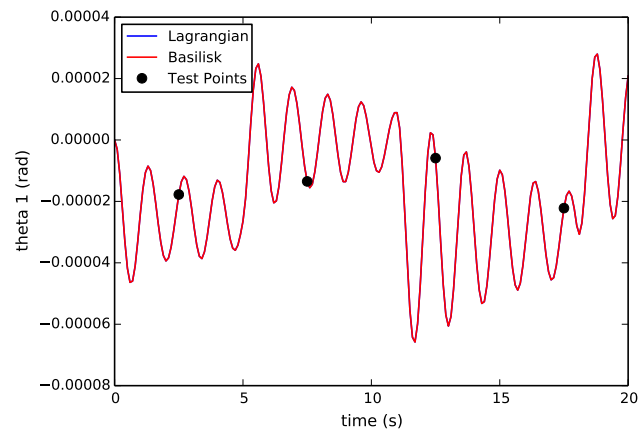


Figure 5.17: Theta 1 Position Lagrangian Vs Basilisk

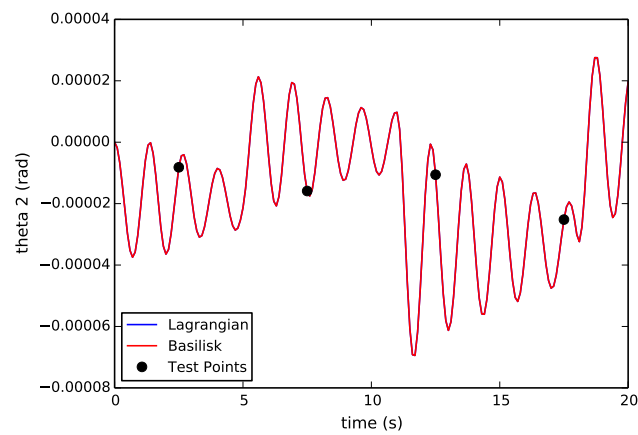


Figure 5.18: Theta 2 Lagrangian Vs Basilisk

5.1.3 ReactionWheelStateEffector

The `reactionWheelStateEffector` class is an instantiation of the `stateEffector` abstract class and is the model attempting to represent the dynamics of a reaction wheel. The reaction wheel can model both balanced reaction wheels, and imbalanced reaction wheels. This validation section goes over the expected functions, assumptions/limitations and a validation test.

5.1.3.1 Model Functions

This model is used to approximate the behavior of a reaction wheel. Below is a list of functions that this model performs:

- Compute it's contributions to the mass properties of the spacecraft
- Provides matrix contributions for the back substitution method
- Compute it's derivatives for θ and Ω
- Adds energy and momentum contributions to the spacecraft

5.1.3.2 Model Assumptions and Limitations

Below is a summary of the assumptions/limitations:

- The reaction wheel is considered a rigid body
- The spin axis is body fixed, therefore does not take into account bearing flexing
- For balanced wheels and simple jitter mode the mass properties of the reaction wheels are assumed to be included in the mass and inertia of the rigid body hub, therefore there is zero contributions to the mass properties from the reaction wheels in the dynamics call when the reaction wheels are balanced
- For fully-coupled imbalanced wheels mode the mass properties of the reaction wheels are assumed to not be included in the mass and inertia of the rigid body hub

- For balanced wheels mode the inertia matrix is assumed to be diagonal with one of its principle inertia axis equal to the spin axis, and the center of mass of the reaction wheel is coincident with the spin axis
- For fully-coupled imbalanced wheels the inertia off-diagonal terms, J_{12} and J_{23} are equal to zero and the remaining inertia off-diagonal term J_{13} is found through the setting of the dynamic imbalance parameter U_d : $J_{13} = U_d$. The center of mass offset, d , is found using the static imbalance parameter U_s : $d = \frac{U_s}{m_{rw}}$

5.1.3.3 Validation Calculation Scenario

The validation test for this scenario can be seen in Figure 5.19. This involves a rigid body hub connected to a reaction wheel with the spin axis being aligned with both the hub's center of mass and the reaction wheel's center of mass. This problem assumes the hub and reaction wheel are fixed to rotate about the the spin axis and so it is a two degree of freedom problem. The test sets up Basilisk so that the initial conditions constrain the spacecraft to rotate about the spin axis.

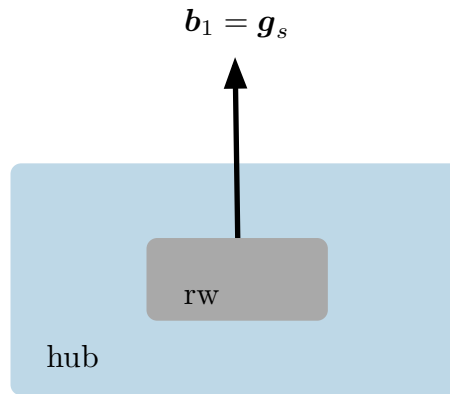


Figure 5.19: Schematic for validation example of reaction wheels

The analytical expressions for the angular velocity of the hub, ω_1 , the angle of the hub, θ and the reaction wheel speed, Ω are found in the below equations.

First, the angular momentum of the spacecraft is defined

$$H_{sc} = I_1\omega_1 + J_s(\omega_1 + \Omega) \quad (5.42)$$

and the corresponding inertial time derivative of H_{sc} is found in the following equation and set to zero since there are no external torques on the spacecraft:

$$\dot{H}_{sc} = I_1\dot{\omega}_1 + J_s(\dot{\omega}_1 + \dot{\Omega}) = 0 = (I_1 + J_s)\dot{\omega}_1 + J_s\dot{\Omega} \quad (5.43)$$

The same approach is completed for the reaction wheel, however, there is an internal torque, u_s :

$$H_{rw} = J_s(\omega_1 + \Omega) \quad (5.44)$$

$$\dot{H}_{rw} = J_s(\dot{\omega}_1 + \dot{\Omega}) = u_s \quad (5.45)$$

The equations of motion are placed into State Space Representation

$$\begin{bmatrix} (I_1 + J_s) & J_s \\ J_s & J_s \end{bmatrix} \begin{bmatrix} \dot{\omega}_1 \\ \dot{\Omega} \end{bmatrix} = \begin{bmatrix} 0 \\ u_s \end{bmatrix} \quad (5.46)$$

and the inverse of the left hand side matrix produces

$$\begin{bmatrix} \dot{\omega}_1 \\ \dot{\Omega} \end{bmatrix} = \begin{bmatrix} -\frac{u_s}{I_1} \\ \frac{(I_1 + J_s)u_s}{I_1 J_s} \end{bmatrix} \quad (5.47)$$

Equation (5.47) is set of linear differential equations that produce the following close form solutions for $\omega_1(t)$, $\theta(t)$ and $\Omega(t)$:

$$\omega_1(t) = -\frac{u_s}{I_1}t + \omega_0 \quad (5.48)$$

$$\theta(t) = -\frac{u_s}{2I_1}t^2 + \omega_0 t + \theta_0 \quad (5.49)$$

$$\Omega(t) = \frac{(I_1 + J_s)u_s}{I_1 J_s}t + \Omega_0 \quad (5.50)$$

The results seen in Figures 5.20-5.22 confirm that the analytical expressions agree with the Basilisk simulation and gives further validation in the software implementation of Basilisk.

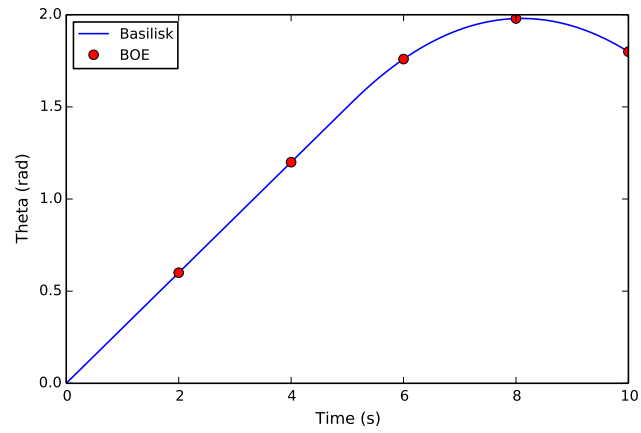


Figure 5.20: Reaction Wheel BOE Theta

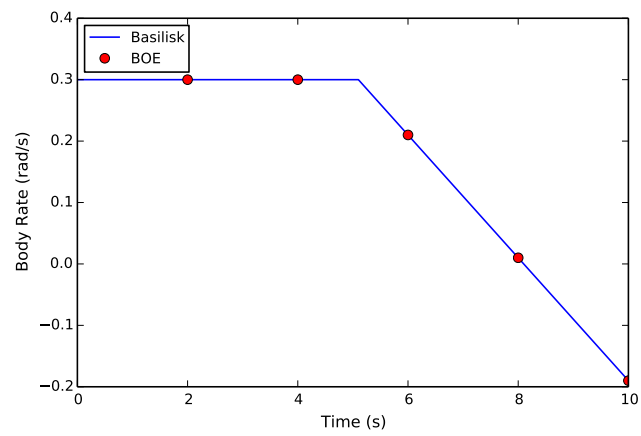


Figure 5.21: Reaction Wheel BOE Body Rate

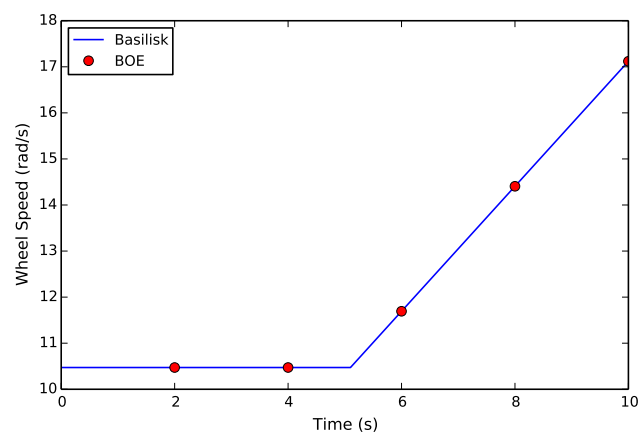


Figure 5.22: Reaction Wheel BOE RW Rate

5.2 Energy and Momentum Conservation Verification

The Basilisk astrodynamics software package was chosen as the implementation code base for the modular dynamics architecture. A key feature that Basilisk needed to retain was the ability to check energy and momentum conservation particularly for verification purposes. For a model to be verified, the model must conserve the four conservation quantities introduced in Section 2: orbital angular momentum, rotational angular momentum, orbital energy, and rotation energy, in the applicable scenarios. This verification process coupled with the validation process, gives confidence in both the analytical development and the software implementation of the equations. This section only gives two examples of the verification results for models: hinged rigid-bodies and the multi-spacecraft architecture. However, the verification results of the remaining models that have been introduced in this dissertation can be seen in the Appendix A. The importance verification tool cannot be stressed enough and is necessary for debugging and verifying software implementation.

5.2.1 Hinged Rigid-Bodies Verification

The scenario that is implemented to verify the conservation quantities for hinged rigid-bodies is a scenario where a spacecraft with two hinged rigid-bodies attached to it is placed into orbit around earth and has a non-zero initial angular velocity and non-zero deflected solar panels. No damping terms were included in this test. The results can be seen in Figure 5.23 and confirms that the hinged rigid-body model is conserving the four conservation quantities. This gives confidence in the analytical and software implementation of the EOMs.

5.2.2 Multiple Attached Spacecraft Verification

One scenario that is implemented to verify the conservation quantities for the multi-spacecraft architecture is a scenario where a spacecraft with one hinged rigid-body attached to it is docked to a spacecraft with no `stateEffectors` attached to it but is docked to another spacecraft with one

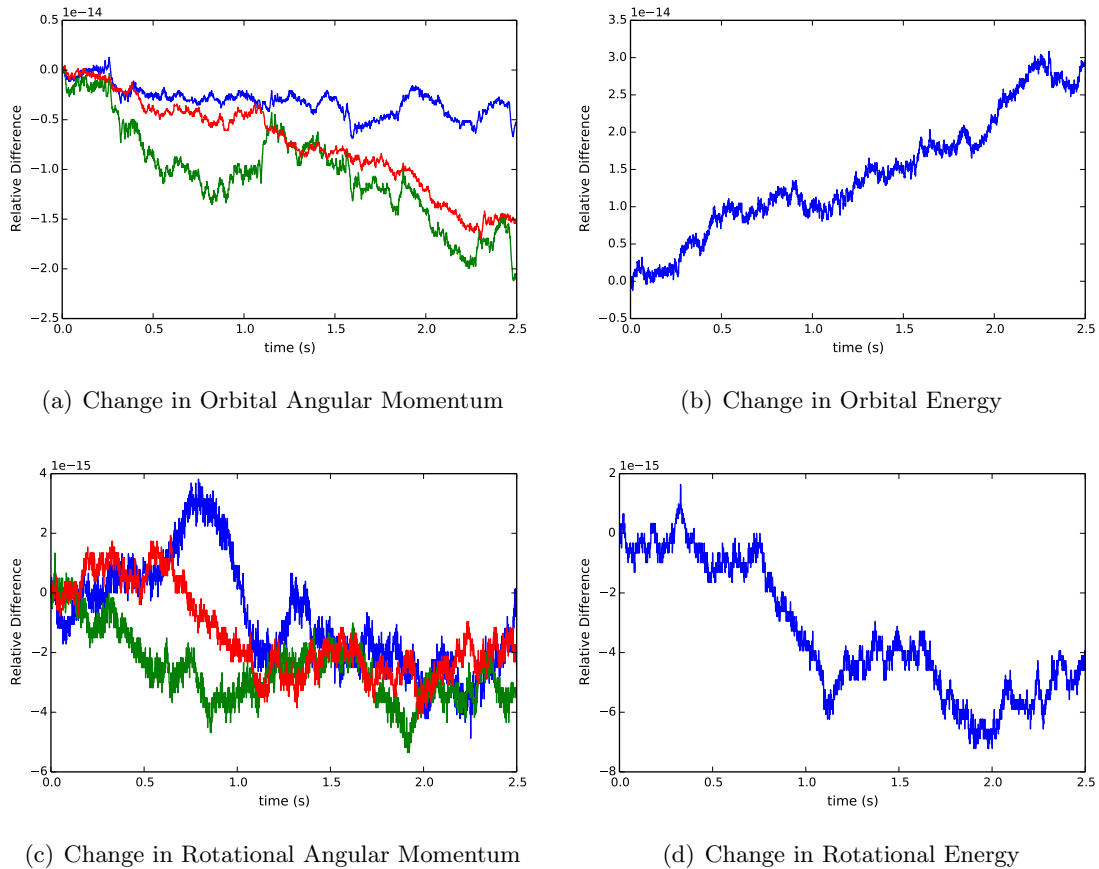
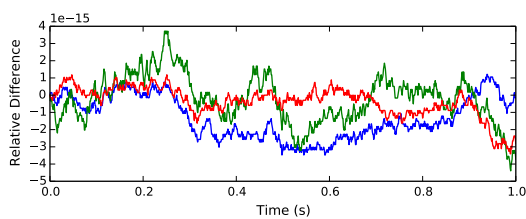
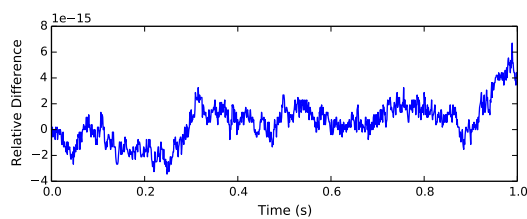


Figure 5.23: Simulation verification results for a rigid hub with two hinged panels

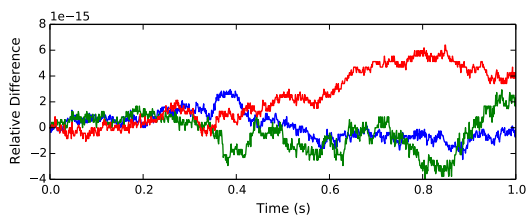
hinged rigid-body attached to it. The total spacecraft system is identical in mass properties the hinged rigid-body verification scenario. The spacecraft system is placed into orbit around earth and has a non-zero initial angular velocity and non-zero deflected solar panels. No damping terms were included in this test. The results can be seen in Figure 5.24 and confirms that the multi-spacecraft architecture is conserving the four conservation quantities. This gives confidence in the analytical and software implementation of the EOMs.



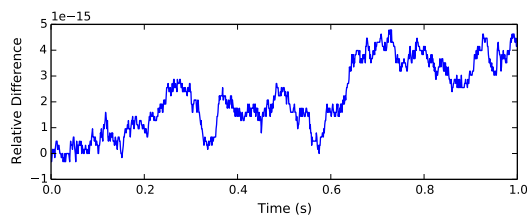
(a) Change in Orbital Angular Momentum



(b) Change in Orbital Energy



(c) Change in Rotational Angular Momentum



(d) Change in Rotational Energy

Figure 5.24: Simulation verification results for two spacecraft attached to the primary spacecraft with two solar panels attached

Chapter 6

Applications, Simulations and Results

6.1 Linearization and Stability Analysis

6.1.1 Introduction

Many spacecraft have appended solar panels or appended bodies that exhibit flexible behavior. Depending on the characteristics of the appended body, the effects due to this flexible phenomenon sometimes cannot be considered negligible. To quantify the closed-loop attitude pointing performance of these effects, a stability analysis can be performed. This will also show how the control system performs while taking the dynamical effect of flexing solar arrays into consideration.

Stability analysis has extensive history and there are many methods to analyze the stability of a system. When the system is linear, or can be linearized, there are classical techniques used to perform stability analysis which include but are not limited to Bode plots, Nyquist plots, Root Locus plots, and gain and phase margins [3, 97, 98]. When the system is nonlinear, there are techniques that can be used with Lyapunov theory to bound the stability of the system [97, 39]. Finally, if the system has multiple inputs and outputs, there are robustness stability analysis techniques such as Nyquist multiple input multiple output stability criteria and h -infinity stability analysis [99]. For this dissertation, the classical techniques are used because the equations of motion can be linearized well using some assumptions.

One task required to perform a stability analysis is developing the equations of motion that describe the system in consideration. In this case, the unique system under consideration is a

spacecraft with flexible solar arrays. One method is to develop the equations of motion considering the appended body as a Bernoulli beam or a continuous flexing structure [100, 40, 39]. Another method is to assume that the appended body is a rigid body but attached to the spacecraft through a torsional spring [41]. For this dissertation, the latter method is chosen because of the ease of linearizing the differential equations.

This dissertation aims to summarize methods that can be used to perform a stability analysis of a spacecraft with flexing solar arrays or appended bodies. The equations of motion are linearized, placed in state space representation, and converted to transfer functions. Then the classical stability analysis tools can be used. This dissertation is also comparing the linear stability analysis results to the full nonlinear simulation results to show the impact of the linearization process. The following section introduces the equations of motion of a spacecraft with flexing solar arrays.

6.1.2 Derivation of Equations

The frame and variable definitions used for the hinged rigid body EOMs development can be seen in Figure 6.1. Using these definitions, Newtonian/Eulerian mechanics [39, 40] and Kane's Method [8, 2] were used independently to derive the equations of motion. The equations of motion are introduced in Reference [41] and are repeated here for convenience. The compact, frame independent translational EOM for the hub was found and can be seen in Eq. (6.1) [41].

$$m_{sc}\ddot{\mathbf{r}}_{B/N} - m_{sc}[\tilde{\mathbf{c}}]\dot{\boldsymbol{\omega}}_{B/N} + \sum_{i=1}^{N_s} m_{sp_i} d_i \hat{\mathbf{s}}_{i,3} \ddot{\theta}_i = \mathbf{F}_{ext} - 2m_{sc}[\tilde{\boldsymbol{\omega}}_{B/N}]\mathbf{c}' - m_{sc}[\tilde{\boldsymbol{\omega}}_{B/N}][\tilde{\boldsymbol{\omega}}_{B/N}]\mathbf{c} - \sum_{i=1}^{N_s} m_{sp_i} d_i \dot{\theta}_i^2 \hat{\mathbf{s}}_{i,1} \quad (6.1)$$

Similarly the hub rotational EOM can be seen in the following equation[41]:

$$m_{sc}[\tilde{\mathbf{c}}]\ddot{\mathbf{r}}_{B/N} + [I_{sc,B}]\dot{\boldsymbol{\omega}}_{B/N} + \sum_i^{N_s} \left\{ I_{s_i,2} \hat{\mathbf{h}}_{i,2} + m_{sp_i} d_i [\tilde{\mathbf{r}}_{S_i/B}] \hat{\mathbf{s}}_{i,3} \right\} \ddot{\theta}_i = \mathbf{L}_B - [\tilde{\boldsymbol{\omega}}_{B/N}][I_{sc,B}]\boldsymbol{\omega}_{B/N} - [I'_{sc,B}]\boldsymbol{\omega}_{B/N} - \sum_i^{N_s} \left\{ \dot{\theta}_i [\tilde{\boldsymbol{\omega}}_{B/N}] \left(I_{s_i,2} \hat{\mathbf{h}}_{i,2} + m_{sp_i} d_i [\tilde{\mathbf{r}}_{S_i/B}] \hat{\mathbf{s}}_{i,3} \right) + m_{sp_i} d_i \dot{\theta}_i^2 [\tilde{\mathbf{r}}_{S_i/B}] \hat{\mathbf{s}}_{i,1} \right\} \quad (6.2)$$

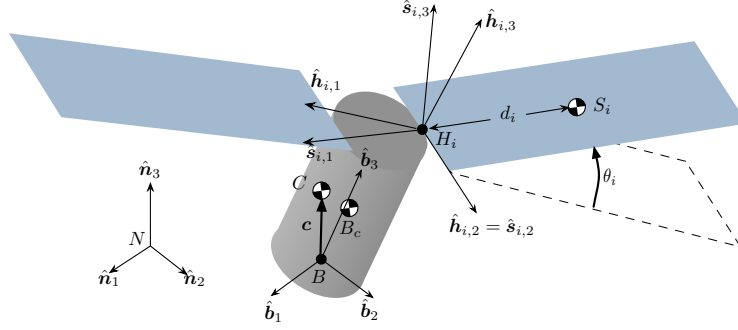


Figure 6.1: Hinged rigid bodies frame and variable definitions

Lastly, the hinged rigid body single degree of freedom differential equation can be seen in Eq. (6.3)[41].

$$\begin{aligned}
 m_{\text{sp}_i} d_i \hat{\mathbf{s}}_{i,3}^T \ddot{\mathbf{r}}_{B/N} + \left[(I_{s_{i,2}} + m_{\text{sp}_i} d_i^2) \hat{\mathbf{s}}_{i,2}^T - m_{\text{sp}_i} d_i \hat{\mathbf{s}}_{i,3}^T [\tilde{\mathbf{r}}_{H_i/B}] \right] \tilde{\boldsymbol{\omega}}_{B/N} \\
 + (I_{s_{i,2}} + m_{\text{sp}_i} d_i^2) \ddot{\theta}_i = -k_i \theta_i - c_i \dot{\theta}_i + \hat{\mathbf{s}}_{i,2}^T \boldsymbol{\tau}_{\text{ext}, H_i} + (I_{s_{i,3}} - I_{s_{i,1}} + m_{\text{sp}_i} d_i^2) \omega_{s_{i,3}} \omega_{s_{i,1}} \\
 - m_{\text{sp}_i} d_i \hat{\mathbf{s}}_{i,3}^T [\tilde{\boldsymbol{\omega}}_{B/N}] [\tilde{\boldsymbol{\omega}}_{B/N}] \mathbf{r}_{H_i/B} \quad (6.3)
 \end{aligned}$$

Eqs. (6.1)-(6.3) provides the $6+N_s$ EOMs required to describe the motion of the spacecraft with flexing appended bodies. Although these equations are general for N_s number of solar panels, for this dissertation the number of appended solar panels will be $N_s = 2$. These equations need to be linearized to use classical stability analysis techniques, and this is performed in the following section.

6.1.2.1 Linearization

To complete a stability analysis using classical techniques, these equations need to be linearized. One of the first steps of the linearization process is assuming the translational and rotational EOMs are decoupled. Looking at Eqs. (6.1) and (6.2), it shows that this coupling comes through the offset vector, \mathbf{c} , between the body frame origin and the center of mass of the spacecraft. Therefore, throughout the remainder of this work, the body frame origin and the center of mass of the spacecraft will be assumed to be coincident. This is a good assumption when the body frame origin is placed at the equilibrium position of the center of mass of the spacecraft, and when the

flexing solar arrays do not change the center of mass location by a substantial amount. For the remainder of this analysis, the cross coupling between the translation and rotational motion is ignored and the translational equation, Eq (6.1), will not be used. Next, it is assumed that nonlinear and other higher order terms are dropped from the rotational equation:

$$\begin{aligned}
 & \cancel{m_{sc}[\tilde{\mathbf{c}}]\ddot{\mathbf{r}}_{B/N}} + [I_{sc,B}]\dot{\boldsymbol{\omega}}_{B/N} + \sum_{i=1}^{N_S} \left\{ I_{s_{i,2}}\hat{\mathbf{s}}_{i,2} + m_{sp_i}d_i[\tilde{\mathbf{r}}_{S_{c,i}/B}]\hat{\mathbf{s}}_{i,3} \right\} \ddot{\theta}_i = \\
 & \cancel{[\tilde{\boldsymbol{\omega}}_{B/N}][I_{sc,B}]\dot{\boldsymbol{\omega}}_{B/N} - [I'_{sc,B}]\dot{\boldsymbol{\omega}}_{B/N} - \sum_{i=1}^{N_S} \left\{ \dot{\theta}_i[\tilde{\boldsymbol{\omega}}_{B/N}] \left(I_{s_{i,2}}\hat{\mathbf{s}}_{i,2} + m_{sp_i}d_i[\tilde{\mathbf{r}}_{S_{c,i}/B}]\hat{\mathbf{s}}_{i,3} \right) \right.} \\
 & \left. + m_{sp_i}d_i\dot{\theta}_i^2[\tilde{\mathbf{r}}_{S_{c,i}/B}]\hat{\mathbf{s}}_{i,1} \right\} + \mathbf{L}_B \quad (6.4)
 \end{aligned}$$

This simplification results in:

$$[I_{sc,B}]\dot{\boldsymbol{\omega}}_{B/N} + \sum_{i=1}^{N_S} \left\{ I_{s_{i,2}}\hat{\mathbf{s}}_{i,2} + m_{sp_i}d_i[\tilde{\mathbf{r}}_{S_{c,i}/B}]\hat{\mathbf{s}}_{i,3} \right\} \ddot{\theta}_i = \mathbf{L}_B \quad (6.5)$$

Following the same linearization techniques for the flex equation, Eq. (6.3) simplifies to:

$$\begin{aligned}
 & \cancel{m_{sp_i}d_i\hat{\mathbf{s}}_{i,3}^T\ddot{\mathbf{r}}_{B/N}} + \left[(I_{s_{i,2}} + m_{sp_i}d_i^2)\hat{\mathbf{s}}_{i,2}^T - m_{sp_i}d_i\hat{\mathbf{s}}_{i,3}^T[\tilde{\mathbf{r}}_{H_i/B}] \right] \dot{\boldsymbol{\omega}}_{B/N} + (I_{s_{i,2}} + m_{sp_i}d_i^2)\ddot{\theta}_i \\
 & = -k_i\theta_i - c_i\dot{\theta}_i + \cancel{\hat{\mathbf{s}}_{i,2} \cdot \boldsymbol{\tau}_{ext,H_i}} + \cancel{(I_{s_{i,3}} - I_{s_{i,1}} + m_{sp_i}d_i^2)\omega_{s_{i,3}}\omega_{s_{i,1}}} \\
 & \quad - \cancel{m_{sp_i}d_i\hat{\mathbf{s}}_{i,3}^T[\tilde{\boldsymbol{\omega}}_{B/N}][\tilde{\boldsymbol{\omega}}_{B/N}]\mathbf{r}_{H_i/B}} \quad (6.6)
 \end{aligned}$$

leading to the following linear relationship:

$$\left[(I_{s_{i,2}} + m_{sp_i}d_i^2)\hat{\mathbf{s}}_{i,2}^T - m_{sp_i}d_i\hat{\mathbf{s}}_{i,3}^T[\tilde{\mathbf{r}}_{H_i/B}] \right] \dot{\boldsymbol{\omega}}_{B/N} + (I_{s_{i,2}} + m_{sp_i}d_i^2)\ddot{\theta}_i = -k_i\theta_i - c_i\dot{\theta}_i \quad (6.7)$$

In Eq. (6.7), k_i is the torsional spring constant and c_i is the torsional damping term. Now the nonlinear coupled equations of motion have been linearized to Eqs. (6.5) and (6.7) and linear stability analysis techniques can be used.

6.1.2.2 State Space Representation

A convenient form to place the equations of motion into is a form called state space representation [3]. This form will allow for the classical stability analysis techniques to be used easily while

leveraging linear algebra techniques. Since the dynamics are second order differential equations, the associated kinematic differential equations need to be introduced. Modified Rodrigues Parameters (MRPs) are chosen for the attitude parameterization set and the associated MRP differential kinematic equations of motion are given by [39]

$$\dot{\boldsymbol{\sigma}}_{B/N} = \frac{1}{4}[B(\boldsymbol{\sigma}_{B/N})]^\mathcal{B}\boldsymbol{\omega}_{B/N} \quad (6.8)$$

However, these equations also need to be linearized seen in the following equation:

$$\dot{\boldsymbol{\sigma}}_{B/N} = \frac{1}{4}\mathcal{B}\boldsymbol{\omega}_{B/N} \quad (6.9)$$

The linear approximation range for MRPs is with principal rotation up to about 120 degrees. The other kinematic differential equation for the hinged rigid bodies is trivial:

$$\dot{\theta}_i = \frac{d}{dt}(\theta_i) \quad (6.10)$$

To simplify these examples to a two dimensional case, let's assume that the solar array hinge axes are directed along the $\hat{\mathbf{b}}_1$ axis, and also assume that spacecraft is constrained to rotate only about the $\hat{\mathbf{b}}_1$ axis. Since the equations are linearized and decoupled, the flexing modes only show up in the $\hat{\mathbf{b}}_1$ axis so this is a good approximation. Additionally, the equilibrium direction $\hat{\mathbf{s}}_1$ for the first solar panel is assumed to be directed along $\hat{\mathbf{b}}_2$, and the equilibrium direction $\hat{\mathbf{s}}_1$ for the second solar panel is assumed to be directed along $-\hat{\mathbf{b}}_2$. This drastically reduces the complexity of the problem. Now the equations are placed into state space representation and yields the following state vector:

$$\mathbf{X} = \left[\sigma_1 \quad \omega_1 \quad \theta_1 \quad \dot{\theta}_1 \quad \theta_2 \quad \dot{\theta}_2 \right]^T \quad (6.11)$$

where σ_1 is the first MRP coordinate and ω_1 is the first body frame component of $\boldsymbol{\omega}_{B/N}$. The following state space form is used[3]:

$$[M]\dot{\mathbf{X}} = [A]\mathbf{X} + [B]\mathbf{u} \quad (6.12)$$

In most cases, the left hand side of the equation is comprised only of the state vector derivative so the following manipulation was completed:

$$\dot{\mathbf{X}} = [M]^{-1}[A]\mathbf{X} + [M]^{-1}[B]\mathbf{u} \quad (6.13)$$

Eqs. (6.5), (6.7), (6.9), and (6.10) are converted into the state space representation matrices beginning with matrix $[M]$:

$$\begin{bmatrix} 1 & 0 & 0 & 0 & 0 & 0 \\ 0 & I_{11} & 0 & -I_{sp,2} - m_{sp}dd_{S_c/B} & 0 & I_{sp,2} + m_{sp}dd_{S_c/B} \\ 0 & 0 & 1 & 0 & 0 & 0 \\ 0 & -(I_{sp,2} + m_{sp}d^2) - m_{sp}dd_{H/B} & 0 & I_{sp,2} + m_{sp}d^2 & 0 & 0 \\ 0 & 0 & 0 & 0 & 1 & 0 \\ 0 & (I_{sp,2} + m_{sp}d^2) + m_{sp}dd_{H/B} & 0 & 0 & 0 & I_{sp,2} + m_{sp}d^2 \end{bmatrix} \quad (6.14)$$

where $I_{sp,2}$ is the inertia of the solar panel about its second solar panel axis seen in Figure 6.1, I_{11} is the inertia of the rigid body hub about the first body axis, $d_{S_c/B}$ is the distance between the body frame origin and the solar panels center of mass, and $d_{H/B}$ is the distance between the body frame origin and the hinge location. Next, matrices $[A]$, $[B]$ and \mathbf{u} are defined:

$$[A] = \begin{bmatrix} 0 & 0.25 & 0 & 0 & 0 & 0 \\ 0 & 0 & 0 & 0 & 0 & 0 \\ 0 & 0 & 0 & 1 & 0 & 0 \\ 0 & 0 & -k & -c & 0 & 0 \\ 0 & 0 & 0 & 0 & 1 & 0 \\ 0 & 0 & 0 & 0 & -k & -c \end{bmatrix} \quad (6.15)$$

$$[B] = \begin{bmatrix} 0 & 1 & 0 & 0 & 0 & 0 \end{bmatrix}^T \quad (6.16)$$

$$\mathbf{u} = [\tau_1] \quad (6.17)$$

where τ_1 is the control torque applied about the first body frame axis, $\hat{\mathbf{b}}_1$.

Next, the output equation is defined in the following equation:

$$\mathbf{Y} = [C]\mathbf{X} + [D]\mathbf{u} = \begin{bmatrix} \sigma_1 & \omega_1 & \theta_1 & \dot{\theta}_1 & \theta_2 & \dot{\theta}_2 \end{bmatrix}^T \quad (6.18)$$

with $[C]$ and $[D]$ defined as

$$[C] = \begin{bmatrix} 1 & 0 & 0 & 0 & 0 & 0 \\ 0 & 1 & 0 & 0 & 0 & 0 \\ 0 & 0 & 1 & 0 & 0 & 0 \\ 0 & 0 & 0 & 1 & 0 & 0 \\ 0 & 0 & 0 & 0 & 1 & 0 \\ 0 & 0 & 0 & 0 & 0 & 1 \end{bmatrix} \quad (6.19)$$

$$[D] = \begin{bmatrix} 0 & 0 & 0 & 0 & 0 & 0 \end{bmatrix}^T \quad (6.20)$$

The output equation is meant to include all of the outputs so that when the equations are converted to transfer functions, eigenvalues can be computed on the resulting matrices.

It should be noted that the matrices included above are the continuous time representation of the system. The system can be converted to a discrete time representation by either using a software package or the analytical conversion. This conversion is not discussed in this document.

Now that the state space representation has been defined (the open loop portion), the closed loop definition of this problem is defined in the next section.

6.1.2.3 Closed Loop State Space Representation

First, the feedback definition for the control in the state space form is defined in the following equation[3].

$$\mathbf{u} = -[K](\mathbf{X} - \mathbf{X}_{\text{ref}}) = \tau_1 \quad (6.21)$$

Where $[K]$ is the gain matrix. The gain matrix chosen for this dissertation is[39]:

$$[K] = \begin{bmatrix} K_1 P - 0.25 K_1^2 I_{11} & P & 0 & 0 & 0 & 0 \end{bmatrix} \quad (6.22)$$

If there is an integral term for σ_1 , then the gain that is associated with $\int \sigma_1$ is $K_I K_1$. This addition can easily be applied to the state space representation since the time derivative of $\int \sigma$ is σ .

Finally, to complete the closed loop state space representation, the following equations are needed:

$$\dot{\mathbf{X}} = [M]^{-1}[A]\mathbf{X} - [M]^{-1}[B][K]\mathbf{X} + [B][K]\mathbf{X}_{\text{ref}} \quad (6.23)$$

$$\dot{\mathbf{X}} = [M]^{-1}([A] - [B][K])\mathbf{X} + [B][K]\mathbf{X}_{\text{ref}} \quad (6.24)$$

The state space representation for both the open loop and closed loop systems are useful for simulating the linear response, and converting to the frequency domain space for completing a phase and gain margin analysis. The following section will summarize the techniques used for converting the between state space and the frequency domain.

6.1.2.4 State Space to Transfer Function Conversion

The following equation is used to convert from the time domain to the frequency domain:

$$[G(s)] = [C](s[I] - [A])[B] \quad (6.25)$$

Where $[G(s)]$ is the transfer function matrix and s is the frequency. where each element corresponds the transfer function that relates an input to an output. This method can be used to find both the open loop and closed loop transfer function matrices using the corresponding $[A]$ and $[B]$ matrices, depending on which form.

However, another way to convert from the time domain to the frequency domain is to use the following two equations:

$$[G(s)]_{OL} = [C](s[I] - [A])[B][K] \quad (6.26)$$

$$[G(s)]_{CL} = \frac{[G(s)]_{OL}}{I + [G(s)]_{OL}} \quad (6.27)$$

Where the subscripts OL and CL are corresponding to open loop and closed loop respectively. Now all of the equations of motion have been developed to perform a phase and gain analysis on the system.

6.1.3 Results

This section uses the stability analysis tools on specific examples to highlight the effects of flexing solar arrays on the stability of the spacecraft. The following table summarizes the physical parameters used for the results in this section. There are two solar panels attached to the spacecraft and they have the same physical parameters seen in Table 6.1.

Table 6.1: Spacecraft parameters for stability analysis

Name	Description	Value	Units
I_{11}	Rigid body hub inertia about \hat{b}_1 axis	500.0	kg-m ²
$I_{sp,2}$	Inertia of solar panel about \hat{s}_2 axis	100	kg-m ²
m_{sp}	mass of solar panel	30	kg
d	distance from hinge location to CoM of solar panel	1.5	m
$d_{H/B}$	distance from body frame location to hinge location	1	m
$d_{S_c/B}$	distance from body frame location to CoM of solar panel	1	m
k	spring constant	1200	N-m/rad
c	damping constant	9	N-m-s/rad

6.1.3.1 Open Loop Stability Analysis Results

In general, an uncontrolled spacecraft is typically considered marginally stable, unless there is some form of passive stability like gravity gradient. In our case, the spacecraft can be assumed to be marginally stable, meaning that the dynamics matrix has values of zero for the pole locations and if the system is perturbed by a step response, the spacecraft will just drift at a constant angular speed.

For this open loop stability analysis, a bode plot is created for three different control gains. These three scenarios are used to show the performance and robustness of the control system with different gains.

The control gains used for each scenario is summarized in Table 6.2. Figures 6.2-6.4 show the results from the bode plots for the open loop system for each set of control gains. These are the

Table 6.2: Gain descriptions for the three scenarios for stability analysis

Scenario	K_1	K_I	P
Scenario 1	0.15	0.0	100
Scenario 2	0.5	0.0	600
Scenario 3	3	25	175

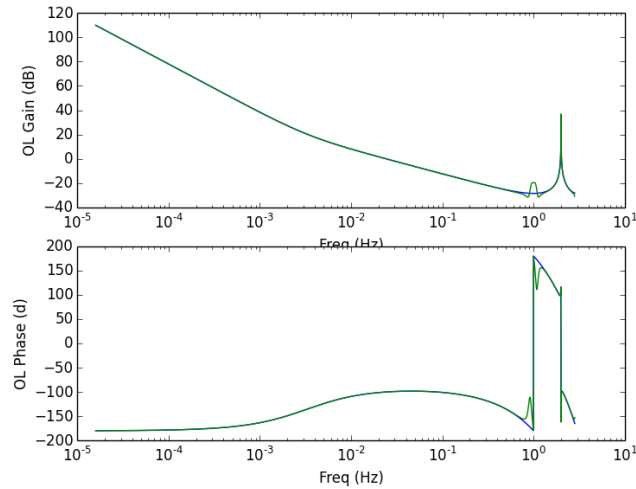


Figure 6.2: Open loop bode plot for Scenario 1 gains (blue is rigid response, green is flexible body response)

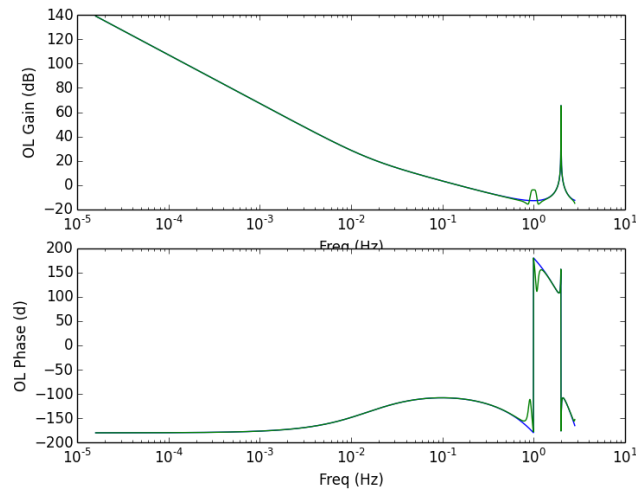


Figure 6.3: Open loop bode plot for Scenario 2 gains

discrete-time systems - with the control frequency set to 2 Hz. The open loop bode plot is useful

because it gives insight into how much the system is close to an instability region. Quantitatively, these values are the gain and phase margins. Using the open loop bode plots the gain and phase margin for each mode was found and can be seen Table 6.3. It should be noted that both the rigid body response and the flexible response is plotted on the bode plots. The green curve is the flexible system response, and blue curve is the rigid body response. There is good agreement between the rigid body and flexible system response at most all frequencies except for close to the frequency of the solar arrays. The solar arrays first mode frequency is at 0.9 Hz, and there is a noticeable difference between the rigid body and flexible system response. However, from the open loop analysis, this does not greatly impact performance.

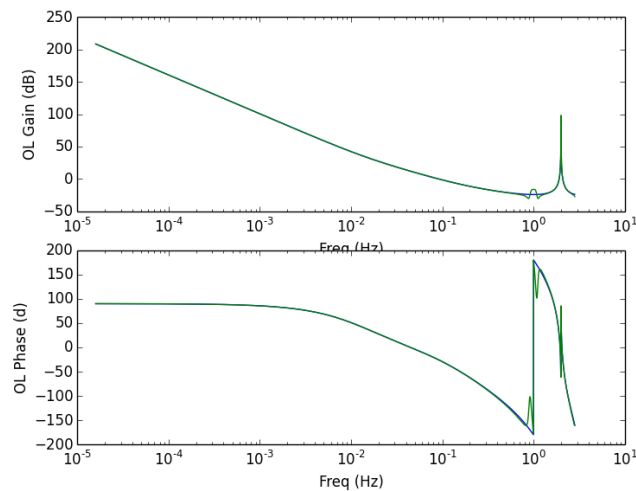


Figure 6.4: Open loop bode plot for Scenario 3 gains

Table 6.3: Gain and phase margins for each scenario

Scenario	Gain (db)	Phase (deg)
Scenario 1	28	81
Scenario 2	12	72
Scenario 3	2.8	153

6.1.3.2 Closed Loop Stability Analysis Results

The closed loop stability analysis is useful for looking at the closed loop performance, the steady state response of the system, and how well the system will track a frequency response over a frequency range. This is particularly useful in systems like this one that are marginally stable, because the system will always be closed loop to elicit the desired control response. Using the analytical development for converting the open loop to a closed loop system and converting the continuous time state space model to the frequency a bode plot analysis was performed. A bode plot was created for each set of control gains. The results from this analysis can be seen in Figures 6.5- 6.7. It should be noted that again the rigid body response curve is in blue, and the green curve is flexible body response. Additionally, simulation results using the Basilisk astrodynamics software package can be seen in Figs. 6.5- 6.7 labeled with the red hash marks. The Basilisk simulation results use the full nonlinear equations of motion. The reason for doing this is to show the agreement between the analytical frequency domain response using the linearized equations and the numerical results from the full nonlinear equations simulation.

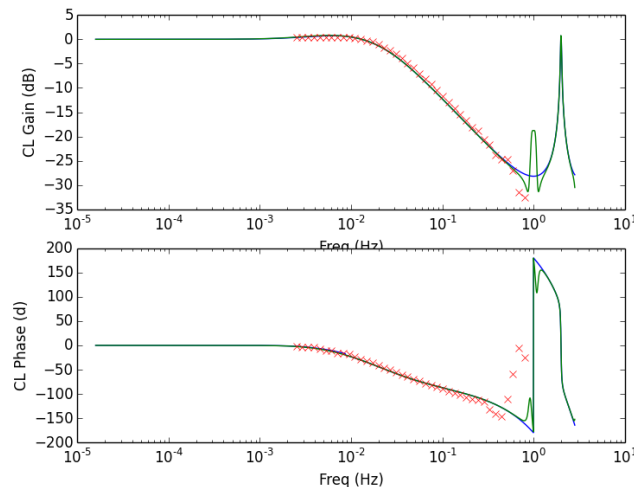


Figure 6.5: Closed loop bode plot for Scenario 1 gains

The results show that the system tracks very well at low frequencies and at high frequencies the performance degrades but the system does not go unstable. Additionally, the numerical sim-

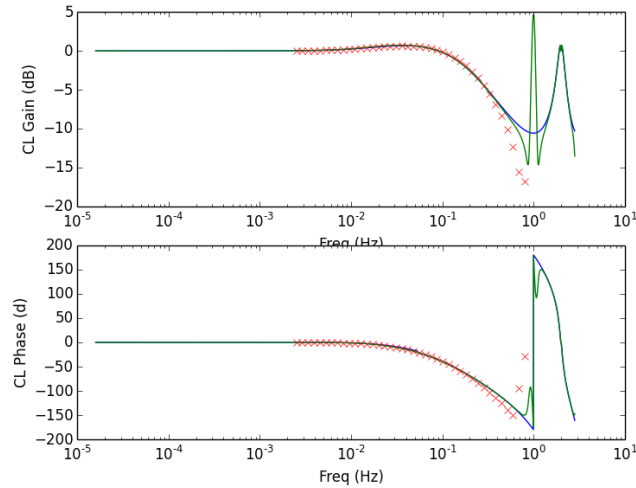


Figure 6.6: Closed loop bode plot for Scenario 2 gains

ulation agrees well with the analytical development, and the flexible dynamics better models the system response than the rigid body response. The spikes in the bode plots that are near the solar array frequency (0.9 Hz) and the Nyquist frequency (1 Hz) are due to the flexible dynamics and the degradation of performance while nearing a Nyquist frequency. Further analysis will be completed in this region, and to see why there is some disagreement between the numerical simulation and the analytical frequency response at these frequencies. However, the results are promising and give confidence in the control gains selected.

6.1.4 Conclusion

This dissertation summarizes some analytical tools that can be used to perform stability analysis of spacecraft with flexing solar arrays using classical methods like Bode plot and gain and phase margins. The stability analysis results include a comparison between rigid body stability analysis and the proposed method. The results highlight the difference between the two and show why this can be important to include in stability studies. Additionally, the linearized stability analysis is compared to the full non-linear equations of motion stability results and these show good agreement. However, there is some disagreement as the results got closer to the solar array

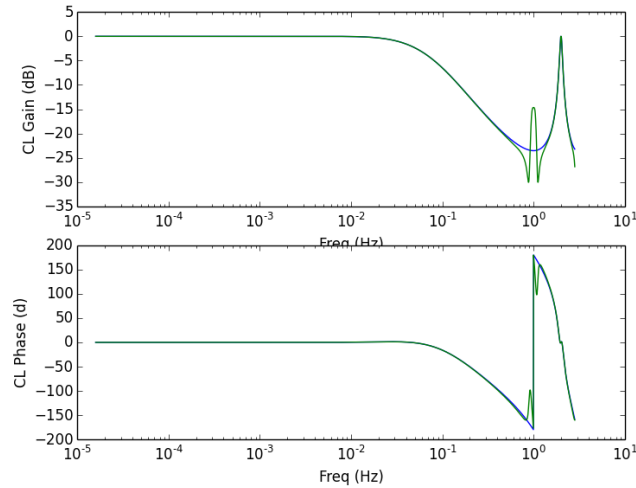


Figure 6.7: Closed loop bode plot for Scenario 3 gains

frequency and the Nyquist frequency. Further investigation needs to be completed to fully quantify the reason for this discrepancy.

6.2 Force and Torque Calculation Example

This section gives an example of how the provided equations of motion in Section 3 could be used to calculate the force and torque that is being imparted on the spacecraft from the considered model. For example, it might be important to know the torque being applied by appended solar panels to ensure that the torque is not exceeding the yield strength of the hinge. Or another example would be it might be helpful to know the time history of the force and torque that fuel slosh is applying to the spacecraft to compare that to experimental data provided by a fuel tank manufacturer.

In this section, the force and torque calculations are shown for hinged rigid bodies and fuel slosh but this methodology could be extended to all of the dynamics models included in this dissertation or other models using the same generalized EOM form.

6.2.1 Force on Spacecraft from Hinged Rigid Bodies and Fuel Slosh

This is the translational EOM for the spacecraft with hinged rigid bodies and fuel slosh:

$$\begin{aligned} \ddot{\mathbf{r}}_{B/N} - [\tilde{\mathbf{c}}]\dot{\boldsymbol{\omega}}_{B/N} + \frac{1}{m_{sc}} \sum_{i=1}^{N_S} m_{sp_i} d_i \hat{\mathbf{s}}_{i,3} \ddot{\theta}_i + \frac{1}{m_{sc}} \sum_{j=1}^{N_P} m_j \hat{\mathbf{p}}_j \ddot{\rho}_j = \ddot{\mathbf{r}}_{C/N} - 2[\tilde{\boldsymbol{\omega}}_{B/N}]\mathbf{c}' \\ - [\tilde{\boldsymbol{\omega}}_{B/N}][\tilde{\boldsymbol{\omega}}_{B/N}]\mathbf{c} - \frac{1}{m_{sc}} \sum_{i=1}^{N_S} m_{sp_i} d_i \dot{\theta}_i^2 \hat{\mathbf{s}}_{i,1} \end{aligned} \quad (6.28)$$

To find the force and torque that each state effector places on the body, both sides of the equation is multiplied by m_{sc} .

$$\begin{aligned} m_{sc} \ddot{\mathbf{r}}_{B/N} - m_{sc} [\tilde{\mathbf{c}}]\dot{\boldsymbol{\omega}}_{B/N} + \sum_{i=1}^{N_S} m_{sp_i} d_i \hat{\mathbf{s}}_{i,3} \ddot{\theta}_i + \sum_{j=1}^{N_P} m_j \hat{\mathbf{p}}_j \ddot{\rho}_j = m_{sc} \ddot{\mathbf{r}}_{C/N} - 2m_{sc} [\tilde{\boldsymbol{\omega}}_{B/N}]\mathbf{c}' \\ - m_{sc} [\tilde{\boldsymbol{\omega}}_{B/N}][\tilde{\boldsymbol{\omega}}_{B/N}]\mathbf{c} - \sum_{i=1}^{N_S} m_{sp_i} d_i \dot{\theta}_i^2 \hat{\mathbf{s}}_{i,1} \end{aligned} \quad (6.29)$$

Influences due to the state effectors are moved to the right-hand side of the equation:

$$\begin{aligned} m_{sc} \ddot{\mathbf{r}}_{B/N} - m_{sc} [\tilde{\mathbf{c}}]\dot{\boldsymbol{\omega}}_{B/N} = \mathbf{F}_{ext} - 2m_{sc} [\tilde{\boldsymbol{\omega}}_{B/N}]\mathbf{c}' \\ - m_{sc} [\tilde{\boldsymbol{\omega}}_{B/N}][\tilde{\boldsymbol{\omega}}_{B/N}]\mathbf{c} - \sum_{i=1}^{N_S} \left(m_{sp_i} d_i \hat{\mathbf{s}}_{i,3} \ddot{\theta}_i + m_{sp_i} d_i \dot{\theta}_i^2 \hat{\mathbf{s}}_{i,1} \right) - \sum_{j=1}^{N_P} m_j \hat{\mathbf{p}}_j \ddot{\rho}_j \end{aligned} \quad (6.30)$$

Also \mathbf{c}' is moved over to the right hand side:

$$\begin{aligned} m_{sc} \ddot{\mathbf{r}}_{B/N} - m_{sc} [\tilde{\mathbf{c}}]\dot{\boldsymbol{\omega}}_{B/N} = \mathbf{F}_{ext} - m_{sc} [\tilde{\boldsymbol{\omega}}_{B/N}][\tilde{\boldsymbol{\omega}}_{B/N}]\mathbf{c} \\ - \sum_{i=1}^{N_S} \left(m_{sp_i} d_i \hat{\mathbf{s}}_{i,3} \ddot{\theta}_i + m_{sp_i} d_i \dot{\theta}_i^2 \hat{\mathbf{s}}_{i,1} + 2[\tilde{\boldsymbol{\omega}}_{B/N}]m_{sp_i} d_i \dot{\theta}_i \hat{\mathbf{s}}_{i,3} \right) - \sum_{j=1}^{N_P} \left(m_j \hat{\mathbf{p}}_j \ddot{\rho}_j + 2[\tilde{\boldsymbol{\omega}}_{B/N}]m_j \dot{\rho}_j \hat{\mathbf{p}}_j \right) \end{aligned} \quad (6.31)$$

The force that each effector place on the spacecraft are as follows:

$$\mathbf{F}_\theta = - \left(m_{sp_i} d_i \hat{\mathbf{s}}_{i,3} \ddot{\theta}_i + m_{sp_i} d_i \dot{\theta}_i^2 \hat{\mathbf{s}}_{i,1} + 2[\tilde{\boldsymbol{\omega}}_{B/N}]m_{sp_i} d_i \dot{\theta}_i \hat{\mathbf{s}}_{i,3} \right) \quad (6.32)$$

$$\mathbf{F}_\rho = - \left(m_j \hat{\mathbf{p}}_j \ddot{\rho}_j + 2[\tilde{\boldsymbol{\omega}}_{B/N}]m_j \dot{\rho}_j \hat{\mathbf{p}}_j \right) \quad (6.33)$$

6.2.2 Torque on Spacecraft from Hinged Rigid Bodies and Fuel Slosh

The next step is to find the torque that each state effector is applying to the body. Here is the rotational EOM with hinged rigid bodies and fuel slosh:

$$\begin{aligned}
m_{sc}[\tilde{\mathbf{c}}]\ddot{\mathbf{r}}_{B/N} + [I_{sc,B}]\dot{\boldsymbol{\omega}}_{B/N} + \sum_{i=1}^{N_S} \left\{ I_{s_{i,2}}\hat{\mathbf{s}}_{i,2} + m_{sp_i}d_i[\tilde{\mathbf{r}}_{S_{c,i}/B}]\hat{\mathbf{s}}_{i,3} \right\} \ddot{\theta}_i + \sum_{j=1}^{N_P} m_j[\tilde{\mathbf{r}}_{P_{c,j}/B}]\hat{\mathbf{p}}_j\ddot{\rho}_j = \\
- [\tilde{\boldsymbol{\omega}}_{B/N}][I_{sc,B}]\boldsymbol{\omega}_{B/N} - [I'_{sc,B}]\boldsymbol{\omega}_{B/N} - \sum_{i=1}^{N_S} \left\{ \dot{\theta}_i[\tilde{\boldsymbol{\omega}}_{B/N}] \left(I_{s_{i,2}}\hat{\mathbf{s}}_{i,2} + m_{sp_i}d_i[\tilde{\mathbf{r}}_{S_{c,i}/B}]\hat{\mathbf{s}}_{i,3} \right) \right. \\
\left. + m_{sp_i}d_i\dot{\theta}_i^2[\tilde{\mathbf{r}}_{S_{c,i}/B}]\hat{\mathbf{s}}_{i,1} \right\} - \sum_{j=1}^{N_P} m_j[\tilde{\boldsymbol{\omega}}_{B/N}][\tilde{\mathbf{r}}_{P_{c,j}/B}]\mathbf{r}'_{P_{c,j}/B} + \mathbf{L}_B \quad (6.34)
\end{aligned}$$

The dynamical effects from the state effectors are moved to the right hand side of the equation:

$$\begin{aligned}
m_{sc}[\tilde{\mathbf{c}}]\ddot{\mathbf{r}}_{B/N} + [I_{sc,B}]\dot{\boldsymbol{\omega}}_{B/N} = -[\tilde{\boldsymbol{\omega}}_{B/N}][I_{sc,B}]\boldsymbol{\omega}_{B/N} \\
- \sum_{i=1}^{N_S} \left\{ \left(I_{s_{i,2}}\hat{\mathbf{s}}_{i,2} + m_{sp_i}d_i[\tilde{\mathbf{r}}_{S_{c,i}/B}]\hat{\mathbf{s}}_{i,3} \right) \ddot{\theta}_i + \left[[I'_{sp_i,S_{c,i}}] - m_{sp_i} \left([\tilde{\mathbf{r}}'_{S_{c,i}/B}][\tilde{\mathbf{r}}_{S_{c,i}/B}] + [\tilde{\mathbf{r}}_{S_{c,i}/B}][\tilde{\mathbf{r}}'_{S_{c,i}/B}] \right) \right] \boldsymbol{\omega}_{B/N} \right. \\
\left. + \dot{\theta}_i[\tilde{\boldsymbol{\omega}}_{B/N}] \left(I_{s_{i,2}}\hat{\mathbf{s}}_{i,2} + m_{sp_i}d_i[\tilde{\mathbf{r}}_{S_{c,i}/B}]\hat{\mathbf{s}}_{i,3} \right) + m_{sp_i}d_i\dot{\theta}_i^2[\tilde{\mathbf{r}}_{S_{c,i}/B}]\hat{\mathbf{s}}_{i,1} \right\} \\
- \sum_{j=1}^{N_P} \left(m_j[\tilde{\mathbf{r}}_{P_{c,j}/B}]\hat{\mathbf{p}}_j\ddot{\rho}_j + m_j[\tilde{\boldsymbol{\omega}}_{B/N}][\tilde{\mathbf{r}}_{P_{c,j}/B}]\mathbf{r}'_{P_{c,j}/B} - m_j \left([\tilde{\mathbf{r}}'_{P_{c,j}/B}][\tilde{\mathbf{r}}_{P_{c,j}/B}] \right. \right. \\
\left. \left. + [\tilde{\mathbf{r}}_{P_{c,j}/B}][\tilde{\mathbf{r}}'_{P_{c,j}/B}] \right) \boldsymbol{\omega}_{B/N} \right) + \mathbf{L}_B \quad (6.35)
\end{aligned}$$

The torque that each effector places on the spacecraft about point B and point C are as follows:

$$\begin{aligned}
\boldsymbol{\tau}_{\theta,B} = - \left\{ \left(I_{s_{i,2}}\hat{\mathbf{s}}_{i,2} + m_{sp_i}d_i[\tilde{\mathbf{r}}_{S_{c,i}/B}]\hat{\mathbf{s}}_{i,3} \right) \ddot{\theta}_i + \left[[I'_{sp_i,S_{c,i}}] - m_{sp_i} \left([\tilde{\mathbf{r}}'_{S_{c,i}/B}][\tilde{\mathbf{r}}_{S_{c,i}/B}] \right. \right. \right. \\
\left. \left. + [\tilde{\mathbf{r}}_{S_{c,i}/B}][\tilde{\mathbf{r}}'_{S_{c,i}/B}] \right) \right] \boldsymbol{\omega}_{B/N} + \dot{\theta}_i[\tilde{\boldsymbol{\omega}}_{B/N}] \left(I_{s_{i,2}}\hat{\mathbf{s}}_{i,2} + m_{sp_i}d_i[\tilde{\mathbf{r}}_{S_{c,i}/B}]\hat{\mathbf{s}}_{i,3} \right) \\
\left. + m_{sp_i}d_i\dot{\theta}_i^2[\tilde{\mathbf{r}}_{S_{c,i}/B}]\hat{\mathbf{s}}_{i,1} \right\} \quad (6.36)
\end{aligned}$$

$$\begin{aligned}
\boldsymbol{\tau}_{\theta,C} = - \left\{ \left(I_{s_{i,2}}\hat{\mathbf{s}}_{i,2} + m_{sp_i}d_i[\tilde{\mathbf{r}}_{S_{c,i}/C}]\hat{\mathbf{s}}_{i,3} \right) \ddot{\theta}_i + \left[[I'_{sp_i,S_{c,i}}] - m_{sp_i} \left([\tilde{\mathbf{r}}'_{S_{c,i}/C}][\tilde{\mathbf{r}}_{S_{c,i}/C}] \right. \right. \right. \\
\left. \left. + [\tilde{\mathbf{r}}_{S_{c,i}/C}][\tilde{\mathbf{r}}'_{S_{c,i}/C}] \right) \right] \boldsymbol{\omega}_{B/N} + \dot{\theta}_i[\tilde{\boldsymbol{\omega}}_{B/N}] \left(I_{s_{i,2}}\hat{\mathbf{s}}_{i,2} + m_{sp_i}d_i[\tilde{\mathbf{r}}_{S_{c,i}/C}]\hat{\mathbf{s}}_{i,3} \right) \\
\left. + m_{sp_i}d_i\dot{\theta}_i^2[\tilde{\mathbf{r}}_{S_{c,i}/C}]\hat{\mathbf{s}}_{i,1} \right\} \quad (6.37)
\end{aligned}$$

$$\begin{aligned} \boldsymbol{\tau}_{\rho,B} = & - \left(m_j [\tilde{\mathbf{r}}_{P_{c,j}/B}] \hat{\mathbf{p}}_j \ddot{\rho}_j + m_j [\tilde{\boldsymbol{\omega}}_{B/N}] [\tilde{\mathbf{r}}_{P_{c,j}/B}] \mathbf{r}'_{P_{c,j}/B} - m_j \left([\tilde{\mathbf{r}}'_{P_{c,j}/B}] [\tilde{\mathbf{r}}_{P_{c,j}/B}] \right. \right. \\ & \left. \left. + [\tilde{\mathbf{r}}_{P_{c,j}/B}] [\tilde{\mathbf{r}}'_{P_{c,j}/B}] \right) \boldsymbol{\omega}_{B/N} \right) \end{aligned} \quad (6.38)$$

$$\begin{aligned} \boldsymbol{\tau}_{\rho,C} = & - \left(m_j [\tilde{\mathbf{r}}_{P_{c,j}/C}] \hat{\mathbf{p}}_j \ddot{\rho}_j + m_j [\tilde{\boldsymbol{\omega}}_{B/N}] [\tilde{\mathbf{r}}_{P_{c,j}/C}] \mathbf{r}'_{P_{c,j}/C} - m_j \left([\tilde{\mathbf{r}}'_{P_{c,j}/C}] [\tilde{\mathbf{r}}_{P_{c,j}/C}] \right. \right. \\ & \left. \left. + [\tilde{\mathbf{r}}_{P_{c,j}/C}] [\tilde{\mathbf{r}}'_{P_{c,j}/C}] \right) \boldsymbol{\omega}_{B/N} \right) \end{aligned} \quad (6.39)$$

6.3 Hinged Rigid-Bodies Numerical Simulations

To provide an example of the flexing behavior, a spacecraft similar to the one in Figure 3.1 is used. The hub is a cylinder with its center of mass located at the geometric center of the cylinder. It has two identical solar panels modeled as rectangular prisms located opposite from each other. There are two scenarios simulated: one that includes flexing and one that models the system as a rigid-body.

Table 6.4: Simulation parameters for the flexing model

Parameter	Notation	Value	Units
Number of solar panels	N_{sp}	2	-
Total spacecraft mass	m_{sc}	950	kg
Hub mass	m_{hub}	750	kg
Solar panel mass	$m_{sp,i}$	100	kg
Hub inertia tensor	$[I_{hub,B_c}]$	${}^B \begin{bmatrix} 499.92 & -1.76 & -2.81 \\ -1.76 & 400.01 & -1.12 \\ -2.81 & -1.12 & 350.08 \end{bmatrix}$	kg·m ²
Hub C.O.M. location w.r.t. B	$\mathbf{r}_{B_c/B}$	${}^B [0 \quad -0.21 \quad 0]^T$	m
Hinge 1 location vector	$\mathbf{r}_{H_1/B}$	${}^B [0.5 \quad 1.0 \quad 0.0]^T$	m
Hinge 2 location vector	$\mathbf{r}_{H_2/B}$	${}^B [0.5 \quad -1.0 \quad 0.0]^T$	m
Body to Hinge 1 DCM	$[H_1B]$	$\begin{bmatrix} -1 & 0 & 0 \\ 0 & 0 & 1 \\ 0 & 1 & 0 \end{bmatrix}$	-
Body to Hinge 2 DCM	$[H_2B]$	$\begin{bmatrix} 1 & 0 & 0 \\ 0 & 0 & -1 \\ 0 & -1 & 0 \end{bmatrix}$	-
C.O.M offset of solar panel	d_i	1.5	m
Torsional linear spring constant	k_i	300	N·m/rad
Torsional linear damping constant	c_i	0	N·m·s/rad

The two simulations are assembled to have the same mass properties when the panels have

zero angular deflection. The spacecraft parameters can be seen in Tables 6.4 and 6.5. Additionally, the rigid-body simulation is chosen to have the center of mass coincident with the body frame origin therefore $\mathbf{r}_{B_c/B} = \mathbf{r}_{C/B} = {}^B \begin{bmatrix} 0 & 0 & 0 \end{bmatrix}^T$. This assumption is common in rigid-body dynamics formulations [39, 40]. The initial conditions of the spacecraft simulations can be seen in Table 6.6 and it should be noted that the two simulations also have the same initial conditions allowing the simulations to be directly comparable; the differences between the two simulations are solely due to the impact of flexing. The simulations are given an impulsive body fixed force, $\mathbf{F}_{\text{ext}} = {}^B \begin{bmatrix} 0 & 100 & 0 \end{bmatrix}^T$ Newtons, from $t = 0$ to $t = 30$ sec, and for the remainder of the simulation there are no external forces or torques on the spacecraft.

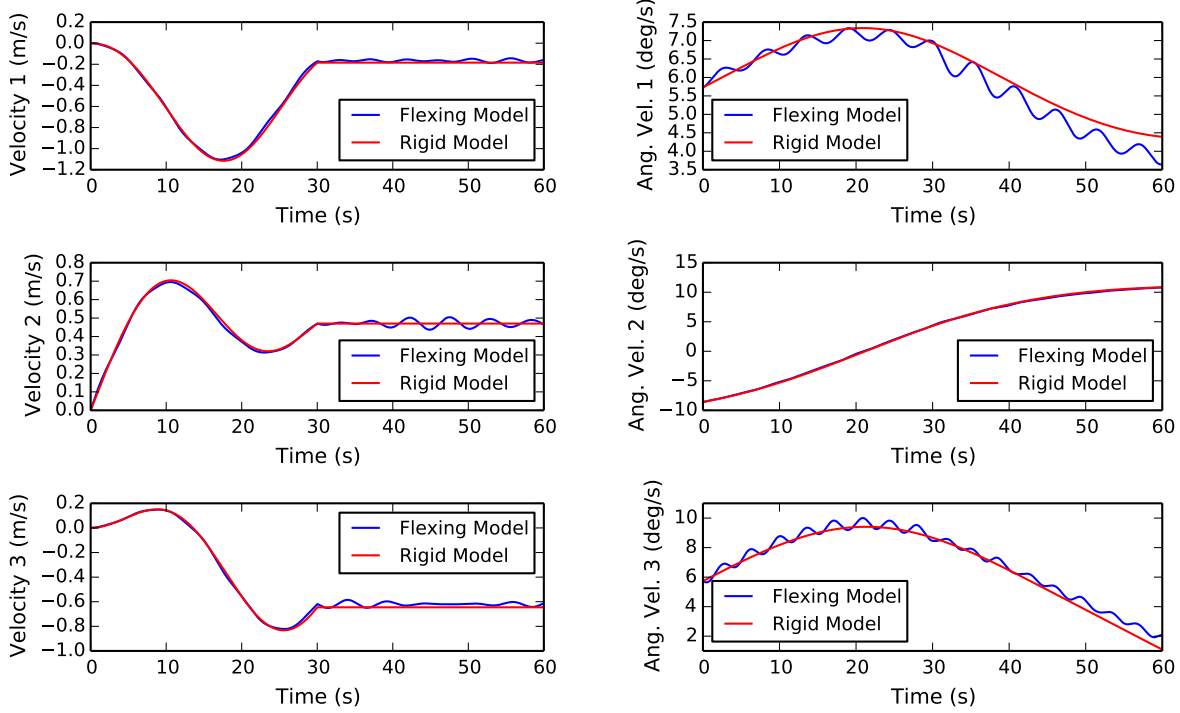
Table 6.5: Simulation parameters for the rigid-body model

Parameter	Notation	Value	Units
Total spacecraft mass	m_{sc}	950	kg
Hub inertia tensor	$[I_{\text{hub},B_c}]$	${}^B \begin{bmatrix} 857.81 & -1.76 & -2.81 \\ -1.76 & 1300.01 & -1.12 \\ -2.81 & -1.12 & 1407.97 \end{bmatrix}$	kg·m ²
Hub C.O.M. location w.r.t. B	$\mathbf{r}_{B_c/B}$	${}^B \begin{bmatrix} 0 & 0 & 0 \end{bmatrix}^T$	m

Table 6.6: Flexing simulation initial conditions

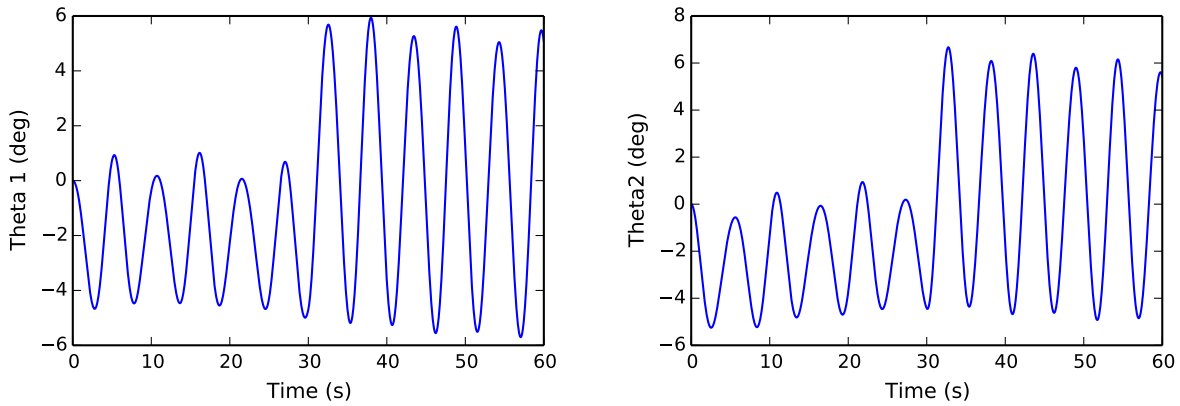
Parameter	Notation	Value	Units
Initial position	$\mathbf{r}_{B/N}$	${}^N \begin{bmatrix} 0 & 0 & 0 \end{bmatrix}^T$	m
Initial velocity	$\dot{\mathbf{r}}_{B/N}$	${}^N \begin{bmatrix} 0 & 0 & 0 \end{bmatrix}^T$	m/s
Initial attitude MRP	$\boldsymbol{\sigma}_{B/N}$	$\begin{bmatrix} 0 & 0 & 0 \end{bmatrix}^T$	-
Initial angular velocity	$\boldsymbol{\omega}_{B/N}$	${}^B \begin{bmatrix} 5.73 & -8.59 & 5.73 \end{bmatrix}^T$	deg/s
External force on spacecraft from $t = 0 : 30$ sec	\mathbf{F}_{ext}	${}^B \begin{bmatrix} 0 & 100 & 0 \end{bmatrix}^T$	N
Initial angular deflection of panels	θ_1, θ_2	0	deg
Initial angular velocity of panels	$\dot{\theta}_1, \dot{\theta}_2$	0	deg/s

The results from these simulations can be seen in Figures 6.8-6.9. In Figure 6.8 the variables, ${}^N \dot{\mathbf{r}}_{B/N}$, and ${}^B \boldsymbol{\omega}_{B/N}$ are plotted for both the flexing model and rigid-body simulations. The flexing impact on the simulations can readily be seen from these plots and visually shows how this can impact simulation fidelity and accuracy of simulated accelerometers. Figure 6.9 shows the angular



(a) Inertial Velocity of Point B in Inertial Frame Components (b) Inertial Angular Velocity of Body Frame in Body Frame Components

Figure 6.8: Inertial Velocity of Point B and Inertial Angular Velocity of the Body Frame



(a) Angular Deflection of Panel 1 (b) Angular Deflection of Panel 2

Figure 6.9: Angular Deflection of the Hinged Rigid-Bodies

deflection of each solar panel and these oscillations are what are driving the oscillations in the

translational and rotational motions.

6.4 Fuel Slosh and Hinged Rigid-Bodies Numerical Simulations

To give an example of the flexing and slosh behavior, a numerical simulation is setup. The spacecraft is composed by a hub, two solar panels, and two slosh masses. The parameters used for the simulation can be seen in Tables 6.7-6.9. Two different simulations are run: with and without damping. The table shows the damping parameters for the damped case. For the undamped case they are all zero.

Table 6.7: Hub simulation parameters

Hub	$m_{\text{hub}} [kg]$	750
	$[I_{\text{hub},B_c}] [kg-m^2]$	$\text{diag}([900 \ 800 \ 600])$
	${}^B\mathbf{r}_{B_c/B}$	$[0.00133 \ -0.267 \ 0]^T$

Table 6.8: Solar panel simulation parameters

Solar Panels	$m_{\text{sp}_1}, m_{\text{sp}_2} [kg]$	100
	$[I_{S_{c,1}}, [I_{S_{c,2}}] [kg-m^2]$	$\text{diag}([100 \ 50 \ 50])$
	${}^B\mathbf{r}_{H_1/N} [m]$	$[0.5 \ 1 \ 0]^T$
	${}^B\mathbf{r}_{H_2/N} [m]$	$[-0.5 \ 1 \ 0]^T$
	$[H_1B]$	$\begin{bmatrix} -1 & 0 & 0 \\ 0 & 0 & 1 \\ 0 & 1 & 0 \end{bmatrix}$
	$[H_2B]$	$\begin{bmatrix} 1 & 0 & 0 \\ 0 & 0 & -1 \\ 0 & 1 & 0 \end{bmatrix}$
	$d_1, d_2 [m]$	1.5
	$k_1, k_2 [N]$	43426.26
	$c_1, c_2 [Ns]$	138.23

For simplicity, the spacecraft is given initial conditions that will constrain its movement to planar motion. No external forces are acting on the body. The non-zero initial values are $\theta_{1_0} = 5^\circ$, $\rho_{1_0} = 5 \text{ cm}$, $\rho_{2_0} = -2.5 \text{ cm}$. All other initial values are set to zero.

Table 6.9: Slosh simulation parameters

Slosh modes	m_1, m_2 [kg]	10, 20
	${}^B\mathbf{r}_{P_{c,1}/B}$ [m]	$[0.1 \ 0 \ 0]^T$
	${}^B\mathbf{r}_{P_{c,2}/B}$ [m]	$[-0.1 \ 0 \ 0]^T$
	${}^B\hat{\mathbf{p}}_1, {}^B\hat{\mathbf{p}}_2$	$[0 \ 1 \ 0]^T$
	k_1, k_2 [N/m]	3.95, 71.06
	c_1, c_2 [Ns/m]	2.51, 7.54

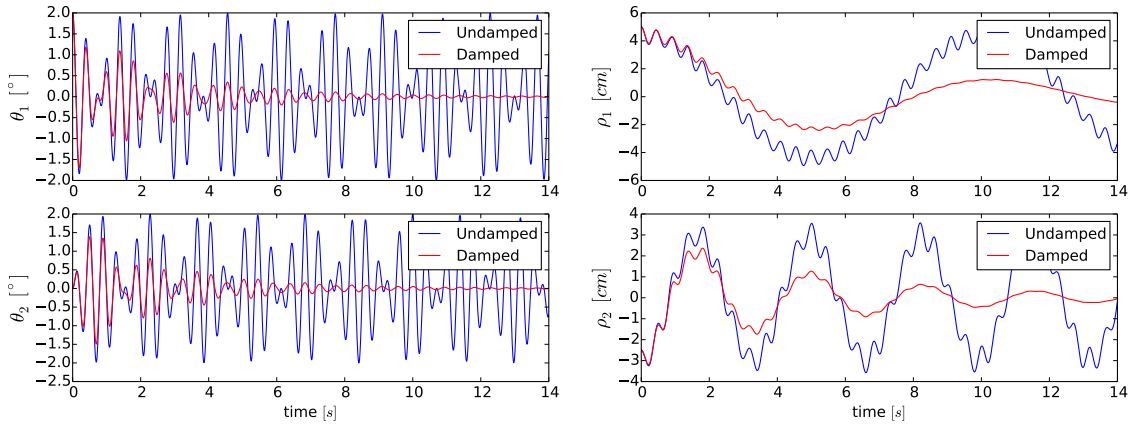
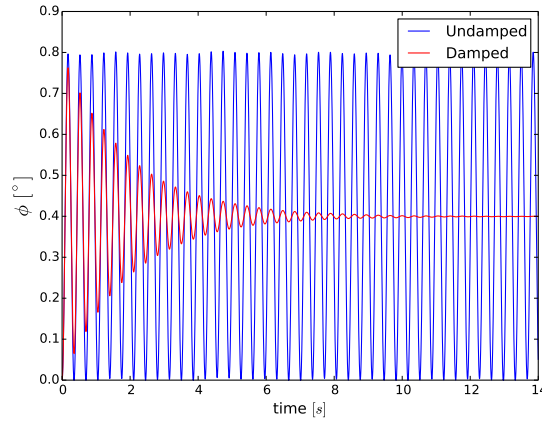
(a) Solar panel angles, θ_1 and θ_2 .(b) Slosh displacements, ρ_1 and ρ_2 .(c) Orientation of body frame, ϕ .

Figure 6.10: Solar panel, slosh, and rotational motion.

To describe the one-dimensional planar rotation, the angle between $\hat{\mathbf{b}}_3$ and $\hat{\mathbf{n}}_3$ is defined as ϕ . It should be noted here that ϕ is only defined for use in this planar case, but otherwise

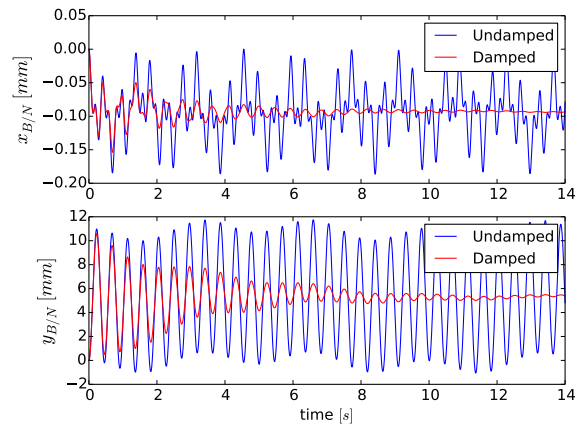


Figure 6.11: Translational motion of spacecraft.

3-dimensional orientation descriptions would need to be used to describe the relationship between the \mathcal{B} and \mathcal{N} frames. The results from this simulation can be seen in Figures 6.10-6.11.

Chapter 7

Conclusion and Future Work

7.1 Summary and Conclusion

Simulations of spacecraft dynamics are becoming increasingly more complex. Due to the increase in complexity, special consideration must be taken with respect to the maintainability, testability, and scalability of the software. However, spacecraft dynamics simulations provide their own unique challenges. For example, the equations of motion (EOM)s of spacecraft can come in an infinite number of different solutions to describe the same system. Once an additional system is being considered, the variability between the EOMs grows very quickly. The assumptions made, the state variables chosen, the coordinate frames used, and the methods used to develop the EOMs all dictate the final form of the EOMs. These considerations require detailed planning throughout the entire design process of the software architecture which begin at the development of the EOMs.

To combat the issue of having non-conformity between different equations of motion, a generalized EOM form is introduced in this dissertation that can apply to a wide range of spacecraft applications. The elegant form is achieved by considering a specific spacecraft dynamical system where a range of dynamical sub-systems are attached to a central rigid hub. Using this standard form for the EOMs ensures that the dynamics solutions developed for a spacecraft mission or spacecraft dynamics software will all adhere to the same form.

A key feature of this generalized EOM form is that a pattern is created in the system mass matrix which creates modularity. One issue with multi-body dynamics is that the system mass matrix is non-diagonal and needs to be inverted to solve the full system dynamics. Leveraging

the pattern in the system mass matrix, a back-substitution method is introduced that analytically solves the mass matrix inverse in the least amount calculations required and removes the need for the system to populate the full system mass matrix. This introduces modularity to the spacecraft dynamics which is leveraged in the design of the software architecture.

In addition to the modularity, since the full solution is being computed with the proposed back-substitution method, energy and momentum tools are available for verification purposes. When developing multi-body dynamics simulation software, energy and momentum tools are vital for ensuring the code is implemented properly. This dissertation includes modularization of the energy and momentum conservation values where each model provides contributions to the energy and momentum calculations but does not need to know any information about other models.

Due to the variability in the dynamics formulations the literature is lacking on common dynamics problems solutions seen by spacecraft that agree with a common form. This results in the necessity to re-derive the equations of motion for complex problems which can be a time consuming task and is susceptible to analytical development errors. This dissertation provides ready-to-implement solutions to common spacecraft dynamics problems that all conform to the general equation of motion form presented. The solutions included in this dissertation are flexing appended bodies, spring mass damper based fuel slosh, pendulum based fuel slosh, thruster based mass depletion, imbalanced reaction wheels, and imbalanced variable speed control moment gyroscopes. These examples are fully tested, ready to be implemented solutions to common phenomenon affecting spacecraft.

This dissertation introduces a modular software architecture for fully-coupled spacecraft dynamics and solves the issue of maintainability, scalability, and testability for this problem. The proposed software architecture is shown to be maintainable, allows for a fixed size system mass matrix to be inverted, allows effectors to be attached to the spacecraft in no particular order, allows for ease of testing the code base through energy and momentum conservation, and does not have scaling limitations.

An additional contribution of this dissertation is the extension of the software architecture

to allow for multiple spacecraft to be simulated at once, and allow for the spacecraft to dock and detach from one another. This is completed by assuming that the connected spacecraft are docked to one another rigidly through their rigid-body hubs. This creates a continuous rigid structure between the spacecraft and essentially creates a larger spacecraft that utilizes the same generalized EOM form. The architecture ensures that only the primary spacecrafts translational and rotational states are integrated by calculating contributions from the other connected spacecraft. After an integration step the software architecture solves for the other connected spacecraft states through kinematic relationships.

The modular software architecture is verified using energy and momentum conservation and is implemented in the Basilisk astrodynamics software package. This provides a fully implemented and tested example of the modular software architecture to provide proof of concept but this architecture could be implemented in any object oriented computer language.

7.2 Recommendations for Future Work

The included examples in this dissertation for common physical phenomenon affecting spacecraft is just a subset of all of the possible dynamics models affecting spacecraft. There are endless possibilities of dynamics models for example dual-gimbal VSCMGs, robotic appendages with multiple arms, more realistic fuel slosh models, etc. If the generalized EOM form is used to develop the EOMs, the modular software architecture could be used to implement these new models seamlessly. The scalability of this architecture was a large consideration of this architecture and was meant to allow for many different models to be added with ease.

Additionally, an assumption that was leveraged throughout this dissertation was the fact that the effectors had to be attached to the the rigid body hub. For example if a developer wanted a reaction wheel attached to a flexible appendage a new model would have to be created that defines that system connected to the spacecraft. Future work could be completed on determining the underlying physics and resulting architecture that would allow for effectors to be chained together or allow for the rigid-body hub to become flexible.

Bibliography

- [1] J.L. Junkins and Y. Kim. Introduction to Dynamics and Control of Flexible Structures. AIAA education series. American Institute of Aeronautics & Astronautics, 1993.
- [2] Thomas R. Kane and David A. Levinson. Formulation of equations of motion for complex spacecraft. Journal of Guidance, Control, and Dynamics, 3(2):99–112, 2017/09/27 1980.
- [3] C.A. Kluever. Dynamic Systems: Modeling, Simulation, and Control. Wiley, 2015.
- [4] Jinlu Kuang, Paul A Meehan, AYT Leung, and Soonhie Tan. Nonlinear dynamics of a satellite with deployable solar panel arrays. International Journal of Non-Linear Mechanics, 39(7):1161–1179, 2004.
- [5] Oskar Wallrapp and Simon Wiedemann. Simulation of deployment of a flexible solar array. Multibody System Dynamics, 7(1):101–125, 2002.
- [6] B Wie, N Furumoto, AK Banerjee, and PM Barba. Modeling and simulation of spacecraft solar array deployment. Journal of Guidance, Control, and Dynamics, 9(5):593–598, 1986.
- [7] Ieee standard glossary of software engineering terminology. IEEE Std 610.12-1990, pages 1–84, Dec 1990.
- [8] T. R. Kane, P. W. Likins, and D. A. Levinson. Spacecraft dynamics. McGraw-Hill Book Co., 1983.
- [9] Motion genesis: Symbolic force, motion, and code-generation tools. October, 2017. www.MotionGenesis.com.
- [10] Simscape multibody - model and simulate multibody mechanical systems. October, 2017. <https://www.mathworks.com/products/simmechanics.html>.
- [11] V. J. MODI. Attitude dynamics of satellites with flexible appendages- a brief review. Journal of Spacecraft and Rockets, 11(11):743–751, 2017/10/12 1974.
- [12] Arun K. Banerjee. Contributions of multibody dynamics to space flight: A brief review. Journal of Guidance, Control, and Dynamics, 26(3):385–394, 2017/09/27 2003.
- [13] Jorge Angeles and A Kecskeméthy. Kinematics and dynamics of multi-body systems, volume 360. Springer, 2014.

- [14] Gerald E Fleischer and Peter W Likins. Attitude dynamics simulation subroutines for systems of hinge-connected rigid bodies. NASA STI, 1975.
- [15] W Jerkovsky. The structure of multibody dynamics equations. Journal of Guidance, Control, and Dynamics, 1(3):173–182, 1978.
- [16] Peter W. Likins. Point-connected rigid bodies in a topological tree. Celestial mechanics, 11(3):301–317, May 1975.
- [17] W. W. HOOKER. A set of r dynamical attitude equations for an arbitrary n -body satellite having r rotational degrees of freedom. AIAA Journal, 8(7):1205–1207, 2017/09/27 1970.
- [18] T. R. Kane and D. A. Levinson. Multibody dynamics. Journal of Applied Mechanics, 50(4b):1071–1078, 12 1983.
- [19] Thomas R. Kane and David A. Levinson. The use of kane’s dynamical equations in robotics. The International Journal of Robotics Research, 2(3):3–21, 2017/09/27 1983.
- [20] Robert Filman, Tzilla Elrad, Siobhán Clarke, and Mehmet Akcsit. Aspect-oriented Software Development. Addison-Wesley Professional, first edition, 2004.
- [21] Bullet: Real-time physics simulation. October, 2017. <http://bulletphysics.org/wordpress/>.
- [22] H. Jeffreys and B. Jeffreys. Methods of Mathematical Physics. Cambridge Mathematical Library. Cambridge University Press, 1999.
- [23] Chrono: An open source framework for the physics-based simulation of dynamic systems. October, 2017. <http://projectchrono.org>.
- [24] Rbdl: Rigid body dynamics library. October, 2017. <https://rbdl.bitbucket.io/>.
- [25] Moby - multi-body dynamics simulation library. September, 2017. <http://physsim.sourceforge.net/index.html>.
- [26] Comsol: Multibody dynamics module. September, 2017. <https://www.comsol.com/multibody-dynamics-module>.
- [27] Interactive computer graphics - position based dynamics library. August, 2017. <http://www.interactive-graphics.de/index.php/downloads/92-positionbaseddynamics-library>.
- [28] Jan Bender, Matthias Müller, and Miles Macklin. Position-based simulation methods in computer graphics. In EUROGRAPHICS 2017 Tutorials. Eurographics Association, 2017.
- [29] Crispin Deul, Patrick Charrier, and Jan Bender. Position-based rigid body dynamics. Computer Animation and Virtual Worlds, 27(2):103–112, 2014.
- [30] Jan Bender. Impulse-based dynamic simulation in linear time. Computer Animation and Virtual Worlds, 18(4-5):225–233, 2007.
- [31] Ibds - impulse-based dynamic simulation and for institut für betriebs- und dialogsysteme. August, 2017.

- [32] Solis: Commercial plug-in to the analytical graphics, inc (agi) systems toolkit (stk). April, 2017. <http://www.go-asi.com/solutions/stk-solis/>.
- [33] Darts: Dynamics algorithms for real-time simulation. June, 2017. <https://dartslab.jpl.nasa.gov/DARTS/index.php>.
- [34] G. Rodriguez and A. Jain. Spatial operator algebra for multibody system dynamics. Journal of the Astronautical Sciences, 1992.
- [35] A. JAIN and G. RODRIGUEZ. Recursive flexible multibody system dynamics using spatial operators. Journal of Guidance, Control, and Dynamics, 15(6):1453–1466, 2017/10/26 1992.
- [36] 42: A comprehensive general-purpose simulation of attitude and trajectory dynamics and control of multiple spacecraft composed of multiple rigid or flexible bodies. September, 2017. <https://software.nasa.gov/software/GSC-16720-1>.
- [37] Orekit: An accurate and efficient core layer for space flight dynamics applications. October, 2017. <https://www.orekit.org/>.
- [38] Cody Allard, Manuel Diaz-Ramos, and Hanspeter Schaub. Spacecraft dynamics integrating hinged solar panels and lumped-mass fuel slosh model. In AIAA/AAS Astrodynamics Specialist Conference, Long Beach, CA, Sept. 12–15 2016.
- [39] Hanspeter Schaub and John L. Junkins. Analytical Mechanics of Space Systems. AIAA Education Series, Reston, VA, 3rd edition, 2014.
- [40] M.J. Sidi. Spacecraft Dynamics and Control: A Practical Engineering Approach. Cambridge Aerospace Series. Cambridge University Press, 1997.
- [41] C. Allard, Hanspeter Schaub, and Scott Piggott. General hinged solar panel dynamics approximating first-order spacecraft flexing. In AAS Guidance and Control Conference, Breckenridge, CO, Feb. 5–10 2016. Paper No. AAS-16-156.
- [42] John Alcorn, Cody Allard, and Hanspeter Schaub. Fully-coupled dynamical modeling of a rigid spacecraft with imbalanced reaction wheels. In AIAA/AAS Astrodynamics Specialist Conference, Long Beach, CA, Sept. 12–15 2016.
- [43] Paolo Panicucci, Cody Allard, and Hanspeter Schaub. Spacecraft dynamics employing a general multi-tank and multi-thruster mass depletion formulation. In AAS Guidance, Navigation and Control Conference, Breckenridge, CO, Feb. 2–8 2017. Paper AAS 17-011.
- [44] John Alcorn, Cody Allard, and Hanspeter Schaub. Fully-coupled dynamical jitter modeling of variable-speed control moment gyroscopes. In AAS/AIAA Astrodynamics Specialist Conference, Stevenson, WA, Aug. 20–24 2017. Paper No. AAS-17-730.
- [45] John Alcorn. Fully-coupled dynamical jitter modeling of momentum exchange devices. Master's thesis, University of Colorado - Boulder, Boulder, CO, May 2017.
- [46] Zhang F. Z. The Schur Complement and Its Applications. 01 2005.
- [47] Eigen: A c++ template library for linear algebra: matrices, vectors, numerical solvers, and related algorithms. August, 2016. <http://eigen.tuxfamily.org>.

- [48] Vladimir S. Aslanov and Vadim V. Yudinsev. Dynamics, analytical solutions and choice of parameters for towed space debris with flexible appendages. Advances in Space Research, 55(2):660 – 667, 2015.
- [49] James Richard Forbes. Identities for deriving equations of motion using constrained attitude parameterizations. Journal of Guidance, Control, and Dynamics, 37(4):1283–1289, 2017/10/20 2014.
- [50] A. Walsh and J. R. Forbes. Modeling and control of flexible telescoping manipulators. IEEE Transactions on Robotics, 31(4):936–947, Aug 2015.
- [51] T. R. Kane and D. A. Levinson. Dynamics, Theory and Applications. McGraw-Hill, 1985.
- [52] Payam Zarafshan and S Ali A Moosavian. Manipulation control of a space robot with flexible solar panels. In Advanced Intelligent Mechatronics (AIM), 2010 IEEE/ASME International Conference on, pages 1099–1104. IEEE, 2010.
- [53] S Ali A Moosavian and Evangelos Papadopoulos. Explicit dynamics of space free-flyers with multiple manipulators via spacemaple. Advanced robotics, 18(2):223–244, 2004.
- [54] Thomas Freud Wiener. Theoretical Analysis of Gimballess Inertial Reference Equipment Using Delta-Modulated Instruments. Ph.D. dissertation, Department of Aeronautics and Astronautics, Massachusetts Institute of Technology, Cambridge, MA, March 1962.
- [55] Malcolm D. Shuster. A survey of attitude representations. Journal of the Astronautical Sciences, 41(4):439–517, 1993.
- [56] S. R. Marandi and V. J. Modi. A preferred coordinate system and the associated orientation representation in attitude dynamics. Acta Astronautica, 15(11):833–843, 1987.
- [57] Hanspeter Schaub and John L. Junkins. Stereographic orientation parameters for attitude dynamics: A generalization of the rodrigues parameters. Journal of the Astronautical Sciences, 44(1):1–19, 1996.
- [58] John E. Hurtado. Interior parameters, exterior parameters, and a cayley-like transform. AIAA Journal of Guidance, Control, and Dynamics, 32(2):653–657, 2009.
- [59] J. Gerrits. Dynamics of Liquid-Filled Spacecraft. PhD thesis, University of Groningen, December 2001.
- [60] R Luppés, J Helder, and A. Veldman. Liquid sloshing in microgravity. In 56th International Astronautical Congress of the International Astronautical Federation, the International Academy of Astronautics, and the International Institute of Space Law, International Astronautical Congress (IAF), Fukuoka, Japan, 2005.
- [61] H. Abramson. The dynamic behavior of liquids in moving containers. Technical Report SP-106, NASA, 1966.
- [62] F. Dodge. The new dynamic behavior of liquids in moving containers. Technical report, Southwest Research Institute, San Antonio, TX, USA, 2000.
- [63] Vreeburg J. and Veldman P. Transient and sloshing motions in an unsupported container. In R. Monti, editor, Physics of Fluids in Microgravity. Taylor and Francis, 1st edition, 2001.

- [64] R. Hung and Y. Chi. Slosh dynamics coupled with spacecraft attitude dynamics part 1: Formulation and theory. Journal of Spacecraft and Rockets, 33(4), July-August 1996.
- [65] B. Marsell, S. Gangadharan, Y. Chatman, J. Sudderemann, K. Schlee, and J. Ristow. A cfd approach to modeling spacecraft fuel slosh. In 47th AIAA Aerospace Sciences Meeting Including The New Horizons Forum and Aerospace Exposition, Orlando, FL, USA, January 2009. Paper No. AIAA 2009-366.
- [66] R. Zhou, M. Vergalla, D. Kirk, and H. Gutierrez. Experimental methodology and numerical technique for 6-dof tank slosh dynamics. In 46th AIAA/ASME/SAE//ASEE Joint Propulsion Conference and Exhibit, Nashville, TN, USA, July 2010. Paper No. AIAA 2010-6977.
- [67] K. Schlee, S. Gangadharan, J. Ristow, J. Sudermann, and C. Walker. Parameter estimation of spacecraft fuel slosh. In Structures, Structural Dynamics, and Materials Conference, Newport, RI, USA, May 2006. Paper No. AIAA 2006-1886.
- [68] D. Theureau, B. Busset, H. Bavestrello, L. Dandaleix, S. Tanguy, J. Mignot, and J. Maureau. Integration of low g sloshing models with spacecraft attitude control simulators. In AIAA Guidance, Navigation, and Control (GNC) Conference, Boston, MA, USA, August 2013.
- [69] R. Buseck and H. Benaroya. Mechanical models for slosh and liquid fuel. In Aerospace Design Conference, Irving, CA, USA, 1993. Paper No. AIAA-93-1093.
- [70] P. Enright and E. Wong. Propellant slosh models for the cassini spacecraft. In Astrodynamics Conference, Guidance, Navigation, and Control, Scottsdale, AZ, USA, 1994. Paper No. AIAA-94-3730-CP.
- [71] D. Kana. A model for nonlinear rotary slosh in propellant tanks. In 27th Structures, Structural Dynamics and Materials Conference Structures, Structural Dynamics, and Materials, San Antonio, TX, USA, 1986.
- [72] Carl Blaurock Kuo-Chia Liu James Alexander Marie Levine Larry Dewell, Nelson Pedreiro. Precision telescope pointing and spacecraft vibration isolation for the terrestrial planet finder coronagraph, 2005.
- [73] J. B. Alcorn R. B. Barclay R. K Barry D. J. Benford A. Dhabal D. J. Fixsen A. S. Gore S. Johnson-Shapoval D. T. Leisawitz S. F. Maher L. G. Mundy A. Papageorgiou E. Pascale A. Rau R. F. Silverberg P. Taraschi T. J. Veach S. Weinreich Maxime J. Rizzo, S. A. Rinehart. Building an interferometer at the edge of space: pointing and phase control system for bettii, 2014.
- [74] Landis Markley and John Crassidis. Fundamentals of Spacecraft Attitude Determination and Control. 01 2014.
- [75] Junyoung Park, Alan Palazzolo, and Raymond Beach. Mimo active vibration control of magnetically suspended flywheels for satellite ipac service. Journal of Dynamic Systems, Measurement, and Control, 130(4):041005–041005–22, 06 2008.
- [76] Junyoung Park and Alan Palazzolo. Magnetically suspended vscmgs for simultaneous attitude control and power transfer ipac service. Journal of Dynamic Systems, Measurement, and Control, 132(5):051001–051001–15, 08 2010.

- [77] R.A. MASTERSON, D.W. MILLER, and R.L. GROGAN. Development and validation of reaction wheel disturbance models: Empirical model. Journal of Sound and Vibration, 249(3):575 – 598, 2002.
- [78] L. Liu. Jitter and basic requirements of the reaction wheel assembly in the attitude control system. Technical report, Massachusetts Institute of Technology, Cambridge, MA, August 2007.
- [79] H. Gutierrez. Performance Assessment and Enhancement of Precision Controlled Structures During Conceptual Design. PhD thesis, Massachusetts Institute of Technology, Cambridge, MA, 1999.
- [80] Homero L. (Homero Luis) Gutierrez. Performance assessment and enhancement of precision controlled structures during conceptual design. 01 2007.
- [81] Scott Miller, Paul Kirchman, and John Sudey. Reaction Wheel Operational Impacts on the GOES-N Jitter Environment. American Institute of Aeronautics and Astronautics, 2017/09/27 2007.
- [82] Dae-Kwan Kim. Micro-vibration model and parameter estimation method of a reaction wheel assembly. Journal of Sound and Vibration, 333(18):4214 – 4231, 2014.
- [83] Yao Zhang and Jingrui Zhang. Disturbance characteristics analysis of cmg due to imbalances and installation errors. 50:1017–1026, 04 2014.
- [84] John Alcorn, Cody Allard, and Hanspeter Schaub. Fully coupled reaction wheel static and dynamic imbalance for spacecraft jitter modeling. Journal of Guidance, Control, and Dynamics, 41(6):1380–1388, 2018/06/08 2018.
- [85] James F Thorpe. On the momentum theorem for a continuous system of variable mass. Am. J. Phys, 30:637–640, 1962.
- [86] Carl Grubin. Mechanics of variable mass systems. Journal of the Franklin Institute, 276(4):305–312, 1963.
- [87] Robert W Fox, Alan T McDonald, and Philip J Pritchard. Introduction to fluid mechanics, volume 7. John Wiley & Sons New York, 1985.
- [88] F.M. White. Fluid Mechanics. McGraw-Hill series in mechanical engineering. McGraw Hill, 2011.
- [89] B.R. Munson, A.P. Rothmayer, and T.H. Okiishi. Fundamentals of Fluid Mechanics, 7th Edition. John Wiley & Sons, Incorporated, 2012.
- [90] Fidelis O Eke. Dynamics of variable mass systems. 1998.
- [91] FO Eke, T Tran, and J Sookgaew. Dynamics of a spinning rocket with internal mass flow. Nonlinear Dynamics and Systems Theory, 6(2):129–142, 2006.
- [92] J Sookgaew and FO Eke. Effects of substantial mass loss on the attitude motions of a rocket-type variable mass system. Nonlinear Dynamics and Systems Theory, 4(1):73–88, 2004.

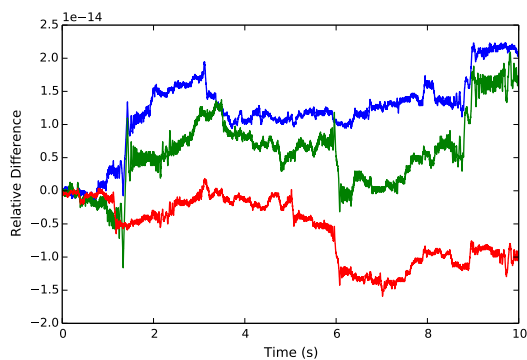
- [93] Marius Ionut Marmureanu and Ion Fuiorea. Attitude dynamics of a spinning rocket with internal fluid whirling motion. INCAS Bulletin, 6(2):75, 2014.
- [94] VS Aslanov and AV Doroshin. The motion of a system of coaxial bodies of variable mass. Journal of Applied Mathematics and Mechanics, 68(6):899–908, 2004.
- [95] Anton V Doroshin. Analysis of attitude motion evolutions of variable mass gyrostats and coaxial rigid bodies system. International Journal of Non-Linear Mechanics, 45(2):193–205, 2010.
- [96] Marco B Quadrelli, Jonathan Cameron, Bob Balaram, Mayank Baranwal, and Alessandro Bruno. Modeling and simulation of flight dynamics of variable mass systems. 2014.
- [97] K.J. Åström and Richard Murray. Feedback systems: An introduction for scientists and engineers. 01 2008.
- [98] B. Friedland. Control system design: an introduction to state-space methods. McGraw-Hill series in electrical engineering: Control theory. McGraw-Hill, 1986.
- [99] S. Skogestad and I. Postlethwaite. Multivariable Feedback Control: Analysis and Design. Wiley, 2005.
- [100] John L. Junkins and Youdam Kim. Introduction to Dynamics and Control of Flexible Structures. AIAA Education Series, Washington D.C., 1993.

Appendix A

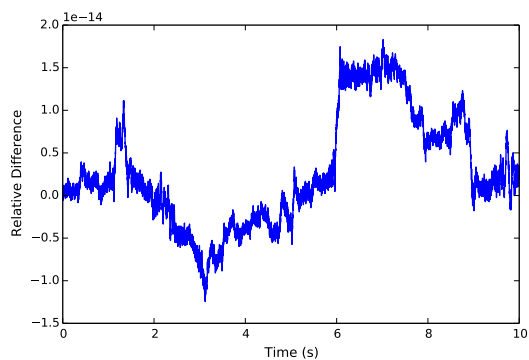
Energy and Momentum Verification

A.1 Rigid-Body Hub Verification

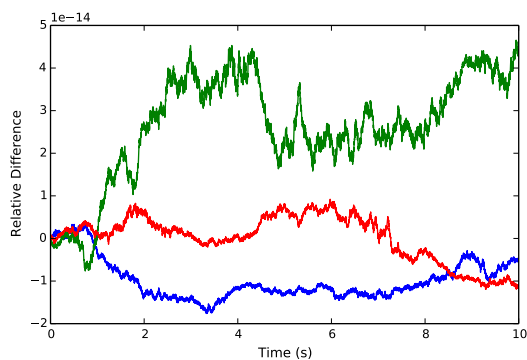
The scenario that is implemented to verify the conservation quantities for a rigid body hub is a scenario where a spacecraft with a rigid body hub is placed into orbit around earth and has a non-zero initial angular velocity. The results can be seen in Figure A.1 and confirms that the rigid body model is conserving the four conservation quantities. This gives confidence in the analytical and software implementation of the EOMs.



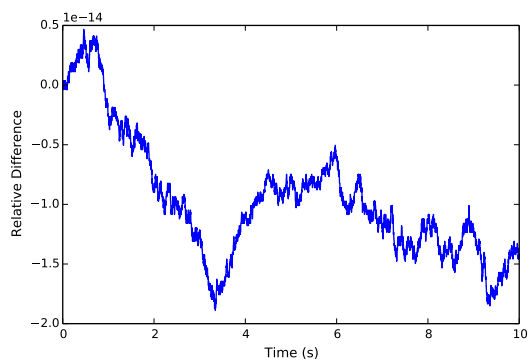
(a) Change in Orbital Angular Momentum



(b) Change in Orbital Energy



(c) Change in Rotational Angular Momentum

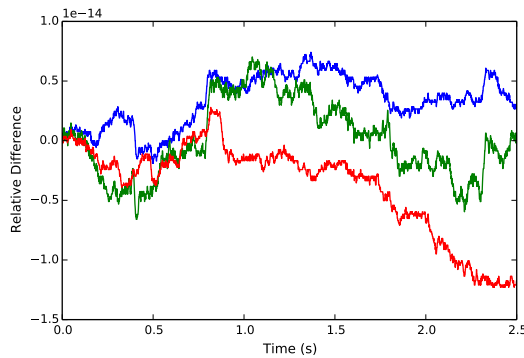


(d) Change in Rotational Energy

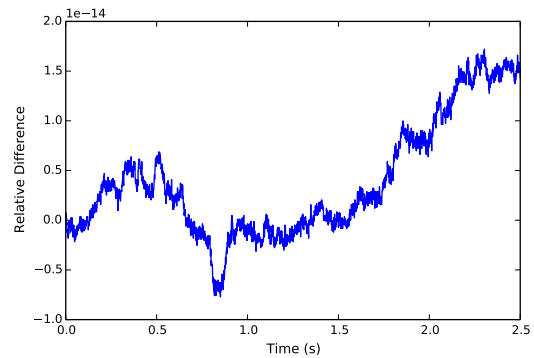
Figure A.1: Simulation verification results for a rigid hub

A.2 Fuel Slosh - Lumped Mass Spring Mass Damper Model Verification

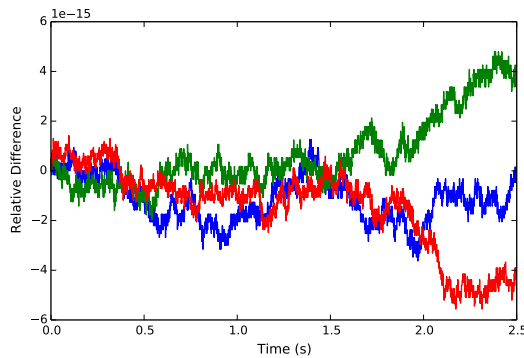
The scenario that is implemented to verify the conservation quantities for the spring mass damper fuel slosh model is a scenario where a spacecraft with three fuel slosh particles attached to it is placed into orbit around earth and has a non-zero initial angular velocity and non-zero deflected fuel slosh particles. No damping terms were included in this test. The results can be seen in Figure A.2 and confirms that the model is conserving the four conservation quantities. This gives confidence in the analytical and software implementation of the EOMs.



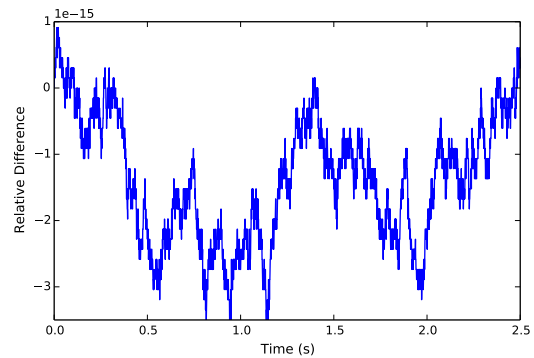
(a) Change in Orbital Angular Momentum



(b) Change in Orbital Energy



(c) Change in Rotational Angular Momentum



(d) Change in Rotational Energy

Figure A.2: Simulation verification results for a rigid hub with three spring mass damper fuel slosh particles

A.3 Reaction Wheels Verification

A.3.1 Balanced Reaction Wheels

The scenario that is implemented to verify the conservation quantities for the balanced reaction wheel model is a scenario where a spacecraft with three balanced reaction wheels are attached to it is placed into orbit around earth and has a non-zero initial angular velocity and non-zero wheel speeds. No friction terms were included in this test. The results can be seen in Figure A.3 and confirms that the model is conserving the four conservation quantities. This gives confidence in the analytical and software implementation of the EOMs.

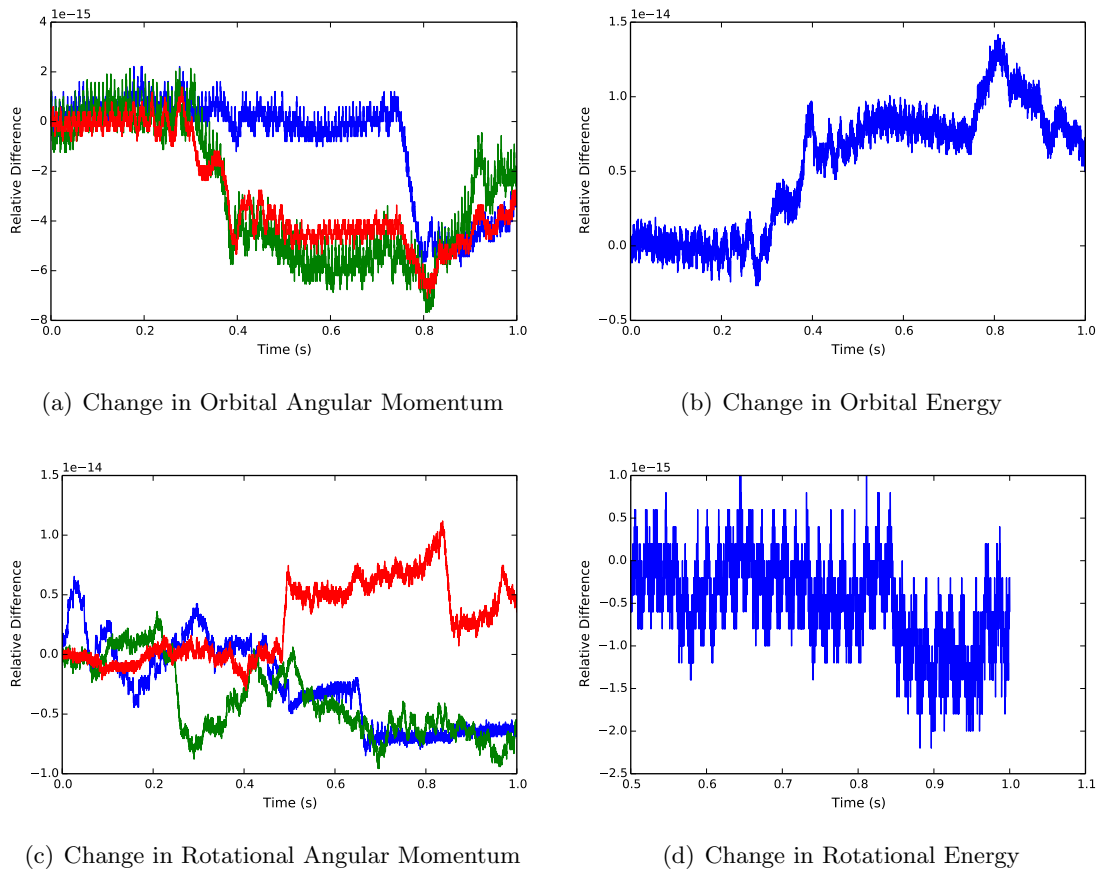


Figure A.3: Simulation verification results for a rigid hub with three balanced reaction wheels

A.3.2 Imbalanced Reaction Wheels

The scenario that is implemented to verify the conservation quantities for the imbalanced reaction wheel model is a scenario where a spacecraft with three imbalanced reaction wheels are attached to it is placed into orbit around earth and has a non-zero initial angular velocity and non-zero wheel speeds. No friction terms were included in this test. The results can be seen in Figure A.4 and confirms that the model is conserving the four conservation quantities. This gives confidence in the analytical and software implementation of the EOMs.

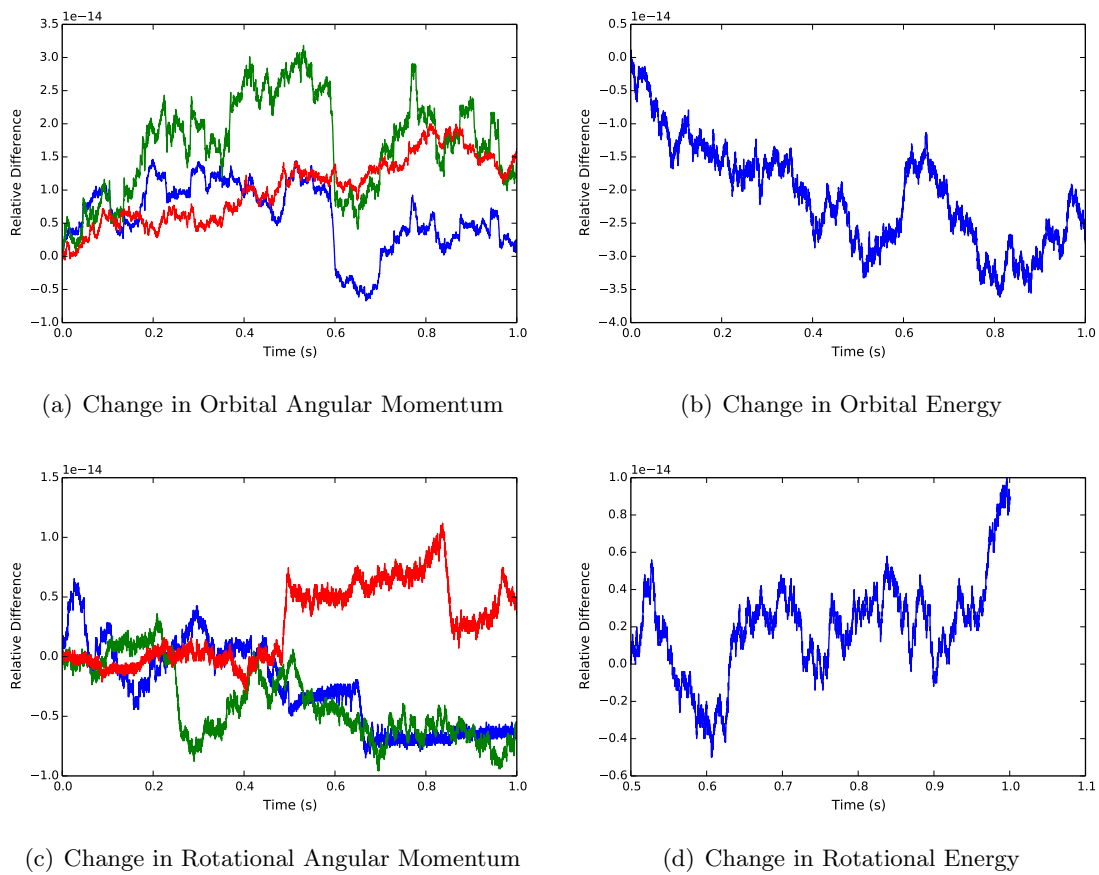


Figure A.4: Simulation verification results for a rigid hub with three imbalanced reaction wheels

A.4 Dual-Hinged Rigid-Bodies Verification

The scenario that is implemented to verify the conservation quantities for dual-hinged rigid-bodies is a scenario where a spacecraft with two sets of dual-hinged rigid-bodies attached to it is placed into orbit around earth and has a non-zero initial angular velocity and non-zero deflected solar panels. No damping terms were included in this test. The results can be seen in Figure A.5 and confirms that the dual-hinged rigid-body model is conserving the four conservation quantities. This gives confidence in the analytical and software implementation of the EOMs.

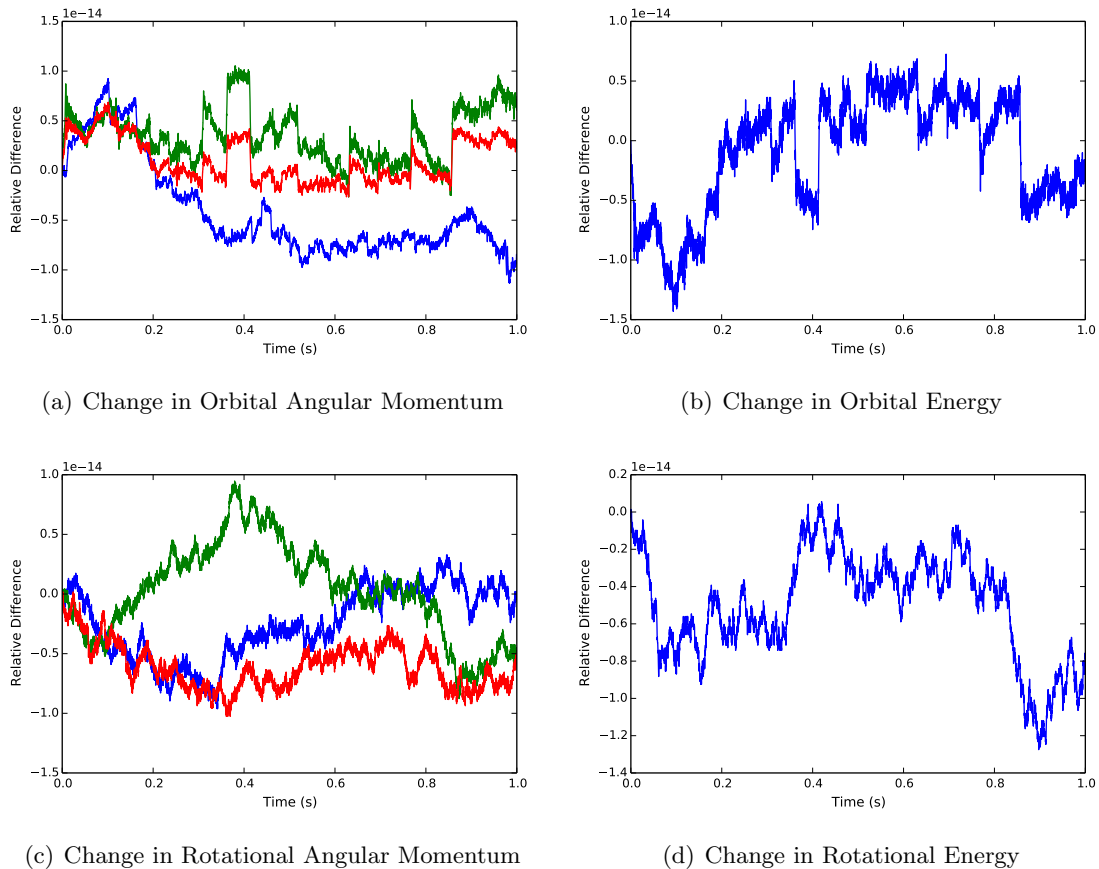


Figure A.5: Simulation verification results for a rigid hub with two sets of dual-hinged rigid-bodies

A.5 Variable Speed Control Moment Gyroscopes Verification

A.5.1 Balanced Variable Speed Control Moment Gyroscopes

The scenario that is implemented to verify the conservation quantities for the balanced VSCMG model is a scenario where a spacecraft with two balanced VSCMGs are attached to it is placed into orbit around earth and has a non-zero initial angular velocity and non-zero wheel speeds and non-zero gimbal speeds. No friction terms were included in this test. The results can be seen in Figure A.6 and confirms that the model is conserving the four conservation quantities. This gives confidence in the analytical and software implementation of the EOMs.

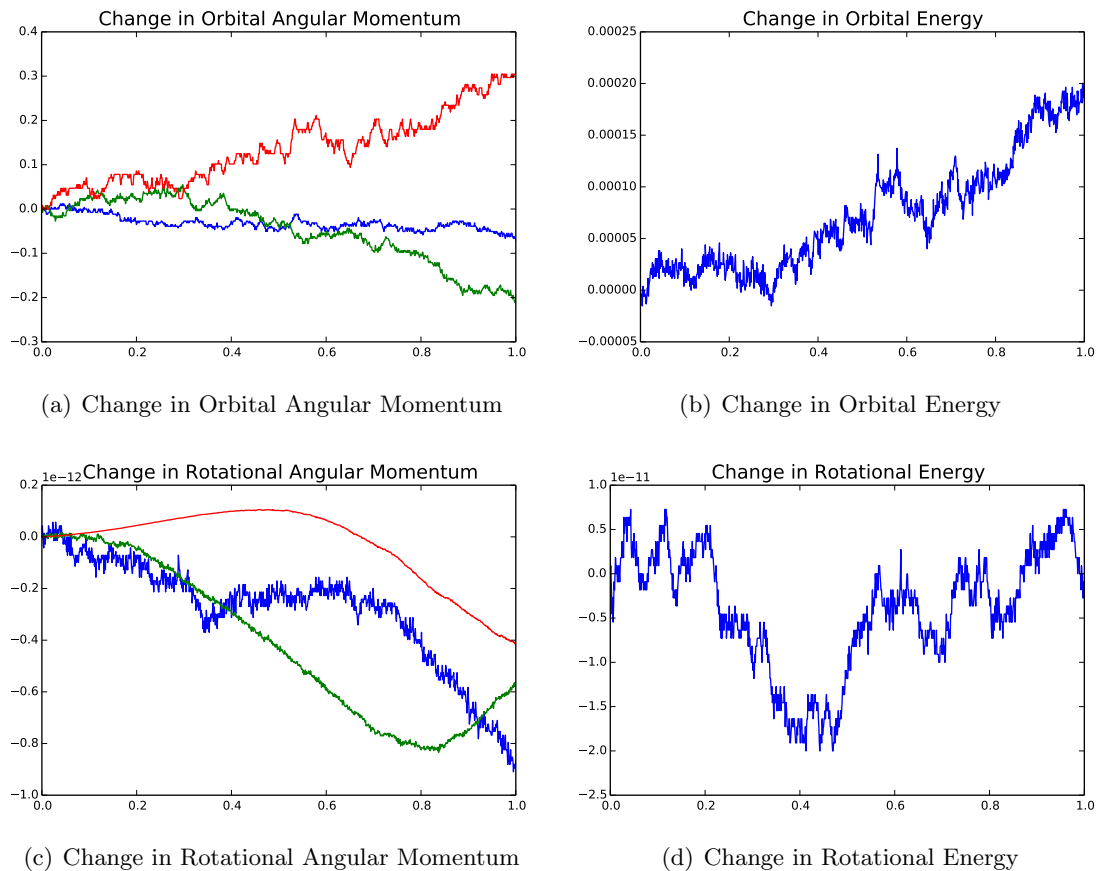


Figure A.6: Simulation verification results for a rigid hub with two balanced variable speed control moment gyroscopes

A.5.2 Imbalanced Variable Speed Control Moment Gyroscopes

The scenario that is implemented to verify the conservation quantities for the imbalanced VSCMG model is a scenario where a spacecraft with two imbalanced VSCMGs are attached to it is placed into orbit around earth and has a non-zero initial angular velocity and non-zero wheel speeds and non-zero gimbal speeds. No friction terms were included in this test. The results can be seen in Figure A.7 and confirms that the model is conserving the four conservation quantities. This gives confidence in the analytical and software implementation of the EOMs.

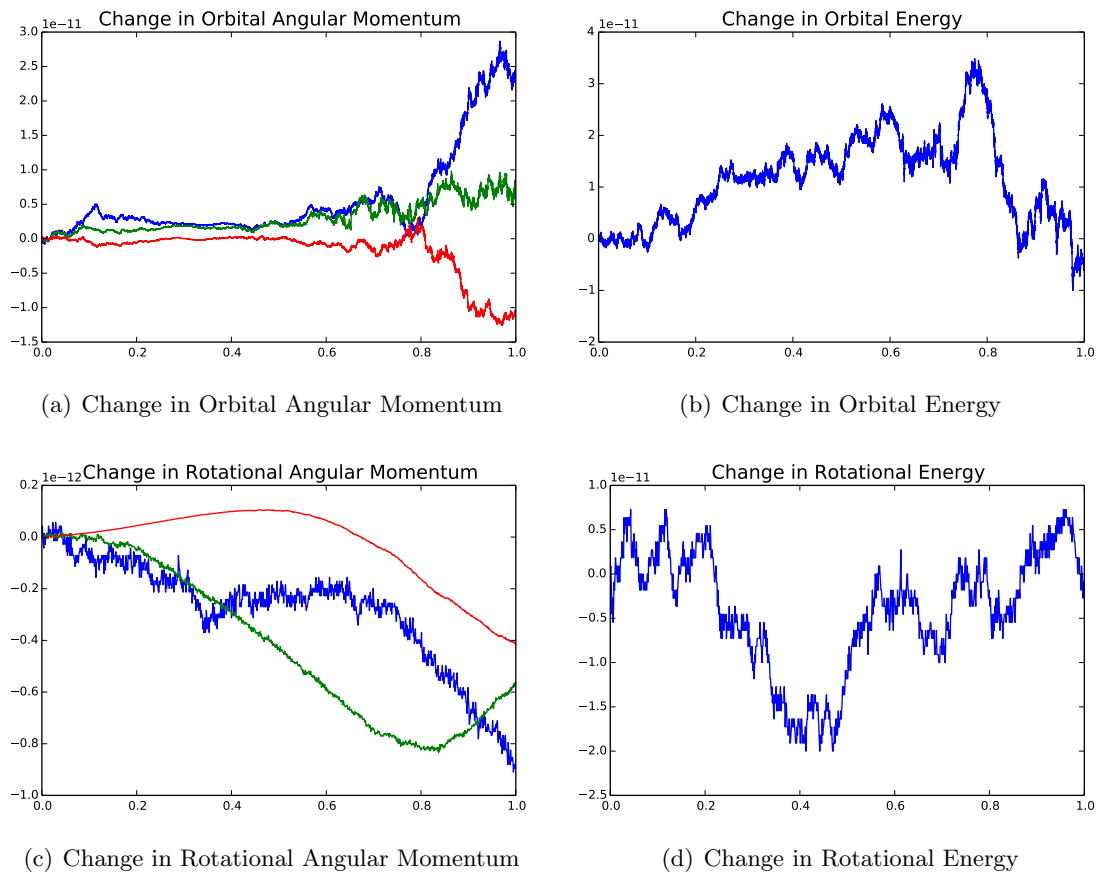


Figure A.7: Simulation verification results for a rigid hub with two imbalanced variable speed control moment gyroscopes

A.6 N-Connected Hinged Rigid-Bodies Verification

The scenario that is implemented to verify the conservation quantities for N-Connected hinged rigid-bodies is a scenario where a spacecraft with two sets of N-Connected hinged rigid-bodies attached to it (one with four panels and one with three panels) is placed into orbit around earth and has a non-zero initial angular velocity and non-zero deflected solar panels. No damping terms were included in this test. The results can be seen in Figure A.8 and confirms that the model is conserving the four conservation quantities. This gives confidence in the analytical and software implementation of the EOMs.

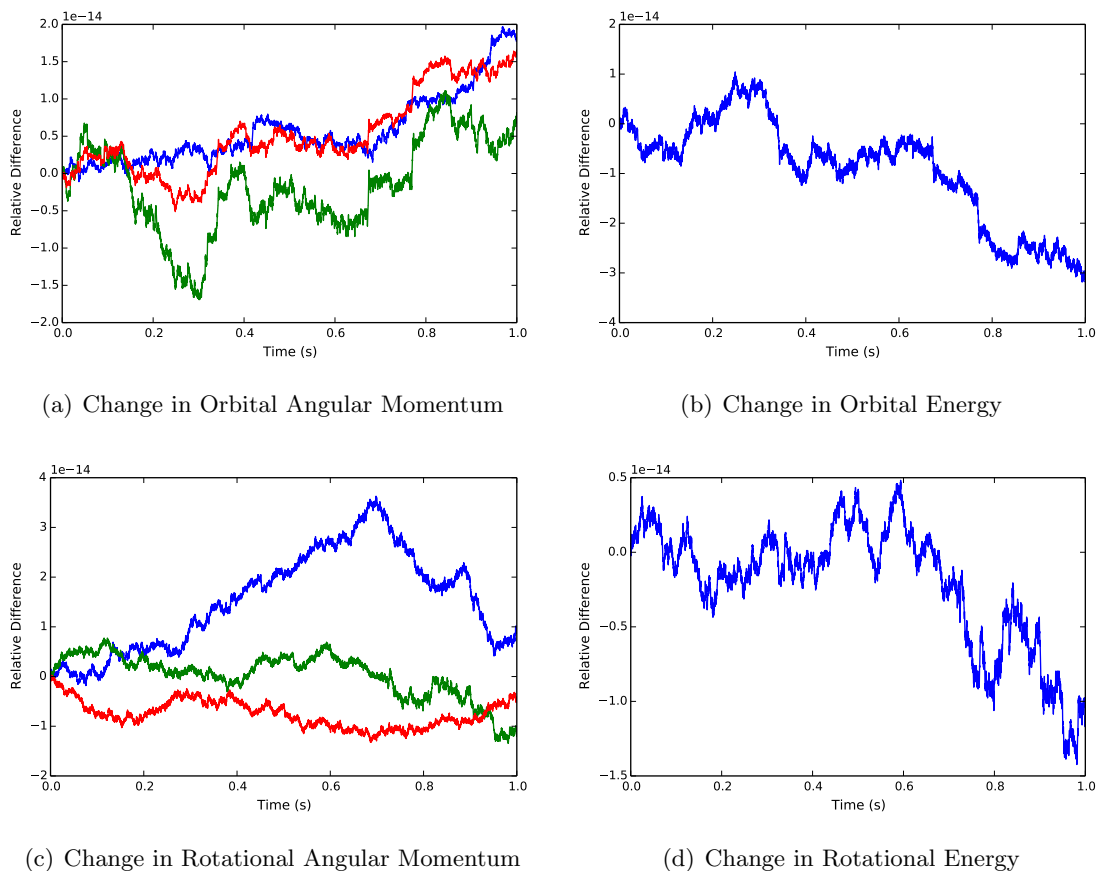


Figure A.8: Simulation verification results for a rigid hub with one panel with four sections and another panel with three sections

A.7 Fuel Slosh - Pendulum Model

The scenario that is implemented to verify the conservation quantities for the pendulum based fuel slosh model is a scenario where a spacecraft with three fuel slosh particles attached to it is placed into orbit around earth and has a non-zero initial angular velocity and non-zero deflected fuel slosh particles. No damping terms were included in this test. The results can be seen in Figure A.9 and confirms that the model is conserving the four conservation quantities. This gives confidence in the analytical and software implementation of the EOMs.

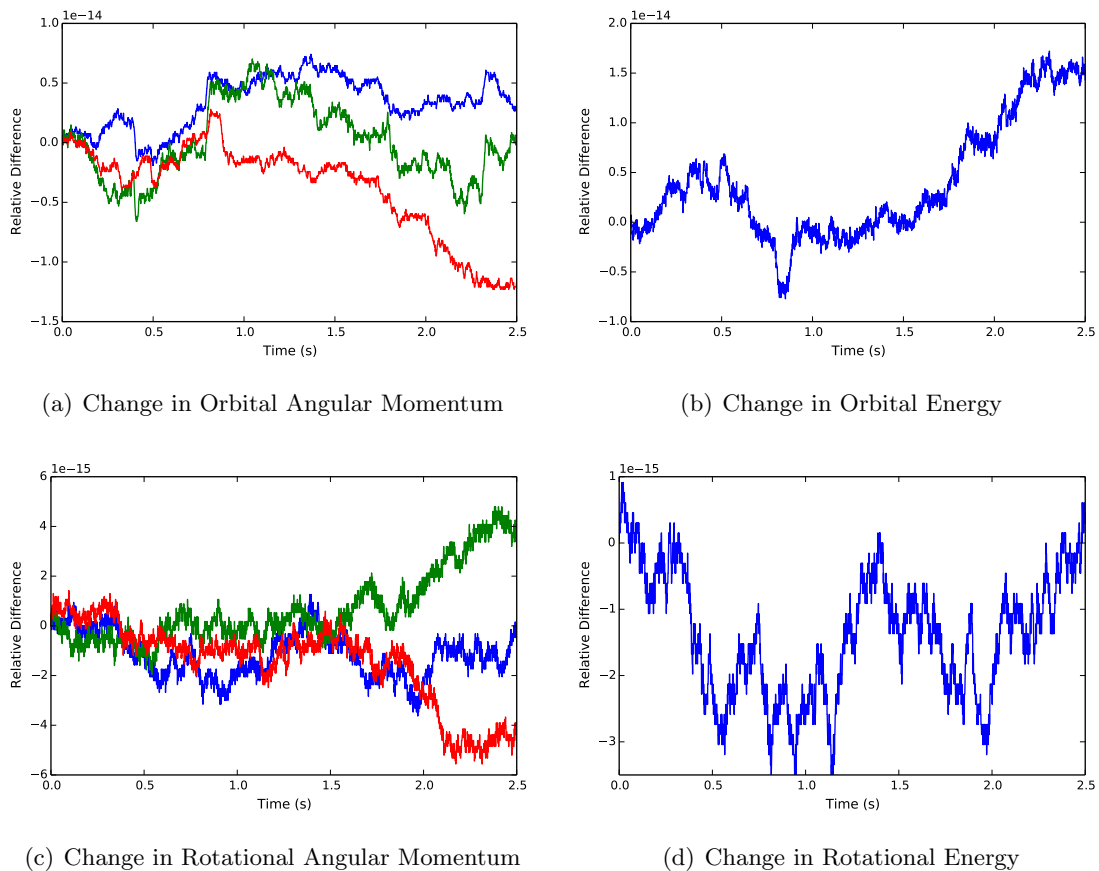


Figure A.9: Simulation verification results for a rigid hub with three pendulum based fuel slosh particles

A.8 Multi-Spacecraft Verification - Attached Spacecraft and Unattached Spacecraft

Another scenario that is implemented to verify the conservation quantities for the multi-spacecraft architecture is a scenario where a spacecraft with one hinged rigid-body attached to it is docked to a spacecraft with no `stateEffectors` attached to it but is docked to another spacecraft with one hinged rigid-body attached to it. Two other spacecraft with rigid body hubs are simulated unattached to the primary spacecraft. The spacecraft system is placed into orbit around earth and has a non-zero initial angular velocity and non-zero deflected solar panels. No damping terms were included in this test. The results can be seen in Figures A.10-A.12 and confirms that the multi-spacecraft architecture is conserving the four conservation quantities for the spacecraft system and the unattached spacecraft. This gives confidence in the analytical and software implementation of the EOMs.

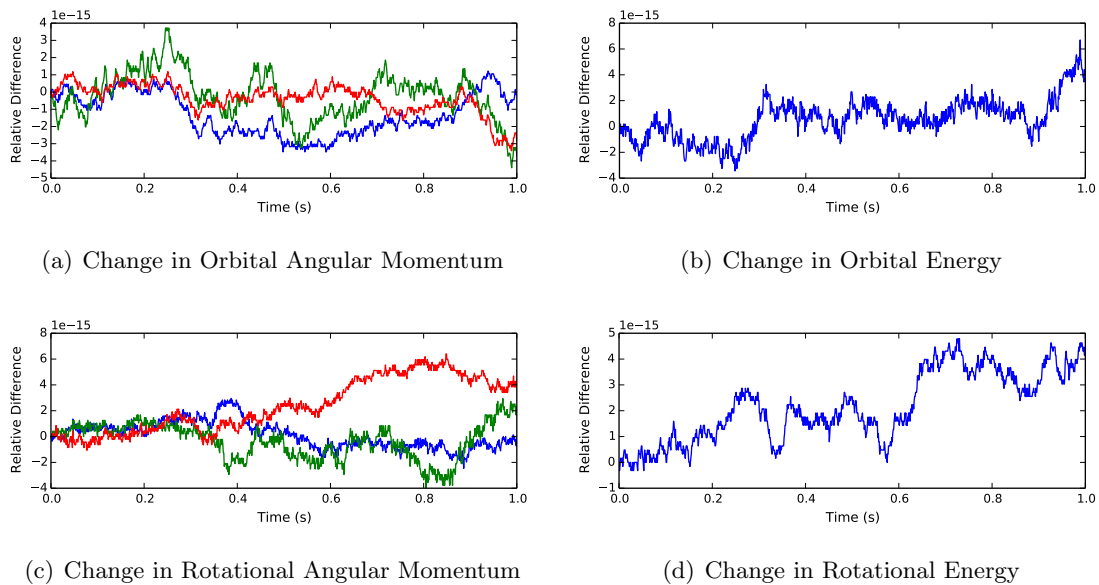
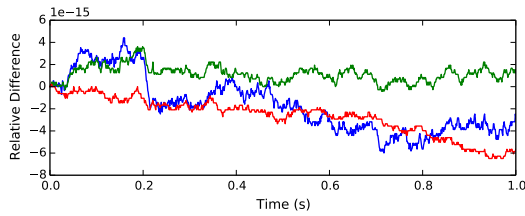
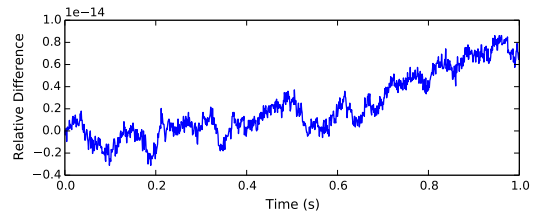


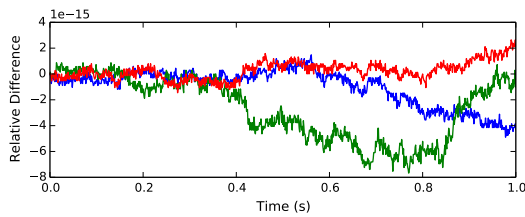
Figure A.10: Simulation verification results for two spacecraft attached to the primary spacecraft with two solar panels attached



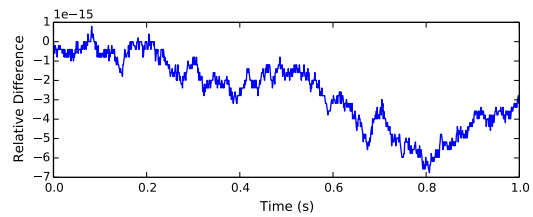
(a) Change in Orbital Angular Momentum



(b) Change in Orbital Energy

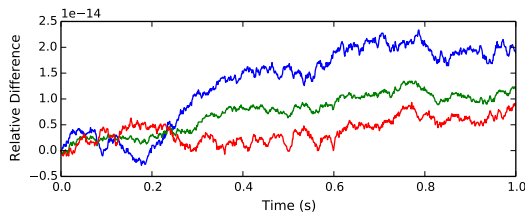


(c) Change in Rotational Angular Momentum

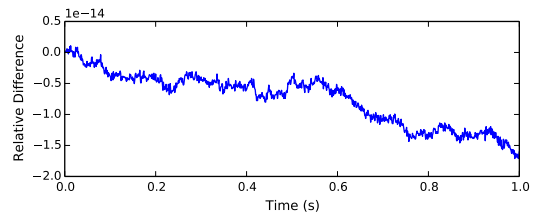


(d) Change in Rotational Energy

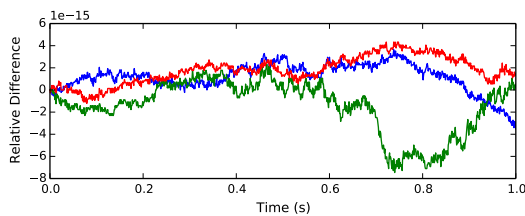
Figure A.11: Simulation verification results for first unattached spacecraft



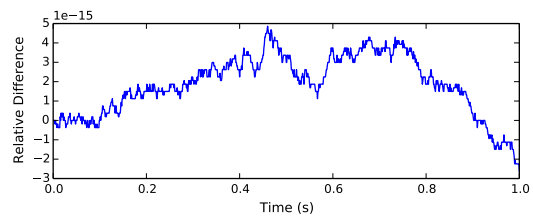
(a) Change in Orbital Angular Momentum



(b) Change in Orbital Energy



(c) Change in Rotational Angular Momentum



(d) Change in Rotational Energy

Figure A.12: Simulation verification results for second unattached spacecraft